Impact of changes in anthropogenic air pollutants on particulate air quality and the attributable burden of disease

Edward William Butt

Submitted in accordance with the requirements for the degree of

Doctor of Philosophy

The University of Leeds

School of Earth and Environment

November 2018

Declaration of Authorship

The candidate confirms that the work submitted in this thesis is his own, except where work formed as part of co-authored publications has been included. The contribution of the candidate and of other co-authors is detailed below. The candidate confirms that appropriate credit has been given where reference has been made to the work of others.

Chapter 3 is the publication Butt EW, Turnock ST, Rigby R, Reddington CL, Yoshioka M, Johnson JS, Regayre LA, Pringle KJ, Mann GW, Spracklen DV. 2017. Global and regional trends in particulate air pollution and attributable health burden over the past 50 years. Environmental Research Letters. 12(10). The manuscript was written by the candidate with advice from supervisors (Spracklen DV), with additional comments from co-authors during its preparation. The analysis of model simulations, evaluation against observations, and health burden calculations was solely undertaken by the candidate. The set-up and running of the climate-composition model was undertaken by Turnock ST. PPE simulation data were provided jointly by Yoshioka M, Johnson JS, Regayre LA, Pringle KJ, and Mann GW. Additional population and health data and simulated aerosol data were provided with help from Rigby R and Reddington CL.

Chapter 4 is the publication Butt EW, Rap A, Schmidt A, Scott CE, Pringle KJ, Reddington CL, Richards NAD, Woodhouse MT, Ramirez-Villegas J, Yang H, Vakkari V, Stone EA, Rupakheti M, Praveen PS, Van Zyl PG, Beukes JP, Josipovic M, Mitchell EJS, Sallu SM, Forster PM, Spracklen DV. 2016. The impact of residential combustion emissions on atmospheric aerosol, human health, and climate. Atmospheric Chemistry and Physics. 16(2). The manuscript was written by the candidate with advice from supervisors (Spracklen DV, Sallu SM, and Forster PM), with additional comments from co-authors during its preparation. The set-up and running of the chemistry-transport model, analysis of model simulations, evaluation against observations, and health burden calculations was solely undertaken by the candidate. Additional support for model set-up and health calculations were provided by Schmidt

A, Scott CE, Pringle KJ, Reddington CL, Richards NAD, Woodhouse MT, Ramirez-Villegas J, and Yang H. The set-up and running of the offline radiative transfer model was conducted by Rap A. Aerosol observations and measurements were provided by Vakkari V, Stone EA, Rupakheti M, Praveen PS, Van Zyl PG, Beukes JP, and Josipovic M.

Chapter 5 is the draft manuscript Butt EW, Gordon H, Pearce H, Kilmont Z, Heyes C, McNorton J, Conibear L, Reddington CL, Arnold SR, Spracklen DV. 2018. Near-term global and regional air quality and health benefits in 2050 due to widespread adoption of clean residential combustion technologies. (in prep). The manuscript was written by the candidate with advice from supervisors (Spracklen DV), with additional (on-going) comments from co-authors during its preparation. The set-up and running of the chemistry-transport model, analysis of model simulations, evaluation against observations, and health burden calculations was solely undertaken by the candidate. Additional support for model set-up was provided by Gordon H, McNorton J and Arnold SR. Information regarding the anthropogenic emissions used was provided by Kilmont Z and Heyes C. Additional simulated aerosol data were provided by Reddington CL.

Acknowledgements

I would like to thank my lead supervisor Dominick Spracklen for all his patience, support and advice throughout my PhD years, for which I am very grateful. I would also like to send a big thanks to my other supervisors (Piers Forster, Susie Sallu, and Jonathan Wild) for their additional support and guidance. In addition, I would like to acknowledge funding from the United Bank of Carbon for my PhD studentship.

I would like to thank members of my research group (BAG) and others who have provided support in all number of areas. In particular, I would to thank Steve Turnock for providing me with model simulations, Carly Reddington and Catherine Scott for early technical support, and Hamish Gordon for more recent technical model support. I would also like to thank Luke Conibear for the lengthy discussions on health related impacts, which were very useful. Finally, a big thanks should go to Richard Rigby for his unbelievable IT support throughout the years.

A big thanks to all those in my office 9.157 for sharing the highs and lows of doing a PhD at Leeds. In particular, I would like to thank Stewart Jennings for being Stewart Jennings and Huiyi Yang for teaching me IDL and imparting his wisdom on all manner of things. In addition, I would like to thank Tom Smith for the weekend bike rides, Kate Massarella and Imogen Rattle for the political discussions, and Tom Whale and Anna Hogg for leading me astray.

I would like to send a special thank you to my family, especially my parents for proving all sorts of support and encouragement over the past few years. I would also like to thank my brother for the daily phone calls of ridiculous banter and general mockery - the distraction was welcome. Finally I would like to extend my biggest thank you to my partner Megan for all her love and support over the past few years. Her support and encouragement has been the rock with which I have seen this through, and I cannot thank her enough. I would also like to thank our dog Lulu for making our lives that little bit harder but altogether brighter.

Abstract

Anthropogenic primary aerosol and aerosol precursor emissions have undergone considerable regional changes over the last 50 years. Reduced anthropogenic emissions across high-income regions, in part due to the implementation of air quality and emission control regulations, have coincided with large economic-related emission growth across large parts of the developing world. These emission changes have undoubtedly led to regional changes in ambient $PM_{2.5}$ concentrations and have affected human health. The global composition climate model, HadGEM3-UKCA, was used to simulate and evaluate regional changes in ambient $PM_{2.5}$ concentrations and human health effects over the period 1960 to 2009. Dominated by regional increases across China and India, global simulated population-weighted $PM_{2.5}$ concentrations was estimated to have increased by 37.5% over the period 1960 to 2009, despite declines across North America and Western Europe. As a result, mortality attributable to long-term $PM_{2.5}$ exposure is estimated to have increased by 89% to 124% over the same period, which were driven largely by demographic transitions, and to a lesser extent by regional $PM_{2.5}$ changes. Understanding the historical changes in ambient $PM_{2.5}$ and their associated effects on human health is not only important for evaluating past efforts, but is also vital for crafting future air quality strategies.

The combustion of residential solid-fuels for cooking and space heating contributes a large proportion to the global burden of primary aerosol emissions in the present-day, with potentially large impacts on ambient air quality, health and the climate. Using a global chemistry-transport model (TOMCAT-GLOMAP), present-day emissions from residential combustion activities were estimated to contribute to between 22% to 33% and 12% to 32% of the global annual mean burden of black carbon (BC) and organic aerosol respectively. In addition, residential emissions were estimated to contribute to regional annual mean surface $PM_{2.5}$ concentrations of between 15%

to $>$ 40%, particularly across low and middle income regions, resulting in an estimated preventable human mortality burden of between 315,000 to 516,600 (if emissions were removed). Using an offline radiative transfer model, residential emissions were estimated to exert a global annual mean direct radiative effect (DRE) of between -66 and $+21$ mW m^{-2} and a global first aerosol indirect effect (AIE) of between -52 and -16 mW m^{-2}. Uncertainties in properties of residential combustion aerosol contributed to a wide range of simulated radiative effects, which makes quantifying the magnitude of their radiative effects difficult. Understanding the present-day impacts from this emission source is an important first step in identifying potential benefits of emission control measures, such as the use of clean cookstoves or cleaner fuels.

Understanding to what extent the widespread near-term implementation of clean residential combustion technologies (e.g., clean cookstoves) can avoid ambient air quality and associated health impacts is important for reviewing options for air quality management strategies. Understanding such measures in the context of future changes in other anthropogenic emissions is also important. Using a global chemistry-transport model (TOMCAT-GLOMAP), the widespread use of clean residential combustion technologies was estimated to avoid 4.9 μg m^{-3} of population-weighted $PM_{2.5}$ concentrations in 2050 globally, resulting in 0.34 [0.28-0.4] million avoided mortalities or 20% of the maximum global preventable mortality. It is expected that low-income regions of Sub-Saharan Africa will gain the most, where half to two thirds of the maximum avoidable $PM_{2.5}$ and mortality, can be attributed to residential emission control technologies alone. In these regions, the use of clean residential combustion technologies could provide an effective measure for tackling poor air quality and public health.

Contents

Declaration of Authorship **ii**

Acknowledgements **iv**

Abstract **v**

List of Figures **xvii**

List of Tables **xxi**

List of Abbreviations **xxii**

1 Introduction **1**

1.1 Ambient air pollutants 1

1.1.1 Processes affecting ambient air pollutant concentrations 3

Emission sources 4

Chemical composition 5

Aerosol microphysical processes 6

Meteorology and transport 8

1.2 Ambient air quality and human health 10

1.2.1 The health link 11

1.2.2 Health-based assessment: recent improvements for estimating the global burden of disease attributable to $PM_{2.5}$ 14

1.2.3 The global burden of disease attributable to $PM_{2.5}$ in the present-day 17

1.2.4 Emission source contributions in the present-day to the global burden of disease 18

1.2.5 Ambient air quality standards and guidelines for protecting health and environment 20
1.3 Atmospheric aerosol effects on the Earth's radiation budget 21
1.4 Trends in anthropogenic emissions 24
1.5 Trends in ambient particulate air pollution 29
1.6 Trends in the global burden of disease attributable to $PM_{2.5}$ 32
1.6.1 Options for reducing particulate air pollution 35
1.7 Summary and motivation 36
1.8 Thesis aims and objectives 38

2 Methods **41**
2.1 Chemistry–climate model (CCM) 42
2.2 Chemistry–transport model (CTM) 44
2.3 GLOMAP-mode aerosol model 45
2.3.1 Aerosol primary and gas-phase precursor emissions 46
2.3.2 Aerosol microphysical processes 48
New particle formation 49
Coagulation 50
Condensation 50
Cloud processing 51
Dry deposition 51
Wet deposition 52
2.4 Off-line radiative transfer model 52
2.5 Simulating $PM_{2.5}$ concentrations 54
2.6 Perturbed Parameter Ensemble 56
2.7 Calculating the attributable burden of disease 57
2.7.1 $PM_{2.5}$ exposure distribution 57
2.7.2 Exposure-response relationships 57
2.7.3 Calculating attributable deaths 60
2.7.4 Demographic and disease data 61
2.8 Thesis experiments 63

3 Global and regional trends in particulate air pollution and attributable health burden over the past 50 years 64

4 The impact of residential combustion emissions on atmospheric aerosol, human health, and climate 75

5 Near-term global and regional air quality and health benefits in 2050 due to widespread adoption of clean residential combustion technologies 109

5.1 Introduction . . . 111

5.2 Methods . . . 114

5.2.1 TOMCAT-GLOMAP description . . . 114

5.2.2 Emission scenarios . . . 116

Future emission changes . . . 119

5.2.3 Evaluating simulated $PM_{2.5}$ concentrations . . . 121

5.2.4 Health impact assessment . . . 124

5.3 Results and Discussion . . . 126

5.3.1 Impacts in the future reference scenario . . . 126

5.3.2 Benefits of the clean residential scenario . . . 132

5.3.3 Comparison to previous work . . . 137

5.3.4 Implications for policy . . . 139

5.3.5 Additional uncertainties and sensitivities . . . 142

5.4 Conclusions . . . 146

6 Discussion and Conclusions 149

6.1 Chapter 3: Global and regional trends in particulate air pollution and attributable health burden over the past 50 years . . . 150

6.2 Chapter 4: The impact of residential combustion emissions on atmospheric aerosol, human health, and climate . . . 153

6.3 Chapter 5: Near-term global and regional air quality and health benefits due to widespread adoption of clean residential combustion technologies . . . 157

6.4 Summary and synthesis . . . 161

6.5 Implications for Future Work . . . 165

6.5.1 Priorities relating to my research 165
Reducing model biases 165
Representing uncertainty in future impacts 168
Health impacts 171
6.5.2 Research priorities for the wider community 172
The of value of PPEs in directing research priorities 172
Need for more air quality epidemiology 173

A Appendix A Supplementary material for Chapter 3 **176**

B Appendix B Supplementary material for Chapter 5 **195**

References **219**

List of Figures

1.1 Overview of the emission sources of aerosol and aerosol precursors, the processes that control their distribution in the atmosphere, and their role in the climate system. 'Exposure zone' is meant to describe the Earth's surface when human populations are exposed to air pollutants. 4

1.2 Summary schematic of aerosol size distribution and microphysical processes. 7

1.3 Time-series of dry season MODIS aerosol optical depth (AOD) over the Amazon region. Drought years are shown in red. Figure taken from Reddington et al., 2014. 10

1.4 Potential pathophysiological pathways linking $PM_{2.5}$ exposure to various cardiovascular and respiratory mortality and morbidity. Figure taken from Pope III and Dockery, 2006. Heart: 'increased dysrhythimc suscepibility' is defined as an is an abnormal heart beat; 'Altered cardiac repolarization' is defined as heart rate variability; 'Myocardial ischemia' in defined as reduced blood flow to the heart. Vasculature: 'Atherosclerosis' defined as a disease in which plaque builds up inside arteries; 'Endothelial dysfunction' defined as the inability of the endothelium (membrane that line vessels) to perform tasks properly; 'Vasoconstriction and hypertension' defined as the constriction of blood vessels, which increases blood pressure causing high blood pressure. Lungs: 'COPD' defined as chronic obstructive pulmonary disease. Blood: 'Altered rheology' defined as disruption of blood flow properties; 'Increased coagulability' defined as increased chance of blood clotting; 'Translocated particles' defined as PM particle traversing into the blood stream; 'Peripheral thrombosis' formation of blood clots. Brain: 'Cerebrovascular ischemia' defined as a condition in which there is insufficient blood flow to the brain to meet metabolic demand. 13

1.5 Example of the annual mean $PM_{2.5}$ exposure distribution used by the recent GBD CRA. Circles represent surface measurement locations and magnitude of underlying population while gridded contour data represents modelled concentrations. Gridded modelled data are provided by the Data Integration Model for Air Quality (DIMAQ) (Shaddick et al., 2018). Taken from the interactive map http://maps.who.int/airpollution/. 15

1.6 Summary of direct and indirect effects of atmospheric aerosols on radiation, including new AR5 definitions. Figure taken from Boucher et al., 2013. 22

1.7 Global drivers of climate change as a measure of effective radiative effect (ERF) relative to the pre-industrial year 1750. The measure of the level of confidence in radiative forcing estimates (furthest column on the right) is represented: very high (VH), high (H), medium (M), low (L), and very low (VL). Figure taken from Stocker, 2014 24

1.8 Annual mean top of the atmosphere radiative forcing due to different aerosol components for the 1750-2010 period. Solid boxes are the AR5 estimates, whereas the hatched box and whiskers are estimates from the AeroCom II models. Figure taken from Boucher et al., 2013. 25

1.9 Global anthropogenic emissions by sector used in the Coupled Model Intercomparison Project phase 6 (CMIP6) compared to other estimates (e.g., CMIP5 and CDIAC). Emissions from aviation and open biomass burning are not included. "RCO" refers residential, commercial and other. Figure taken Hoesly et al., 2018. 26

1.10 Global anthropogenic emissions by region used in the Coupled Model Intercomparison Project phase 6 (CMIP6) compared to other estimates (e.g., CMIP5 and CDIAC). Emissions from aviation and open biomass burning are not included. Figure taken Hoesly et al., 2018. 27

1.11 Global annual anthropogenic emissions of CO_2, CH_4 and air pollutants (SO_2, NO_x and BC) from the ECLIPSE emission inventory for the current legislation (CLE), no further controls (NFC) and short-lived climate pollutants (SLCP) mitigation scenario. Also shown for comparison is the range of the RCP emission scenarios (grey shading). Figure taken from Stohl et al., 2015. 28

1.12 Time-series of the European observations of total suspended particulate matter (SPM) and PM_{10} $PM_{2.5}$ (mass particulate matter with an median aerodynamic dry diameter of < 10 μm) from the EMEP network over the period 1978 to 2010. Coloured lines represent individual measurement locations with the solid black lines representing the mean. Figure taken from Turnock et al., 2015. 29

1.13 Time-series of the US observations of PM_{10} (left) and $PM_{2.5}$ (right) for measurement locations across the US. Dark blue line is mean across all locations with the light blue shaded area representing the 5th and 95th percentile range. Data taken from the US Environmental Protection Agency (EPA) https://www.epa.gov/air-trends/. 30

1.14 Time-series of population-weighted $PM_{2.5}$ concentrations in China and India from 1990-2016. Data taken from State of Global Air 2018 https://www.stateofglobalair.org/data/. 31

1.15 Regional annual mean population weighted $PM_{2.5}$ concentrations ($\mu g\ m^{-3}$) (left axis) in 2005 and 2050 under different emission scenarios including 'Reference' or Shared Socio-Economic Pathway (SSP) scenarios (blue color bars) and average of 3 RCP scenarios (grey bar). Green, orange and red colored markers indicate the fraction of the population exposed to <10, <25 and <35 $\mu g\ m^{-3}$ respectively (right axis), and contribution of natural $PM_{2.5}$ is represented by the hatched area. Figure taken from Rao et al., 2017 32

1.16 Total global deaths attributable to ambient $PM_{2.5}$ pollution by year and cause. Figure taken from Cohen et al., 2017. 33

1.17 Changes in attributable deaths from ambient $PM_{2.5}$ exposure due to the changing contribution from population growth, ageing, background disease mortality, and exposure. Figure taken from Cohen et al., 2017 . 34

2.1 Summary of microphysical processes that control atmospheric aerosol size distributions, lifetime and chemical composition. Figure taken from Raes et al., 2000. 49

2.2 Annual mean surface $PM_{2.5}$ concentrations in the present-day from TOMCAT-GLOMAP-mode (coupled chemistry) in year 2015 **a**, TOMCAT-GLOMAP-mode (uncoupled chemistry or prescribed oxidants) in year 2000 **b**, and HadGEM3-UKCA in year 2008 **c**. 55

2.3 Integrated-exposure response relationships used to relate $PM_{2.5}$ exposure to cause-specific diseases endpoints: all-ages lower respiratory infections, lung cancer, chronic obstructive pulmonary disease, and age-specific ischaemic heart disease and cerebrovascular disease (ischaemic stroke and haemorrhagic stroke). Solid lines represent the up-to-date IER version used in Chapter 5, whereas the dotted lines represent the an older IER version used in the Chapter 4. 60

2.4 Gridded population count data for the year 2015 taken from the Gridded Population of the World (GPW) dataset. Spatial resolution is on 15 arc-minute (0.25 degree) grid. 62

5.1 Energy consumption of combustible fuels in the residential sector in 2015 and 2050, split by geographical super region (see Figure A.1 for super region breakdown). Projected energy use estimates for consumption in 2050 are based on IEA forecasts (IEA, 2012) consistent with 2050 ECLIPSE reference (i.e., CLE) and MTFR scenarios. 117

5.2 Anthropogenic air pollutant emissions (million tonnes (Mt) for individual scenarios split by broad geographical super region as identified in Figure A.1, including international shipping. Air pollutants include, BC (black carbon), OC (organic carbon), SO_2 (sulfur dioxide), NO_x (nitrogen oxides), CO (carbon monoxide), and VOCs (volatile organic compounds). Total residential sector emissions for each scenario are also included and represented by the smaller bar to the right. 120

5.3 Comparison of simulated (scaled) $PM_{2.5}$ concentrations with measurements collected across multiple locations and regions. **a** 2015 TOMCAT simulated surface annual mean $PM_{2.5}$ concentrations (background) compared to measurements (filled circles). **b** Comparison of $PM_{2.5}$ concentrations, best fit line (red line), 1:1 (solid black line), 2:1 and 1:2 (dashed black lines). Best fit line has slope = 0.32 and Pearson's correlation coefficient (r) = 0.87. **c** Normalised mean bias factor (NMBF) box and whisker by sub-region, showing the minimum, maximum and median distribution values, as well as the 10^{th}, 25^{th}, 75^{th}, and 90^{th} percentiles. 123

5.4 Absolute (left) and percentage (right) change in annual mean surface $PM_{2.5}$ concentrations in the 2050 reference scenario, relative to the present-day 2015. 126

5.5 Annual mean population-weighted $PM_{2.5}$ concentrations in 2015 and the 2050 reference scenario per sub region (bars). Horizontal lines in bars represent the absolute population-weighted $PM_{2.5}$ concentrations due to residential combustion emissions (left axis). Also shown is the fraction or relative contribution of residential emissions to population-weighted $PM_{2.5}$ concentrations, and fraction of the population in each region exposed to $PM_{2.5}$ concentration levels above the WHO annual mean standards including the air quality guideline (AQG) (10 μg m^{-3}) and interim target 1 (IT-1) (35 μg m^{-3}) (right axis). 128

5.6 Mortality attributable (millions) to long-term ambient $PM_{2.5}$ exposure in 2015 and 2050 reference per sub region (bars). Horizontal lines in bars represent mortality attributable to residential emissions (attribution method), while small circles in bars represent averted mortality due to the removal of residential emissions (subtraction method) (see Section A.4). Note that the left axis is used for global, East Asia and South Asia, while the right axis is for all other regions. 129

5.7 Attributable mortality rates (deaths per 10^5) due to long-term ambient $PM_{2.5}$ exposure in 2015 and 2050. Bars show per capita (e.g., crude) mortality rates while squares show age-standardised mortality rates. Horizontal lines in bars represent mortality attributable to residential emissions (attribution method), while small circles in bars represent averted mortality due to the removal residential emissions (subtraction method) (see Section A.4). 130

5.8 Absolute (left) and percentage (right) change in annual mean surface $PM_{2.5}$ concentrations in 2050 under the clean residential scenario relative to the 2050 reference scenario. 132

5.9 Avoided population-weighted $PM_{2.5}$ concentrations in 2050 due to the clean residential scenario and maximum feasible reduction (MTFR) scenario (bars, left axis), and change (reduction) in population-weighted $PM_{2.5}$ concentrations in 2050 due to both scenarios, relative to the reference scenario (right axis) **a**. Also shown is the maximum avoidable population-weighted $PM_{2.5}$ concentration potential due to the clean residential scenario (i.e., clean residential avoided / MTFR avoided) (**a** (left axis) and **b**). 134

5.10 Avoided attributable mortality in 2050 due to clean residential scenario maximum feasible reduction (MTFR) scenario (bars, left and right axis), and change (reduction) in attributable mortality in 2050 due to both scenarios, relative to the reference scenario (left axis) **a**. Also shown is the maximum avoidable mortality potential due to the clean residential scenario (i.e., clean residential avoided / MTFR avoided) (**a** (left axis) and **b**). 135

List of Tables

1.1 Summary of common aerosol primary and precursor air pollutants and gas-phase air pollutants, their sources, and formation pathways. . 3

1.2 Global emission flux estimates and broad size category for atmospheric aerosols classes. Figure adapted from Seinfeld and Pandis, 2012. 5

1.3 Summary of key aerosol microphysical processes. 8

1.4 Overview of the adverse health effects of various air pollutant exposures. Disease acronyms can be found on the list of abbreviations at the front of this thesis. 14

1.5 Global burden of disease estimates due to air pollution and their global risk factor rank as of GBD CRA 2016. Data taken from GBD compare tool (https://vizhub.healthdata.org/gbd-compare/). Death and DALYs are reported in millions. Deaths for GBD CRA 2008 are also included (far right). 18

1.6 Present-day emission source contribution [%] of total attributable mortality due to long-term exposure to $PM_{2.5}$. Source contributions to ambient $PM_{2.5}$ include, Res = Residential, Agr = Agriculture, Pow = Power generation, Ind = Industry, Bio = open biomass burning, and Tra = land transport. Bold values indicate the largest health contribution [%] due to an emission source. Data taken from Lelieveld et al., 2015. 20

1.7 World Health Organization (WHO) air quality guidelines and interim targets for annual mean ambient $PM_{2.5}$ concentration levels. 21

2.1 Summary of key differences among the models configurations used in this thesis. TOMCAT-GLOMAP in Chapter 4 refers to the prescribed oxidant configuration, while TOMCAT-GLOMAP in Chapter 5 refers to the coupled chemistry configuration. 43

2.2 Reactions of gas-phase chemistry used in GLOMAP-mode with oxidants provide by either HadGEM3-UKCA or TOMCAT (Table 2.1), adapted from (Mann et al., 2010). Reactions for sulfur species include: dimethyl sulphide (DMS,DMSO), sulfur dioxide (SO_2), sulphuric acid (H_2SO_4), methane sulphonic acid (MSA), carbonyl sulphide (COS) and carbonyl sulphide (CS_2), and semi-prognostic hydrogen peroxide (H_2O_2). Formation of sulfate (SO_4^{2-}) aerosol, includes gas-phase reactions by the hydroxyl radical (OH), as well as aqueous-phase formation through the oxidation of sulphur species (S(IV) to S(VI)) by H_2O_2 and ozone O_3 dissolved in cloud drops present in low-level clouds. In addition, secondary organic aerosol formation includes reactions of biogenic monoterpene to form low volatility oxidation products. Here, monoterpene are oxidised at a 13% yield following reaction rates for α–pinene. [(a)] Atkinson et al., 1992, [(b)] Pham et al., 1995, and [(c)] Jones et al., 2001. 45

2.3 Key differences in natural aerosol primary and gas-phase precursor emissions used in the different thesis chapters and models. TOMCAT-GLOMAP in Chapter 4 referrers to the prescribed oxidant configuration, while TOMCAT-GLOMAP in Chapter 5 refers to the coupled chemistry configuration. 47

2.4 Key differences in anthropogenic aerosol primary and gas-phase precursor emissions used in the different thesis chapters and models. TOMCAT-GLOMAP in Chapter 4 refers to the prescribed oxidant configuration, while TOMCAT-GLOMAP in Chapter 5 refers to the coupled chemistry configuration. 47

2.5 Summary of GLOMAP-mode set up. Dp (dry diameter); SU (sulfate), POM (particulate organic matter), BC (black carbon), SS (sea salt), DU (mineral dust). Sigma reflects geometric standard deviation of mode. TOMCAT-GLOMAP in Chapter 4 refers to the prescribed oxidant configuration, while TOMCAT-GLOMAP in Chapter 5 refers to the coupled chemistry configuration. 48

2.6 Summary of the key difference between the model configurations that likely contribute to differences in simulated surface $PM_{2.5}$ concentrations reported in Figure 2.2. TOMCAT-GLOMAP in Chapter 4 refers to the prescribed oxidant configuration, while TOMCAT-GLOMAP in Chapter 5 refers to the coupled chemistry configuration. 56

2.7 Summary of exposure-response relationships used in each thesis Chapter and model configuration. 'IER' represents integrated exposure-response and the subscript indicates different versions used. TOMCAT-GLOMAP in Chapter 4 refers to the prescribed oxidant configuration, while TOMCAT-GLOMAP in Chapter 5 refers to the coupled chemistry configuration. 58

2.8 Summary of the differences in the demographic and background disease data used in each thesis Chapter. 'GPW' represents Gridded population of the World dataset, 'IHME' represents Institute Health Metrics and Evaluation data, 'UN' United Nations, and 'IFs' represents the International Futures socio-economic modelling system. TOMCAT-GLOMAP in Chapter 4 refers to the prescribed oxidant configuration, while TOMCAT-GLOMAP in Chapter 5 refers to the coupled chemistry configuration. 61

2.9 Summary of the different experiments presented in this thesis. 63

5.1 Air quality emission scenarios used. All scenarios include natural emissions consistent with present-day meteorology. 116

5.2 Residential control technology options used in the clean residential scenario. Control options are based on laboratory and field emission factors using best available control technologies. Table data adapted from Klimont et al., 2017. 119

List of Abbreviations

ACCMIP - The **A**tmospheric **C**hemistry and **C**limate **M**odel **I**ntercomparison **P**roject

AeroCom - **Aerosol** modelling inter**Com**parison project

AIE - **A**erosol **I**ndirect **E**ffect

AOD - **A**erosol **O**ptical **D**epth

AQG - **A**ir **Q**uality **G**uideline

AR5 - **5**th **A**ssessment **R**eport of the IPPCC

BC - **B**lack **c**arbon

CCM - **C**limate **C**omposition **M**odel

CCN - **C**loud **C**ondensation **N**uclei

CDNC -**C**loud **D**rop **N**umber **C**oncentration

CLE - **C**urrent **Le**gislation

COPD - **C**hronic **O**bstructive **P**ulmonary **D**isease

CRA - **C**omparative **R**isk **A**ssessment of the GBD

CRF - **C**oncentration **R**esponse **F**unction

CTM - **C**hemistry **T**ransport **M**odel

DALYs - **D**isability **A**djusted **L**ife **Y**ears

DIMAQ - **Data I**ntegration **M**odel for **A**ir **Q**uality

DRE - **D**irect **R**adiative **E**ffect

ECLIPSE - Evaluating the Climate and Air Quality Impacts of Short-Lived Pollutants

ECMWF - **E**uropean **C**entre for **M**edium-Range **W**eather **F**orecasts

EMEP - **E**uropean **M**onitoring and **E**valuation **P**rogramme

GBD - **G**lobal **B**urden of **D**isease

GLOMAP - **GLO**bal **M**odel of **A**erosol **P**rocesses

HAP - **H**ousehold **A**ir **P**ollution

IER - **I**ntegrated **E**xposure **R**esponse

IHD - **I**schemic **H**eart **D**isease

IMPROVE - **I**ntegrated **M**onitoring of **PRO**tected **V**isual **E**nvironment

LRI - **L**ower **R**espiratory **I**nfection

MACCity - MACC and CityZEN project

MTFR - **M**aximum **T**echnology **F**easible **R**eduction

NMBF - **N**ormalised **M**ean **B**ias **F**actor

PAF - **P**opulation **A**ttribution **F**raction

PAH - **P**olycyclic **A**romatic **H**ydrocarbon **$PM_{2.5}$** - **P**articulate **m**atter with a diameter less **2.5** micrometres

PM_{10} - **P**articulate **m**atter with a diameter less **10** micrometres

POM - **P**articulate **O**rganic **M**atter

PPE - **P**erturbed **P**arameter **E**nsemble

RCP - **R**epresentative **C**oncentration **P**athway

RR - **R**elative **R**isk

RSF - **R**esidential **S**olid **F**uel

SOA - **S**econdary **O**rganic **A**erosol

TMREL - **T**heoretical **M**inimum **R**isk **E**xposure **L**evel

UKCA - **U**nited **K**ingdom **C**hemistry and **A**erosol programme

VOC - **V**olatile **O**rganic **C**ompounds

WHO - **W**orld **H**ealth **O**rganisation

Chapter 1

Introduction

Air pollution in the form of atmospheric aerosols vary both spatially and temporally in terms of their size, concentrations, and chemical composition, all of which are determined by their emission sources, meteorological conditions (e.g., precipitation, transport processes), and aerosol microphysical processes (e.g., removal processes, secondary formation). Given their short residence time and complex life cycle in the atmosphere, modelling atmospheric aerosol and their effects is challenging. Long-term exposure to aerosol fine particulate matter ($PM_{2.5}$) is a leading present-day global risk factor to the global burden of disease, contributing to 4.1 million deaths annually. Atmospheric aerosols also affect the climate directly and indirectly via modification of the Earth's radiative balance. The large regional changes in anthropogenic pollutant emissions over the last 50 years has undoubtedly changed aerosol concentrations and their effects on air quality and public health, with future impacts likely also related to future changes in anthropogenic emissions. This thesis examines the impact of atmospheric aerosol on air quality, human health and climate, over different time periods, with specific focusses on key polluting sources.

1.1 Ambient air pollutants

Air pollution is defined as the accumulation of air pollutants in the lower troposphere in sufficient concentrations to impair visibility, damage ecosystems, and have

adverse effects on human health (Seinfeld and Pandis, 2012). Air pollution, typically measured in terms of air quality, is a complex mixture of aerosol particles or particulate matter (PM), aerosol precursor-gases, and gas-phase species that vary temporally and spatially. Air pollutants such as aerosols can also affect the climate directly by scattering and absorbing solar and terrestrial radiation, and indirectly via the interaction with clouds and chemistry of greenhouse gases.

Table 1.1 describes some of the most common air pollutants, their sources and formation pathways. The chemical and physical properties of air pollutants are a result of their different emission sources and the chemical reactions that transform them as they are transported, mixed and removed from the atmosphere. Air pollutants can either be emitted directly (primary) or formed via chemical reactions (secondary).

Primary air pollutants are typically associated with anthropogenic combustion activities such as the emission of black carbon (BC) and particulate organic matter (POM) aerosol from diesel vehicles or combustion of biomass in small-scale residential or household cooking and heating stoves. Anthropogenic primary pollutants can also include gas-phase species such as sulphur dioxide (SO_2) and nitrogen oxides (NO_x) generated by the combustion of fossil-fuels from power stations and motor vehicles.

Secondary pollutants include the formation of sulphate aerosol (SO_4^{2-}) via gas-phase and aqueous-phase oxidation of SO_2 within the atmosphere. Tropospheric ozone (O_3), a major constituent of photochemical smog, can also be formed when precursor-gases, NO_x, carbon monoxide (CO) and volatile organic compounds (VOCs) react in the presence of sunlight. Vehicle, industrial and chemical solvent emissions are all important anthropogenic sources for tropospheric O_3 precursor-gases.

Natural sources can also contribute to the burden of air pollutants in the atmosphere. Examples of natural sources include sulphate precursor SO_2 emissions from volcanic and biogenic sources, windblown mineral dust, and secondary organic aerosol formation from biogenic VOCs emitted from vegetation.

Under certain atmospheric conditions, pollutants such as $PM_{2.5}$ (mass of aerosol with an median aerodynamic dry diameter of < 2.5 μm) and tropospheric O_3 can

accumulate in high enough concentrations to degrade air quality and pose a risk to human health. In addition, atmospheric stability and circulation can determine the transport distances of pollutants but also the height at which aerosols can be lofted influencing their interaction with radiation and clouds. The transport of air pollutants over large distances also highlights air pollution as a transboundary issue that does not respect national borders.

Pollutant	Gas-phase	Particulate-phase	Formation	Sources
PM_1, $PM_{2.5}$, PM_{10}	-	Yes; mass of particles < aerodynamic dry diameter of 2.5 μm	Dependent on emissions, meteorology, transport and microphysical processes	Mixture dependent on components included
Black Carbon (BC)	-	Yes	Primary	Incomplete combustion of fossil fuel and biomass
Particulate Organic Matter (POM)	-	Yes	Primary emission from combustion sources, pollen spores and algae. Also secondary from gas-to-particle conversion of biogenic, combustion solvent VOCs	Biomass and fossil fuel combustion, natural biogenic sources, industrial solvents
Sulphate (SO_4^{2-}) or ammonium sulphate ($(NH_4)_2SO_4$) after reaction of H_2SO_4 with NH_3	-	Yes	Secondary from gas-phase oxidation products of SO_2, Dimethyl sulfide (DMS), H_2S. Also aqueous-phase in-cloud secondary formation after reaction of SO_2 with H_2O_2 and O_3	SO_2 from fossil fuel and biomass combustion, volcanic activity, DMS emissions from marine phytoplankton
Nitrate (NO_3^-) or ammonium nitrate (NH_4NO_3) after reaction of HNO_3 with NH_3	-	Yes	Secondary formed from reactions of Nitric acid (HNO_3) and NO_x	NO_x from high temperature combustion of fossil fuel and biomass, electrical storms and anaerobic processes in soils
Sea salt (NaCl)	-	Yes	Primary emission from ocean surface	Bursting of air bubble during white cap formation or tearing of drops from wave tops
Mineral Dust	-	Yes	Primary emissions	Wind attrition on bare soil. Anthropogenic construction and agricultural activities
Sulphur Dioxide (SO_2)	Yes	-	Primary. Also secondary from DMS oxidation	Primarily from anthropogenic combustion sources such as coal. DMS emissions produced naturally from marine phytoplankton
Nitric Oxide (NO)	Yes	-	Primary	Emitted by natural sources (e.g., forest fires, anaerobic processes in soils and electrical storms) and high temperature anthropogenic combustion of fossil fuels
Nitrogen Dioxide (NO_2)	Yes	-	Primary. Also secondary from NO oxidation	High temperature combustion. See sources of NO above
Carbon Monoxide (CO)	Yes	-	Primary. Also secondary from Methane (CH_4) and VOC oxidation	CH_4 and VOC emissions from biosphere and natural forest fires, as well as and anthropogenic combustion and agriculture. Primary emissions primarily from incomplete combustion sources
Volatile Organic Compounds (VOCs)	Yes	-	VOCs denote a numerous set of gas-phase atmospheric organic compounds, typically with high vapour pressures	Anthropogenic and naturally occurring compounds
Tropospheric ozone (O_3)	Yes	-	Secondary $NO \rightarrow NO_2$ conversion	Natural and anthropogenic induced $NO \rightarrow NO_2$ conversion

TABLE 1.1: Summary of common aerosol primary and precursor air pollutants and gas-phase air pollutants, their sources, and formation pathways.

1.1.1 Processes affecting ambient air pollutant concentrations

This thesis focuses on the effect of atmospheric aerosols because of their adverse effect on human burden of disease (Section 1.2) and climate through interaction with

radiation and clouds (Section 1.3). The spatial and temporal distribution of atmospheric aerosol concentrations depends on the interaction of processes highlighted in Figure 1.1. These processes include emission sources, microphysical processes, meteorology and transport. The interaction of these processes can mean that changes in the anthropogenic emissions can produce non-linear responses which in turn may affect air quality, human health and climate.

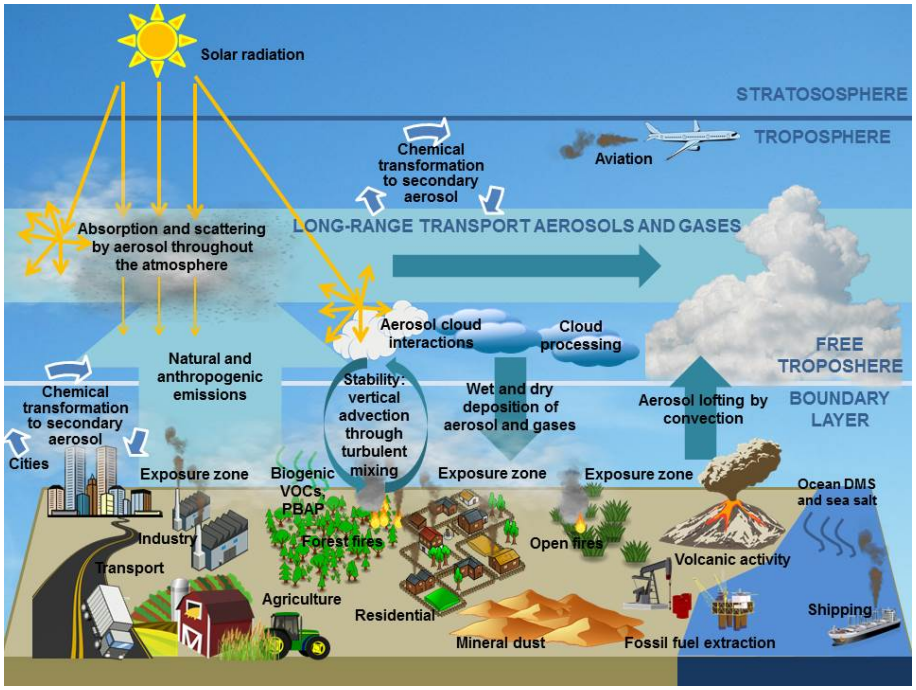

FIGURE 1.1: Overview of the emission sources of aerosol and aerosol precursors, the processes that control their distribution in the atmosphere, and their role in the climate system. 'Exposure zone' is meant to describe the Earth's surface when human populations are exposed to air pollutants.

Emission sources

Figure 1.1 and Table 1.2 shows that atmospheric aerosols are diverse in terms of their emission sources, size, composition and formation pathways. Primary aerosols are emitted directly into the atmosphere (e.g., BC and windblown mineral dust) whereas secondary aerosols are formed via gas-to-particle chemical reactions (e.g., sulfate production from dry and aqueous-phase oxidation of sulfur species).

Primary aerosols from natural sources (e.g., mineral dust and sea salt) largely dominate the global emission mass flux of atmospheric aerosol. However, these particles

Source	Estimate Flux (Tg/yr)	Particle Size Category
Natural primary		
mineral dust	1000-3000	Mainly coarse
Sea salt	1000-10000	Mainly coarse
Volcanic dust	2-10000	Coarse
Biological particles	26-80	Coarse
Natural secondary		
Biogenic sulfate (e.g., from DMS)	80-150	Fine
Sulfate from volcanic SO_2	5-60	Fine
Organic aerosol from biogenic VOCs	40-200	Fine
Nitrate from NO_x (e.g., soil, oceanic)	15-50	Fine and Coarse
Total Natural	2200-23500	
Anthropogenic primary		
Industrial dust (excluding black carbon)	40-130	Fine and coarse
Black carbon	5-20	Mainly fine
Organic aerosol		
Anthropogenic secondary		
Sulfate from SO_2	170-250	Mainly fine
Nitrate from NO_x	25-65	Mainly coarse
Organic aerosol from VOCs	5-25	fine
Total anthropogenic	300-650	
Total	2500-24000	

TABLE 1.2: Global emission flux estimates and broad size category for atmospheric aerosols classes. Figure adapted from Seinfeld and Pandis, 2012.

tend to be emitted at coarse size ranges and thus exist in the atmosphere with relatively short residence times (lifetime). In contrast, while anthropogenic emission sources have a smaller mass flux, they tend to be made up of particles in the accumulation size range. These particle sizes are not only more important for human health effects, due to their smaller sizes and general proximity to human populations, but are also important for climate interactions as they have longer residence times in the atmosphere.

Whilst anthropogenic aerosol and precursor emissions have changed significantly over the industrial period (Section 1.4), especially during the last 50 years, the contribution from natural sources is thought to have been relative constant in comparison. However despite this, spatial and temporal changes to atmospheric aerosol concentrations cannot be inferred from changes in anthropogenic emissions alone. In such cases, it is important to consider the impact of anthropogenic emission sources on aerosol properties and processes.

Chemical composition

Atmospheric aerosol particles contain a mixture of components with different chemical compositions. These include inorganic secondary sulfate, ammonium and nitrate, secondary organics, and primary and secondary carbonaceous material, mineral dust and sea salt (Table 1.1). The chemical composition of atmospheric aerosol

are important for removal efficient from the atmosphere, particularly wet deposition (see below), as well as determining their interaction with radiation and clouds (Section 1.3) (Seinfeld and Pandis, 2012). Aerosol mixing state is also important for radiation and cloud interactions (Jacobson, 2001; Bond et al., 2013; Cappa et al., 2012), with the extent of mixing determined by proximity of emission sources and atmospheric ageing. Changes in aerosol precursor emissions can change the composition and ageing rate of aerosol particles thus influence their mixing state. For human health impacts, while aerosol composition is thought to be very important (Thurston et al., 2016; Tuomisto et al., 2008), lack of epidemiological evidence currently limit composition effects for health-based assessments (Section 1.2).

Changes in anthropogenic emissions can not only change the magnitude and location of primary emission particles, which can for example, influence new particle formation, but can also change the abundance of precursor gases and influence levels of atmospheric oxidants. For example, declines in anthropogenic emissions across North America and Europe (Section 1.4) together with increases in Asia over the last few decades have shifted the oxidation efficiency of the atmosphere in the same direction, which can influence the spatial efficiency of secondary aerosol formation such as sulfate (Manktelow et al., 2007).

Aerosol microphysical processes

The size distribution of atmospheric aerosols is important for determining how they interact with radiation, clouds and human health. Figure 1.2 shows a typical aerosol size distribution as a function of microphysical processes not shown in Figure 1.1. Based on particle diameter (Dp), the aerosol size distribution is commonly split into 4 mode: nucleation (dry diameter (Dp) <10 nm), Aitken (Dp 10–100 nm), accumulation (Dp 100 nm to 1 μm) and coarse (Dp >1 μm). Greater particle number concentrations can be found in the nucleation and Aitken modes, which are dominated by secondary aerosols such as sulfate and organics due to new particle formation and condensation. In contrast, greater volume and mass concentrations are found in the coarse mode, where primary natural particles such as windblown mineral dust

and primary biological particles (e.g., spores and pollen) dominate. Aerosol particles of intermediate sizes, such as in the accumulation mode, typically have longer lifetimes due to less efficient removal rates (see below), tend to be more important for radiation (Section 1.3) and human health (Section 1.2) interactions.

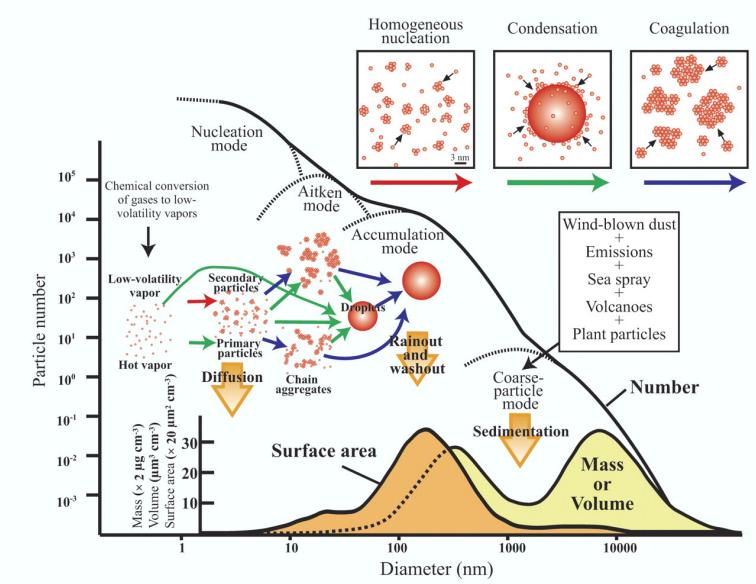

FIGURE 1.2: Summary schematic of aerosol size distribution and microphysical processes.

The overall shape of the size distribution, composition and lifetime of atmospheric aerosols is governed by the microphysical processes also summarised in Table 1.3. Changes in aerosol primary and precursor emissions can lead to changes in microphysical processes and subsequently to changes in aerosol composition and size distribution. For example, changes in anthropogenic primary aerosol and precursor emissions can affect the magnitude and location of new particle formation events by increasing/decreasing the condensational sink due to primary particles and/or increasing/decreasing low volatility vapours available for nucleation (Spracklen et al., 2010; Forouzanfar et al., 2015). Such changes have the ability to affect climate through, for example, changes in the ability of aerosols to interact with clouds (Section 1.3). Additionally, increases in anthropogenic primary aerosol emissions will lead to a greater abundance of fine particles which may ultimately impact on human health.

The main sink for atmospheric aerosol is wet deposition via in-cloud nucleation scavenging (i.e. the rain-out of aerosol after the formation of a water droplet around

Process	Description	Example
New particle formation	Homogeneous nucleation of low volatility vapours to form new clusters that can growth through coagulation and condensation.	Low volatility products from VOC oxidation to form SOA
Condensation	Heterogeneous nucleation of vapours on pre-existing particles to increase mass but conserving number	VOC and H_2SO_4 vapour
Coagulation	Collision and coalescence of particles due to random motions to form larger particles resulting in less numerous particle numbers	Collision and coalescence of pre-existing particles
Activation	Activation and growth of aerosol particles as water droplets	Soluble particles of a certain size and supersaturation

TABLE 1.3: Summary of key aerosol microphysical processes.

an activated aerosol particle) and below-cloud impaction scavenging (i.e. washout of aerosol particles by falling rain drops). Both wet removal mechanisms are strongly dependant on aerosol particle size and composition. Dry deposition is also an important removal mechanism, which is similarly dependant on particle size, as well as the underlying land surface type. Dry deposition tends to be more efficient at remove larger sized particles through gravitational settling and small particles through Brownian diffusion to the Earth's surface. As a result, dry deposition is less efficient for particles in intermediate size ranges (i.e. 100 nm to 1 μm in diameter) resulting in the accumulation of accumulation mode size particles, which can remain the in atmosphere from a number of days to weeks, but also can be removed via wet deposition given the right soluble properties and size (Seinfeld and Pandis, 2012). Similarly to changes in emissions, removal processes are an important mechanism for aerosol burdens and lifetimes. However, the representation of removal processes in chemistry-composition models are highly uncertain, leading to the one of the largest sources of uncertainty for simulated aerosol (Lee et al., 2013).

Meteorology and transport

The atmospheric boundary layer (BL) is defined as the lowest part of the atmosphere and is continuously interacting with the Earth's surface due to friction, heating and cooling. BL processes play a critical role in determining the magnitude and location of atmospheric aerosol concentrations since most primary and secondary aerosol are emitted and formed in the BL, respectively (Figure 1.1). These processes together with meteorology and atmospheric circulation are thus important for human exposures such that under stagnant conditions of high pressure, low wind-speed and dispersion and precipitation, high concentrations of aerosol number and mass

are able to accumulate (e.g. Whiteaker, Suess, and Prather, 2002; Tai, Mickley, and Jacob, 2010).

BL stability determines the vertical mixing and lofting of aerosol from their sources at the surface, controlling the height of aerosol layers, which in turn will affect the ability and magnitude of aerosol radiation and cloud interactions. Processes such as turbulent mixing and convection are able to transport aerosol particles to higher altitudes (Figure 1.1). Convective transport is thought to be very important for controlling the vertical profile of aerosol components by mass, whilst BL stability mixing plays a more dominant role for sea-salt and mineral dust particles (Kipling et al., 2016).

The lateral distribution of atmospheric aerosol are largely determined by the atmospheric circulation though wind regimes. Depending on the injection height of emissions (e.g., from the surface or smoke stack) and vertical mixing related to LB stability, aerosol and aerosol precursor emissions can be transported over large distances before they are removed from the atmosphere by wet or dry deposition. This long-range transport (Figure 1.1) can contribute and degrade air quality hundreds to thousands of kilometres away downwind. For example, Vieno et al., 2016 found that high aerosol loading events observed in recent years over the United Kingdom (UK) originated largely from continental European outflow, with agricultural emissions of ammonia playing an important contribution. Similarly, wildfires across Southern Sumatra were found to contribute the greatest proportion (42-62%) of enhanced aerosol concentrations in Singapore in recent years (Reddington et al., 2014). Large-scales weather systems typically control the transport of atmospheric aerosol to remote continents and regions. Desert mineral dust and aerosol from open biomass burning (wildfires) are important aerosol components and can to travel across oceans to remote continents, which is of particularly important for transport to the Arctic region due to their particle absorbing abilities acting to enhance Arctic warming.

Meteorology and atmospheric circulation can determine the surface flux of natural aerosol and precursor emissions such as windblown mineral dust (Todd et al.,

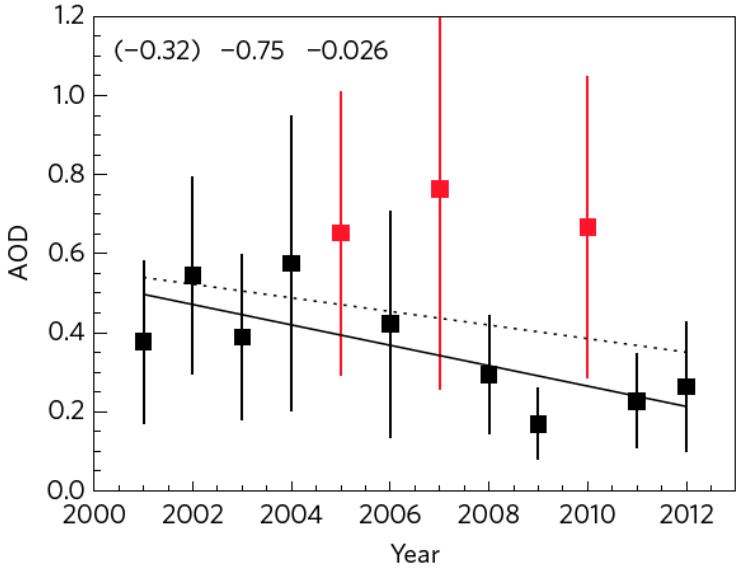

FIGURE 1.3: Time-series of dry season MODIS aerosol optical depth (AOD) over the Amazon region. Drought years are shown in red. Figure taken from Reddington et al., 2014.

2013; Dentener et al., 2006; Woodward, 2001), wind-speed dependant sea salt (Gong, 2003; Mårtensson et al., 2003; Monahan, Spiel, and Davidson, 1986), temperature dependant biogenic VOCs, and the frequency of wildfire episodes (Brown, Hall, and Westerling, 2004; Moriondo et al., 2006; Westerling and Bryant, 2008). Specific meteorological conditions such as droughts can reduced wet deposition leading to the accumulation of high aerosol concentrations. In some regions, such as the over the Amazon, drought conditions can also result in lowering of soil moisture creating the ideal conditions for enhanced wilfire emissions leading to a positive feedback on aerosol concentrations with effects on air quality and human health (e.g. Reddington et al., 2015; Smith et al., 2014b) (Figure 1.3). It is uncertain however, how climate change will affect both the flux of natural emissions and meteorological effects on aerosol concentrations in the future.

1.2 Ambient air quality and human health

This thesis focuses on the human burden of disease associated with atmospheric aerosols in the form of particulate matter (PM) exposure. This focus on PM is based on years of epidemiological evidence regarding their adverse impacts on human

health. The following section describes the evidence base for PM impacts on health, with the rest of the section providing an overview on the current assessment used estimate the global disease burden due PM exposure.

1.2.1 The health link

By the 1970s and 1980s, the link between respiratory and cardiovascular morbidity and mortality outcomes due to extreme episodes of PM air pollution was generally accepted (Pope III and Dockery, 2006). By the mid-1990s, however, the health evidence associated with low-to-moderate PM exposure was mounting. Epidemiological time-series studies conducted in North America cities were consistently linking short-term daily changes in PM to daily counts of all-cause, cause-specific mortality and/or hospital admissions using various regression techniques, while prospective cohort studies (e.g., that controlled for individual confounder risk factors, including smoking, age, sex, income, education etc.) were finding strong associations between long-term PM exposure and respiratory and cardiovascular mortality (Dockery et al., 1993; Pope, Dockery, and Schwartz, 1995; Pope et al., 1995). The health risks from short-term exposure, while consistent across studies and regions (Atkinson et al., 2014; Pope III and Dockery, 2006), were found to be small compared to long-term risks, suggesting they captured only a small fraction of the overall cumulative health effect of long-term cumulative exposure to PM (Beverland et al., 2012; Pope III, 2007; Pope III and Dockery, 2006). The body of evidence from long-term prospective cohort studies have also been bolstered in recent by reanalysis of earlier North American data (Krewski et al., 2009; Krewski et al., 2000; Laden et al., 2006), with similar health associations being found across cohort studies conducted in other high-income regions such as in Western Europe (Burnett et al., 2014; Cohen et al., 2017).

The evidence from prospective cohort studies also suggested stronger respiratory and cardiovascular disease associations from exposure to fine PM (PM with a median aerodynamic dry diameter of < 2.5 μm, $PM_{2.5}$), thus supporting physiological and toxicological considerations that $PM_{2.5}$ exposure adversely affects human

health. For example, $PM_{2.5}$ particles are small enough to reach the smallest airways and alveoli of the lungs, while the ultrafine size fraction of $PM_{2.5}$, PM_1, may penetrate the blood-air barrier (alveolar-capillary membrane), eventually leading to the cardiovascular system. In addition, $PM_{2.5}$ particles can more readily penetrate indoor environments, be transported over greater distances, and can remain suspended for longer time periods. $PM_{2.5}$ particles may be more toxic because they include multiple inorganic and organic particles, metals, and absorption of various chemicals species on particle surfaces such as PAHs.

Figure 1.4 shows some of the potential pathophysiological pathways linking $PM_{2.5}$ exposure to various cardiovascular and respiratory mortality and morbidity. Epidemiological, biomedical and clinical evidence suggests that long-term exposure to $PM_{2.5}$ is responsible for chronic cardiovascular outcomes directly through toxicity effects or indirectly by inducing systemic inflammation and oxidative stress (e.g., Du et al., 2016). Long-term exposure to $PM_{2.5}$ also affects the respiratory system through irritation and corroding of the alveolar wall, leading to inflammation and impaired lung function, as well as promoting lung cancer (e.g., Xing et al., 2016).

There is a growing body of research that has observed how health effects relate to the body's response to the complex mixture, composition and multiple sources of air pollution (West et al., 2016). For example, of the very few studies that have been conducted, evidence has emerged of stronger cardiovascular effects associated with $PM_{2.5}$ components originating from fossil-fuel combustion (coal and diesel combustion) compared to mineral dust and biomass burning sources (Thurston et al., 2016). However, at present, there is not enough evidence to draw conclusive associations between the biological effects of individual $PM_{2.5}$ components and emission sources at the population level. The result of this is that current risk associations used for health-based assessments, such as the methods used in this thesis (see Methods Chapter), consider all $PM_{2.5}$ mass as equally toxic regardless of composition and source (Burnett et al., 2014).

While the health risk evidence for $PM_{2.5}$ exposure is compelling, adverse health effects are associated with other air pollutants. Table 1.4 reports a range of different

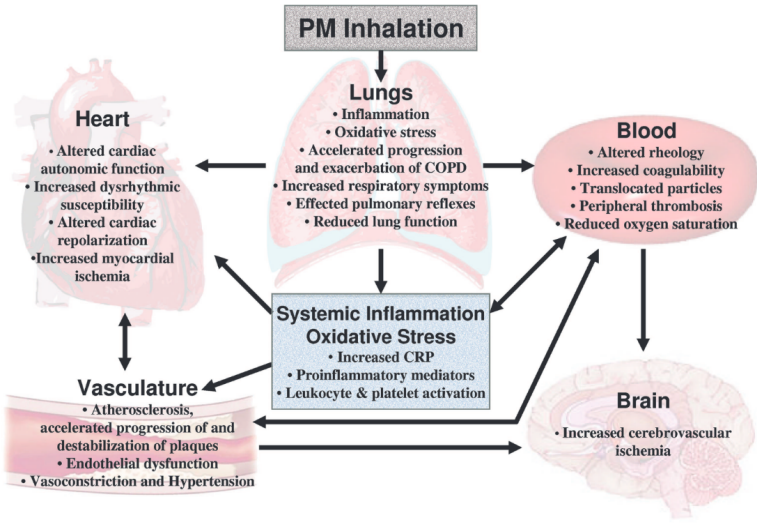

FIGURE 1.4: Potential pathophysiological pathways linking $PM_{2.5}$ exposure to various cardiovascular and respiratory mortality and morbidity. Figure taken from Pope III and Dockery, 2006. Heart: 'increased dysrhythimc suscepibility' is defined as an is an abnormal heart beat; 'Altered cardiac repolarization' is defined as heart rate variability; 'Myocardial ischemia' in defined as reduced blood flow to the heart. Vasculature: 'Atherosclerosis' defined as a disease in which plaque builds up inside arteries; 'Endothelial dysfunction' defined as the inability of the endothelium (membrane that line vessels) to perform tasks properly; 'Vasoconstriction and hypertension' defined as the constriction of blood vessels, which increases blood pressure causing high blood pressure. Lungs: 'COPD' defined as chronic obstructive pulmonary disease. Blood: 'Altered rheology' defined as disruption of blood flow properties; 'Increased coagulability' defined as increased chance of blood clotting; 'Translocated particles' defined as PM particle traversing into the blood stream; 'Peripheral thrombosis' formation of blood clots. Brain: 'Cerebrovascular ischemia' defined as a condition in which there is insufficient blood flow to the brain to meet metabolic demand.

air pollutants and their effects on health outcomes. Unlike other air pollutants, there is enough evidence for $PM_{2.5}$ effects to conduct reasonably well informed health based-assessments for various disease endpoints. As such, $PM_{2.5}$ health effects are the focus of this thesis. The only other air pollutant with enough evidence for health based-assessments is O_3, which has enough evidence for causally associated respiratory mortality in the form of COPD (Turner et al., 2016; Jerrett et al., 2009; Malley et al., 2017; Gakidou et al., 2017). However, this thesis does not examine O_3 impacts on health.

Air pollutants	Associated	Likely causal	Enough evidence for global health-based assessments?
$PM_{2.5}$	Asthma, cognitive functions, low birthweight, other cancers, Alzheimer's disease, tuberculosis, cataracts	COPD, LRI, IHD, CEV, lung cancer, type 2 diabetes	Yes, for causally associated diseases
O_3	Possibly cardiovascular disease	COPD	Yes, for COPD
CO	Likely cardiovascular morbidity. Suggestive central nervous system effect, respiratory morbidity and mortality, birth and developmental effects.	Not clear yet	Not yet
NO_2	Likely respiratory and cardiovascular disease, cancer and all cause-mortality	Not clear yet	Still some debate on whether it is an indicator pollutant for fossil fuel $PM_{2.5}$ or whether it is a toxic gas by itself.
SO_2	Likely respiratory mortality and morbidity	Not clear yet	Not yet
PAHs	Cause of DNA damage, thus cancer	Cancers	Not yet

TABLE 1.4: Overview of the adverse health effects of various air pollutant exposures. Disease acronyms can be found on the list of abbreviations at the front of this thesis.

1.2.2 Health-based assessments: recent improvements for estimating the global burden of disease attributable to $PM_{2.5}$

As mentioned in the previous section, this thesis focuses on the disease burden associated with long-term exposure to $PM_{2.5}$. Global health-based assessments aiming to estimate the burden of disease to known risk factors require firstly, a detailed understanding of the population-level exposure distribution of a given risk factor, and secondly, the expected exposure-response within a given population per level of exposure. For $PM_{2.5}$, knowledge of these two terms have undergone major developments over the past few years. These developments have been documented by the Global Burden of Disease (GBD) Comparative Risk Assessment (CRA) (e.g., Gakidou et al., 2017), which describes mortality and morbidity from all major risk factors (or the current disease that would be eliminated if known risk factors were reduced to a theoretical minimum risk exposure level in the present-day) at global and regional levels.

Until relatively recently, $PM_{2.5}$ health-based assessments as part of the GBD CRA were restricted to urban populations because of the larger pool of $PM_{2.5}$ measurements by which population-level exposure distributions could be derived (Cohen et al., 2004; Ostro and WHO, 2004). However, more recent CRA (e.g. Gakidou et al., 2017; Lim et al., 2012; Forouzanfar et al., 2015) have taken advantage of new techniques, and employ high resolution spatially explicit exposure distributions across

the entire Earth's surface. Figure 1.5 shows an example of these new exposure distributions, which are produced by combining satellite retrievals of aerosol column extinction (e.g., aerosol optical depth (AOD)) with surface measurements and global chemistry-transport model (CTM) simulations (e.g., Brauer et al., 2015; Van Donkelaar et al., 2010; Shaddick et al., 2018). The recent use of such methods now makes it possible for researchers and policy makers to construct $PM_{2.5}$ exposure distributions across all global regions and populations, even where surface $PM_{2.5}$ measurements are unavailable. In Chapter 3 and Chapter 5, I make use of such datasets to compliment my simulated $PM_{2.5}$ concentrations.

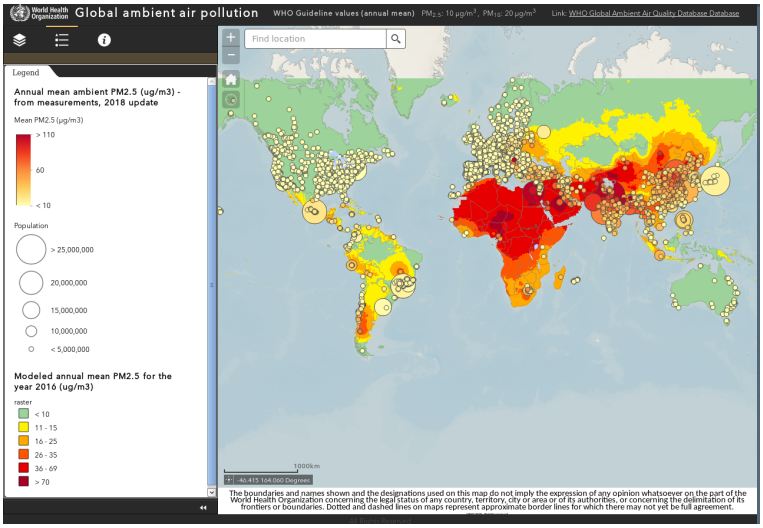

FIGURE 1.5: Example of the annual mean $PM_{2.5}$ exposure distribution used by the recent GBD CRA. Circles represent surface measurement locations and magnitude of underlying population while gridded contour data represents modelled concentrations. Gridded modelled data are provided by the Data Integration Model for Air Quality (DIMAQ) (Shaddick et al., 2018). Taken from the interactive map http://maps.who.int/airpollution/.

In addition to accurate exposure distributions, understanding of the exposure-response relationship (i.e., how an exposure translates to an expected health response within a given population) and associated theoretical minimum risk exposure level (TMREL) (i.e., below which no risk is assumed) are needed to conduct health-based assessments. Moreover, for global health-based assessments like the CRA, exposure-response relationships are needed at all global ranges of exposure distribution (e.g., Figure 1.5). However, until relatively recently, the GBD CRA prior to 2010 relied exclusively on exposure-response relationships derived from ambient air quality prospective cohort studies conducted in North America and or Western Europe only.

Thus, while these older relationships were valuable for quantifying risks (i.e., relative risk) at low exposure distributions typical of North America and Western Europe (e.g., usually <30 $\mu g\ m^{-3}$), they could not be used to estimate risk at high exposure distributions (above 30 $\mu g\ m^{-3}$) experienced in many low and middle-income countries where most of the global population is exposed (Figure 1.5). To address this problem, older generation relationships employed linear (Cohen et al., 2004) and log-linear (Ostro and WHO, 2004) approaches to extrapolate risk to high exposure distributions. However, because of a lack of ambient air pollution epidemiological observations at these high exposure distributions, such approaches inherently ran the possibility of predicting implausible and biologically inconsistent risk estimates (Ostro et al., 2018).

In recent years, a new generation of exposure-response relationships were developed to overcome these limitations by linking or integrating risk observations from different prospective cohort studies associated with different combustion sources. The development of these integrated exposure-response (IER) relationships, compile observed risks estimates not only from prospective cohort studies associated with ambient air quality from North America and Europe, but also from household air pollution (HAP) studies from solid fuel combustion (using randomised control trials), second-hand (passive) tobacco smoke, and active tobacco smoking studies (Burnett et al., 2014). These other combustion sources provide the high exposure distributions needed to construct a globally relevant exposure distribution appropriate for use in global health-based assessments. The use of IER in recent GBD CRA thus provides a an improvement on previous methods because it allows researchers and policy makers to estimate health risk based on empirical evidence for the entire global range of exposure distributions without the need for extrapolation. As such, in this thesis, IERs are used to estimate the global burden of disease associated with $PM_{2.5}$ exposure.

1.2.3 The global burden of disease attributable to $PM_{2.5}$ in the present-day

Following improvement to health-based assessment methods highlighted in the previous subsection, the GBD CRA place air pollution as a leading global risk factor to the global burden of disease and the most important environmental risk factor (Gakidou et al., 2017). Table 1.5 reports global mortality and morbidity attributable to air pollution and their risk ranking as of GBD CRA 2016 (Gakidou et al., 2017). For comparison, Table 1.5 also shows attributable deaths due to urban ambient $PM_{2.5}$ as estimated by the GBD CRA 2008.

Long-term exposure to ambient $PM_{2.5}$ is ranked the 5th largest risk factor to the global burden of disease in CRA 2016, which is now considered among more well known risk factors such as active tobacco smoking (2nd) and high body mass index (7th). It typically ranked within the top ten risk factors for the 195 countries studied, including the 3rd and 4th largest risk factor in India and China, respectively. Globally, ambient $PM_{2.5}$ was responsible for 4.1 (3.6-4.6) million deaths in 2016 (7.6% of total global deaths), including 105.7 (94.2-117.8) million disability-adjusted life-years (DALYs) (4.2% of total global DAYLs). In contrast, the CRA 2008 estimated only 1.3 million global deaths attributable to ambient $PM_{2.5}$ in 2008. The mortality estimate in CRA 2016 compared to CRA 2008 largely reflects the improvements made to the global exposure distribution and exposure-response relationships (IER) described in the previous section.

Recent GBD CRA also provide disease burden estimates for other individual air pollution risk factors (Table 1.5). These include ambient tropospheric O_3 exposure and exposure to household $PM_{2.5}$ air pollution (HAP) from cooking with solid fuels (Smith et al., 2014a). Exposure to HAP contributed to 2.7 (2.2–2.9) million deaths and 77.16 (66.1–88.04) million DALYs global deaths in 2016, most of which were located in low and middle-income countries where the use of solid fuels to meet basic household needs are common place (Gakidou et al., 2017; Smith et al., 2014a; Lim et al., 2012). Exposure to ambient O_3 contributed to 233.6 (90.1–385.3) thousand deaths and 3.79 (1.5-6.3) million DALYs in 2016, 91% lower than ambient $PM_{2.5}$.

Recent CRA also provide joint disease burden estimates for air pollution as the combination of ambient $PM_{2.5}$, ozone and HAP. This is estimated to be 6.1 (5.6–6.6) million deaths and 163 (151–176) million DALYs in 2016. However, this joint estimate for air pollution should be considered only as an approximation with an assumption of independence, little correlation and/or interaction. For example, because disease outcomes are often caused by more than one risk factor all interacting to the overall disease outcome, the estimated proportion of the outcome per individual risk factor can often overlap or add up to more than one. In the case of joint air pollution sources, the assumption of independence relates to a lack of epidemiological evidence on the population exposure distribution between ambient and HAP, and how individual level exposures correlate (e.g., because HAP also contributes to ambient air pollution and vice versa), as well as other non-linear interactions (Ezzati et al., 2003; Smith et al., 2014a). In this thesis, only ambient $PM_{2.5}$ health impacts are considered which means that health burden estimates will not capture the full health impact of overall air pollution.

Air pollution risk	Deaths	DALYs	Rank 2016	CRA 2008 deaths
Air pollution (joint)	6.1 [5.6 to 6.6]	163 [151 to 176]	-	-
Ambient particulate matter ($PM_{2.5}$) pollution	4.1 [3,6 to 4.8]	106 [95 to 118]	5^{th} (deaths), 6^{th} (DALYs)	1.3
Household air pollution (HAP) from solid fuels	2.6 [2.2 to 2.9]	77 [66 to 88]	10^{th} (deaths), 8^{th} (DALYs)	-
Ambient ozone pollution	0.23 [0.01 to 0.39]	3.8 [1.5 to 6.3]	-	-

TABLE 1.5: Global burden of disease estimates due to air pollution and their global risk factor rank as of GBD CRA 2016. Data taken from GBD compare tool (https://vizhub.healthdata.org/gbd-compare/). Death and DALYs are reported in millions. Deaths for GBD CRA 2008 are also included (far right).

1.2.4 Emission source contributions in the present-day to the global burden of disease

Global health-based assessments, such the GBD CRA described in the previous section, estimate disease burdens using total exposure distributions (e.g., Figure 1.5). However, understanding the contribution of different emissions sources on air pollution concentrations and their subsequent health burden is important. Understanding these source contributions is necessary for crafting sound air quality legislation

in order for policies to effectively target sources of ambient air pollution that are having the greatest adverse effects.

The CRA does not apply or provide sources contributions to their estimates of ambient $PM_{2.5}$ and their associated disease burden simply because their global exposure distributions (e.g., Figure 1.5) are not fractionated by emission source. However, two recent GBD studies have estimated source contributions nationally for both China and India. In those two studies, ambient $PM_{2.5}$ and health burden attribution was simulated using the GEOS-Chem chemical-transport model (CTM) under an assumption that the attributed burden of disease scaled linearly with the simulated fraction of $PM_{2.5}$ per emission source. This linear attribution method is currently recommended by the GBD as the most palatable method for policy makers to understand, and is also applied in Chapter 5 of this thesis.

Using the same linear attribution method, Lelieveld et al., 2015 was the first to examine the present-day contribution of emission sources to the attributable burden of disease at global level (see Table 1.6). In that study, Lelieveld et al., 2015 found that emissions from the residential sector were the largest global contributor, contributing 31% of all global attributable deaths due to ambient $PM_{2.5}$ (about 1 million deaths). Most of these deaths were concentrated in low and middle-income regions where the common combustion of residential solid fuels in simple and inefficient cooking and heating stoves resulted in large $PM_{2.5}$ related emissions. Emissions from agriculture and power generation were found to be more important contributors to ambient $PM_{2.5}$ and associated disease burdens in high-income countries (e.g., North America and Europe), while natural emission sources in the form of wind-blown dust were found to be large contributors across North Africa and the Middle East. In this thesis, the contribution of residential emissions to ambient $PM_{2.5}$ concentrations and associated health disease burdens are explored in greater detail (Chapter 4 and 5).

Country	Res	Agr	Nat	Pow	Ind	Bio	Tra
China	**32**	29	9	18	8	1	3
India	**50**	6	11	14	7	7	5
Pakistan	31	2	**57**	2	2	2	3
Bangladesh	**55**	10	0	15	7	7	6
Nigeria	14	1	**77**	0	0	8	0
Russia	7	**43**	1	22	8	8	11
USA	6	**29**	2	31	6	5	21
Indonesia	**60**	2	0	5	4	27	2
Ukraine	6	**52**	0	18	9	5	10
Vietnam	**51**	12	0	13	8	12	4
Egypt	1	3	**92**	2	1	0	1
Germany	8	**45**	0	13	13	1	20
Turkey	9	**29**	15	19	11	6	11
Iran	1	6	**81**	4	3	1	4
Japan	12	**38**	0	17	18	5	10
World	**31**	20	18	14	7	5	5

TABLE 1.6: Present-day emission source contribution [%] of total attributable mortality due to long-term exposure to $PM_{2.5}$. Source contributions to ambient $PM_{2.5}$ include, Res = Residential, Agr = Agriculture, Pow = Power generation, Ind = Industry, Bio = open biomass burning, and Tra = land transport. Bold values indicate the largest health contribution [%] due to an emission source. Data taken from Lelieveld et al., 2015.

1.2.5 Ambient air quality standards and guidelines for protecting health and environment

Air quality standards and guidelines can be set by individual countries as part of national environmental regulations to help protect human health, as well as achieving other environmental goals. Standards vary across different countries based on approaches used to balance public health risks, technological feasibility, and other various political and social-economic considerations and factors.

Over the past number of decades ambient legislation on air quality standards across the North America and many European countries have been instrumental in improving air quality. In the European Union (EU), standards are designed to protect both human health and environmental effects of ambient air pollution. For ambient $PM_{2.5}$, the EU directive on ambient air quality and cleaner air for Europe (EU, 2008) requires that member states achieve annual ambient $PM_{2.5}$ exposure levels of 25 $\mu g\ m^{-3}$ by the year 2015, with a second phase of reducing to 20 $\mu g\ m^{-3}$ by the year 2020. Based on epidemiological evidence, the United States (US) Environmental Protection Agency (EPA) recently reduced the annual ambient $PM_{2.5}$ standard in 2012 from 15 $\mu g\ m^{-3}$ to 12 $\mu g\ m^{-3}$.

In contrast, many low and middle-income countries across Asia, Africa, Latin America and the Middle East, have not established or enforced national air pollution

standards (Giannadaki, Lelieveld, and Pozzer, 2016), which have in part resulted in air quality degradation. However, while annual $PM_{2.5}$ standards have been introduced in some highly polluted countries, such as India (40 $\mu g\ m^{-3}$) and China (35 $\mu g\ m^{-3}$), they are often not legally binding (e.g., in India) and are consistently exceeded (Archer-Nicholls et al., 2016; Conibear et al., 2018a).

In response to guidance on air pollution standards, the World Health Organization (WHO) has proposed a number of interim targets for countries to strive for, all of which are designed to protect human health based on epidemiological evidence. For annual mean $PM_{2.5}$, these standards, though not legally binding, incorporate a three tier system to the ultimate desirable standard of the Air Quality Guidelines (WHO AQG) standard of 10 $\mu g\ m^{-3}$ (see Table 1.7). However, recent epidemiological evidence suggests that mortality risk can exist at low exposures, low than even the AQG. This suggest that the desired target of AQG may not fully protect public health (Cohen et al., 2017).

	$PM_{2.5}$ $\mu g\ m^{-3}$	Basis for selection
Interim target-1 (IT-1)	35	Approximately 15% higher long-term mortality risk relative to the AQG level
Interim target-2 (IT-2)	25	Approximately 6% lower mortality risk relative to IT-1
Interim target-3 (IT-3)	15	Approximately 6% lower mortality risk relative to IT-2
Air quality guideline (AQG)	10	Lowest levels that mortality risk has been shown to increase (as of evidence in 2005)

TABLE 1.7: World Health Organization (WHO) air quality guidelines and interim targets for annual mean ambient $PM_{2.5}$ concentration levels.

1.3 Atmospheric aerosol and the Earth's radiation budget

Air pollutants can affect the climate system by interacting with the Earth's radiation balance (Figure 1.1). The Earth's energy budget accounts for the balance between radiation received by the Earth-system (i.e. the surface and atmosphere) from the Sun and the energy radiated back to space. Anything that increases or decreases the amount of incoming and outgoing radiation (short-wave and long-wave) will disturb this balance with implications for the Earth's climate system.

Atmospheric aerosols can interact with climate directly by absorbing and scattering incoming short-wave radiation and by absorbing outgoing long-wave radiation,

known as aerosol direct effects. The magnitude of the direct effect at any given time and location is generally dependant on the aerosol size, burden and optical properties (and solar zenith angle). Absorption of atmospheric aerosol can also lead to surface cooling and local heating of the atmosphere, which can reduce the formation of clouds and precipitation, known as aerosol semi-direct effects (Lohmann and Feichter, 2005). Atmospheric aerosols of a certain size and composition can act as cloud condensation nuclei (CCN), which can activate to form cloud droplets influencing cloud-droplet number concentrations (CDNC). The aerosol influence on CDNC can indirectly affect the Earth's radiation balance by modifying properties of clouds, known as aerosol indirect effects. Aerosol indirect effects can be further sub-categorised into two effects: 1) The *cloud albedo effect* (sometimes referred to as the *Twomey effect* or *first indirect effect*) where the albedo of clouds are enhanced by aerosols acting to produce more numerous smaller cloud droplets under an assumption of fixed liquid water content (Twomey, 1959; Twomey, 1977); 2) The *cloud lifetime effect* (sometime referred to as the *second direct effect*) where more numerous smaller cloud droplets result in a decrease in precipitation efficiency and prolonged cloud lifetime (Albrecht, 1989).

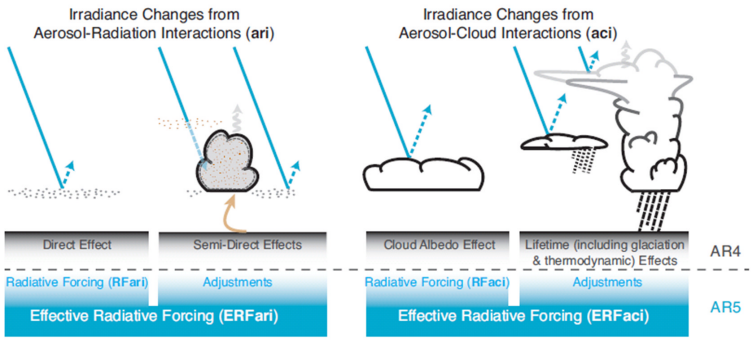

FIGURE 1.6: Summary of direct and indirect effects of atmospheric aerosols on radiation, including new AR5 definitions. Figure taken from Boucher et al., 2013.

Figure 1.6 shows a summary of these interactions. In the 5th Assessment Report (AR5) of the Intergovernmental Panel on Climate Change (IPCC), new definitions for these interactions were termed. Aerosol radiation interactions (ari) represent the former direct and semi-direct effects, while aerosol-cloud interactions (aci) represents the former cloud albedo and cloud lifetime effects (Boucher et al., 2013). Additional distinctions have also been made for radiative forcing effects (representing

both direct and cloud albedo effects) and rapid adjustment effects (representing both semi-direct and cloud lifetime effects), which combined leads to overall effective radiative forcing (EFR) from both ari (ERFari) and aci (ERFaci). Here, ERF is defined as the change in net top of the atmosphere downward radiative flux after allowing for atmospheric temperatures, water vapour, and clouds to adjust, but with surface temperature or a portion of surface conditions unchanged (Myhre et al., 2013).

Figure 1.7 summarises the anthropogenic drivers of EFR relative to the pre-industrial year of 1750. Instantaneous RF is given as a measure of the change in net radiative flux in both shortwave and longwave radiation at the top of the atmosphere (climatological tropopause). Instantaneous radiative forcing (RF) does not include changes from rapid adjustments or feedbacks, such as those from aerosol cloud changes (i.e. cloud lifetime and semi-direct effects), which are included in the measure of ERF, but are measured relative to the pre-industrial. In addition, the term instantaneous radiative effect (RE) is distinct from ERF, as the measure of the radiative radiative flux imbalance of an atmospheric constituent in the present-day atmosphere only.

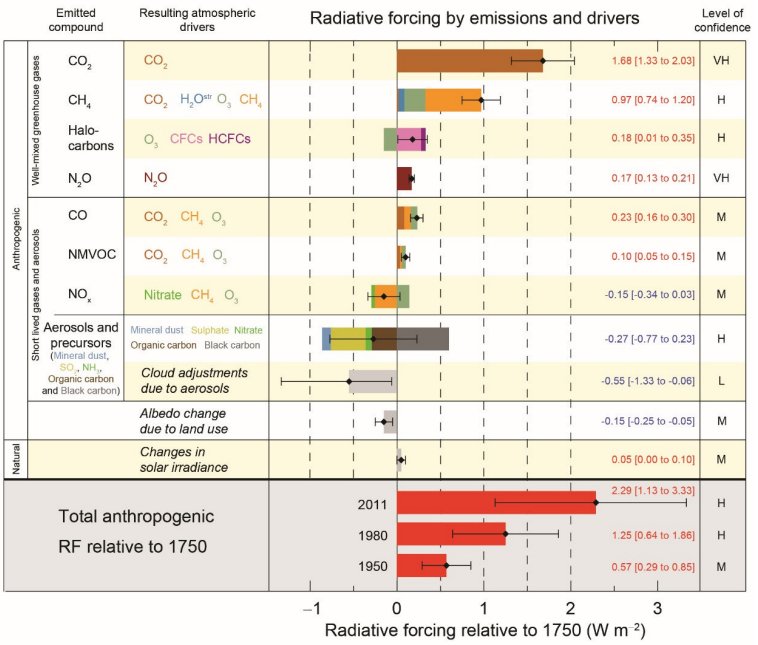

FIGURE 1.7: Global drivers of climate change as a measure of effective radiative effect (ERF) relative to the pre-industrial year 1750. The measure of the level of confidence in radiative forcing estimates (furthest column on the right) is represented: very high (VH), high (H), medium (M), low (L), and very low (VL). Figure taken from Stocker, 2014

The relatively small error bars due to well-mixed greenhouse gases reflect the high level of confidence in their mean positive radiative forcing (e.g., + 1.68 [1.33 to 2.03] W m $^{-2}$ for CO_2, see Figure 1.7). However, the radiative forcing due to atmospheric aerosol is estimated to be negative (-0.27 [-0.77 to -0.23] W m $^{-2}$ for aerosol and -0.55 [-1.33 to -0.08] W m $^{-2}$ for aerosol cloud adjustments), with large error bars, representing the largest source of uncertainty to net anthropogenic radiative forcing.

The radiative effect of an aerosol population depends on the size aerosol particles and the chemical composition of the particles through their respective refractive indices. Figure 1.8 shows the different radiative effects (RFari) of aerosol components as reported in AR5. Sulphate aerosol is estimated to have the most negative RFari (-0.4 [-0.6 to -0.2] W m $^{-2}$), with BC exerting the largest positive RFari ($+0.4$ [$+0.05$ to $+0.8$] W m $^{-2}$). In total, the RFari for all aerosol components combined is estimated to be -0.35 [-0.85 to $+0.15$] W m $^{-2}$. Shortly after the publication of AR5, Bond et al., 2013 reported a larger direct radiative forcing for BC of $+0.71$ [$+0.08$ to $+1.27$] W m $^{-2}$, which was based by scaling BC absorption to remote sensing observations and considering enhanced absorption due to optical mixing states. In addition, they also argued that modelled BC burdens were too low over many regions (e.g. Africa and Asia), which are likely dominated by underestimates of emissions from BC rich sources such as the residential sector.

1.4 Trends in anthropogenic emissions

Understanding how anthropogenic emissions changed over time is important for understanding how ambient air pollution and air quality have changed over time. Figure 1.9 shows the historical trend in global anthropogenic aerosol primary and precursor emissions, as well as other climate relevant pollutants. Global emissions have increased since the start of the industrial period. Emissions from residential cooking and space heating dominated emissions of black carbon (BC), organic carbon (OC), carbon monoxide (CO), and non-methane volatile organic compounds (NMVOCs or VOCs) in the mid-18th to mid-19th century. By the late-19th to mid-20th century, growing industrial, energy and transport emissions started to build

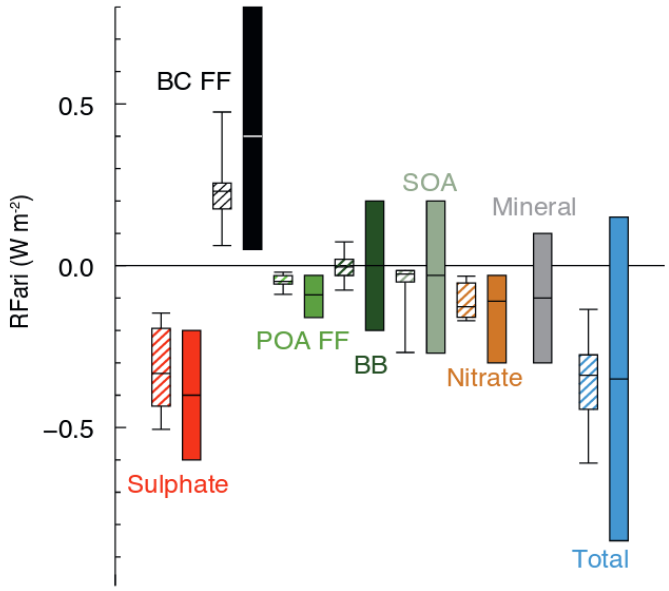

FIGURE 1.8: Annual mean top of the atmosphere radiative forcing due to different aerosol components for the 1750-2010 period. Solid boxes are the AR5 estimates, whereas the hatched box and whiskers are estimates from the AeroCom II models. Figure taken from Boucher et al., 2013.

and increased on the relatively steady emission base of the residential sector (Hoesly et al., 2018). Growing activities in the industrial and transport sectors during the 20th century increased global pollutants of sulfur dioxide (SO_2), oxides of nitrogen (NO_x), and NMVOCs, while the steady growth in global BC and OC emissions were dominated by residential activities. The process of ammonia synthesis over the past 100 years, together with population growth, resulted in the rapid increase in global NH_3 emissions (Erisman et al., 2008).

For the period after 1950, global emissions increase rapidly for most pollutants, but with regional differences (Figure 1.10). Dominated by the industrial and power sectors, SO_2 emissions declined across North America and Europe due to greater environmental air quality legislation, but continued to increase across Asia due to economic and population growth, and lack of environmental legislation (Figure 1.10). For CO emissions, while the introduction of catalytic converters in North America and Europe (and more recently in other regions) led to a reduction in global CO emissions from the transport sector, CO emissions have continued to increase in

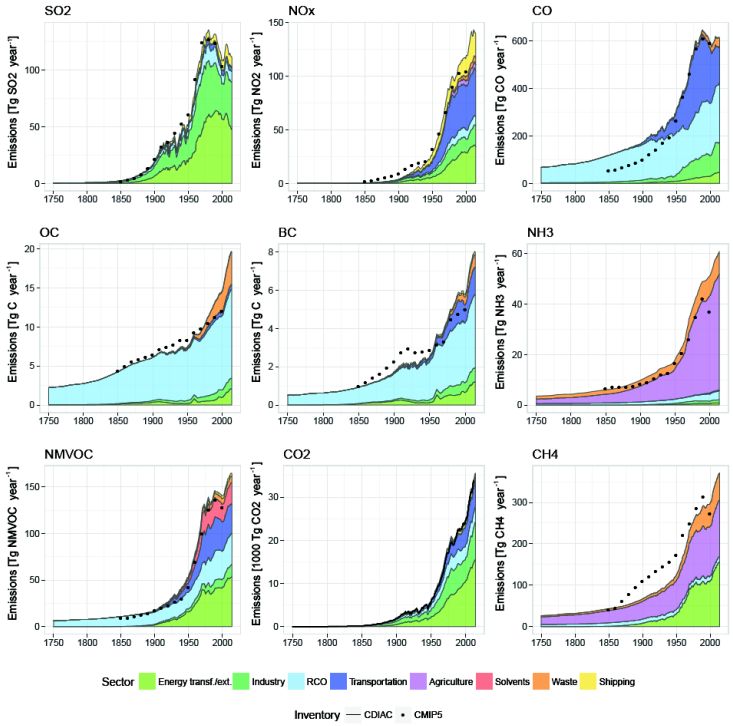

FIGURE 1.9: Global anthropogenic emissions by sector used in the Coupled Model Intercomparison Project phase 6 (CMIP6) compared to other estimates (e.g., CMIP5 and CDIAC). Emissions from aviation and open biomass burning are not included. "RCO" refers residential, commercial and other. Figure taken Hoesly et al., 2018.

Africa and Asia due to population growth and residential biomass burning contributions (Lamarque et al., 2010; Hoesly et al., 2018; Granier et al., 2011). Similarly, while NO_x emissions from the transport sector have decreased, economic growth across much of Asia has resulted in large increases in global NO_x emissions since the year 2000 (Figure 1.10). Global increases in BC and OC emissions since 1950 have been dominated by growth in Africa and Asia largely to due to residential combustion activities responding to population growth, but the use of diesel vehicles has also added to the global growth, especially for BC emissions. The large regional changes in anthropogenic emissions over the past 50 years or so has thus undoubtedly influenced regional changes in ambient $PM_{2.5}$ concentrations and associated health burdens, and is a focus of this thesis in Chapter 3.

Figures 1.9 and 1.10 also highlight the uncertainties in estimates among difference emission inventories. These different estimates are largely a result of uncertainties relating to energy consumption patterns and emission factors, which can be particularly sparse for certain sectors and geographical regions where data are not routinely

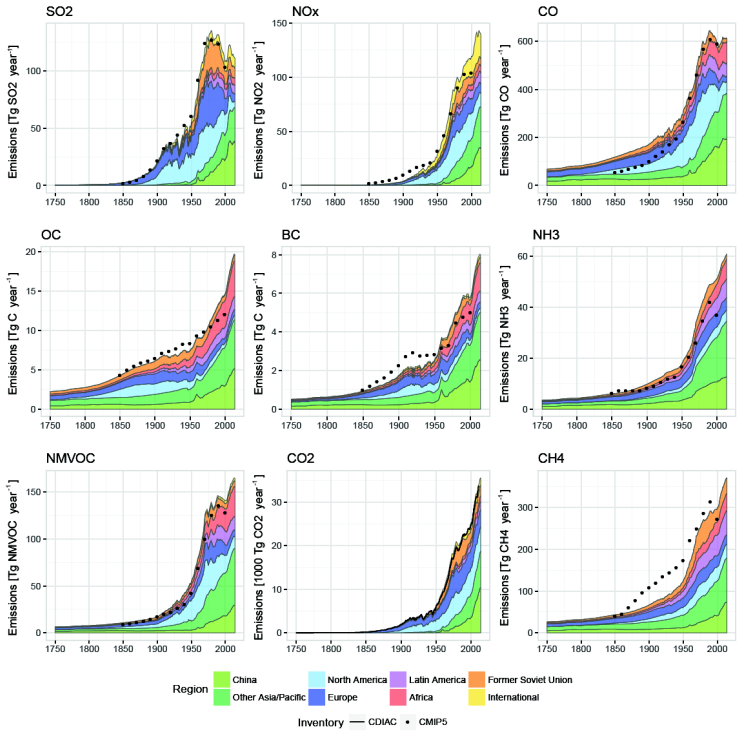

FIGURE 1.10: Global anthropogenic emissions by region used in the Coupled Model Intercomparison Project phase 6 (CMIP6) compared to other estimates (e.g., CMIP5 and CDIAC). Emissions from aviation and open biomass burning are not included. Figure taken Hoesly et al., 2018.

documented and where emission testing is limited. The collection of consumption patterns for residential solid-fuel burning (e.g., for cooking and heating in low and middle-income countries) is one such example. Together with a limited number of field-based emission factors, the residential emission sector represents one the largest sources of uncertainty when it comes to anthropogenic emission mass flux (Bond et al., 2013; Winijkul, Fierce, and Bond, 2016), and is a point of interested explore in this thesis in Chapter 4. It is therefore important to have accurate emission inventory data when quantifying their impacts on air quality and climate.

While uncertainties in estimating historical anthropogenic emissions are apparent, understanding future emission trends may be more uncertain. Future scenarios emission pathways are generally estimate emission changes in response to projected changes in economic growth, population, energy consumption, land-use and agriculture (Rao et al., 2017; Moss et al., 2010). Examples include the Representative Concentration Pathway (RCP) scenarios (Van Vuuren et al., 2011), which examine

a range of climate forcings without socioeconomic narratives, and are based under assumptions of the Kuznets hypothesis where future air pollutants decline in response to income growth (Rao et al., 2017). As such, RCPs show general declines in aerosol primary and precursor emissions (and ozone precursor emissions) over the 21st century (Stohl et al., 2015; Amann, Klimont, and Wagner, 2013). However, more recent emission pathway scenarios include alternative assumptions based on 'reference' scenarios and co-benefits of climate change mitigation policy (Rao et al., 2017; Stohl et al., 2015). In these scenarios, a range of emission pathways can be examined that do not necessarily follow that of the Kuznets hypothesis, resulting in a greater diversity of emission pathways than predicted under the RCPs alone (Figure 1.11).

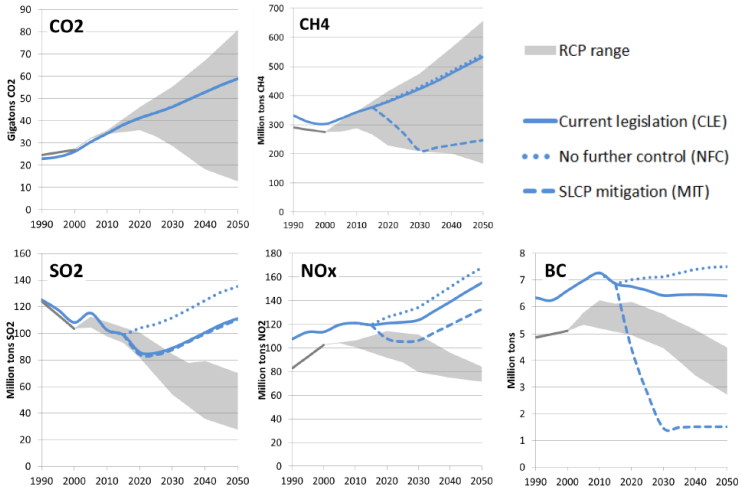

FIGURE 1.11: Global annual anthropogenic emissions of CO_2, CH_4 and air pollutants (SO_2, NO_x and BC) from the ECLIPSE emission inventory for the current legislation (CLE), no further controls (NFC) and short-lived climate pollutants (SLCP) mitigation scenario. Also shown for comparison is the range of the RCP emission scenarios (grey shading). Figure taken from Stohl et al., 2015.

1.5 Trends in ambient particulate air pollution

Following the implementation of air quality legislation and standards, regional monitoring networks were established to evaluate air quality performance both temporally and spatially. The longest operated networks are those based in North America (e.g., Integrated Monitoring of Protected Visual Environments, IMPROVE (Malm et al., 1994)) and Europe (e.g., European Monitoring and Evaluation Programme,

EMEP (Tørseth et al., 2012)), with measurements of aerosol mass from total suspended particles (TSP) dating since the 1970s. More recently (i.e., past two decades or so), $PM_{2.5}$ measurements have taken priority due to epidemiological concerns highlighting the health risk associated with these particles sizes.

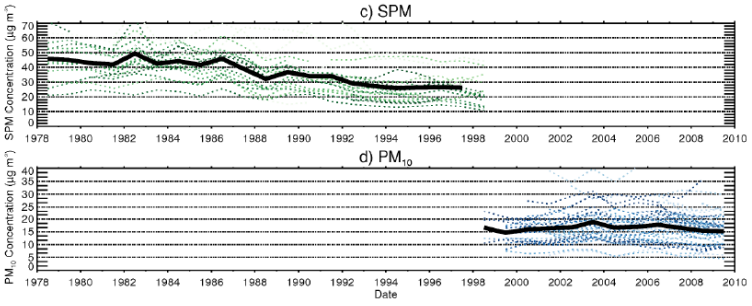

FIGURE 1.12: Time-series of the European observations of total suspended particulate matter (SPM) and PM_{10} $PM_{2.5}$ (mass particulate matter with an median aerodynamic dry diameter of < 10 μm) from the EMEP network over the period 1978 to 2010. Coloured lines represent individual measurement locations with the solid black lines representing the mean. Figure taken from Turnock et al., 2015.

Recent anthropogenic emission reductions across Europe and North America (Figure 1.10) have resulted in regional reductions in ambient PM. In Europe, TSP decreased by 40% during the period 1978-1998, with a smaller reduction in observed PM_{10} and $PM_{2.5}$ (not shown) between 2000-2009 (Figure 1.12), representing an 18% and 27% reduction respectively (Turnock et al., 2015; Tørseth et al., 2012). Across the United States (US), annual PM_{10} and $PM_{2.5}$ decreased by 34% and 41% during the period 1990-2017 and 2000-2017, respectively (Figure 1.13). The above reductions in ambient PM can be attributed to the implementation of air quality legislation and emission control technologies in both these regions.

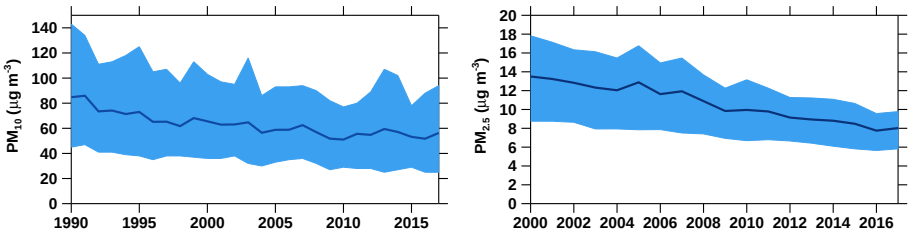

FIGURE 1.13: Time-series of the US observations of PM_{10} (left) and $PM_{2.5}$ (right) for measurement locations across the US. Dark blue line is mean across all locations with the light blue shaded area representing the 5th and 95th percentile range. Data taken from the US Environmental Protection Agency (EPA) https://www.epa.gov/air-trends/.

While reductions in PM have been observed across high-income regions in recent decades, increases in anthropogenic emissions and lack air quality regulation has contributed to rising PM concentrations across many low and middle-income countries, especially in Asia. However, while monitoring networks are being established at increasing rates across some countries, such as in China (e.g. Archer-Nicholls et al., 2016) and India (e.g. Conibear et al., 2018a), few long-term measurements (e.g., $>$ 10 yrs) exist, apart from a few in heavily urbanised locations. This presents a problem for evaluating simulations from chemistry-composition models, and thus for understanding air quality effects on human health and climate over the last decade or more.

Satellite retrievals AOD, which is a measure the amount of light extinction through the atmospheric column due to aerosols, have a global temporal coverage extending more than a decade and are spatially explicit in extent. Satellite AOD can thus be used to evaluate model simulated AOD over regions void of surface observations. The relationship between AOD and surface $PM_{2.5}$ concentrations, which depends on the aerosol profile distribution through the column, aerosol optical properties and humidity, can also be used to estimate $PM_{2.5}$ concentrations in regions where surface observations are lacking (Liu et al., 2004; Van Donkelaar, Martin, and Park, 2006). This technique uses the ratio of $PM_{2.5}$ to AOD simulated by a CTM to infer surface $PM_{2.5}$ concentrations directly from satellite AOD retrievals. Such estimates can be provided at relatively high spatial resolutions with a temporal coverage extending from the start of the satellite period (e.g., 1998) to the present-day. More recent examples of this technique also include the inclusion of surface $PM_{2.5}$ measurements (where available), and are used as the official exposure distributions in GBD CRA (Brauer et al., 2015; Van Donkelaar et al., 2016; Shaddick et al., 2018).

Figure 1.14 shows the trend in population-weighted $PM_{2.5}$ concentrations in China and India for period 2000-2016, which are based on satellite AOD retrievals and surface observations. These estimates show that population-weighted $PM_{2.5}$ concentrations increased by 8% and 25% in China and India respectively over this period. It can also be seen that that after 2010, $PM_{2.5}$ concentrations started to slow and decline in China, which is largely attributable to China's efforts of curb emissions in

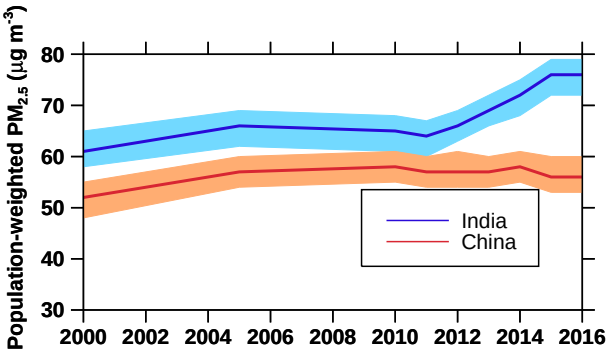

FIGURE 1.14: Time-series of population-weighted $PM_{2.5}$ concentrations in China and India from 1990-2016. Data taken from State of Global Air 2018 https://www.stateofglobalair.org/data/.

key polluting regions (e.g. Zheng et al., 2017).

Understanding how ambient $PM_{2.5}$ concentrations will change into the future is complex and depends on a number of different factors such as changes in anthropogenic emissions, climate and meteorology, and natural emissions. However, considering anthropogenic emissions alone, regional changes will be dependant on the emission pathway scenario assumed (Figure 1.15). That said, it is important to consider how changes or emission abatement in key polluting anthropogenic sectors might affect and improve ambient levels of $PM_{2.5}$ in the near-term (Chapter 5).

1.6 Trends in the global burden of disease attributable to $PM_{2.5}$

In addition to providing disease burden estimates for the present-day, the GBD CRA also provided trends for the burden of disease attributable to individual known risk factors (1990 to present-day). In the most recent CRA (Gakidou et al., 2017; Feigin, 2016; Cohen et al., 2017), the global burden of disease attributable to long-term ambient $PM_{2.5}$ exposure was found to increase 20% from 3.5 (3.0 to 4.0) million deaths in 1990 to 4.2 (3.7-4.8) million deaths in 2015 (Figure 1.16).

Figure 1.17 shows the change in ambient $PM_{2.5}$ attributable mortality over the same period (1990 to 2015) for ten populous countries together with the contribution of individual factors that influence mortality changes. The increase in the number of attributable deaths globally was largely caused by increases in $PM_{2.5}$ exposure and

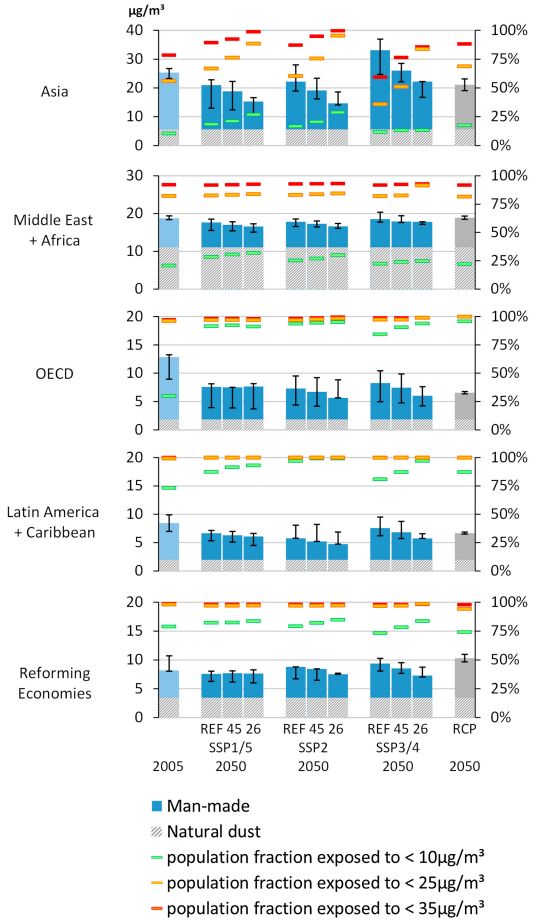

FIGURE 1.15: Regional annual mean population weighted $PM_{2.5}$ concentrations (µg m^{-3}) (left axis) in 2005 and 2050 under different emission scenarios including 'Reference' or Shared Socio-Economic Pathway (SSP) scenarios (blue color bars) and average of 3 RCP scenarios (grey bar). Green, orange and red colored markers indicate the fraction of the population exposed to <10, <25 and <35 µg m^{-3} respectively (right axis), and contribution of natural PM $_{2.5}$ is represented by the hatched area. Figure taken from Rao et al., 2017

the absolute numbers of deaths from non-communicable diseases in highly populated countries such as India and China, where populations are growing and ageing rapidly. These changes were enough to counteract the reduction in attributable mortality experienced across high-income countries (e.g. US) where reductions in $PM_{2.5}$ have been achieved since 1990, and where populations are not growing rapidly.

In contrast, age-standardised death rates from ambient $PM_{2.5}$ decreased by 12.3% from 65.6 per 10^5 deaths (56.9-74.9) in 1990 to 57.5 per 10^5 deaths (50.2-64.8) in 2015. This reduction was a result of improved air quality across high-income countries and overall global improvements in global healthcare, which resulted in overall declines in background disease rates that are causally associated with $PM_{2.5}$ exposure (Cohen

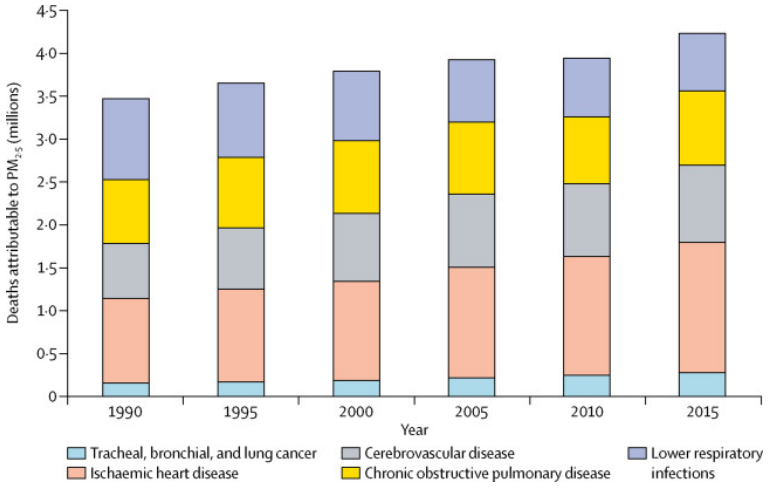

FIGURE 1.16: Total global deaths attributable to ambient $PM_{2.5}$ pollution by year and cause. Figure taken from Cohen et al., 2017.

et al., 2017).

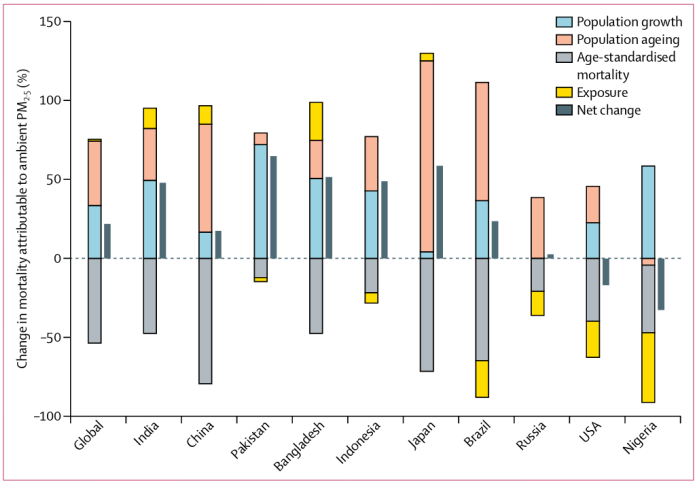

FIGURE 1.17: Changes in attributable deaths from ambient $PM_{2.5}$ exposure due to the changing contribution from population growth, ageing, background disease mortality, and exposure. Figure taken from Cohen et al., 2017

Given the large risk factor to public health, understanding historical changes in ambient $PM_{2.5}$ disease burden is vital for informing future air quality policy design. However, current estimates are restricted to examining changes over the last 25 years only (Figure 1.16), when satellite and ground-based observations are typically available. Few studies have investigated changes in attributable disease burdens associated with changes in ambient $PM_{2.5}$ over the last 50 years or so, a period of widespread implementation of air quality regulation and emission controls across North America and Western Europe coincided with extensive economic growth and

limited emission controls across developing Asia (Figures 1.10). Such changes would have undoubtedly resulted in regional contrasts in ambient $PM_{2.5}$ and associated disease burden trends, and thus a focus of this thesis in Chapter 3.

Understanding how the $PM_{2.5}$ disease burden will change in the future is complex and depends not only on changes in $PM_{2.5}$ concentrations (previous section), but also on changes in demographics and background disease epidemiology. Given the large demographic contribution to changes in $PM_{2.5}$ disease burden over the last 25 years (Figure 1.17), future changes in demographics will likely play an important role in future attributable disease burdens. Regional studies have shown that future population growth and ageing will increase deaths from $PM_{2.5}$ in China and India, even when $PM_{2.5}$ levels have been substantially reduced relative to the present-day (GBD MAPS Working Group, 2016; GBD MAPS Working Group, 2018; Conibear et al., 2018b).

Studies that examine changes in $PM_{2.5}$ mortality under future emission pathway scenarios, report global increases of between 50-335% by 2050 relative to the present-day (Lelieveld et al., 2015; Stohl et al., 2015; IEA, 2016), while other studies predict reductions (Silva et al., 2016; IEA, 2016). These differences are attributable to the differences in assumed emissions and demographic pathways. Nevertheless, few global studies have examined the likely contribution of changes in demographics and background disease to future changes in $PM_{2.5}$ mortality, which is focus of this thesis in Chapter 5. Understanding these contributions may be important for crafting future air quality policy.

1.6.1 Options for mitigating particulate air pollution

Air pollution in the form of PM will persist as a major public health problem until governments take the necessary action to mitigate its effects. PM air pollution can be mitigated through control or end-of-pipe technologies that reduce emissions at the point of emission (e.g., vehicle catalytic converters and smokestack scrubbers), and more structural shifts that avoid the occurrence of emissions (e.g., fuel switching,

energy efficiency and low or non-combustion technologies). However, with the evidence base for PM health effects growing at an ever increasing rate, the need to take action quickly using the range of mitigation options available should nevertheless be modulated by the need to find a long-term path that also does not compromise other policy goals (IEA, 2016). The optimum policy path is one that takes decisive action in coordination with others, which should include both the setting of ambitious long-term air quality goals and a clean air strategy for the important polluting sectors, with effective monitoring, enforcement, evaluation and communication (IEA, 2016).

Reducing air pollution can also bring desirable co-benefits. Climate change co-benefits have recently gained attention through high profile political initiatives, such as the Climate and Clean Air Coalition (CCAC) (www.ccacoalition.org). However, decision makers need to be made aware that while action may provide benefits in one area (e.g., climate), they can worsen the situation in another (e.g., air quality). For example, climate policy favouring low emitting CO_2 diesel vehicles replacing equivalent petrol vehicles can lead to detrimental effects on air quality (e.g. Jonson et al., 2017). Another example includes the shift from light fossil fuel used for space heating to 'carbon-neutral' biomass (wood), which may have greater adverse effects on PM air quality (e.g. Haluza et al., 2012). While this last example may be an growing problem facing wealthy regions (e.g., Europe), providing appropriate 'win-win' solutions for the 3 billion users of residential (household) solid fuels (mainly solid biomass) in low and middle-income countries (Bonjour et al., 2013), which contribute both to household and ambient PM pollution, and climate change, (Smith et al., 2014a; Chafe et al., 2014; Lelieveld et al., 2015) is a complex but pressing issue.

The large scale adoption and implementation of clean burning solid fuel cookstoves has been suggested as a possible 'win-win' solution (e.g. Anenberg et al., 2013). However, others argue that use such cookstoves are being driven by an international policy agenda focussing on climate goals (i.e., one promoting carbon-neutral solid biomass) rather than a promoting cleaner burning light fossil fuels (e.g., LPG), which would provide greater reductions in PM air pollution (both household and

ambient) and benefits for health (Goldemberg et al., 2018; Smith and Sagar, 2014). It is thus important to consider how future changes in emissions (e.g., residential energy) due to policy measures might impact on both air quality (and human health) and climate, which is a focus of this of this thesis in Chapter 5.

1.7 Summary and motivation

Long-term exposure to fine particulate matter ($PM_{2.5}$) air pollution is the 5th largest risk factor to the global burden of disease, contributing to 4.1 million deaths annually in the present-day. The large regional changes in anthropogenic emissions over the last 50 years has undoubtedly changed aerosol concentrations and thus their effects on air quality and public health. Understanding these historical changes, using chemistry-composition models combined with long-term observations, is vital for informing air quality policy design. Previous studies have tended to focus on trends in $PM_{2.5}$ air pollution and associated public health impacts over the last 25 years (e.g. Cohen et al., 2017), when satellite and ground-based measurements were typically available. For this reason, little is known about impacts between 1960 and 1990, a period where large regional changes in anthropogenic emission occurred. Using a detailed chemistry-climate model simulation, this thesis will build on current knowledge and examine trends in $PM_{2.5}$ air pollution and associated public health impacts over the past 50 years (Chapter 3).

Atmospheric aerosols also have substantial impacts on climate via modification of the Earth's radiative balance. This aerosol radiative effect is large and of opposite sign to the greenhouse gas effect. However, large uncertainties remain to their precise effects (Boucher et al., 2013). The aerosol radiative effect from substantial anthropogenic emission sources such as combustion of residential solid fuels (e.g., for household cooking and space heating) is thought to be large. This source sector contributes a considerable fraction of anthropogenic BC and OC emissions in the present-day(Bond et al., 2013). Combustion of residential solid fuels are also responsible for one-quarter of the attributable deaths associated with ambient $PM_{2.5}$ air pollution. The large scale adoption and implementation of clean burning solid

fuel cookstoves (and clean fuel such as gas and electricity) across low and middle-income regions has been suggested as a possible option for mitigating the adverse effects of traditional solid fuel combustion (e.g. Anenberg et al., 2013). Quantifying the present-day impact of residential solid fuel combustion on climate, ambient air quality and health is thus an important first step in understanding the likely effects of large scale adoption and implementation of clean cookstoves and fuels. Using a chemistry-transport model, this thesis seeks to examine the extent of these present-day impacts from the residential sector (Chapter 4).

Understanding the potential benefits of large scale adoption of clean cookstove technologies as a means of reducing emissions from the residential sector is important. However, quantifying any potential benefits to air quality and health needs to be done in the context of future changes in other anthropogenic emission sources, residential solid fuel usage, and demographic transitions. Previous studies examining potential future benefits of reducing emissions from the residential sector have relied on unrealistic assumptions of complete removal of emissions (e.g. Lacey et al., 2017a). This thesis will apply chemistry-transport model simulations using technology-based scenarios to quantify the potential near-term air quality and associated public health benefits of reducing emissions in the residential sector (Chapter 5). Understanding of these benefits will be particularly useful for decision makers across low and middle-income countries where the public health burden due to air pollution associated with residential solid fuel combustion is considerable.

1.8 Thesis aims and objectives

The overall aim of this thesis to quantify how changes in anthropogenic air pollutants have affected air quality and attributable disease burdens. It will also evaluate the present-day and future impact of residential combustion emissions, and how adoption of clean residential combustion technologies might reduce adverse impacts.

Individual aims for each result chapter are set out below:

1. How have changes in anthropogenic aerosol primary and precursor emissions affected global and regional trends in surface $PM_{2.5}$ concentrations and associated health burdens over the past 50 years from 1960 to 2009?

   (a) Can simulated changes in regional $PM_{2.5}$ concentrations reproduce long-term observed changes?

   (b) What are main sources of uncertainty in the model that are influencing the comparison to long-term measurements?

   (c) How have global and regional simulated $PM_{2.5}$ concentrations changed over the period 1960 to 2009?

   (d) How has the global and regional burden of disease attributable to long-term exposure to ambient $PM_{2.5}$ changed over the period 1960 to 2009?

   (e) What factors have dominated the contribution to the change in total $PM_{2.5}$ mortality over the period 1960 to 2009?

   (f) How can trends in historical $PM_{2.5}$ concentrations help inform policy makers about the impacts of future changes in $PM_{2.5}$ mortality?

2. How important is the present-day contribution of residential solid fuel combustion to atmospheric aerosol, human health and climate?

   (a) Can a global model simulate observed aerosol mass and number concentrations at locations where influence of residential combustion on atmospheric aerosol are thought to be important?

   (b) What are the global regional contributions of residential combustion emissions to atmospheric aerosol mass in the near present-day?

   (c) What is the near present-day global and regional burden of disease attributable residential combustion emissions on ambient $PM_{2.5}$ concentrations?

(d) What is the near present-day direct and first indirect radiative effect of residential combustion aerosol on the Earth's radiation budget?

(e) What might the uncertainties in residential combustion emission mass flux and emitted size distributions mean for quantifying residential impacts on air quality, human health and radiative effect?

3. How are ambient $PM_{2.5}$ concentrations and associated disease burdens expected to change by 2050? To what extend can the adoption of clean residential combustion technologies in the near-term offset adverse air quality and attributable health impacts?

(a) To what extent can a global chemical-transport model reproduce annual mean observed $PM_{2.5}$ concentrations across multiple global regions?

(b) How do annual mean ambient $PM_{2.5}$ concentrations change regionally under a reference scenario in the year 2050?

(c) How does the disease burden attributable to ambient $PM_{2.5}$ exposure change in the year 2050 under the reference scenario?

(d) How does the widespread adoption and sustained use of clean residential combustion technologies improve ambient $PM_{2.5}$ air quality relative to a reference scenario and a maximum anthropogenic emission reduction scenario?

(e) How does the widespread adoption and sustained use of clean residential combustion technologies improve the $PM_{2.5}$ mortality burden relative to a reference scenario and a maximum anthropogenic emission reduction scenario?

(f) How can near-term scenarios of clean residential emission controls inform ambient air quality management strategies?

Chapter 2

Methods

The amount of aerosol present in the atmosphere can strongly affect air quality resulting in adverse impacts on human health. Aerosols can also impact the climate directly through the absorption and scattering of radiation or indirectly via interaction with clouds. While measurements of aerosol such as their mass and number concentrations are valuable in quantifying some of these impacts, models can be used to simulate and understand aerosol impacts over spatial and temporal dimensions where measurements are not available. Models can simulate atmospheric aerosol through calculation of anthropogenic and natural emissions fluxes and the microphysical processes that govern the mass and number size distributions of aerosol components, which are important for air quality and climate impacts. However, aerosol measurements cannot be replaced by model simulations as the inclusion of observations are essential for understanding real atmosphere conditions, which are crucial for evaluating the models.

Models make it possible to simulate atmospheric aerosol impacts not only for past and present-day conditions, but also into the future, allowing for investigations of future mitigation scenarios. Models can be run at different spatial resolutions, with computational expense currently limiting global models to low resolutions greater than 100 km. Low spatial resolutions result in large scale mean aerosol properties which struggle to resolve gradients associated with urban scale locations. In addition, computational expense means that global models often include simplified aerosol size distribution representations.

In general, atmospheric aerosol are simulated in one of two types of global models; chemistry transport models (CTM) or chemistry-climate models (CCM). CTMs simulate atmospheric chemistry and aerosols using input meteorological data prescribed from a general circulation or climate model, where the CTM is run as a separate program off-line. Simulated atmospheric chemistry and aerosol from a CTM are thus not able to feedback and impact on meteorology, which is distinct from a CCM where meteorology, chemistry and aerosols are all calculated on-line allowing for feedbacks and interactions.

In this thesis, atmospheric aerosol is simulated using a CTM and CCM both of which are configured with the same aerosol scheme, the Global Model of Aerosol Processes (GLOMAP-mode). The following chapter describes both the CTM and CCM configuration used in thesis Chapters, with Table 2.1 presenting some key differences. In addition, a full description of the GLOMAP-mode model is also provided, as well as descriptions for the methods used to estimate aerosol radiative effects and the disease burden associated with ambient $PM_{2.5}$ exposure.

2.1 Chemistry–climate model (CCM)

The CCM HadGEM3-UKCA was applied using the same setup described in Turnock et al., 2015. HadGEM3-UKCA incorporates on-line treatment of chemistry and aerosols through the United Kingdom Chemistry and Aerosols (UKCA) programme (O'Connor et al., 2014). The dynamical core of the model is the Met Office's Unified Model (UM), which provides meteorological components including the large scale processes of advection, convection and boundary layer mixing (Davies et al., 2005).

In this thesis, HadGEM3-UKCA is used in atmosphere-only mode (Hewitt et al., 2011) with at spatial resolution of $1.875^\circ \times 1.25^\circ$ (approximately 140 km at mid latitudes) with 63 vertical levels to a height of 40km. The model was run over a simulation period from 1960 to 2009, with meteorological fields nudged at 6-hourly intervals to the European Centre for Medium-Range Weather Forecasts (ECMWF)

Reanalysis ERA-40 (period 1960 to 2000) (Uppala et al., 2005) and ERA-Interim (period 2000 to 2009) (Dee et al., 2011). Nudging to meteorological reanalysis is a simple form of data assimilation whereby dynamic variables of the free running CCM are adjusted to allow an accurate representation of meteorological conditions under which observations were collected. Sea ice fields and sea surface temperatures were prescribed to those used in the Coupled Model Intercomparison Project Phase 5 (CIMP5) (Hurrell et al., 2008), while the coupling of the land surface and atmosphere were prescribed using the Met Office's Surface Exchange Scheme (MOSES) (Essery et al., 2003).

Atmospheric chemistry within HadGEM3-UKCA is calculated based on the scheme (TropIsop) described in O'Connor et al., 2014 and includes reactions of odd oxygen (O_x), nitrogen (NO_y), hydrogen (HO_x = OH + HO_2), as well as carbon monoxide (CO), methane (CH_4) and short chain non-methane volatile organic compounds (VOCs). The chemistry scheme has a total of 41 species and simulates approximately 120 chemical reactions. The photolysis scheme (Fast-J) (Wild, Zhu, and Prather, 2000) is used to calculate photolysis rates on-line based on the distribution of simulated clouds, ozone and aerosol fields.

To allow coupling to the aerosol model (GLOMAP-mode), the chemistry scheme also includes additional chemistry with sulfur (Mann et al., 2010), monoterpene (Spracklen et al., 2006) and isoprene (Scott et al., 2014) species (Table 2.2). This coupling allows for the interaction and feedback of aerosol and chemistry. However, feedbacks and interactions on meteorology are suppressed through nudging to the meteorology reanalysis.

	HadGEM3-UKCA (Chapter 3)	TOMCAT-GLOMAP (Chapter 4)	TOMCAT-GLOMAP (Chapter 5)
Spatial resolution	1.875° × 1.25°	2.8° × 2.8°	2.8° × 2.8°
Vertical resolution	63 levels	31 levels	31 levels
Meteorology	Nudged to ECMWF	Off-line ECMWF	Off-line ECMWF
Chemistry	Coupled chemistry	Prescribed oxidants	Coupled chemistry
Aerosol	GLOMAP-mode	GLOMAP-mode	GLOMAP-mode
Thesis chapter	3	4	5

TABLE 2.1: Summary of key differences among the models configurations used in this thesis. TOMCAT-GLOMAP in Chapter 4 refers to the prescribed oxidant configuration, while TOMCAT-GLOMAP in Chapter 5 refers to the coupled chemistry configuration.

2.2 Chemistry–transport model (CTM)

In this thesis, the CTM TOMCAT was used (Chipperfield, 2006; Monks et al., 2017), which has a horizontal resolution of 2.8° × 2.8° (approximately 300 km at mid latitudes) and 31 hybrid vertical σ–p levels extending from the surface to 10 hPa (30Km). The model is run off-line with prescribed large-scale transport and meteorology (e.g., winds, temperature and humidity fields) from ECMWF ERA-Interim re-analyses data (Dee et al., 2011) at 6 hourly intervals. Large-scale tracer advection in the meridional, zonal and vertical is based on Prather, 1986, while sub-grid transport (boundary layer mixing and convective transport) is based on the schemes by Holtslag and Boville, 1993 and Tiedtke, 1989. The use of prescribed meteorology means that simulated chemistry and aerosol are not able to feedback and interact on the meteorology, which is also the case for the CCM setup described above.

The chemistry scheme in TOMCAT includes detailed tropospheric gas-phase chemistry inclusive of reactions of odd oxygen (O_x), nitrogen (NO_y), hydrogen (HO_x = OH + HO_2), as well as CO, CH_4 and short chain VOCs (Chipperfield, 2006; Monks et al., 2017). The photolysis scheme calculates photolysis rates on-line at each chemical time step based on a two-stream method considering direct and scattered radiation, and are coupled through TOMCAT simulated temperature and ozone concentration profiles. Surface albedo and monthly mean climatological cloud fields are supplied to the photolysis scheme from the International Satellite Cloud Climatology Project (ISCCP-D2) (Rossow and Schiffer, 1999), while aerosol concentrations are supplied by GLOMAP-mode (coupled or prescribed, see below).

The TOMCAT-GLOMAP-mode configuration is described as one of two setups (Table 2.1). The first describes a coupled chemistry configuration where oxidants are interactively regenerated allowing for the oxidation with sulfur and biogenic monoterpene species (Table 2.2) that can interact and feedback on atmospheric chemistry and aerosol. The second configuration describes GLOMAP-mode run with prescribed 6 hourly oxidant fields from a previous TOMCAT simulation (Arnold, Chipperfield, and Blitz, 2005), which are linearly interpolated to the GLOMAP-mode model time step. Under the prescribed oxidant set up, interaction and feedback of atmospheric

chemistry such as changes in oxidant concentrations, due to changes in aerosol primary and gas-phase precursor emissions (e.g. sulfur and biogenic species), are not accounted for.

Reactions
$DMS + OH \rightarrow SO_2$ [(a)]
$DMS + OH \rightarrow 0.6\ SO_2 + 0.4\ DMSO$ [(b)]
$DMSO + OH \rightarrow 0.6\ SO_2 + 0.4\ MSA$ [(b)]
$DMS + NO_3 \rightarrow SO_2$ [(a)]
$CS_2 + OH \rightarrow SO_2$ [(b)]
$COS + OH \rightarrow SO_2$ [(b)]
$SO_2 + OH + M \rightarrow H_2SO_4$ [(b)]
monoterpene + OH $\rightarrow$ 0.13 secondary-organic [(a)]
monoterpene + NO_3 $\rightarrow$ 0.13 secondary-organic [(a)]
monoterpene + O_3 $\rightarrow$ 0.13 secondary-organic [(a)]
$HO_2 + HO_2 \rightarrow H_2O_2$ [(c)]

TABLE 2.2: Reactions of gas-phase chemistry used in GLOMAP-mode with oxidants provide by either HadGEM3-UKCA or TOMCAT (Table 2.1), adapted from (Mann et al., 2010). Reactions for sulfur species include: dimethyl sulphide (DMS,DMSO), sulfur dioxide (SO_2), sulphuric acid (H_2SO_4), methane sulphonic acid (MSA), carbonyl sulphide (COS) and carbonyl sulphide (CS_2), and semi-prognostic hydrogen peroxide (H_2O_2). Formation of sulfate (SO_4^{2-}) aerosol, includes gas-phase reactions by the hydroxyl radical (OH), as well as aqueous-phase formation through the oxidation of sulphur species (S(IV) to S(VI)) by H_2O_2 and ozone O_3 dissolved in cloud drops present in low-level clouds. In addition, secondary organic aerosol formation includes reactions of biogenic monoterpene to form low volatility oxidation products. Here, monoterpene are oxidised at a 13% yield following reaction rates for α–pinene. [(a)] Atkinson et al., 1992, [(b)] Pham et al., 1995, and [(c)] Jones et al., 2001.

2.3 GLOMAP-mode aerosol model

The Global Model of Aerosol Processes (GLOMAP) is a global microphysical model of aerosol processes that simulates the evolution of size-resolved mass and number concentrations of aerosol particles with different compositions. In this thesis, the modal version of GLOMAP (GLOMAP-mode) is used (Mann et al., 2010). GLOMAP-mode simulates the shape of the aerosol size distribution as a series of log-normal modes (with the width of each mode being fixed) and includes a number of size-resolved processes including primary emissions, new particle formation, particle growth through coagulation, condensation, and cloud-processing, as well as the removal of particles by dry deposition and wet in-cloud and below-could scavenging.

2.3.1 Aerosol primary and gas-phase precursor emissions

Subject to the aim of the research study, different combinations of emission inventories have been used in this thesis, with each Chapter describing specific emissions used. Key differences in natural and anthropogenic emissions used in each chapter are described in Table 2.3 and Table 2.4, respectively.

Natural emissions of volcanic SO_2 are provided for both continuous (Andres and Kasgnoc, 1998) and explosive (Halmer, Schmincke, and Graf, 2002) eruptions. Wildfire emissions of BC, OC and SO_2 are taken from the Global Fire Emission Database (GFED) (Van Der Werf et al., 2004) or from the MACCity (MACC/CityZEN EU projects) inventory (Granier et al., 2011) and REanalysis of the TROposhperic chemical composition (RETRO) inventory (Schultz et al., 2008) (Table 2.3). Oceanic dimethylsulfide (DMS) emissions are calculated using an ocean surface DMS concentration database (Kettle and Andreae, 2000) combined with a wind speed dependant sea–air exchange parametrisation from Nightingale et al., 2000 or Liss and Merlivat, 1986. Emissions of oceanic sea salt are calculated using the scheme of Gong, 2003 and are emitted into the accumulation and coarse modes. Emissions of oceanic sea salt are also calculated using the schemes of Mårtensson et al., 2003 and Monahan, Spiel, and Davidson, 1986 which includes a more observationally driven treatment of submicron sea salt particles. Monoterpene emissions from vegetation are prescribed as monthly mean fields from the Global Emissions Inventory Activity database based on Guenther et al., 1995. Mineral dust emissions are either provided by daily-varying fluxes as recommended by AeroCom (Dentener et al., 2006) or from a separate six-bin scheme of Woodward, 2001 or are not included (Table 2.3).

Annual mean anthropogenic emissions of BC, OC and SO_2 are provided by the Atmospheric Chemistry and Climate Model Intercomparison Project (ACCMIP) (Lamarque et al., 2010) or as monthly mean varying emissions by the MACCity inventory (Granier et al., 2011) and ECLIPSE (Evaluating the Climate and Air Quality Impacts of Short-Lived Pollutants) inventory version v5a (Stohl et al., 2015) (Table 2.4). Emissions were provided for different years typically for the following anthropogenic

Emission source	HadGEM3-UKCA (Chapter 3)	TOMCAT-GLOMAP (Chapter 4)	TOMCAT-GLOMAP (Chapter 5)
Wildfires emissions			
Years	1960-2009	Averaged (1997-2002)	Averaged (1997-2010)
Reference	MACCity and RETRO	GFED	GFED
Oceanic sea salt			
Years	Present-day, wind-speed dependant	Present-day, wind-speed dependant	Present-day, wind-speed dependant
Reference	Gong, 2003	Gong, 2003	Mårtensson et al., 2003 and (Monahan, Spiel, and Davidson, 1986)
Windblown dust			
Years	Present-day, wind-speed dependant	Present-day	Not included
Reference	Separate scheme Woodward, 2001	GLOMAP, daily flux from Dentener et al., 2006	Not included

TABLE 2.3: Key differences in natural aerosol primary and gas-phase precursor emissions used in the different thesis chapters and models. TOMCAT-GLOMAP in Chapter 4 referrers to the prescribed oxidant configuration, while TOMCAT-GLOMAP in Chapter 5 refers to the coupled chemistry configuration.

sectors: power, industry, transport, residential and commercial, agriculture, waste treatment and international shipping.

Anthropogenic SO_2 emissions are emitted into the lowest model layer for low-level sources (i.e. residential and commercial and land transport sectors) but are injected at altitudes ranging 100-300 m for the energy and industrial sectors accounting for smoke stack heights. Wildfire SO_2 emissions are injected uniformly between the surface and 3 km, whereas wildfire BC and OC are injected between the surface and 6 km (Dentener et al., 2006). Volcanic SO_2 emissions are injected at heights based on volcano-top altitudes (Dentener et al., 2006).

Emission source	HadGEM3-UKCA (Chapter 3)	TOMCAT-GLOMAP (Chapter 4)	TOMCAT-GLOMAP (Chapter 5)
Anthropogenic emissions			
Years	1960-2009	2000	2015-2050
Data source	MACCity	MACCity and ACCMIP	ECLIPSE

TABLE 2.4: Key differences in anthropogenic aerosol primary and gas-phase precursor emissions used in the different thesis chapters and models. TOMCAT-GLOMAP in Chapter 4 refers to the prescribed oxidant configuration, while TOMCAT-GLOMAP in Chapter 5 refers to the coupled chemistry configuration.

To account for sub-grid nucleation and formation of SO_4^{2-} particles in volcanic, power-plant, and transport exhaust plumes, 2.5% of all SO_2 emissions are emitted as primary SO_4^{2-} particles based on the size distribution of Stier et al., 2005. To account for the size distribution of primary BC and OC emissions at the point of emission and sub-grid-scale processing at short time-scales after emission, BC and OC are emitted with an initial log-normal size distribution. This log-normal size distribution has a specified geometric mean diameter of 150 nm for wildfire and other biomass burning

emissions and 60 nm for fossil fuel emissions (regardless of specific source), with a geometric standard deviation set at 1.59. The distribution of BC and OC particles are then incorporated into the Aitken insoluble mode. Additionally, to account for the additional mass of oxygen, hydrogen and nitrogen atoms associated with particulate organic matter (POM) aerosol, OC emissions are multiplied by a OC:POM ratio of 1.4 or 2 based on AeroCom (Dentener et al., 2006) and other recommendations (Philip et al., 2014).

2.3.2 Aerosol microphysical processes

GLOMAP-mode is a two-moment scheme where information on aerosol number and mass concentrations of different components are carried in a series of log-normal size modes: nucleation (dry diameter (Dp) <10 nm), Aitken (Dp 10–100 nm), accumulation (Dp 100 nm to 1 μm) and coarse (Dp >1 μm). GLOMAP-mode simulates multiple components in soluble and insoluble modes where aerosol components can be a combination of internal and external mixtures. Typical aerosol components include sulfate (SU, SO_4^{2-}), sea-salt (SS, NaCl), black carbon (BC), particulate organic matter (POM) and mineral dust (DU). Table 2.5 reports key differences in the GLOMAP-mode set up used in each thesis Chapter and model configuration.

Mode	Size (Dp)	HadGEM3-UKCA (Chapter 3) Components	TOMCAT-GLOMAP (Chapter 4) Components	TOMCAT-GLOMAP (Chapter 5) Components
Nucleation	Dp <10 nm	SU,POM	SU,POM	SU,POM
Aitken soluble	Dp 10–100 nm	SU,POM,BC	SU,POM,BC	SU,POM,BC
Accumulation soluble	Dp 100 nm to 1 μm	SU,POM,BC,SS	SU,POM,BC,SS,DU	SU,POM,BC,SS
Coarse soluble	Dp >1 μm	SU,POM,BC,SS	SU,POM,BC,SS,DU	SU,POM,BC,SS
Aitken insoluble	Dp 10–100 nm	BC,POM	BC,POM	BC,POM
Accumulation insoluble	Dp 100 nm to 1 μm	-	DU	-
Coarse insoluble	Dp >1 μm	-	DU	-

TABLE 2.5: Summary of GLOMAP-mode set up. Dp (dry diameter); SU (sulfate), POM (particulate organic matter), BC (black carbon), SS (sea salt), DU (mineral dust). Sigma reflects geometric standard deviation of mode. TOMCAT-GLOMAP in Chapter 4 refers to the prescribed oxidant configuration, while TOMCAT-GLOMAP in Chapter 5 refers to the coupled chemistry configuration.

To simulate the evolution of aerosol concentrations, each mode has a fixed geometric standard deviation but a changeable particle geometric mean dry diameter. When

microphysical processes (coagulation, condensational growth and in-cloud processing) act to exceed the geometric mean dry diameter above the upper size limit of the respective mode, particle number and mass are transferred between the modes.

Microphysical processes include the new particle formation in the boundary layer and free troposphere, ageing of insoluble to soluble aerosol particles through condensational ageing, as well as complete removal of aerosol particles via wet and dry deposition processes. Figure 2.1 presents a summary of the microphysical processes in GLOMAP-mode that govern aerosol size distributions, composition and lifetime.

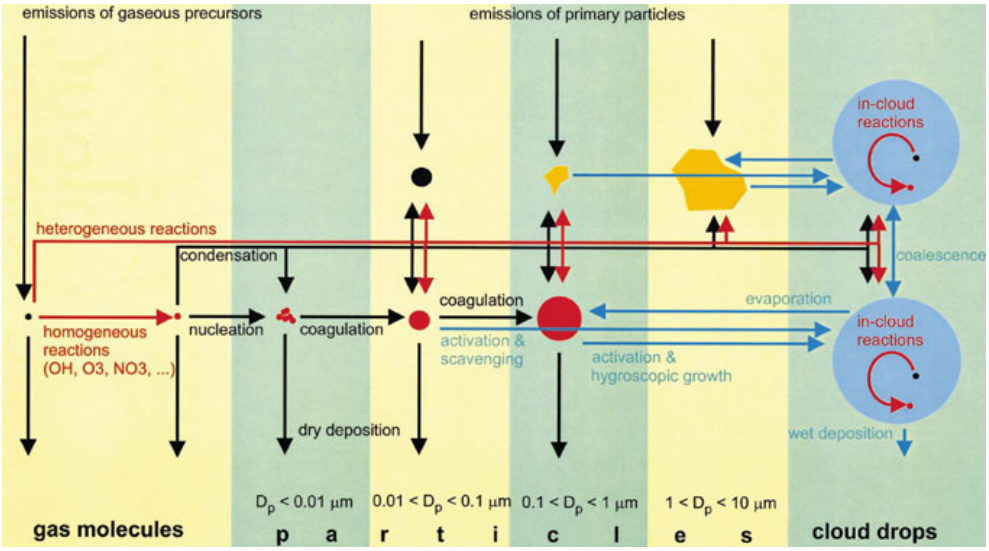

FIGURE 2.1: Summary of microphysical processes that control atmospheric aerosol size distributions, lifetime and chemical composition. Figure taken from Raes et al., 2000.

New particle formation

New particle formation through the nucleation of new particle clusters is simulated in GLOMAP-mode by the binary homogeneous nucleation of H_2SO_4–H_2O (Kulmala, Laaksonen, and Pirjola, 1998) in the free and upper troposphere and in the boundary layer (boundary layer nucleation) using an empirical mechanism (Kulmala, Lehtinen, and Laaksonen, 2006; Sihto et al., 2006). Binary homogeneous nucleation is the dominant source of new particles in the free and upper troposphere due to its preference for low temperature, high relative humidity, and low particle surface areas (Spracklen et al., 2005a; Spracklen et al., 2005c). However, boundary

layer nucleation is more important for new particle formation in remote continental locations (Spracklen et al., 2006).

Updated mechanisms for the formation of inorganic new particles have been made to TOMCAT-GLOMAP-mode coupled chemistry version used in Chapter 5. Here new particle formation is expressed as the sum of binary homogeneous nucleation (H_2SO_4–H_2O) and ternary sulfuric acid-ammonia-water (H_2SO_4–NH_3–H_2O) components, as described in Gordon et al., 2017. New particle formation from H_2SO_4 with oxidation products of monoterpenes with the hydroxyl radical (OH) has also been included in this version of the model (Riccobono et al., 2014).

Coagulation

Coagulation is the process by which aerosol particles can collide due to random motions and coalesce to form larger particles resulting in less numerous particle numbers. Using a mass conserving scheme Seinfeld and Pandis, 1998, GLOMAP-mode simulates coagulation through Brownian diffusion (i.e., random motion of particles) of both intra-modal collisions of particles in the same mode and inter-modal collisions of particles between different modes (Mann et al., 2010; Spracklen et al., 2005a). Coagulation is an important mechanism for the growth of sub-micron particles in the nucleation and Aiken size ranges, due to the random Brownian motion of particles within these size ranges.

Condensation

In GLOMAP-mode, oxidants react with SO_2 and monoterpenes (at reaction rates for α–pinene) to produce low volatility oxidation products H_2SO_4 and gaseous secondary organic vapour from a 13% production yield (Table 2.2). These vapours have the ability to condense onto all pre-existing particles acting not only as a condensational sink for these low volatility vapours, but acting to increase the size and mass

of existing particles without changing overall number concentrations. The nucleation of new particles and potential for condensational growth are in direct competition, as the existence of particle surface areas act as a condensational sink limiting the available low volatility vapours for nucleation events. The condensation of low volatility soluble vapours can also age insoluble aerosol particles into soluble modes thus influencing time-scales for wet deposition.

Cloud processing

In GLOMAP-mode, cloud processes are simulated by the growth of aerosol particles as water droplets and the aqueous phase oxidation of SO_2 in non-precipitating clouds. This process leads to a gap in the growth of activated and non-activated aerosol particles, resulting in a minimum in the particle size distribution, which defines both the Aitken and accumulation modes (i.e., 'Hopple gap') (Hoppel et al., 1994). For HadGEM3-UKCA, information on low-level cloud liquid water path are taken from the coupled climate model, whereas they are taken from off-line ISCCP-D2 data (Rossow and Schiffer, 1999) in the TOMCAT-GLOMAP-mode configuration. Following Spracklen et al., 2005b, cloud processing of aerosol in GLOMAP-mode is determined using a global uniform activation dry radius (defined as the smallest particles activated to cloud droplets) of 37.5 nm corresponding to a stratocumulus cloud supersaturation of 0.2% for H_2SO_4.

Dry deposition

The removal of atmospheric aerosol by dry deposition processes in GLOMAP-mode is parameterised using the scheme of Zhang et al., 2001, which represents gravitational settling, Brownian diffusion, impaction interception of the surface, and particle rebound of the surface. The particle sizes, underlying land surface type (i.e. forest, ocean, ice) and wind speed determine the deposition velocity. In general, dry deposition velocity is less efficient for particles of an intermediate size ranges (i.e. 100 nm to 1 μm in diameter), leading to the accumulation of accumulation mode

size aerosol particles. Dry deposition velocities on the other hand, are more efficient for larger size particles through gravitational settling processes, as well as for smaller size particles through diffusion to the surface.

Wet deposition

The wet removal of atmospheric aerosol is treated in GLOMAP-mode through in-cloud nucleation scavenging (i.e. the rain-out of aerosol after the formation of a water droplet around an activated aerosol particle) and below-cloud impaction scavenging (i.e. washout of aerosol particles by falling rain drops). Removal is simulated for both large-scale and convective-scale precipitation events based on prescribed ECMWF reanalysis (i.e., TOMCAT-GLOMAP-mode configuration) or nudged climate model (i.e., HadGEM3-UKCA). For large-scale precipitation events, all in-cloud activated particles in the soluble accumulation and coarse modes are removed at a constant rate in the cloudy fraction of grid boxes containing precipitating clouds. However, for sub-grid convective precipitation events, in-cloud nucleation scavenging of aerosol is assumed to occur in 30% of the model grid box. For both large scale and convective precipitation events, GLOMAP-mode removes aerosol particles at a rate proportional to the amount of condensed water converted to rain. For removal of aerosol through below-cloud impaction scavenging, GLOMAP-mode uses a raindrop aerosol collection efficiency lookup table based on geometric mean dry radius of mode and raindrop size distribution (Sekhon and Srivastava, 1971).

2.4 Off-line radiative transfer model

In chapter 4 (TOMCAT-GLOMAP-mode configuration), the Edwards and Slingo, 1996 off–line radiative transfer model is used to quantify the radiative effects of aerosol. The radiative transfer model uses nine radiation bands in the longwave

(LW) and six bands in the shortwave (SW), together with monthly-mean climatologies of water vapour, temperature and O_3 based on ECMWF re-analysis. Information on surface albedo and climatological clouds is also provided by the ISCCP-D2 dataset.

Following Rap et al., 2013, the aerosol direct effect (DRE) is calculated by the difference in net (SW and LW) top of atmosphere (TOA) all-sky radiative flux between a control unperturbed and perturbed TOMCAT-GLOMAP-mode simulation. For each spectral band and aerosol mode, aerosol optical properties are calculated as described in Bellouin et al., 2013. Optical properties are the specific scattering and absorption coefficients, which calculates the magnitude of scattering and absorption per unit aerosol mass, and the dimensionless asymmetry parameter, describing the angular dependence of the scattering (Bellouin et al., 2013). he quantification of DRE here is based under the unrealistic assumption that BC is internally or homogeneously mixed with scattering aerosol species (i.e. does not account for different BC optical mixing states), providing an upper bound for BC DRE (Kodros et al., 2015; Jacobson, 2001). Additionally, DRE calculated here does not account for light absorbing effect of brown carbon, which is thought to be important for absorption at visible to ultraviolet wavelengths (Sun, Biedermann, and Bond, 2007).

To determine the first aerosol indirect effect (AIE) or cloud albedo effect, the contribution of aerosol concentrations to cloud droplet number concentrations (CDNC) needs to be calculated. The maximum supersaturation (SS_{max}) of an ascending cloud parcel depends on the competition between increasing water vapour saturation with decreasing pressure and temperature, and the loss of water vapour through condensation onto activated particles. CDNC are calculated here using a physically based method based on the scheme of Nenes and Seinfeld, 2003, which has been evaluated previously in GLOMAP (Pringle et al., 2009). For a given updraught velocity, monthly mean aerosol size distributions are converted to a supersaturation distribution where the number of activated particles can be determined for SS_{max}. Here, CDNC are calculated in a post-processing procedure in all model grid boxes (and at all levels) using a constant up-draught velocity of 0.15 ms^{-1} over the ocean and 0.2

ms^{-1} over the land, consistent with observations of low-level stratus and stratocumulus clouds (Pringle et al., 2012). While up-draught velocities will vary substantially at such locations, the use of average velocities in previous GLOMAP studies have shown to capture observed relationships between particle number and CDNC (Pringle et al., 2009), as well as reproducing realistic CDNCs (Merikanto et al., 2010). For calculating AIE (see below), a cloud mask from ISCCP data are used, and only CDNDs for low-level clouds (i.e., below 600 hPa) are considered.

Following previous methodologies (Scott et al., 2014; Schmidt et al., 2012; Spracklen et al., 2011b), AIE is calculated assuming fixed water content where a control uniform cloud droplet effective radius re_1 = 10 μm is assumed to maintain consistency with the ISCCP derivation of liquid water path:

$$re_2 = re_1 \times \left[\frac{CDNC_1}{CDNC_2}\right]^{\frac{1}{3}}$$

where $CDNC_1$ represents a control unperturbed simulation (e.g. with residential emissions) and $CDNC_2$ represents a perturbed simulation (e.g. without residential emissions). The AIE is calculated by comparing the net TOA radiative fluxes using the different re_2 values derived for each perturbation experiment, to that of the control where re_1 is fixed.

2.5 Simulating $PM_{2.5}$ concentrations

The mass of particles with a median aerodynamic dry diameter of < 2.5 μm ($PM_{2.5}$) is strongly associated with mortality and morbidity epidemiological evidence and thus is used in air quality health burden assessments. In this thesis, $PM_{2.5}$ concentrations from GLOMAP-mode output are calculated in a post processing procedure based on a mathematical function that calculates the cumulative of a log-normal distribution up to a specific radius (i.e. 1.25 μm for $PM_{2.5}$). Using this function, the mass fraction of particles at or below a median aerodynamic dry diameter of < 2.5 μm ($PM_{2.5}$) can be calculated and summed over all aerosol modes. Calculation of

the mass of water associated with individual aerosol components under specific relative humidities (RH) can also be quantified, which is useful for comparing to $PM_{2.5}$ measurements under certain RH conditions. Here, a hygroscopicity parameter k is assigned to individual components in soluble modes to estimate the mass of water associated.

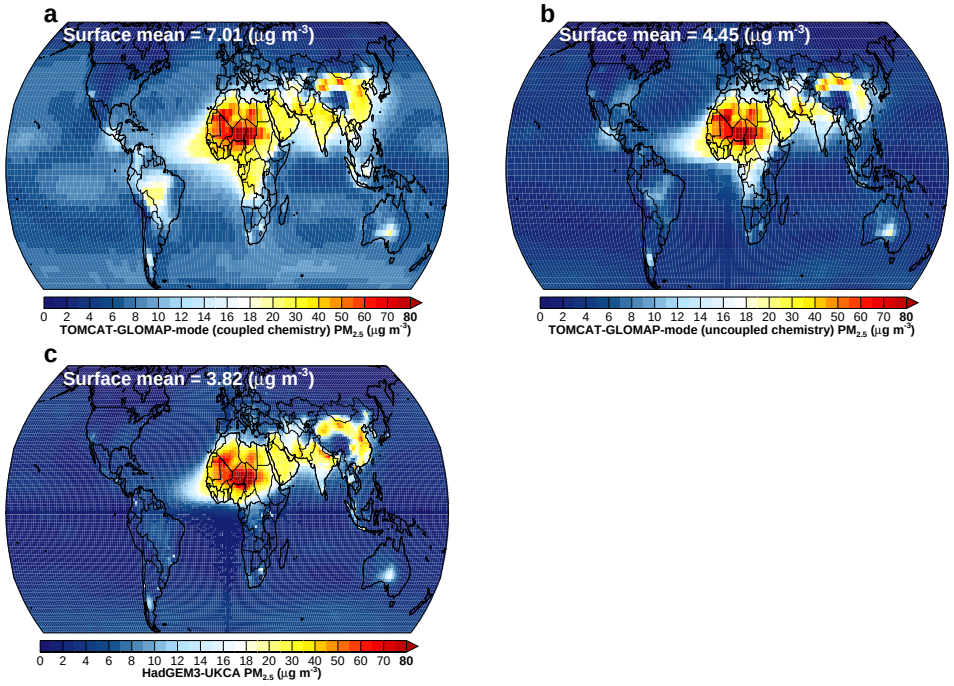

FIGURE 2.2: Annual mean surface $PM_{2.5}$ concentrations in the present-day from TOMCAT-GLOMAP-mode (coupled chemistry) in year 2015 **a**, TOMCAT-GLOMAP-mode (uncoupled chemistry or prescribed oxidants) in year 2000 **b**, and HadGEM3-UKCA in year 2008 **c**.

The use of GLOMAP-mode within the different model configurations used in this thesis makes it hard to compare the magnitude of differences in simulated PM $PM_{2.5}$ concentrations as shown in Figure 2.2. Differences likely stem from a number of different reasons such as spatial resolution used, chemical scheme, anthropogenic and natural emissions and meteorological year used, as well as other structural differences.

Table 2.6 summarises some of the key differences between model configurations that likely contribute to differences in simulated surface $PM_{2.5}$ concentrations 2.2. The use of a higher spatial resolution in HadGEM3-UKCA leads to noticeable $PM_{2.5}$ 'hotspots' or plumes over heavily urbanised areas, which cannot be resolved under

the relatively coarse resolution of TOMCAT-GLOMAP. Elevated $PM_{2.5}$ concentrations over the oceans in the TOMCAT-GLOMAP (coupled chemistry) configuration are more apparent than in the other two model configurations, which contributes to the larger mean surface $PM_{2.5}$ estimate of 7.01 $\mu g\ m^{-3}$. Elevated $PM_{2.5}$ over the oceans in this model configuration is due to a more robust representation of submicron sea salt particles using a parametrisation more consistent with observations (Mårtensson et al., 2003). Organic aerosol is an important constituent of $PM_{2.5}$ and differences in the assumed ratio of OC:POM can lead to noticeable differences in simulated concentrations. For example, the use of a larger ratio of 2 in the TOMCAT-GLOMAP (coupled chemistry) configuration is responsible for a large proportion of elevated $PM_{2.5}$ concentrations in biomass combustion regions (e.g. wildfire regions of the Amazon, Congo basin and South East Asia, and residential and agricultural biomass burning regions of India and China).

	HadGEM3-UKCA (Chapter 3)	TOMCAT-GLOMAP (Chapter 4)	TOMCAT-GLOMAP (Chapter 5)
Spatial resolution	1.875° × 1.25°	2.8° × 2.8°	2.8° × 2.8°
Sea salt	Gong, 2003 parametrisation	Gong, 2003 parametrisation	Mårtensson et al., 2003 parametrisation
OC:POM ratio	1.4	1.4	2
Meteorology	2008	2000	2015
Anthropogenic emissions	2008, MACCity	2000, ACCMIP	2015, ECLIPSE

TABLE 2.6: Summary of the key difference between the model configurations that likely contribute to differences in simulated surface $PM_{2.5}$ concentrations reported in Figure 2.2. TOMCAT-GLOMAP in Chapter 4 refers to the prescribed oxidant configuration, while TOMCAT-GLOMAP in Chapter 5 refers to the coupled chemistry configuration.

2.6 Perturbed Parameter Ensemble

In Chapter 3, a perturbed parameter ensemble (PPE) is used (Lee et al., 2011; Regayre et al., 2018) to explore the uncertainty in simulated $PM_{2.5}$ concentrations from HadGEM3-UKCA CCM (see Appendix A for further details). The PPE used in Chapter 3 represented 235 simulations from a separate group of HadGEM3-UKCA runs for the year 2008 where 26-related parameters are perturbed simultaneously (Yoshioka, 2017). In brief, the PPE approach uses expert elicitation and statistical sampling methods such as Latin hypercube sampling to produce a large number of variations

of one model to represent the full parametric uncertainty space of simulated output variables (e.g., $PM_{2.5}$ concentrations). Latin hypercube sampling is key to the PPE because it stratifies uncertainty among input parameters so that sampling can cover the full parametric uncertainty space with a limited sample size, which means a reduced number of simulations are required compared to a more common Monte Carlo sampling approach.

2.7 Calculating the attributable burden of disease to $PM_{2.5}$ exposure

Estimating the burden of disease attributable to long-term $PM_{2.5}$ exposure are similar to those employed by the GBD CRA (e.g. Lim et al., 2012; Gakidou et al., 2017). Estimating the health burden due to ambient $PM_{2.5}$ exposure requires an understanding of three key factors; 1) population-level $PM_{2.5}$ exposure distributions, 2) exposure-response relationships together with theoretical minimum risk exposure levels (TMREL, below which no risk is assumed), and 3) demographic and background disease characteristics.

2.7.1 $PM_{2.5}$ exposure distribution

The $PM_{2.5}$ exposure distributions used in the GBD CRA are taken from gridded surface estimates based on combining CTM modelling, ground measurements and satellite retrievals of AOD (e.g. Brauer et al., 2015; Van Donkelaar et al., 2010; Shaddick et al., 2018). In this thesis, $PM_{2.5}$ exposure distribution estimates are taken from GLOMAP-mode, as well as the satellite based estimates used in the GBD. As in the GBD CRA and other health burden assessments, annual mean surface concentrations of ambient $PM_{2.5}$ are assumed a proxy for long-term personal exposures.

2.7.2 Exposure-response relationships

To translate a health outcome or risk in a population given a level of $PM_{2.5}$ exposure, knowledge of the exposure-response relationship and TMREL is required. Exposure-response relationships usually take the form of relative risk (RR) estimates based on epidemiological evidence from prospective cohort studies. RR is expressed as the ratio of the probability of cumulative incidences for disease mortality in an exposed population π_1 over the probability of cumulative incidences in an unexposed population π_2 over an observation period:

$$RR = \frac{\pi_1}{\pi_2}$$

After controlling for other individual confounder risk factors, RR represents the differences in population level health outcomes due to differences in $PM_{2.5}$ exposure levels, with risk being limited to above the lowest measured exposure distribution among cohort studies (e.g., TMREL).

Two different types of exposure-response relationship are used in this thesis (see Table 2.7), representing old and new generation relationships. The two relationships chart the improvement in scientific understanding regarding the estimated $PM_{2.5}$ exposure-response over the past few years.

The older relationship, typically used before GBD CRA 2010 (Lim et al., 2012), is based entirely on ambient air quality prospective cohort studies from North America and Western Europe. However, because $PM_{2.5}$ concentrations rarely exceeded 30 μm^{-3} across these regions, older relationships employed linear or log-linear functions to estimate excess risk at high exposure distributions more typical of low and middle-income countries with poor ambient air quality (e.g., India and China where cohort studies do not exist) (Cohen et al., 2004; Ostro and WHO, 2004). Thus, risk estimates at concentrations typically above 30 μm^{-3} were dependant on the extrapolation model (e.g., linear or log-linear), which are not constrained by observations. Following (Ostro and WHO, 2004; Schmidt et al., 2011), a log-linear exposure-response relationship is used in Chapter 4 of this thesis.

	HadGEM3-UKCA (Chapter 3)	TOMCAT-GLOMAP (Chapter 4)	TOMCAT-GLOMAP (Chapter 5)
Exposure-response relationship	IER_1	Log-linear	IER_2

TABLE 2.7: Summary of exposure-response relationships used in each thesis Chapter and model configuration. 'IER' represents integrated exposure-response and the subscript indicates different versions used. TOMCAT-GLOMAP in Chapter 4 refers to the prescribed oxidant configuration, while TOMCAT-GLOMAP in Chapter 5 refers to the coupled chemistry configuration.

There are a number of limitations and concerns associated with the use of older generation relationships similar to the log-linear approach used in Chapter 4. Most are concerned with the risk of simulating implausible and biologically inconsistent risk estimates at high exposure distributions not constrained by epidemiological evidence (Ostro et al., 2018).

To overcome this limitation, researchers looked to combine observed epidemiological risks from high exposure distribution activities such as active tobacco and passive (second hand) smoking (Pope III et al., 2011, e.g.,). Following this body of research, integrated exposure-response (IER) relationships were developed that could, for the first time, predict observationally-constrained risk estimates for the entire global range of ambient $PM_{2.5}$ exposures (Burnett et al., 2014). The IER works by compiling observed risks from different epidemiological prospective cohort studies and randomised control trials of different combustion sources, including ambient air pollution, household air pollution (HAP) from solid fuel combustion, second-hand (passive) tobacco smoke, and active tobacco smoking. The IER relationship is thus far more superior than the older generation relationships (e.g., log-linear relationship) (Ostro et al., 2018).

In addition, the IER predicts a greater number of individual cause-specific diseases than older generation relationships that have been deemed consistent with causal relationships: ischaemic heart disease (IHD), cerebrovascular disease (ischaemic stroke and haemorrhagic stroke; CEV), lung cancer, chronic obstructive pulmonary disease (COPD), and lower respiratory infections (LRI).

Two different versions of the IER are used in this thesis (see Table 2.7 and Figure

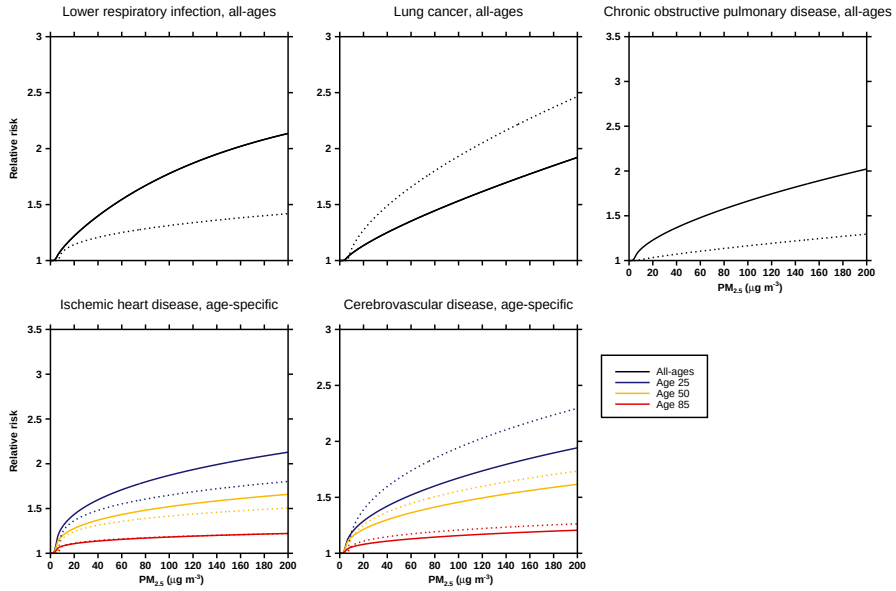

FIGURE 2.3: Integrated-exposure response relationships used to relate $PM_{2.5}$ exposure to cause-specific diseases endpoints: all-ages lower respiratory infections, lung cancer, chronic obstructive pulmonary disease, and age-specific ischaemic heart disease and cerebrovascular disease (ischaemic stroke and haemorrhagic stroke). Solid lines represent the up-to-date IER version used in Chapter 5, whereas the dotted lines represent the an older IER version used in the Chapter 4.

2.3). The differences between the two versions represent the greater inclusion of epidemiological evidence in recent years. For example, the more up-to-date version of the IER used in Chapter 5 includes data from many more prospective cohort studies compared to the older version used in Chapter 3. In addition, the up-to-date version includes a lower TMREL due to the inclusion of a greater number cohort studies in very clean regions. Figure 2.3 show a comparison of the two IER versions. In general, IER curves are non-linear, with reduced sensitivity to changes in $PM_{2.5}$ at higher concentrations, particularly for cardiovascular diseases (IHD and CEV). Age-specific cardiovascular RRs also show a decline with age as supported by health evidence (Singh et al., 2013). Health assessments employing different versions of the IER or altogether different exposure-response relationships, make comparisons between health burden estimates difficult (Ostro et al., 2018).

2.7.3 Calculating attributable deaths

Once an appropriate exposure-response relationship is selected, the number of deaths attributable to long-term $PM_{2.5}$ exposure can be quantified. Following GBD CRA methods, the number of attributable deaths for a given year, country, sex and cause-specific disease, can be estimated using the population attributable fraction (PAF):

$$PAF = \frac{P_{fage}(RR_{age} - 1)}{P_{fage}(RR_{age})}$$

where RR_{age} is the all-age or age-specific IER-derived RR estimate derived from country-level population-weighted $PM_{2.5}$ concentrations and P_{fage} is the fraction of the age-group population of interest. Total attributable deaths or mortality ($Mort_{PM_{2.5}}$) are then calculated by multiplying the (PAF) by the annual total age and cause-specific background disease mortality $Mort_{background_{age}}$:

$$Mort_{PM_{2.5}} = PAF \times Mort_{background_{age}}$$

Attributable disease burden (deaths) can either be calculated at the national or country-level using population-weighted $PM_{2.5}$ concentrations (Chatper 5) or calculated on the grid-level (Chapter 3 and 4) using grid-level $PM_{2.5}$ concentrations. Both methods produce very similar burden results at the national-level.

2.7.4 Demographic and disease data

Subject to the aim of the research study, different combinations of demographic and background disease data have been used to estimate attributable health burdens. Table 2.8 reports the different data sources used in each thesis Chapter.

The Gridded Population of the World (GPW) dataset (CIESIN, 2005; Doxsey-Whitfield et al., 2015) are used to estimate the total number of people exposed to ambient $PM_{2.5}$ spatially (Figure 2.4). The GPW dataset is generated by collecting detailed spatial resolution data from the most available rounds of population and housing censuses and extrapolating them to produce gridded estimates for different years (typically

	HadGEM3-UKCA (Chapter 3)	TOMCAT-GLOMAP (Chapter 4)	TOMCAT-GLOMAP (Chapter 5)
Gridded population	GPW	GPW	GPW and IFs
Background disease	IHME	UN	IHME and IFs
Age-group estimates	UN	UN	IFs

TABLE 2.8: Summary of the differences in the demographic and background disease data used in each thesis Chapter. 'GPW' represents Gridded population of the World dataset, 'IHME' represents Institute Health Metrics and Evaluation data, 'UN' United Nations, and 'IFs' represents the International Futures socio-economic modelling system. TOMCAT-GLOMAP in Chapter 4 refers to the prescribed oxidant configuration, while TOMCAT-GLOMAP in Chapter 5 refers to the coupled chemistry configuration.

at 5-year intervals). Information on age-group structures used to estimate the faction of the population within specific age-groups are taken from either the United Nations (UN) Population Division estimates (https://esa.un.org/unpd/wpp/) or from Institute Health Metrics and Evaluation (IHME) (Health Metrics and (IHME), 2015). Estimates of cause-specific background disease data are taken from the cause of disease the IHME (Health Metrics and (IHME), 2015), which use statistical and analytical methods to redistribute modelled or reported deaths by their probable underlying causes.

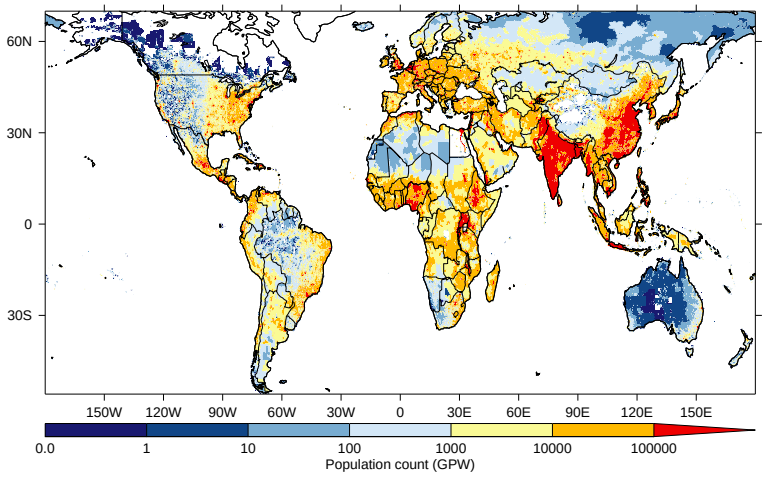

FIGURE 2.4: Gridded population count data for the year 2015 taken from the Gridded Population of the World (GPW) dataset. Spatial resolution is on 15 arc-minute (0.25 degree) grid.

The data described above represents historical estimates. However, for the study design in Chapter 5, estimates of demographic and background disease in the year 2050 were required. Here, the International Futures (IFs) socio-economic modelling system (Hughes et al., 2011) was used. The IFs model draws on drivers of health and

population, including demographic, economic, educational, socio-political, agricultural and environmental to forecast estimates into the future. The model is initialised with present-day conditions (based on UN and IHME estimates) and is run under a future base case scenario where present-day dynamic patterns and relationships relating to demographic and disease outcomes continue to unfold and evolve to 2050. IFs forecasts were obtained through the downloadable model version v7.31 (https://pardee.du.edu/access-ifs).

2.8 Thesis experiments

Table 2.9 summarizes the different experiments presented in this thesis. Using time varying emissions from the MACCity emission inventory together with HadGEM3-UKCA model (Turnock et al., 2015), the experiment presented in Chapter 3 investigates the global and regional health burden impacts due to changes in ambient $PM_{2.5}$ concentrations over the past 50 years (e.g., period 1960 to 2009). In Chapter 4, the TOMCAT-GLOMAP configuration (with prescribed oxidants) was used with anthropogenic emissions from the MACCity and ACCIMP inventories to examine the present-day (year 2000) impact of small-scale residential combustion activities (e.g., cooking and heating with solid fuels) on atmospheric aerosol and climate and $PM_{2.5}$ air quality on human health. Finally in Chapter 5, the TOMCAT-GLOMAP configuration (with coupled chemistry) with anthropogenic emissions from the ECLIPSE emission inventory was used to examine $PM_{2.5}$ air quality and health burden impacts in the year 2050 and the potential for clean residential combustion technologies (e.g., widespread implementation of clean cookstoves) to avoid impacts.

	Chapter 3	Chapter 4	Chapter 5
Experiment description	Examining changes in $PM_{2.5}$ and associated health impacts from 1960 to 2009.	Examining the impact of residential combustion emissions in the present-day on atmospheric aerosol, climate and health.	Investigating $PM_{2.5}$ and health impacts in 5050 and potential benefits of clean combustion measures (e.g., clean cookstoves)
Model configuration	HadGEM3-UKCA	TOMCAT-GLOMAP, prescribed oxidants	TOMCAT-GLOMAP, coupled chemistry
Simulation period	1960 to 2009	2000	2015 to 2050

TABLE 2.9: Summary of the different experiments presented in this thesis.

Chapter 3

Global and regional trends in particulate air pollution and attributable health burden over the past 50 years

Environmental Research Letters

LETTER

Global and regional trends in particulate air pollution and attributable health burden over the past 50 years

E W Butt[1,4], S T Turnock[2], R Rigby[1], C L Reddington[1], M Yoshioka[1], J S Johnson[1], L A Regayre[1], K J Pringle[1], G W Mann[3] and D V Spracklen[1]

[1] School of Earth and Environment, University of Leeds, Leeds, United Kingdom
[2] Met Office Hadley Centre, Fitzroy Road, Exeter, Devon, United Kingdom
[3] National Centre for Atmosphere Science, University of Leeds, Leeds, United Kingdom
[4] Author to whom any correspondence should be addressed.

E-mail: e.butt@leeds.ac.uk

OPEN ACCESS

RECEIVED
11 July 2017

ACCEPTED FOR PUBLICATION
23 August 2017

PUBLISHED
18 October 2017

Keywords: $PM_{2.5}$, emissions, historical, health burden, attributable deaths

Supplementary material for this article is available online

Abstract

Long-term exposure to ambient particulate matter ($PM_{2.5}$, mass of particles with an aerodynamic dry diameter of < 2.5 μm) is a major risk factor to the global burden of disease. Previous studies have focussed on present day or future health burdens attributed to ambient $PM_{2.5}$. Few studies have estimated changes in $PM_{2.5}$ and attributable health burdens over the last few decades, a period where air quality has changed rapidly. Here we used the HadGEM3-UKCA coupled chemistry-climate model, integrated exposure-response relationships, demographic and background disease data to provide the first estimate of the changes in global and regional ambient $PM_{2.5}$ concentrations and attributable health burdens over the period 1960 to 2009. Over this period, global mean population-weighted $PM_{2.5}$ concentrations increased by 38%, dominated by increases in China and India. Global attributable deaths increased by 89% to 124% over the period 1960 to 2009, dominated by large increases in China and India. Population growth and ageing contributed mostly to the increases in attributable deaths in China and India, highlighting the importance of demographic trends. In contrast, decreasing $PM_{2.5}$ concentrations and background disease dominated the reduction in attributable health burden in Europe and the United States. Our results shed light on how future projected trends in demographics and uncertainty in the exposure–response relationship may provide challenges for future air quality policy in Asia.

1. Introduction

Long-term exposure to ambient concentration of particles withan aerodynamic dry diameter of < 2.5 μm ($PM_{2.5}$) is associated with mortality and morbidity and shortens life expectancy (Dockery *et al* 1993, Pope and Dockery 2006, Pope *et al* 1995). It is estimated that ~87% of the global population live in areas exceeding the World Health Organisation's (WHO) air quality guidelines for annual mean ambient $PM_{2.5}$ (10 μg m^{-3}) (Apte *et al* 2015). Recent assessments of the Global Burden of Disease (GBD) estimate that exposure to ambient $PM_{2.5}$ is a major contributing risk factor to regional and global burden of disease (Forouzanfar *et al* 2016, Forouzanfar *et al* 2015, Lim *et al* 2013).

Previous studies have reported present day and future (Lelieveld *et al* 2015, Silva *et al* 2016b) attributable health burdens assessments. Few studies have estimated changes in $PM_{2.5}$ attributable health burdens over the last few decades (e.g. Wang *et al* 2017), a period where widespread implementation of air quality regulation and emission controls in North America and Europe coincided with extensive economic growth and limited emission controls across Asia. Over Europe and the United States, emissions of sulphur dioxide (SO_2) have decreased by more than 70% over the last few decades (Leibensperger *et al* 2012, Vestreng *et al* 2007), resulting in substantial reductions in $PM_{2.5}$ concentrations (Leibensperger *et al* 2012, Tørseth *et al* 2012, Turnock *et al* 2015). In contrast, SO_2 emissions over Asia have increased by a

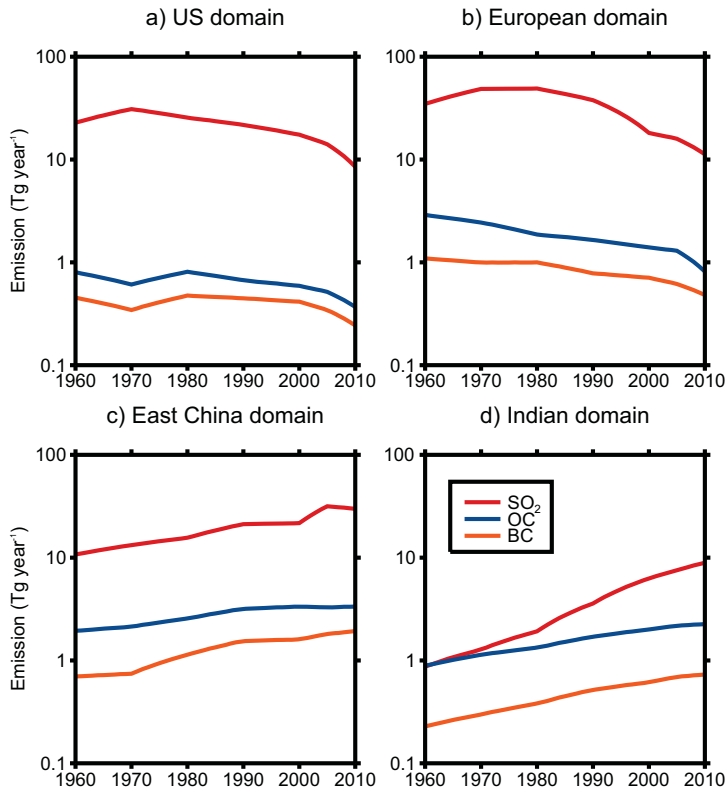

Figure 1. Annual emissions (Tg yr^{-1}) of sulfur dioxide (SO_2), organic carbon (OC) and black carbon (BC) from the MACCity emission inventory for the period 1960 to 2010. Regional domains (identified in figure S1) for (*a*) US (United States), (*b*) Europe, (*c*) East China and (*d*) India.

factor of 7 between 1960 and 2005 (Smith *et al* 2011), resulting in increased $PM_{2.5}$ concentrations (Brauer *et al* 2015). Understanding these historical changes in $PM_{2.5}$ concentrations and attributable burdens across these regions is vital to inform future air quality policy design.

Estimating the health burden attributable to long-term exposure to $PM_{2.5}$ requires an understanding of the exposure-response relationship, an accurate representation of $PM_{2.5}$ concentrations and demographic and background disease trends. $PM_{2.5}$ concentrations can be simulated using global chemical transport models (Anenberg *et al* 2010, Lelieveld *et al* 2013, Silva *et al* 2016a), or through a combination of modelling, satellite remote sensing data, ground-based observations, and land-use regression (Brauer *et al* 2012, Brauer *et al* 2015, Jerrett *et al* 2016, van Donkelaar *et al* 2010). Global health assessments (Forouzanfar *et al* 2016, Forouzanfar *et al* 2015, Lim *et al* 2013, Wang *et al* 2017) are restricted to the last few decades (1990 onwards), when satellite and ground-based observations are typically available. For this reason, little is known about how $PM_{2.5}$ attributable burden changed prior to 1990. Here we combine a global climate model, with exposure-response relationships, demographic and background disease data to provide the first estimate of the changes in global and regional $PM_{2.5}$ attributable health burdens over the period 1960 to 2009.

2. Methods

2.1. $PM_{2.5}$ concentrations

We used the coupled chemistry–climate model HadGEM-3-UKCA, known hereafter as 'UKCA', to simulate $PM_{2.5}$ concentrations for the period 1960 to 2009. We use the same model setup described in detail in Turnock *et al* (2015) with a horizontal resolution of 1.875° × 1.25° (approximately 140 km at mid latitudes). Meteorological fields were nudged at 6 h intervals to the European Centre for Medium-Range Weather Forecasts Reanalysis (ERA-40) (Uppala *et al* 2005) for the years 1960 to 2000 and ERA-Interim (Dee *et al* 2011) for 2001 to 2009.

UKCA simulates sulfate (SO_4), black carbon (BC), organic carbon (OC) and sea salt aerosol in five log-normal modes (four soluble modes and one insoluble Aitken mode) (Mann *et al* 2010) (see supplementary information (SI) 1.1 available at stacks.iop.org/ERL/12/104017/mmedia). Monthly mean anthropogenic emissions of CO, SO_2, NO_x, OC and BC from 1960 to 2009 are taken from the MACCity emission inventory (Granier *et al* 2011). Figure 1 shows the 1960 to 2010 trends in SO_2, BC and OC. Emissions in Europe and the United States (US) have declined from a maximum in the 1970s due to the implementation of air quality regulation and emission controls, while emissions have increased substantially in China and India. SO_2 emissions in the region of East China

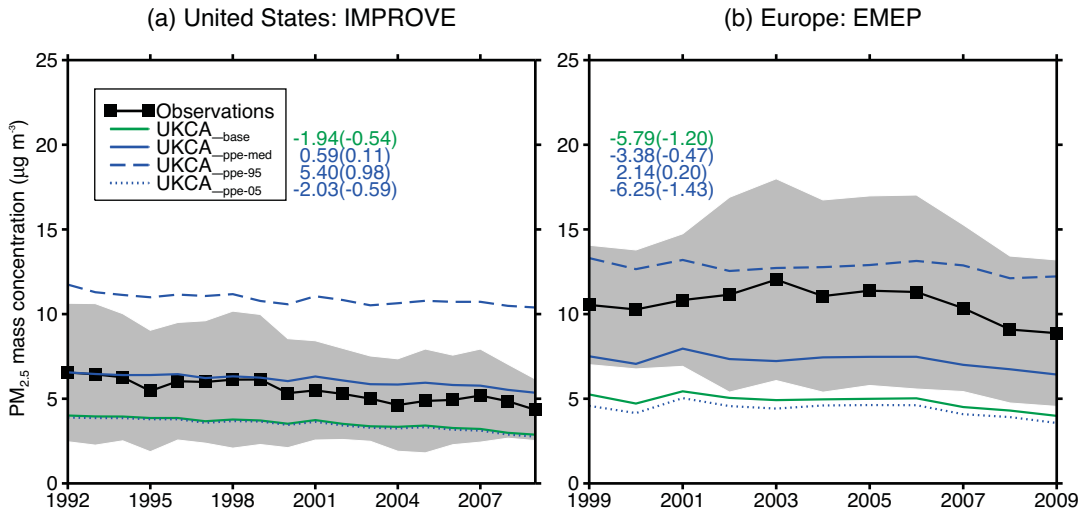

Figure 2. Average annual mean $PM_{2.5}$ concentrations at (*a*) IMPROVE sites in the United States and (*b*) EMEP sites in Europe. Measured concentrations (black line with filled squares, shading represents standard deviation of annual mean concentrations across all sites) are compared to simulated concentrations from the baseline of UKCA (green lines) and UKCA-PPE estimates (blue lines). The mean bias ($\mu g\ m^{-3}$) and normalised mean bias factor (in brackets) for each UKCA simulation is shown on each panel in legend order.

in the 2000s were a similar magnitude to US emissions in the 1970s, but less than European emissions during the same period. Other emission sources are described in detail in Turnock *et al* (2015). Mineral dust concentrations are taken from a 10 year GLOMAP-mode climatology taken from Reddington *et al* (2015). We therefore assume no interannual variability or trends in dust over the study period. There is no representation of ammonium nitrate in this version of the model.

To account for uncertainty in $PM_{2.5}$ estimated by UKCA we used a perturbed parameter ensemble (PPE) of 235 UKCA simulations for the year 2008 where 26 aerosol related parameters were perturbed simultaneously. The PPE represents the aerosol parametric uncertainty in the model (see SI 1.3 and figure S2). We use the median value of $PM_{2.5}$ simulated across the PPE as our best estimate of PM2.5 and the 5th and 95th percentile values as an indication of uncertainty in our estimate. We increment the baseline model ($UKCA_{\_base}$) by the absolute difference in the year 2008 between the baseline and the median ($UKCA_{\_ppe-med}$), 5th ($UKCA_{\_ppe-05}$) and 95th ($UKCA_{\_ppe-95}$) percentile of the PPE (see SI 1.3 and figure S3). We assume that the same increment across the entire 1960 to 2009 simulation period.

We also used satellite-derived $PM_{2.5}$ estimates (Brauer *et al* 2015) known hereafter as 'GBD-PM'. This dataset provides annual mean $PM_{2.5}$ concentrations at $0.1° \times 0.1°$ horizontal resolution for the period 1990 to 2010 at five year intervals. In this dataset, $PM_{2.5}$ is estimated through a $PM_{2.5}$ to aerosol optical depth (AOD) relationship using the GEOS-Chem model and satellite remote sensing products calibrated to ground-based measurements (Brauer *et al* 2015). This dataset was used in the GBD2013 (Forouzanfar *et al* 2015) and we use it compare with UKCA.

Figure 2 compares simulated $PM_{2.5}$ against measurements at surface sites in the US and Europe (see figure S1). In the US we use observations from the Interagency Monitoring of Protected Visual Environments (IMPROVE) and in Europe we use observations from the European Monitoring and Evaluation Programme (EMEP) network (see SI 1.2). There are few long-term observations of $PM_{2.5}$ outside of Europe and the US with which to evaluate UKCA. The baseline UKCA model ($UKCA_{\_base}$) underestimates observed concentrations in both Europe (normalised mean bias factor (NMBF) = −1.2) and the US (NMBF = −0.54). Similarly, Turnock *et al* (2015) found UKCA underestimated total suspended particles and PM_{10} observed over Europe using the same model setup. We find that $UKCA_{\_ppe-med}$ better matches observations in both Europe (NMBF = −0.47) and the US (NMBF = 0.11), The 5th to 95th percentile of the PPE brackets surface observations in both Europe and the US. We therefore report the results from these three simulations for the rest of the paper.

2.2. Background disease and demographic data

We used national level population and age group distribution data from the United Nations (UN) Population Division (UN 2015), which are available for the period 1960 to 2010 (see figure S3). We used gridded population from the Gridded Population of the World v3 (GPWv3) (CIESIN 2015), at a resolution of 2.5 arc-minutes for the period 1990 to 2010. We extrapolated the GPWv3 to 1960 applying the rate of change observed in the UN national level data (see SI 1.4).

We used age and cause-specific background disease data for the period 1980 to 2010 from the Institute for Health Metrics and Evaluation (IHME 2014). This

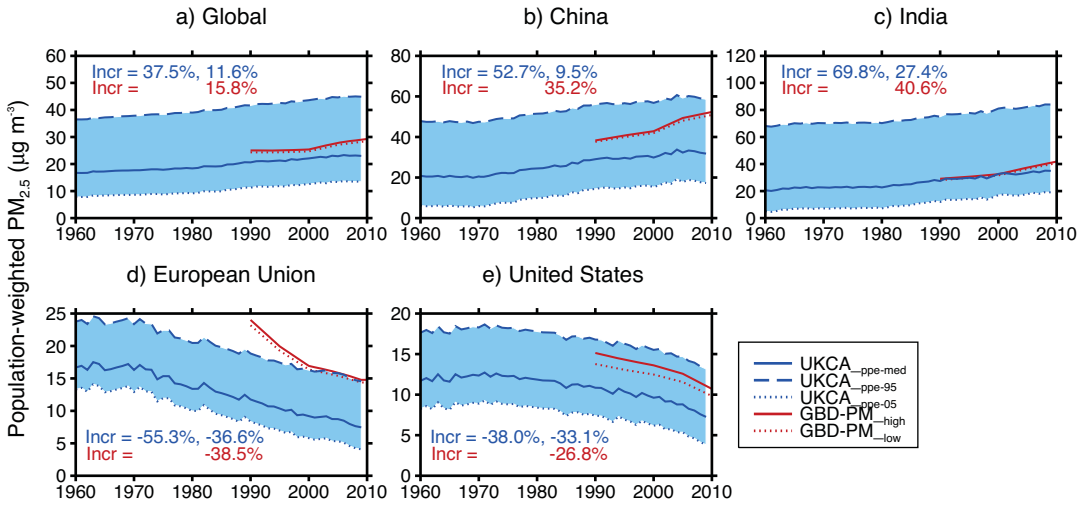

Figure 3. Annual mean population-weighted $PM_{2.5}$ concentrations for (*a*) global, (*b*) China, (*c*) India, (*d*) European Union and (*e*) United States. Regional values are reported for the shaded regions identified in figure S1. Percentage changes are shown for $UKCA_{\_ppe-med}$ (Incr = (2009−1960)/1960, (2009−1990)/1990 in blue) and $GBD\text{-}PM_{\_high}$ (Incr = (2009−1990)/1990 in red).

dataset provides national level background disease endpoint data for cardiovascular ischemic heart disease (IHD) and stroke (cerebrovascular disease), lung cancer (LungC), chronic obstructive pulmonary disease (COPD) and lower respiratory infections (LRI). Disease data is not available prior to 1980, so we take a conservative assumption and assume that background disease rates remain constant at 1980 levels. In a sensitivity study, we assume that background disease rates between 1960 and 1980 follow the same trend as that between the period 1980 to 1990 (see SI 1.4).

2.3. Attributable health burden calculation

We calculate relative risk (RR) due to long-term exposure to $PM_{2.5}$ using the integrated exposure-response (IER) relationship (Burnett *et al* 2014), which compiles epidemiological evidence across a wide range of $PM_{2.5}$ exposures from different combustion sources. The IER allows for age-dependent (i.e. ≥ 25 years of age at five year intervals to age 80+) calculation of RR for IHD and stroke, adult (≥ 25 years of age) for LC and COPD, and all ages for lower respiratory infections (LRI). We develop a lookup table compatible with the IER used in GBD2013 (Forouzanfar *et al* 2015) (see SI 1.5). This lookup table is provided in SI data 1. IER relationships are non-linear with respect to $PM_{2.5}$ exposure (figure S4), with reduced sensitivity of RR to $PM_{2.5}$ at higher concentrations (Pope *et al* 2009a, Pope *et al* 2011), particularly for IHD, stroke and LRI.

We use IER derived RRs to estimate attributable deaths at the grid cell level using attributable fraction type relationship described in Apte *et al* (2015) (see SI 1.5). Years of lost life (YLLs) are calculated by summing attributable deaths in each age group and multiplying by the associated expected life expectancy taken from the standard life table provide by Murray *et al* (2013). We estimate attributable deaths using $PM_{2.5}$ concentrations from UKCA for the period 1960 to 2009 and from GBD-PM for the period 1990 to 2010. We calculated attributable deaths at original resolution of the GBD-PM data (0.1° × 0.1°) ($GBD\text{-}PM_{\_high}$) and at the same resolution of UKCA (1.875° × 1.25°) ($GBD\text{-}PM_{\_low}$). We find that attributable deaths estimated using GBD-PM closely match GBD2013, within 3%–4% globally, with similar regional mortalities (Forouzanfar *et al* 2015). We also explored the relative contribution of estimated attributable deaths over the period 1980 to 2009 to changing $PM_{2.5}$ concentrations, population demographics and background disease (see SI 1.6).

3. Results and discussion

Figure 3 shows annual mean population-weighted $PM_{2.5}$ concentrations over the period 1960 to 2009. Population-weighted $PM_{2.5}$ concentrations simulated by the median PPE ($UKCA_{\_ppe-med}$) closely match those from GBD-PM over India but are lower in other regions. We explored whether the coarser spatial resolution of UKCA (1.875° × 1.25°) compared to $GBD\text{-}PM_{\_high}$ (0.1° × 0.1°) is responsible for this difference. When $GBD\text{-}PM_{\_high}$ (Brauer *et al* 2015) is averaged to the same spatial resolution as UKCA ($GBD\text{-}PM_{\_low}$), mean population-weighted $PM_{2.5}$ typically decreased by less than ~4% (~1 $\mu g\ m^{-3}$), showing that lower $PM_{2.5}$ concentrations simulated by $UKCA_{\_ppe-med}$ is not entirely due to the coarse resolution of UKCA. The upper ($UKCA_{\_ppe95}$) and lower ($UKCA_{\_ppe05}$) range of UKCA bracket values from GBD-PM, except over Europe.

During the period 1990 to 2009, global population-weighted $PM_{2.5}$ concentrations simulated by $UKCA_{\_ppe-med}$ increased by 11.6%, smaller than the 15.8% increase estimated by GBD-PM. At the

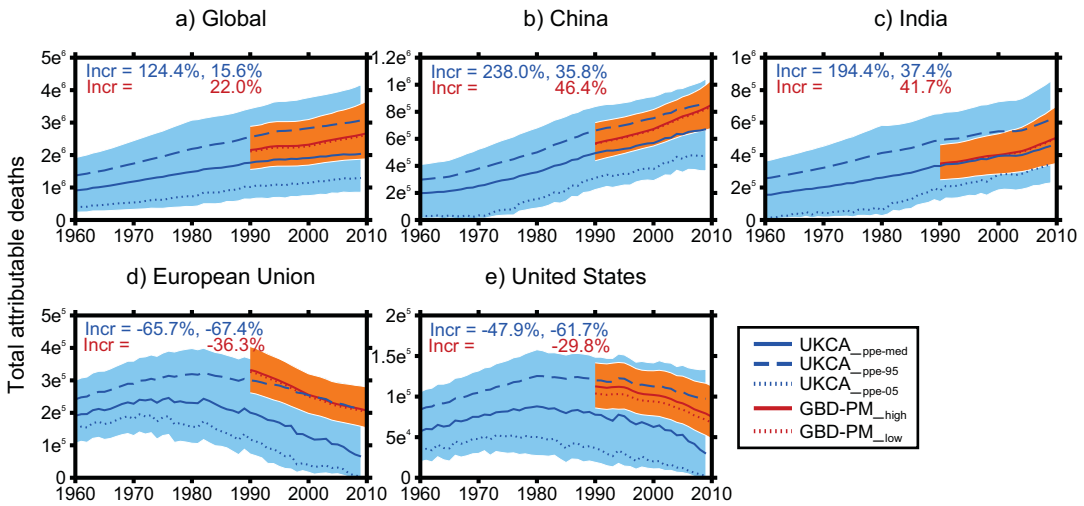

Figure 4. Annual total attributable deaths for (*a*) global, (*b*) China, (*c*) India, (*d*) European Union and (*e*) United States. Shaded areas represent upper and lower range of UKCA-PPE estimates (light blue) and GBD-PM (orange). Regional values are reported for the shaded regions identified in figure S1 and use a fixed background disease rate (year 1980) for years prior to 1980. Percentage changes as for figure 3.

regional scale, $UKCA_{\_ppe-med}$ simulated broadly similar fractional changes to GBD-PM in the EU and US, but smaller changes in China and India. During the period 1960 to 2009, global population-weighted $PM_{2.5}$ simulated by UKCA increased by 37.5%, dominated by large increases in China and India of 52.7% and 69.8%, respectively. In contrast, population-weighted $PM_{2.5}$ reduced in the EU and US by −55.3% and −38%, respectively. Because of the positive correlation between the spatial distribution of $PM_{2.5}$ concentrations and population, population-weighted $PM_{2.5}$ concentrations are higher than the regional average (see figure S8). We find that the ratio of population-weighted to regional average $PM_{2.5}$ in the EU and US has decreased over the period 1960 to 2009 (1.3 to 1.0 and 2.0 to 1.6, respectively), whereas the ratio has increased in both China and India (1.4 to 1.6 and 1.1 to 1.3, respectively). These changes match those reported previously (Wang *et al* 2017) and are driven by anthropogenic emission changes (figure 1) and changes in population (figure S5).

Figure 4 shows the estimated attributable deaths over the period 1960 to 2009 (see SI data 2 for all data values). Using $PM_{2.5}$ concentrations from $GBD\text{-}PM_{\_high}$, we estimate 2.6 million global attributable deaths in the year 2009, with a lower and upper uncertainty interval of 1.87 to 3.57 million. Estimated attributable deaths from $UKCA_{\_ppe-med}$ are 22.5% lower at 2.0 (1.4 to 2.9) million for the same year, due to lower estimated $PM_{2.5}$ concentrations. When $GBD\text{-}PM_{\_high}$ is averaged to the same resolution as UKCA ($GBD\text{-}PM_{\_low}$), global attributable deaths are reduced by less than 3%, again demonstrating that the coarse resolution of UKCA is not the dominant reason for the lower global mortality estimate in $UKCA_{\_ppe-med}$. Larger regional differences occur in regions with low $PM_{2.5}$ concentrations such as the US where estimated attributable deaths from $GBD\text{-}PM_{\_low}$ are ∼10% lower than $GBD\text{-}PM_{\_high}$. This greater sensitivity occurs because the IER relationship is non-linear and particularly sensitive to changes in $PM_{2.5}$ just above the theoretical minimum risk exposure level (TMREL) (∼6 $\mu g\,m^{-3}$). This sensitivity also explains the large difference in deaths estimated in $UKCA_{\_ppe-med}$ compared to GBD-PM in the EU and US. Estimated attributable deaths from UKCA and GBP-PM are in better agreement over China and India, where higher $PM_{2.5}$ concentrations are associated with reduced sensitivity in the IER. Attributable deaths estimated using the upper and lower bound of the PPE bracket GBD-PM, showing the contribution of uncertainty in model processes to estimated mortality.

During the period 1990 to 2009, $UKCA_{\_ppe-med}$ estimated global deaths increased by 15.6%, similar to the 22% change in GBD-PM. At the regional scale, $UKCA_{\_ppe-med}$ simulates broadly similar fractional changes to GBD-PM in both China and India, but only simulates half the fractional change in the EU and US. During the period 1960 to 2009, global attributable deaths increased by an average of 124.4%. If we assume background disease rates prior to 1980 vary, this increase is reduced to 88.5% (see figure S9) because background diseases are comparatively higher in 1960. The percentage increase in attributable deaths is substantially greater than increases in population-weighted $PM_{2.5}$ concentrations over the same period, owing to the non-linear IER and to increases in population. Our results imply that global attributable deaths are now larger in the present day than at any other point since 1960.

Global increases in attributable deaths were dominated by large increases in China (238%) and India

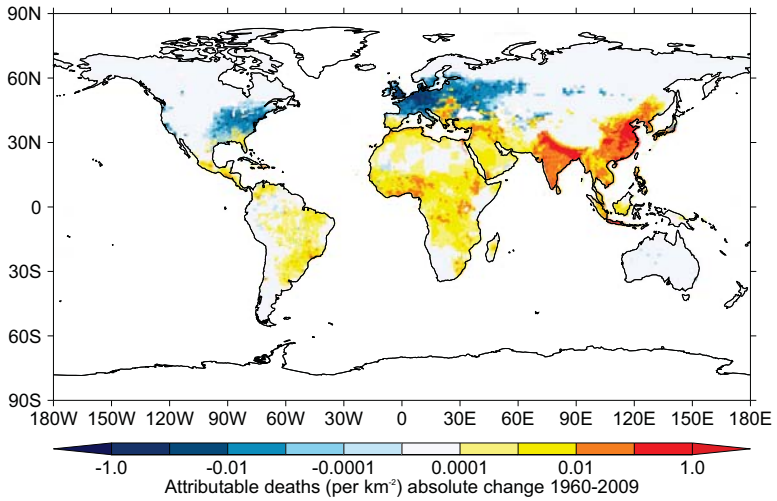

Figure 5. Absolute change in attributable deaths (km^{-2} yr^{-1}) between 1960 and 2009. Results are shown for $UKCA_{\_ppe-med}$ using a fixed background disease rate (year 1980) for years prior to 1980.

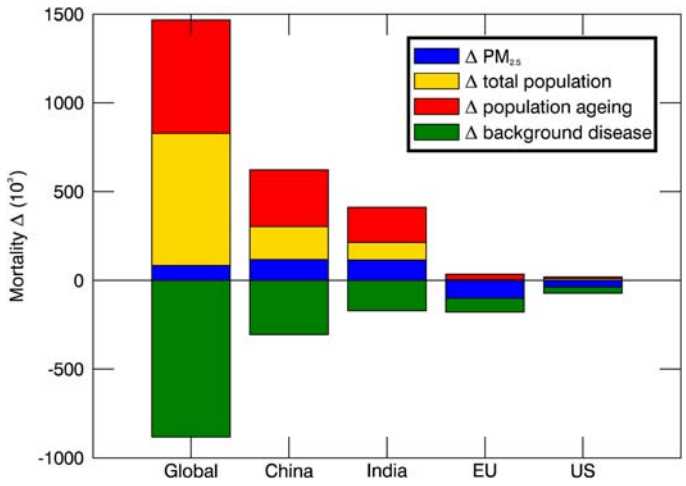

Figure 6. Relative contribution of changes in $PM_{2.5}$, population growth, population ageing, and background disease endpoint rates to changes in total attributable deaths between 1980 and 2009. Results are shown for $UKCA_{\_ppe-med}$.

(194%). China and India accounted for 39% of global deaths attributable to $PM_{2.5}$ in 1960 growing to 55% in 2009. In contrast, attributable deaths reduced in the EU (−65.7%) and US (−47.9%) over this period. The US and EU accounted for 27% of global attributable deaths in 1960 falling to ∼1% in 2009. If we assume that background disease rates prior to 1980 vary, attributable deaths in the EU and US peak in early-1970s following that of population-weighted $PM_{2.5}$ concentrations rather than peaking in early-1980s (see figure S9).

Figure 5 shows the spatial pattern of change in attributable deaths between 1960 and 2009. Large increases in deaths attributable to $PM_{2.5}$ are simulated in China and India as well as parts of Africa, the Middle East, and Central and South America. In contrast, reductions are simulated across much of Western Europe and North America.

Attributable deaths from cardiovascular disease contribute most to total global and regional attributable deaths (see figure S10). Figure 6 explores the relative contribution to changes in attributable deaths for the period 1980 to 2009 (see SI 1.6). Population growth and ageing act to increase attributable deaths, whereas declining background disease acts to reduce attributable deaths. In China and India, population growth and ageing and to a lesser extent increasing $PM_{2.5}$ concentrations act to increase mortality offset by reductions in background disease rates. In contrast, in the US and EU, reductions in background cardiovascular disease and $PM_{2.5}$ concentrations offset the contribution from population growth and ageing. Our results imply that air quality regulation and emission controls in Europe and North America are acting to reduce attributable burdens as observed in the US (Correia *et al* 2013, Pope *et al* 2009b).

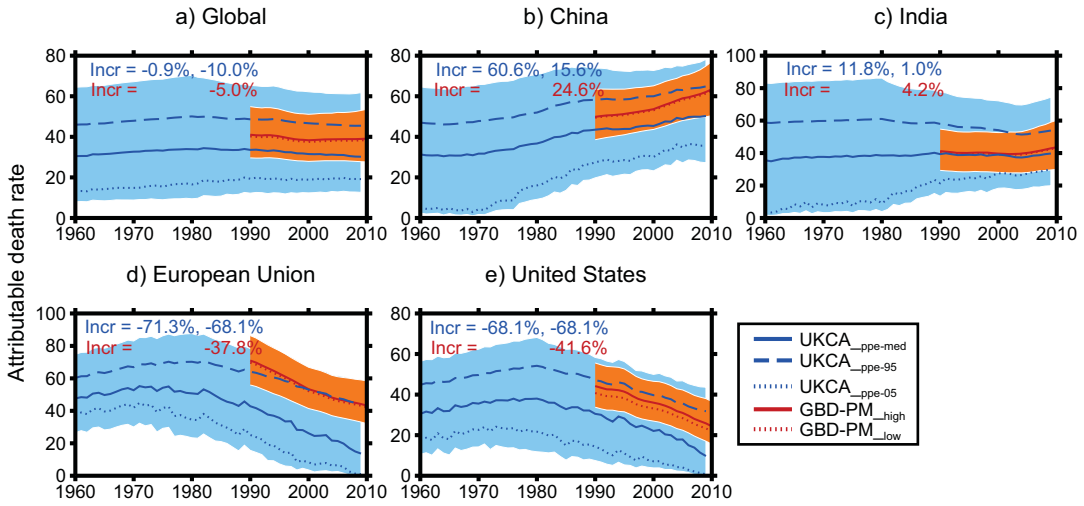

Figure 7. Attributable deaths rate per 100 000 persons for (*a*) global, (*b*) China, (*c*) India, (*d*) European Union and (*e*) United States. Shaded areas represent upper and lower range of UKCA-PPE estimates (light blue) and GBD-PM (orange). Regional values are reported for the shaded regions identified in figure S1 and use a fixed background disease rate (year 1980) for years prior to 1980. Percentage changes as for figure 3.

Since the end of our simulation period (year 2009) regional changes in $PM_{2.5}$ concentrations and population demographics may have occurred. For example in China, population-weighted $PM_{2.5}$ concentrations stabilised between 2010 and 2015 (Brauer *et al* 2015, Cohen *et al* 2017), but attributable deaths continued to increase (Cohen *et al* 2017, Forouzanfar *et al* 2016). Our findings suggest that while primary and precursor emissions in China (and other parts of Asia) are likely to decrease over the next few decades (Zhao *et al* 2013, Zhao *et al* 2014), attributable deaths are likely to increase in the near future because of projected population growth and ageing (UN 2015). This highlights the need of strict control of $PM_{2.5}$ in the face of changing demographics.

Figure 7 shows the attributable death rate per 10^5 of population for the period 1960 to 2009, which removes the influence of population growth. China had the highest attributable death rate in 2009, comparable to the EU in 1960. In contrast to the growth in total global attributable deaths, global attributable death rates reduced (−0.9%) over the period 1960 to 2009, a result of overall decreasing background disease rates and health benefits of cleaner air quality in North America and Western Europe. Decreasing background disease rates played an important role in influencing changes in attributable years of life lost (YLLs). For example, YLLs in India were markedly reduced between 1990 and 2010 (see figure S11) because of declines in infant (<5 yr) attributable mortality from LRI (see figure S10), a result of reduced disease rates (see figure S7), in part due to improved vaccination efforts, poverty alleviation and access to health care (Naghavi *et al* 2015).

Calculating the uncertainty in our attributable burdens is challenging because there are multiple sources of uncertainty. We have quantified uncertainty using the lower and upper uncertainty bounds in the IER and background disease rates. Applying an exposure-response relationship (IER) based on epidemiological data from North America and Europe to the rest of the world, where lifestyles, age-structures, healthcare systems and $PM_{2.5}$ composition differ, is a critical source of uncertainty.

The IER neglects $PM_{2.5}$ particle composition and toxicity, which may be important (Lelieveld *et al* 2015, Thurston *et al* 2016, Tuomisto *et al* 2008). Further research is needed to establish the health implications of particle toxicity and source which may differ for each region.

The shape of the IER remains uncertain, particularly in very clean and polluted regions. We follow the GBD2013 and use a TMREL (~6 $\mu g\ m^{-3}$) below which we assume zero risk. However, there is limited evidence for such a threshold. Additional research to constrain relative risks in very clean regions (Crouse *et al* 2012, Shi *et al* 2016, Tomczak *et al* 2016), where there is a lack of epidemiological data, is needed. Similarly, because of a lack of data, relative risks in polluted regions are based extrapolations from active and passive smoking cohort studies (Pope *et al* 2009a, Pope *et al* 2011), leading to uncertainty in the IER at high exposure levels. This is important as the predicted shape of the IER is highly non-linear in polluted settings (figure S4). This implies that polluted regions will display the smallest reductions in relative risk from incremental pollution reduction. Our results suggest that current $PM_{2.5}$ concentrations in China and India are higher than those experienced in the EU and US during the 1960s and 1970s (figure 3). This suggests that stringent emission controls will be required to reduce population-weighted $PM_{2.5}$ concentrations and attributable health burdens.

Simulated $PM_{2.5}$ concentrations are uncertain due to uncertainties in emissions, meteorological input and

model processes. We have evaluated our estimated $PM_{2.5}$ concentrations using available long-term observations in North America and Europe. In regions where long-term observations are not available, we compare against satellite derived $PM_{2.5}$ data. There is an urgent need for more $PM_{2.5}$ observations, particularly in polluted and data sparse regions. We used the range of $PM_{2.5}$ concentrations from the PPE as an indication of the contribution of uncertain model processes, which indicated large uncertainties associated with dry deposition of accumulation mode particles in all regions, and mass flux of small scale residential combustion carbonaceous emissions in Asia (see SI 1.3 and figure S2). This analysis confirms a large contribution of residential emissions to $PM_{2.5}$ over Asia that has been shown previously (Butt *et al* 2016, Lelieveld *et al* 2015). Future research should prioritise constraining these large model uncertainties. UKCA does not include nitrate or anthropogenic secondary organic aerosol formation which may contribute to the underestimation of $PM_{2.5}$ concentrations. Multi-decadal global simulations of $PM_{2.5}$ are currently restricted to relatively coarse resolution, as used here. Differences in model spatial resolutions have been found to affect estimated attributable burdens (Ford and Heald 2015, Punger and West 2013, Thompson *et al* 2014). Although we find small differences between estimates at $0.1° \times 0.1°$ versus the resolution of UKCA ($1.875° \times 1.25°$), further research using higher resolution estimates below $0.1° \times 0.1°$ like those used in Jerrett *et al* (2016) may provide more realistic personal exposures and thus attributable burdens.

Our estimates are subject to increased uncertainty prior to 1980 where we do not have data on background diseases. We find that varying assumptions about trends in background disease prior to 1980 increases global attributable deaths in 1960 by 16%. Information on historical background diseases trends would improve our attributable burden estimates prior to 1980. Background disease data is also provided at the national level, which does not account for any subnational variability, which may be important (Apte *et al* 2015, Chowdhury and Dey 2016, Cossman *et al* 2010). Similarly, we use national level data for different age groups, which is also unrealistic. Future research using subnational background disease and age group distribution data would improve future attributable burden estimates.

4. Conclusions

We used the HadGEM3-UKCA global coupled chemistry–climate model to investigate changes in ambient $PM_{2.5}$ concentrations and attributable burdens over the period 1960 to 2009. We found that the uncertainty in the model, estimated using a perturbed parameter ensemble of 235 simulations across 26 aerosol parameters, brackets long-term $PM_{2.5}$ measurements and satellite derived $PM_{2.5}$ concentrations used in the Global Burden of Disease (GBD) 2013.

We estimate that global population-weighted $PM_{2.5}$ concentrations increased by 37.5% over the period 1960 to 2009, dominated by increases in China and India, a result of economic expansion and growth in emissions. In contrast, air quality regulation and emission controls in the European Union (EU) and United States (US) has reduced population-weighted $PM_{2.5}$ concentrations over the same period.

We found that global attributable deaths increased by 89% to 124% over the period 1960 to 2009, much larger than the changes in $PM_{2.5}$ over the same period. Global changes were dominated by large increases China and India. In contrast, attributable deaths decreased in the EU and US.

Increases in attributable deaths in China and India were dominated by population growth and ageing, and to a lesser extent increasing $PM_{2.5}$ concentrations. Reduced attributable deaths in the EU and US were driven by reductions in background disease rate and $PM_{2.5}$ concentrations. Our results suggest that projected changes in demography in China and India will pose challenges as policy makers attempt to reduce attributable deaths in the near future. Our results provide the first estimate of how $PM_{2.5}$ concentrations and associated health burden has changed over the 1960 to 2009 period. Understanding the reasons for these changes is required to help policy makers craft sound policies to reduce future health impacts.

Acknowledgments

E W Butt would like to thank the United Bank of Carbon and University of Leeds for providing the funding for his PhD studentship. We acknowledge funding from Natural Environment Research Council (NERC) under grants AEROS, ACID-PRUF, GASSP and SAMBBA (NE/G006172/1, NE/I020059/1, NE/J024252/1 and NE/J009822/1). This work used the ARCHER UK National Supercomputing Service (www.archer.ac.uk). ARCHER project allocation n02-FREEPPE and the Leadership Project allocation n02-CCPPE were used to create the PPE. S T Turnock was supported by funding for his PhD studentship from NERC and the UK Met Office Hadley Centre. He also acknowledges use of the MONSooN system, a collaborative facility supplied under the Joint Weather and Climate Research Programme, a strategic partnership between the UK Met Office Hadley Centre and the NERC. L Regayre was funded by a NERC Doctoral Training Grant and a CASE studentship with the UK Met Office Hadley Centre. J S Johnson was funded by the UK-China Research & Innovation Partnership Fund through the Met Office Climate Science for Service Partnership (CSSP) China as part of the Newton Fund. G W Mann was funded by the National Centre for Atmospheric Science.

References

Anenberg S C, Horowitz L W, Tong D Q and West J 2010 An estimate of the global burden of anthropogenic ozone and fine particulate matter on premature human mortality using atmospheric modeling *Environ. Health Perspect.* **118** 1189–95

Apte J S, Marshall J D, Cohen A J and Brauer M 2015 Addressing global mortality from ambient $PM_{2.5}$ *Environ. Sci. Technol.* **49** 8057–66

Brauer M, Amann M, Burnett R T, Cohen A, Dentener F, Ezzati M, Henderson S B, Krzyzanowski M, Martin R V and Van Dingenen R 2012 Exposure assessment for estimation of the global burden of disease attributable to outdoor air pollution *Environ. Sci. Technol.* **46** 652–60

Brauer M *et al* 2015 Ambient air pollution exposure estimation for the global burden of disease 2013 *Environ. Sci. Technol.* **50** 79–88

Burnett R T *et al* 2014 An integrated risk function for estimating the global burden of disease attributable to ambient fine particulate matter exposure *Environ. Health Perspect.* **122** 397

Butt E W *et al* 2016 The impact of residential combustion emissions on atmospheric aerosol, human health, and climate *Atmos. Chem. Phys.* **16** 873–905

Chowdhury S and Dey S 2016 Cause-specific premature death from ambient $PM_{2.5}$ exposure in India: estimate adjusted for baseline mortality *Environ. Int.* **91** 283–90

CIESIN 2015 Gridded Population of the World, Version 3 (GPWv3) Data Collection

Cohen A J, Brauer M, Burnett R, Anderson H R, Frostad J, Estep K, Balakrishnan K, Brunekreef B, Dandona L and Dandona R 2017 Estimates and 25 year trends of the global burden of disease attributable to ambient air pollution: an analysis of data from the global burden of diseases study 2015 *Lancet* **389** 1907–18

Correia A W, Pope III C A, Dockery D W, Wang Y, Ezzati M and Dominici F 2013 The effect of air pollution control on life expectancy in the United States: an analysis of 545 US counties for the period 2000 to 2007 *Epidemiology* **24** 23–31

Cossman J S, James W L, Cosby A G and Cossman R E 2010 Underlying causes of the emerging nonmetropolitan mortality penalty *Am. J. Public Health* **100** 1417–9

Crouse D L *et al* 2012 Risk of nonaccidental and cardiovascular mortality in relation to long-term exposure to low concentrations of fine particulate matter: a Canadian national-level cohort study *Environ. Health Perspect.* **120** 708

Dee D, Uppala S, Simmons A, Berrisford P, Poli P, Kobayashi S, Andrae U, Balmaseda M, Balsamo G and Bauer P 2011 The ERA-interim reanalysis: configuration and performance of the data assimilation system *Q. J. R. Meteorol. Soc.* **137** 553–97

Dockery D W, Pope C A, Xu X, Spengler J D, Ware J H, Fay M E, Ferris B G Jr and Speizer F E 1993 An association between air pollution and mortality in six US cities *N. Engl. J. Med.* **329** 1753–9

Ford B and Heald C 2015 Exploring the uncertainty associated with satellite-based estimates of premature mortality due to exposure to fine particulate matter *Atmos. Chem. Phys. Discuss.* **15** 25329–80

Forouzanfar M H *et al* 2016 Global, regional, and national comparative risk assessment of 79 behavioural, environmental and occupational, and metabolic risks or clusters of risks, 1990–2013: a systematic analysis for the global burden of disease study 2015 *Lancet* **388** 1659–724

Forouzanfar M H, Alexander L, Anderson H R, Bachman V F, Biryukov S, Brauer M, Burnett R, Casey D, Coates M M and Cohen A 2015 Global, regional, and national comparative risk assessment of 79 behavioural, environmental and occupational, and metabolic risks or clusters of risks in 188 countries, 1990–2013: a systematic analysis for the global burden of disease study 2013 *Lancet* **386** 2287–323

Granier C, Bessagnet B, Bond T, D'Angiola A, van Der Gon H D, Frost G J, Heil A, Kaiser J W, Kinne S and Klimont Z 2011 Evolution of anthropogenic and biomass burning emissions of air pollutants at global and regional scales during the 1980–2010 period *Clim. Change* **109** 163–90

IHME 2014 (http://vizhub.healthdata.org/cod/) (Accessed: 30 September 2015)

Jerrett M *et al* 2016 Comparing the health effects of ambient particulate matter estimated using ground-based versus remote sensing exposure estimates *Environ. Health Perspect.* **125** 552

Leibensperger E, Mickley L J, Jacob D J, Chen W-T, Seinfeld J, Nenes A, Adams P, Streets D, Kumar N and Rind D 2012 Climatic effects of 1950–2050 changes in US anthropogenic aerosols–Part 1: aerosol trends and radiative forcing *Atmos. Chem. Phys.* **12** 3333–48

Lelieveld J, Barlas C, Giannadaki D and Pozzer A 2013 Model calculated global, regional and megacity premature mortality due to air pollution *Atmos. Chem. Phys.* **13** 7023–37

Lelieveld J, Evans J, Fnais M, Giannadaki D and Pozzer A 2015 The contribution of outdoor air pollution sources to premature mortality on a global scale *Nature* **525** 367–71

Lim S S, Vos T, Flaxman A D, Danaei G, Shibuya K, Adair-Rohani H, AlMazroa M A, Amann M, Anderson H R and Andrews K G 2013 A comparative risk assessment of burden of disease and injury attributable to 67 risk factors and risk factor clusters in 21 regions, 1990–2010: a systematic analysis for the global burden of disease study 2010 *Lancet* **380** 2224–60

Mann G, Carslaw K, Spracklen D, Ridley D, Manktelow P, Chipperfield M, Pickering S and Johnson C 2010 Description and evaluation of GLOMAP-mode: a modal global aerosol microphysics model for the UKCA composition-climate model *Geosci. Model Dev.* **3** 519–51

Murray C J, Vos T, Lozano R, Naghavi M, Flaxman A D, Michaud C, Ezzati M, Shibuya K, Salomon J A and Abdalla S 2013 Disability-adjusted life years (DALYs) for 291 diseases and injuries in 21 regions, 1990–2010: a systematic analysis for the global burden of disease study 2010 *Lancet* **380** 2197–223

Naghavi M, Wang H, Lozano R, Davis A, Liang X, Zhou M, Vollset S E, Ozgoren A A, Abdalla S and Abd-Allah F 2015 Global, regional, and national age-sex specific all-cause and cause-specific mortality for 240 causes of death, 1990–2013: a systematic analysis for the global burden of disease study 2013 *Lancet* **385** 117–171

Pope C A, Burnett R T, Krewski D, Jerrett M, Shi Y, Calle E E and Thun M J 2009a Cardiovascular mortality and exposure to airborne fine particulate matter and cigarette smoke shape of the exposure-response relationship *Circulation* **120** 941–8

Pope C A, Burnett R T, Turner M C, Cohen A, Krewski D, Jerrett M, Gapstur S M and Thun M J 2011 Lung cancer and cardiovascular disease mortality associated with ambient air pollution and cigarette smoke: shape of the exposure-response relationships *Environ. Health Perspect.* **119** 1616

Pope C A and Dockery D W 2006 Health effects of fine particulate air pollution: lines that connect *J. Air. Waste Manage. Assoc.* **56** 709–42

Pope C A, Dockery D W and Schwartz J 1995 Review of epidemiological evidence of health effects of particulate air pollution *Inhal. Toxicol.* **7** 1–18

Pope C A, Ezzati M and Dockery D W 2009b Fine-particulate air pollution and life expectancy in the United States *N. Engl. J. Med.* **360** 376–86

Punger E M and West J J 2013 The effect of grid resolution on estimates of the burden of ozone and fine particulate matter on premature mortality in the USA *Air Qual. Atmos. Health* **6** 563–73

Reddington C, Butt E, Ridley D, Artaxo P, Morgan W, Coe H and Spracklen D 2015 Air quality and human health improvements from reductions in deforestation-related fire in Brazil *Nat. Geosci.* **8** 768–71

Shi L, Zanobetti A, Kloog I, Coull B A, Koutrakis P, Melly S J and Schwartz J D 2016 Low-concentration $PM_{2.5}$ and mortality: estimating acute and chronic effects in a population-based study *Environ. Health Perspect.* **124** 46

Silva R A, Adelman Z, Fry M M and West J J 2016a The impact of individual anthropogenic emissions sectors on the global burden of human mortality due to ambient air pollution *Environ. Health Perspect.* **124** 1776

Silva R A, West J J, Lamarque J-F, Shindell D T, Collins W J, Dalsoren S, Faluvegi G, Folberth G, Horowitz L W and Nagashima T 2016b The effect of future ambient air pollution on human premature mortalityto 2100 using output from the ACCMIP model ensemble *Atmos. Chem. Phys.* **16** 9847–62

Smith S J, Aardenne J V, Klimont Z, Andres R J, Volke A and Delgado Arias S 2011 Anthropogenic sulfur dioxide emissions: 1850–2005 *Atmos. Chem. Phys.* **11** 1101–16

Thompson T M, Saari R K and Selin N E 2014 Air quality resolution for health impact assessment: influence of regional characteristics *Atmos. Chem. Phys.* **14** 969–78

Thurston G D, Burnett R T, Turner M C, Shi Y, Krewski D, Lall R, Ito K, Jerrett M, Gapstur S M and Diver W R 2016 Ischemic heart disease mortality and long-term exposure to source-related components of US fine particle air pollution *Environ. Health Perspect.* **124** 785

Tomczak A, Miller A, Weichenthal S, To T, Wall C, van Donkelaar A, Martin R, Crouse D and Villeneuve P 2016 Long-term exposure to fine particulate matter air pollution and the risk of lung cancer among participants of the Canadian National Breast Screening Study *Int. J. Cancer* **139** 1958–66

Tørseth K, Aas W, Breivik K, Fjæraa A, Fiebig M, Hjellbrekke A, Myhre Lund C, Solberg S and Yttri K 2012 Introduction to the european monitoring and evaluation programme (EMEP) and observed atmospheric composition change during 1972–2009 *Atmos. Chem. Phys.* **12** 5447–81

Tuomisto J T, Wilson A, Evans J S and Tainio M 2008 Uncertainty in mortality response to airborne fine particulate matter: combining European air pollution experts *Reliab. Eng. Syst. Safe.* **93** 732–44

Turnock S, Spracklen D, Carslaw K, Mann G, Woodhouse M, Forster P, Haywood J, Johnson C, Dalvi M and Bellouin N 2015 Modelled and observed changes in aerosols and surface solar radiation over europe between 1960 and 2009 *Atmos. Chem. Phys.* **15** 9477–500

UN 2015 *World Population Prospects: The 2015 Revision* (New York: UN Department of Economic and Social Affairs, Population Division)

Uppala S M, Kållberg P, Simmons A, Andrae U, Bechtold V D, Fiorino M, Gibson J, Haseler J, Hernandez A and Kelly G 2005 The ERA-40 re-analysis *Q. J. R. Meteorol. Soc.* **131** 2961–3012

van Donkelaar A, Martin R V, Brauer M, Kahn R, Levy R, Verduzco C and Villeneuve P J 2010 Global estimates of ambient fine particulate matter concentrations from satellite-based aerosol optical depth: development and application *Environ. Health Perspect.* **118** 847–55

Vestreng V, Myhre G, Fagerli H, Reis S and Tarrasón L 2007 Twenty-five years of continuous sulphur dioxide emission reduction in Europe *Atmos. Chem. Phys.* **7** 3663–81

Wang J, Xing J, Mathur R, Pleim J, Wang S, Hogrefe C, Gan C, Wong D and Hao J 2017 Historical trends in $PM_{2.5}$-related premature mortality during 1990–2010 across the Northern Hemisphere *Environ. Health Perspect.* **125** 400

Zhao B, Wang S, Liu H, Xu J, Fu K, Klimont Z, Hao J, He K, Cofala J and Amann M 2013 NO_x emissions in China: historical trends and future perspectives *Atmos. Chem. Phys.* **13** 9869–97

Zhao Y, Zhang J and Nielsen C P 2014 The effects of energy paths and emission controls and standards on future trends in China's emissions of primary air pollutants *Atmos. Chem. Phys.* **14** 8849–68

Chapter 4

The impact of residential combustion emissions on atmospheric aerosol, human health, and climate

Atmos. Chem. Phys., 16, 873–905, 2016
www.atmos-chem-phys.net/16/873/2016/
doi:10.5194/acp-16-873-2016

Atmospheric Chemistry and Physics Open Access EGU

The impact of residential combustion emissions on atmospheric aerosol, human health, and climate

E. W. Butt[1], A. Rap[1], A. Schmidt[1], C. E. Scott[1], K. J. Pringle[1], C. L. Reddington[1], N. A. D. Richards[1], M. T. Woodhouse[1,2], J. Ramirez-Villegas[1,3], H. Yang[1], V. Vakkari[4], E. A. Stone[5], M. Rupakheti[6], P. S. Praveen[7], P. G. van Zyl[8], J. P. Beukes[8], M. Josipovic[8], E. J. S. Mitchell[9], S. M. Sallu[10], P. M. Forster[1], and D. V. Spracklen[1]

[1]Institute for Climate and Atmospheric Science, School of Earth and Environment, University of Leeds, Leeds, UK
[2]CSIRO Oceans and Atmosphere, Aspendale, Victoria, Australia
[3]International Centre for Tropical Agriculture, Cali, Colombia
[4]Finnish Meteorological Institute, Helsinki, Finland
[5]Department of Chemistry, University of Iowa, Iowa City, Iowa 52242, USA
[6]Institute for Advanced Sustainability Studies, Potsdam, Germany
[7]International Centre for Integrated Mountain Development, Kathmandu, Nepal
[8]North-West University, Unit for Environmental Sciences and Management, 2520 Potchefstroom, South Africa
[9]Energy Research Institute, School of Chemical and Process Engineering, University of Leeds, Leeds, UK
[10]Sustainability Research Institute, School of Earth and Environment, University of Leeds, Leeds, UK

Correspondence to: E. W. Butt (e.butt@leeds.ac.uk)

Received: 29 May 2015 – Published in Atmos. Chem. Phys. Discuss.: 29 July 2015
Revised: 10 November 2015 – Accepted: 6 January 2016 – Published: 26 January 2016

Abstract. Combustion of fuels in the residential sector for cooking and heating results in the emission of aerosol and aerosol precursors impacting air quality, human health, and climate. Residential emissions are dominated by the combustion of solid fuels. We use a global aerosol microphysics model to simulate the impact of residential fuel combustion on atmospheric aerosol for the year 2000. The model underestimates black carbon (BC) and organic carbon (OC) mass concentrations observed over Asia, Eastern Europe, and Africa, with better prediction when carbonaceous emissions from the residential sector are doubled. Observed seasonal variability of BC and OC concentrations are better simulated when residential emissions include a seasonal cycle. The largest contributions of residential emissions to annual surface mean particulate matter ($PM_{2.5}$) concentrations are simulated for East Asia, South Asia, and Eastern Europe. We use a concentration response function to estimate the human health impact due to long-term exposure to ambient $PM_{2.5}$ from residential emissions. We estimate global annual excess adult (> 30 years of age) premature mortality (due to both cardiopulmonary disease and lung cancer) to be 308 000 (113 300–497 000, 5th to 95th percentile uncertainty range) for monthly varying residential emissions and 517 000 (192 000–827 000) when residential carbonaceous emissions are doubled. Mortality due to residential emissions is greatest in Asia, with China and India accounting for 50 % of simulated global excess mortality. Using an offline radiative transfer model we estimate that residential emissions exert a global annual mean direct radiative effect between −66 and +21 mW m^{-2}, with sensitivity to the residential emission flux and the assumed ratio of BC, OC, and SO_2 emissions. Residential emissions exert a global annual mean first aerosol indirect effect of between −52 and −16 mW m^{-2}, which is sensitive to the assumed size distribution of carbonaceous emissions. Overall, our results demonstrate that reducing residential combustion emissions would have substantial benefits for human health through reductions in ambient $PM_{2.5}$ concentrations.

Published by Copernicus Publications on behalf of the European Geosciences Union.

1 Introduction

Combustion of fuels within the household for cooking and heating, known as residential fuel combustion, is an important source of aerosol emissions with impacts on air quality and climate (Ramanathan and Carmichael, 2008; Lim et al., 2012). In most regions, residential emissions are dominated by the combustion of residential solid fuels (RSFs, see Table A1 for list of acronyms used in the study) such as wood, charcoal, agricultural residue, animal waste, and coal. Nearly 3 billion people, mostly in the developing world, depend on the combustion of RSFs as their primary energy source (Bonjour et al., 2013). RSFs are usually burnt in simple stoves or open fires with low combustion efficiencies, resulting in substantial emissions of aerosol. It has been suggested that reducing RSF emissions would be a fast way to mitigate climate and improve air quality (UNEP, 2011), but the climate impacts of RSF emissions are uncertain (Bond et al., 2013). Whilst it is clear that RSF combustion has substantial adverse impacts on human health through poor indoor air quality, there have been few studies quantifying the impacts on outdoor air quality and human health. Here, we use a global aerosol microphysics model to estimate the impacts of residential fuel combustion on atmospheric aerosol, climate, and human health.

Residential emissions due to the small-scale combustion of biomass and fossil fuels used for cooking, heating, lighting, and auxiliary engines include black carbon (BC), particulate organic matter (POM), primary inorganic sulfate, and gas-phase SO_2. Residential emissions contribute substantially to the global aerosol burden, accounting for 25 % of global energy-related BC emissions (Bond et al., 2013). In China and India, residential emissions are even more important, accounting for 50–60 % of BC and 60–80 % of organic carbon (OC) emissions (Cao et al., 2006; Klimont et al., 2009; Lei et al., 2011). The combustion of residential fuels also emit volatile and semi-volatile organic compounds that lead to the production of secondary organic aerosols via atmospheric oxidation. Residential emissions are dominated by emissions from RSFs in many regions, due to poor combustion efficiency of RSFs and extensive use across the developing world (Bond et al., 2013). In China, residential combustion of both biomass (referred to as "biofuel") and coal is important, whereas across other parts of Asia and Africa residential combustion of biofuel is dominant (Lu et al., 2011; Bond et al., 2013).

Estimates of residential emissions are typically "bottom-up", combining information on fuel consumption rates with laboratory or field emission factors. Obtaining reliable estimates of residential fuel use is difficult because these fuels are often collected by consumers and are not centrally recorded (Bond et al., 2013). Emission factors are hugely variable, depending on the type, size, and moisture content of fuel, as well as stove design, operation, and combustion conditions (Roden et al., 2006, 2009; Li et al., 2009; Shen et al., 2010). As a result, uncertainty in residential emissions may be as large as a factor 2 or more (Bond et al., 2004). There is a range of evidence that residential emissions may be underestimated. Firstly, emission factors for RSF combustion derived from laboratory experiments are often less than those derived under ambient conditions (Roden et al., 2009). Secondly, models typically underestimate observed aerosol absorption optical depth, BC, and OC over regions associated with large RSF emissions such as in South and East Asia (Park et al., 2005; Koch et al., 2009; Ganguly et al., 2009; Menon et al., 2010; Nair et al., 2012; Fu et al., 2012; Moorthy et al., 2013; Bond et al., 2013; Pan et al., 2015). A further complication is that residential emissions, particularly from residential heating, also exhibit seasonal variability (Aunan et al., 2009; Stohl et al., 2013), but this is rarely implemented within global modelling studies.

Atmospheric aerosols interact with the Earth's radiation budget directly through the scattering and absorption of solar radiation (direct radiative effect – DRE – or aerosol–radiation interactions) and indirectly by modifying the microphysical properties of clouds (aerosol indirect effect – AIE – or aerosol–cloud interactions) (Forster et al., 2007; Boucher et al., 2013). The interaction of aerosol with radiation and clouds depends on properties of the aerosol, including mass concentration, size distribution, chemical composition, and mixing state (Boucher et al., 2013). BC is strongly absorbing at visible and infrared wavelengths, exerting a positive DRE5. BC particles coated with a non-absorbing shell have greater absorption compared to a fresh BC core due to a lensing effect (Fuller et al., 1999; Jacobson, 2001). More recent studies have shown that a fraction of organic aerosol can absorb light (Kirchstetter et al., 2004; Chen and Bond, 2010; Arola et al., 2011), with the light absorbing fraction termed "brown carbon". The net DRE of residential combustion emissions is a complex combination of these warming and cooling effects.

Aerosol also impacts climate through altering the properties of clouds. The cloud albedo or first AIE is the radiative effect due to a change in cloud droplet number concentration (CDNC), assuming a fixed cloud water content. The change in CDNC is governed by the number concentration of aerosols that are able to act as cloud condensation nuclei (CCN), which is determined by aerosol size and chemical composition (Penner et al., 2001; Dusek et al., 2006). Modelling studies have shown the importance of carbonaceous combustion aerosols to global CCN concentrations (Pierce et al., 2007; Spracklen et al., 2011a) and modification of cloud properties (Bauer et al., 2010; Jacobson, 2010). However, there is considerable variability in the size of particles emitted by combustion sources including those from residential sources (Venkataraman and Rao, 2001; Shen et al., 2010; Pagels et al., 2013; Bond et al., 2006) that will impact simulated CCN concentrations (Pierce et al., 2007, 2009; Reddington et al., 2011; Spracklen et al., 2011a; Kodros et al., 2015) and AIE (Bauer et al., 2010; Spracklen et

al., 2011a; Kodros et al., 2015). Aerosols can further alter cloud properties through the second aerosol indirect effect and through semi-direct effects (Koch and Del Genio, 2010).

The net radiative effect (RE) of residential emissions depends on the fuel and combustion process (Bond et al., 2013). Carbonaceous emissions from residential biofuel exhibit higher POM : BC mass ratios compared to residential coal, which emits more BC and sulfur (Bond et al., 2013). Aunan et al. (2009) found that despite large BC emissions over Asia, RSF combustion emissions exerted a small net negative DRE because of co-emitted scattering aerosols; however, this study did not include aerosol–cloud effects. Jacobson (2010) reported increased cloud cover and depth from biofuel aerosol and gases as well as a net positive RE. In contrast, Bauer et al. (2010) found the negative AIE from residential biofuel combustion to be 3 times greater than the positive DRE, resulting in a negative net RE. Unger et al. (2010) used a mass-only aerosol model to calculate a positive AIE due to the residential sector. The review of Bond et al. (2013) identified a net negative RE (DRE and AIE) for biofuel with large uncertainty but a slight net positive RE (with low certainty) from residential coal (Bond et al., 2013). However, a recent detailed global modelling study found that the climate effects of residential biofuel combustion aerosol are largely unconstrained because of uncertainties in emission mass flux, emitted size distribution, optical mixing state, and ratio of BC to POM (Kodros et al., 2015)

In addition to impacting climate, aerosol from residential fuel combustion degrades air quality with adverse implications for human health. Epidemiologic research has confirmed a strong link between exposure to particulate matter (PM) and adverse health effects, including premature mortality (Pope III and Dockery, 2006; Brook et al., 2010). Exposure to $PM_{2.5}$ (PM with an aerodynamic dry diameter of $< 2.5\,\mu m$) is thought to be particularly harmful to human health (Pope III and Dockery, 2006; Schlesinger et al., 2006). Household air pollution, mostly from RSF combustion (Smith et al., 2014) in low and middle income countries, is estimated to cause 4.3 million deaths annually (WHO, 2014a), making it one of the leading risk factors for global disease burden (Lim et al., 2012). Global estimates of premature mortality attributable to ambient (outdoor) air pollution range from 0.8 million to 3.7 million deaths per year, most of which occur in Asia (Cohen et al., 2005; Anenberg et al., 2010; WHO, 2014b). These estimates rely on $PM_{2.5}$ concentrations from coarse global models with mean spatial resolutions of ~ 200 km. At these resolutions, human health estimates are likely underestimated at urban and semi-urban scales. Emission inventories highlight residential combustion as one of the most important contributors to ambient $PM_{2.5}$, accounting for 55 % in Europe (EEA, 2014) and 33 % in China (Lei et al., 2011). However, while previous studies have estimated the human health impacts from ambient air pollution due to fossil fuel combustion (Anenberg et al., 2010), open biomass burning (Johnston et al., 2012; Marlier et al., 2013), and wind-blown dust (Giannadaki et al., 2014), fewer studies have quantified the impact of residential combustion on ambient quality and human health. Lim et al. (2012) estimated that 16 % of the global burden of ambient $PM_{2.5}$ was due to RSF sources but did not estimate premature mortality. Another study concluded that ambient $PM_{2.5}$ from cooking was responsible for 370 000 deaths in 2010 (Chafe et al., 2014), but it did not include residential heating emissions, which will cause additional adverse impacts on human health (Johnston et al., 2013; Allen et al., 2013; Y. Chen et al., 2013).

Here we use a global aerosol microphysics model to make an integrated assessment of the impact of residential emissions on atmospheric aerosol, radiative effect, and human health. We used a radiative transfer model to calculate the DRE and first AIE due to residential emissions. To improve our understanding of the health impacts associated with these emissions, we combined simulated $PM_{2.5}$ concentrations with concentration-response functions from the epidemiological literature to estimate excess premature mortality.

2 Methods

2.1 Model description

We used the GLOMAP global aerosol microphysics model (Spracklen et al., 2005a), which is an extension to the TOMCAT 3-D global chemical transport model (Chipperfield, 2006). We used the modal version of the model, GLOMAP-mode (Mann et al., 2010), where aerosol mass and number concentrations are carried in seven log-normal size modes: four hydrophilic (nucleation, Aitken, accumulation, and coarse) and three non-hydrophilic (Aitken, accumulation, and coarse) modes. The model includes size-resolved aerosol processes including primary emissions, secondary particle formation, particle growth through coagulation, condensation, and cloud-processing and removal by dry deposition, in-cloud, and below-cloud scavenging. The model treats particle formation from both binary homogenous nucleation (BHN) of H_2SO_4–H_2O (Kulmala et al., 1998) and an empirical mechanism to simulate nucleation within the model boundary layer or boundary layer nucleation (BLN). The formation rate of 1 nm clusters (J1) within the BL is proportional to the gas-phase H_2SO_4 concentration ($[H_2SO_4]$) to the power of 1 (Sihto et al., 2006; Kulmala et al., 2006) according to $J1 = A[H_2SO_4]$, where A is the nucleation rate coefficient of $2 \times 10^{-6}\,s^{-1}$ (Sihto et al., 2006). GLOMAP-mode simulates multi-component aerosol and treats the following components: sulfate, dust, BC, POM, and sea salt. Primary carbonaceous combustion particles (BC and POM) are emitted as a non-hydrophilic distribution (Aitken insoluble mode). Dust is emitted into the insoluble accumulation and coarse modes. Non-hydrophilic particles are transferred

into hydrophilic particles through coagulation and condensation processes. The model uses a horizontal resolution of 2.8° by 2.8° and 31 vertical levels between the surface and 10 hPa. Large-scale transport and meteorology is specified at 6 h intervals from the European Centre for Medium-Range Weather Forecasts (ECMWF) analyses interpolated to model timestep. All model simulations are for the year 2000, completed after a 3-month model spin up. Oxidants of OH, O_3, H_2O_2, NO_3, and HO_2 are specified using 6 h mean offline concentrations from a TOMCAT simulation with detailed tropospheric chemistry (Arnold et al., 2005).

2.2 Emissions

The model uses gas-phase SO_2 emissions for both continuous (Andres and Kasgnoc, 1998) and explosive (Halmer et al., 2002) volcanic eruptions. Open biomass burning emissions are from the Global Fire Emission Database (van der Werf et al., 2004). Oceanic dimethyl-sulfide (DMS) emissions are calculated using an ocean surface DMS concentration database (Kettle and Andreae, 2000) combined with a sea–air exchange parameterization (Nightingale et al., 2000). Emissions of sea salt were calculated using the scheme of Gong (2003). Biogenic emissions of terpenes are taken from the Global Emissions Inventory Activity database and are based on Guenther et al. (1995). Daily-varying dust emission fluxes are provided by AeroCom (Dentener et al., 2006).

Annual mean anthropogenic emissions of gas-phase SO_2 and carbonaceous aerosol for the year 2000 are taken from the Atmospheric Chemistry and Climate Model Intercomparison Project (ACCMIP) (Lamarque et al., 2010). This data set includes emissions from energy production and distribution, industry, land transport, maritime transport, residential and commercial, and agricultural waste burning on fields. To test the sensitivity to anthropogenic emissions, we completed sensitivity studies (see Sect. 2.6) using anthropogenic emissions from the MACCity (MACC/CityZEN projects) emission data set for the year 2000 (Granier et al., 2011). MACCity emissions are derived from ACCMIP and apply a monthly varying seasonal cycle for anthropogenic emissions (Granier et al., 2011). In both emissions data sets, anthropogenic carbonaceous emissions are based on the Speciated Particulate Emissions Wizard (SPEW) inventory (Bond et al., 2007). In GLOMAP, anthropogenic carbonaceous emissions are added to the lowest model layer, while open biomass burning emissions are emitted between the surface and 6 km (Dentener et al., 2006).

We isolate the impact of residential fuel combustion through simulations where we switch off emissions from the "residential and commercial" sector. The term "residential" includes emissions from household activities, while "commercial" refers to emissions from commercial business activities (excluding agricultural activities). Both residential and commercial activities use similar fuels for similar purposes, but because emissions are dominated by residential activities, we refer to the "residential and commercial" sector collectively as the "residential" sector. Residential fuels used in small-scale combustion for cooking, heating, lighting, and auxiliary engines, consist of many different types such as RSFs (biomass/biofuel and coal) and hydrocarbon-based fuels including kerosene, liquefied petroleum gas, gasoline, and diesel. The ACCMIP and MACCity residential data sets do not allow us to isolate the impacts of different RSFs separately from other residential hydrocarbon-based fuels, but according to the results from the Greenhouse Gas and Air Pollution Interactions and Synergies (GAINS) model, typically ≥ 90 % of PM emissions can be attributed to RSFs within most regions, of which a large proportion is from biomass sources. Compared with residential hydrocarbon-based fuels, RSFs typically burn at lower combustion efficiencies, resulting in substantially higher aerosol emissions (Venkataraman et al., 2005). Residential kerosene wick lamps can produce substantial emissions (Lam et al., 2012); however, these are not included in the ACCMIP and MACCity data sets. Residential biofuel and coal emissions from ACCMIP and MACCity differ to previous global emission inventories (Bond et al., 2004, 2007) through the incorporation of updated emissions factors from field measurements (Roden et al., 2006, 2009; Johnson et al., 2008) and laboratory experiments for biofuel sources in India (Venkataraman et al., 2005; Parashar et al., 2005) and residential coal sources in China (Chen et al., 2005, 2006; Zhi et al., 2008). In both the ACCMIP and MACCity emission data sets, global emissions for the residential and commercial sectors are BC ($\sim 1.9\,\mathrm{Tg\,yr^{-1}}$), POM ($\sim 11.0\,\mathrm{Tg\,POM\,yr^{-1}}$), and SO_2 ($\sim 8.3\,\mathrm{Tg\,SO_2\,yr^{-1}}$).

Figure 1 shows the spatial distribution of BC, POM, and SO_2 emissions from the residential sector in the ACCMIP data set (Lamarque et al., 2010). Residential emissions are greatest over densely populated regions of Africa and Asia where infrastructure and income do not allow access to clean sources of residential energy. The dominant fuel type varies spatially resulting in distinct patterns in pollutant emission ratios (Fig. 1d–e). Residential emissions are dominated by biofuel (biomass) combustion in sub-Saharan Africa, South Asia, and parts of Southeast Asia and characterised by low BC : POM and high BC : SO_2 ratios. Residential coal combustion is more important in parts of Eastern Europe, the Russian Federation, and East Asia, characterised by higher BC : POM and lower BC : SO_2 ratios. In the ACCMIP and MACCity data sets, residential sources account for 38 % of global total anthropogenic BC and 61 % of total global anthropogenic POM emissions. The regional contribution of residential emissions can be even greater (Fig. 1f). For China, residential emissions represent 40 % of anthropogenic BC and 60 % of anthropogenic POM emissions. In India, residential emissions represent 63 % of anthropogenic BC and 78 % of anthropogenic POM emissions.

We assume primary particles from combustion sources are emitted with a fixed log-normal size distribution with a specified geometric mean diameter (D) and standard de-

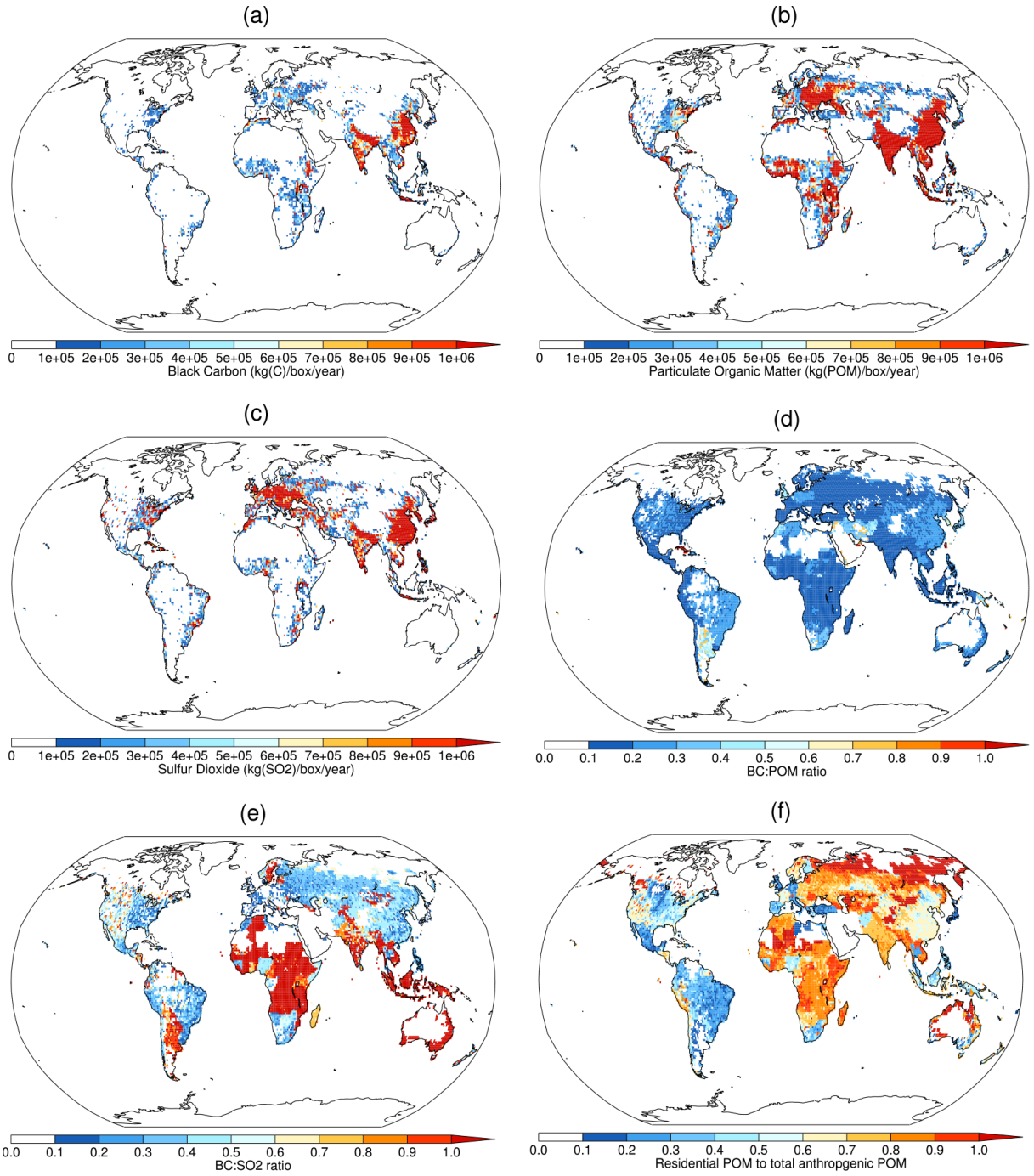

Figure 1. Annual residential emissions from the ACCMIP emission data set for BC **(a)**, POM **(b)**, SO_2 **(c)**, BC : POM ratio **(d)**, BC : SO_2 ratio **(e)**, and residential POM to total anthropogenic POM **(f)**.

viation (σ). Assumptions regarding D and σ for each experiment are detailed in the footnotes of Table 2. This assumption accounts for both the size of primary particles at the point of emission and the sub-grid-scale dynamical processes that contribute to changes in particle size and number concentrations at short timescales after emission (Pierce and Adams, 2009; Reddington et al., 2011). Subsequent aging and growth of the particles are determined by microphysical processes such as coagulation, condensation, and cloud processing simulated by the model. We assume that 2.5 % of SO_2 from anthropogenic and volcanic sources is emitted as primary sulfate particles.

2.3 In situ measurements

To evaluate our model, we synthesised in situ measurements of BC, OC, and $PM_{2.5}$ concentrations, aerosol number size distribution, and estimates of the contribution of biomass derived BC from ^{14}C analysis. GLOMAP has been evaluated for locations in North America (Mann et al., 2010; Spracklen et al., 2011a), the Arctic (Browse et al., 2012; Reddington et al., 2013), and Europe (Schmidt et al., 2011). Here, we focus our evaluation at locations that may be strongly influenced by residential emissions (Fig. 1) and where the model has not been previously evaluated. We focus on rural and background locations because these are more appropriate for comparison to global models with coarse spatial resolutions.

Figure 2 shows the locations of observations used in this study. Information on the measurements for each location is reported in Table 1. Note that the coloured geographical regions in Fig. 2 are only used to distinguish differences in mortality across different regions (see Sect. 3.3). The technique and instruments used to measure BC and OC vary across the different sites (see Table 1). Thermal–optical techniques measure elemental carbon (EC) whereas optical techniques measure BC. Previous studies have documented systematic differences between these techniques but concluded that measurement uncertainties are generally larger than the differences between the measurement techniques (Bond et al., 2004, 2007). We therefore treat different measurement techniques identically and consider EC and BC to be equivalent. For sites in Eastern Europe, we used BC and OC mass concentrations from the Czech Republic and Slovenia (Table 1). For sites in South Africa, we used $PM_{2.5}$ and BC mass and aerosol number size distribution (Vakkari et al., 2013). For sites in South Asia, we used BC mass from the Integrated Campaign for Aerosols gases and Radiation Budget (ICARB) field campaign at eight locations across the Indian mainland and islands (Moorthy et al., 2013). For South Asian sites, we also used $PM_{2.5}$, EC, and OC mass, aerosol number size distribution from the island of Hanimaadhoo in the Maldives (Stone et al., 2007), and EC and OC measurements from Godavari in Nepal (Stone et al., 2010). For sites in East Asia, we used EC and OC mass data compiled by Fu et al. (2012) for two background (Qu et al., 2008) and seven rural sites (Zhang et al., 2008; Han et al., 2008) in China, while measurements from Gosan, South Korea, were taken from Stone et al. (2011). Few long-term observations of CCN are available, so instead we use the number concentration of particles greater than 50 nm dry diameter (N_{50}) and 100 nm (N_{100}) as a proxy for CCN number concentrations. We calculated N_{50} and N_{100} concentrations from aerosol number size distribution measurements at Hanimaadhoo, Botsalano, Marikana, and Welgegund (see Table 1). We note this approach does not account for the impact of particle composition on CCN activity.

We also use information on BC fossil and non-fossil fractions as obtained from three separate source apportionment studies (Gustafsson et al., 2009; Sheesley et al., 2012; Bosch et al., 2014) that use ^{14}C analysis of carbonaceous aerosol taken at Hanimaadhoo in the Indian Ocean. This technique determines the fossil and non-fossil fractions of carbonaceous aerosol, since ^{14}C is depleted in fossil fuel aerosol (half-life 5730 years), whereas non-fossil aerosol (e.g. biofuel, open biomass burning, and biogenic emissions) shows a contemporary ^{14}C content. As previously mentioned, residential emissions consist of a mixture of both fossil and non-fossil sources, with a greater proportion coming from the former. To make distinctions on the fossil versus non-fossil fraction of residential BC emissions, we make assumptions based on information from other emission inventories and models over the South Asian region (see Sect. 3.2 for more details).

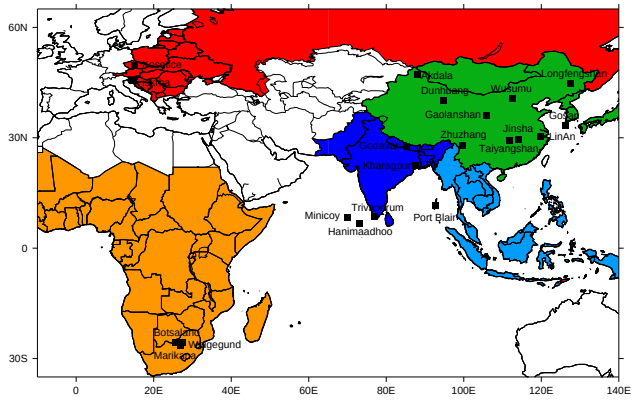

Figure 2. Locations of aerosol measurements used in this study and geographical regions of Eastern Europe and the Russian Federation (red), Africa (orange), South Asia (dark blue), Southeast Asia (light blue), and East Asia (green). Note that geographical regions are only used to distinguish difference in mortality across different regions (see Sect. 3.3).

2.4 Calculating health effects

We calculate annual excess premature mortality from exposure to ambient $PM_{2.5}$ using concentration response functions (CRFs) from the epidemiological literature that relate changes in $PM_{2.5}$ concentrations to the relative risk (RR) of disease. CRFs are uncertain and have been previously based on the relationship between RR and $PM_{2.5}$ concentrations using either a log-linear model (Ostro, 2004) or a linear model (Cohen et al., 2004). These CRFs were based on the American Cancer Society Prevention cohort study, where observed annual mean $PM_{2.5}$ concentrations were typically below 30 $\mu g\,m^{-3}$. The log-linear model was recommended by the WHO for use in ambient air pollution burden of disease estimates at the national level (Ostro, 2004) due to the concern that linear models would produce unrealistically large RR estimates when extrapolated to higher $PM_{2.5}$ concentrations above that of 30 $\mu g\,m^{-3}$. The log-linear models have been used in various modelling studies (Anenberg et al.,

Table 1. Summary of aerosol observations used in this study.

Region and measurement location/site name	Site description	Measurement	Measurement period	Measurement technique	Reference
		Eastern European sites			
Košetice (49.34° N, 15.4° E)	Rural site in central Czech Republic	EC and OC in size fraction $PM_{2.5}$	2010	EC and OC: thermal–optically	*
Iskrba (45.34° N, 14.52° E)	Rural site in southern Slovenia	EC and OC in size fraction $PM_{2.5}$	2010	EC and OC: thermal–optically	*
		South African sites			
Botsalano (25.54° S, 25.75° E)	Rural site in northeastern South Africa	$PM_{2.5}$ mass and aerosol number distribution	2007	$PM_{2.5}$ mass: TEOM Monitor; aerosol number distribution: DMPS	Vakkari et al. (2013)
Marikana (25.70° S, 27.48° E)	Semi-urban site in northeastern South Africa	BC and aerosol number distribution	2008	BC: thermo model 5012 multiangle absorption photometer; aerosol number distribution: DMPS	Vakkari et al. (2013)
Welgegund (26.57° S, 26.94° E)	Semi-rural site in northeastern South Africa	Aerosol number distribution	2011	Aerosol number distribution: DMPS	Tiitta et al. (2014)
		South Asian sites			
Hanimaadhoo (6.87° N, 73.18° E)	Background site in Maldives	$PM_{2.5}$ mass, EC, and OC in size fraction $PM_{2.5}$; aerosol number distribution and fossil and non-fossil BC and EC fractions	Oct–Jan 2004–2005; Jan–Jul 2005 See references for 14C analysis dates	$PM_{2.5}$: gravimetrically; EC and OC: thermal–optically; aerosol number distribution: SMPS ^{14}C analysis	Stone et al. (2007) Gustafsson et al. (2009) Sheesley et al. (2012) Bosch et al. (2014)
Godavari (27.59° N, 85.31° E)	Rural/near-urban site in the foothills of the Himalayas	EC and OC in size fraction $PM_{2.5}$	Jan–Dec 2006	EC and OC: thermal–optically	Stone et al. (2010)
Port Blair (11.6° N, 92.7° E)	Background site located on an island in the Bay of Bengal	BC concentration	2006	BC: optically by aethalometer	Moorthy et al. (2013)
Minicoy (8.3° N, 73.0° E)	Background site located on an island in the Arabian Sea	BC concentration	2006	BC: optically by aethalometer	Moorthy et al. (2013)
Kharagpur (22.5° N, 87.5° E)	Semi-urban site in the Indo-Gangetic Plain	BC concentration	2006	BC: optically by aethalometer	Moorthy et al. (2013)
Trivandrum (8.55° N, 76.9° E)	Semi-urban coastal site in southern India	BC concentration	2006	BC: optically by aethalometer	Moorthy et al. (2013)

Table 1. Continued.

Region and measurement location/site name	Site description	Measurement	Measurement period	Measurement technique	Reference
		East Asia sites			
Gosan (33.38° N, 126.25° E)	Background site on Jeju Island, South Korea	$PM_{2.5}$ mass, EC, and OC in size fraction $PM_{2.5}$	Jan–Jul 2007	$PM_{2.5}$: gravimetrically; EC and OC: thermal–optically	Stone et al. (2011)
Akdala (47.1° N, 87.97° E)	Background site in northwestern China	EC and OC in size fraction PM_{10}	Aug, Sep, Nov, and Dec 2004; Jan–Mar 2005	EC and OC: thermal–optically	Qu et al. (2008)
Zhuzhang (28° N, 99.72° E)	Background site in southern China	EC and OC in size fraction PM_{10}	Aug–Dec 2004; Jan–Feb 2005	EC and OC: thermal–optically	Qu et al. (2008)
Dunhuang (40.15° N, 94.68° E)	Rural site in northwestern China	EC and OC in size fraction PM_{10}	2006	EC and OC: thermal–optically	Zhang et al. (2008)
Gaolan Shan (36° N, 105.85° E)	Rural site in central China	EC and OC in size fraction PM_{10}	2006	EC and OC: thermal–optically	Zhang et al. (2008)
Wusumu (40.56° N, 112.55° E)	Rural site in northeastern China	EC and OC in size fraction PM_{10}	Sep 2005; Jan and Jul 2006; May 2007	EC and OC: thermal–optically	Han et al. (2008)
Longfengshan (44.73° N, 127.6° E)	Rural site in northeastern China	EC and OC in size fraction PM_{10}	2006	EC and OC: thermal–optically	Zhang et al. (2008)
Taiyangshan (29.17° N, 111.71° E)	Rural site in central China	EC and OC in size fraction PM_{10}	2006	EC and OC: thermal–optically	Zhang et al. (2008)
Jinsha (29.63° N, 114.2° E)	Rural site in central China	EC and OC in size fraction PM_{10}	Jun–Nov 2006	EC and OC: thermal–optically	Zhang et al. (2008)
Linan (30.3° N, 119.73° E)	Rural site in eastern China	EC and OC in size fraction PM_{10}	2004–2005	EC and OC: thermal–optically	Zhang et al. (2008)

* Data obtained through the EBAS atmospheric database (http://ebas.nilu.no/Default.aspx).

2010; Schmidt et al., 2011; Partanen et al., 2013; Reddington et al., 2015). More recent models have been proposed to relate disease burden to different combustion sources in order to capture RR over a larger range of $PM_{2.5}$ concentrations up to 300 µg m^{-3} (Burnett et al., 2014). However, given that we use a global model with relatively coarse spatial resolution where $PM_{2.5}$ concentrations very rarely exceed 100 µg m^{-3}, we employ the log-linear model of Ostro (2004). We calculate RR for cardiopulmonary diseases and lung cancer following Ostro (2004):

$$\mathrm{RR} = \left[\frac{(\mathrm{PM}_{2.5,\mathrm{control}} + 1)}{(\mathrm{PM}_{2.5,\mathrm{R\_off}} + 1)}\right]^{\beta}, \quad (1)$$

where $PM_{2.5,control}$ is annual mean simulated $PM_{2.5}$ concentrations of the control experiments and $PM_{2.5,R\_off}$ is a perturbed experiment where residential emissions have been removed. The cause-specific coefficient (β) is an empirical parameter with separate values for lung cancer (0.23218, 95 % confidence interval of 0.08563–0.37873) and cardiopulmonary diseases (0.15515, 95 % confidence interval of 0.05624–0.2541). To calculate the disease burden attributable to the RR, known as the attributable fraction (AF), we follow Ostro (2004):

$$\mathrm{AF} = (\mathrm{RR} - 1)/\mathrm{RR}. \quad (2)$$

To calculate the number of excess premature mortality in adults over 30 years of age, we apply AF to the total number of recorded deaths from the diseases of interest:

$$\Delta M = \mathrm{AF} \times M_0 \times P_{30+}, \quad (3)$$

where M_0 is the baseline mortality rate for each disease risk and P_{30+} is the exposed population over 30 years of age. We only calculate premature mortality for persons over the age of 30 years because this fraction of the population is more susceptible to cardiopulmonary disease and lung cancer. We use country-specific baseline mortality rates from the WHO "The global burden of disease: 2004 update" (Mathers et al., 2008) for the year 2004 and human population data from the Gridded World Population (GWP, version 3) project (SEDAC, 2004) for the year 2000.

2.5 Calculating radiative effects

We quantified the DRE and first AIE of residential emissions using an offline radiative transfer model (Edwards and Slingo, 1996). With nine radiation bands in the longwave (LW) and six bands in the shortwave (SW). We use a monthly mean climatology of water vapour, temperature, and ozone based on ECMWF reanalysis data, together with surface albedo and cloud fields from the International Satellite Cloud Climatology Project (ISCCP-D2) (Rossow and Schiffer, 1999) for the year 2000.

Following the methodology described in Rap et al. (2013) and Scott et al. (2014), we estimate the DRE using the radiative transfer model to calculate the difference in net (SW + LW) top-of-atmosphere (TOA) all-sky radiative flux between model simulations with and without residential emissions. A refractive index is calculated for each individual mode separately, as the volume-weighted mean of the refractive indices for the individual components (including water) present (given at 550 nm in Table A1 of Bellouin et al., 2011). Coefficients for absorption and scattering, and asymmetry parameters, are then obtained from look-up tables containing all realistic combinations of refractive index and Mie parameter (particle radius normalised to the wavelength of radiation), as described by Bellouin et al. (2013). The assumption that BC is internally or homogeneously mixed with scattering species is unrealistic, providing an upper bound for DRE (Jacobson, 2001; Kodros et al., 2015).

To determine the first AIE we calculate the contribution of residential emissions to CDNC. We calculate CDNC using the parameterisation of cloud drop formation (Nenes and Seinfeld, 2003; Fountoukis and Nenes, 2005; Barahona et al., 2010) as described by Pringle et al. (2009). The maximum supersaturation (SS_{max}) of an ascending cloud parcel depends on the competition between increasing water vapour saturation with decreasing pressure and temperature and the loss of water vapour through condensation onto activated particles. Monthly mean aerosol size distributions are converted to a supersaturation distribution where the number of activated particles can be determined for the SS_{max}. CDNC are calculated using a constant up-draught velocity of 0.15 ms^{-1} over sea and 0.3 ms^{-1} over land, which is consistent with observations for low-level stratus and stratocumulus clouds (Pringle et al., 2012). In reality, up-draught velocities vary, but the use of average velocities in previous GLOMAP studies has been shown to capture observed relationships between particle number and CDNC (Pringle et al., 2009), as well as reproducing realistic CDNC (Merikanto et al., 2010). The AIE is calculated using the methodology described previously (Spracklen et al., 2011a; Schmidt et al., 2012; Scott et al., 2014) where a control uniform cloud droplet effective radius $r_{e1} = 10$ µm is assumed to maintain consistency with the ISCCP determination of liquid water path. For each perturbation experiment the effective radius r_{e2} is calculated:

$$r_{e2} = r_{e1} \times (\mathrm{CDNC}_1/\mathrm{CDNC}_2)^{\frac{1}{3}}, \quad (4)$$

where $CDNC_1$ represents a control simulation including residential emissions and $CDNC_2$ represents a simulation where residential emissions have been removed. The AIE is calculated by comparing the net TOA radiative fluxes using the different r_{e2} values derived for each perturbation experiment, to that of the control where r_{e1} is fixed. We do not calculate the cloud lifetime (second indirect effect), semi-direct effects, or snow albedo changes. We also do not account for light absorbing brown carbon and the lensing effect of BC particles coated with a non-absorbing shell, and thus we are

unable to estimate the full climate impact of residential combustion emissions.

2.6 Model simulations

Table 2 reports the model experiments used in this study. These simulations explore uncertainty in residential emission flux and emitted carbonaceous aerosol size distributions and the impact of particle formation. We test two different emission data sets (see Sect. 2.2 for details) allowing us to explore the role of seasonally varying emissions compared to annual mean emissions. We refer to the simulation using the ACCMIP emissions (annual mean emissions) with the standard model setup as the baseline simulation (res_base), while all other simulations explore key uncertainties relative to res_base or use the MACCity emission database of monthly varying anthropogenic emissions (res_monthly). To allow us to quantify the impact of residential emissions we conduct simulations where residential emissions (BC, OC and SO_2) have been switched off (res_base_off and res_monthly_off). To account for uncertainties in the nucleation scheme, we conduct simulations where only BHN is able to contribute to new particle formation (res_BHN and res_BHN_off), while all other simulations include both BHN and BLN. For the majority of our simulations, we use D and σ recommended by Stier et al. (2005) ($D = 150$ nm $\sigma = 1.59$). To account for the uncertainty in the size of emitted residential carbonaceous combustion aerosol and uncertainty of sub-grid ageing of the size distribution, we conduct simulations spanning the range of observed size distributions for primary BC and OC residential combustion particles, while keeping emission mass fixed. We use AeroCom (Dentener et al., 2006) recommended particle size settings (res_aero) (D = 80nm σ = 1.8) and, following a similar approach to Bauer et al. (2010), we use the range identified by Bond et al. (2006) for lower (res_small) ($D = 20$ nm $\sigma = 1.8$) and upper (res_large) ($D = 500$ nm $\sigma = 1.8$) estimates. To account for possible low biases in residential emission flux, we conduct simulations where residential primary carbonaceous combustion aerosol mass (BC and OC) are doubled relative to the baseline simulation (res_$\times$ 2) and the simulation using monthly mean anthropogenic emissions (res_monthly_$\times$ 2). We also perform experiments where only residential BC and OC emissions are doubled separately relative to the baseline simulation (res_BC$\times$ 2 and res_POM$\times$ 2) to explore uncertainties in both emission mass flux and emission ratio. While the uncertainties in primary carbonaceous aerosol emissions are thought to be higher than for gas-phase SO_2 (Klimont et al., 2009), we also conduct an experiment where we double residential SO_2 emissions (res_SO2$\times$ 2).

3 Results

3.1 Model evaluation

Figure 3 compares observed and simulated monthly mean BC, OC, and $PM_{2.5}$ concentrations and normalised mean bias factor (NMBF) (Yu et al., 2006), where M_i are the simulated concentrations by the model and O_i are the observed concentrations at each measurement location, i,

$$\mathrm{NMBF} = \frac{\sum (M_i - O_i)}{\sum O_i} \text{ if } \overline{M} \geq \overline{O} \text{ and}$$
$$\mathrm{NMBF} = \frac{\sum (M_i - O_i)}{\sum M_i} \text{ if } \overline{M} < \overline{O}. \quad (5)$$

The baseline simulation underestimates observed BC (NMBF $= -2.33$), OC (NMBF $= -5.02$), and $PM_{2.5}$ (NMBF $= -1.33$) concentrations. The greatest model underprediction is across East Asia (BC: NMBF $= -2.61$, OC: NMBF $= -6.56$, and $PM_{2.5}$: NMBF $= -1.94$). Over South Asia the model is relatively unbiased against OC (NMBF $= 0.41$) but underestimates BC (NMBF $= -2.54$). In contrast, over Eastern Europe the model is unbiased against BC (NMBF $= 0.01$) but underestimates OC (NMBF $= -2.63$). The simulation with monthly varying emissions compares slightly better with observations compared to the baseline simulation but still underestimates BC (NMBF $= -2.29$), OC (NMBF $= -4.92$), and $PM_{2.5}$ (NMBF $= -1.34$), suggesting that seasonality in emissions has little impact on reducing model bias. The low bias in our model, particularly for BC and OC, is consistent with previous modelling studies using bottom-up emission inventories in South Asia (Ganguly et al., 2009; Menon et al., 2010; Nair et al., 2012; Moorthy et al., 2013; Pan et al., 2015) and East Asia (Park et al., 2005; Koch et al., 2009; Fu et al., 2012). The contribution of residential emissions is illustrated by the model simulation where these emissions are switched off, with substantially greater underestimation of BC (NMBF $= -5.12$), OC (NMBF $= -11.46$), and $PM_{2.5}$ (NMBF $= -1.60$) concentrations (Fig. 3d). Doubling residential carbonaceous emissions improves model agreement with observations, but the model still underestimates BC (NMBF $= -1.33$), OC (NMBF $= -2.96$), and $PM_{2.5}$ (NMBF $= -1.17$) concentrations.

Figure 4 compares observed and simulated concentrations for South Asian locations. The baseline simulation underestimates carbonaceous aerosol concentrations at all locations, although there is better agreement at Godavari and Hanimaadhoo. BC measurements at these two sites were made through thermal–optical methods, whereas other locations in South Asia used optical methods (Table 1). Different measurement techniques result in different mass concentrations (Stone et al., 2007) and may contribute to model–observation errors. The emission inventory that we use is based on carbonaceous measurements using thermal–optical

Table 2. Summary of model simulations and global annual mean values and changes to BC and POM burden, continental surface $PM_{2.5}$, surface total particle number (N_3, diameter > 3 nm), N_{50} (diameter > 50 nm), low-cloud level (850–900 hPa) CDNC concentrations (0.15 and 0.3 ms^{-1} cloud updraft velocity over sea and land respectively), and all-sky DRE and first AIE, relative to an equivalent experiment where residential emissions have been removed. We estimate annual global mortality for cardiopulmonary disease (CPD) and lung cancer (LC) following Ostro (2004) showing 95 % confidence interval (total in bold). Emissions used are either the ACCMIP data set (A) or the MACCity data set (M) with perturbations to residential emissions applied as detailed. For emitted carbonaceous size distributions, see Table footnote.

Expt. no.	Description	Emissions	BC burden (Tg)	POM burden (Tg)	$PM_{2.5}$ ($\mu g\,m^{-3}$)	N_3 (cm^{-3})	N_{50} (cm^{-3})	CDNC (cm^{-3})	Mortality (000)	All-sky DRE ($mW\,m^{-2}$)	First AIE ($mW\,m^{-2}$)
1	**res_base_off**	None	–	–	–	–	–	–	–	–	–
2	**res_base** All annual mean anthropogenic emissions (including residential emissions)[a]	A	0.11 +0.024 (+25.68 %)	1.07 +0.135 (+14.33 %)	4.19 +0.08 (+2.01 %)	778.51 −7.99 (−1.01 %)	381.81 +17.20 (+4.72 %)	214.61 +4.41 (+2.10 %)	CPD: 289 (106–467) LC: 26 (10–41) Total: **315 (115–508)**	**–5**	**–25**
3	**res_aero** AeroCom recommended size distribution for residential primary carbonaceous particles[b]	A	0.12 +0.025 (+26.69 %)	1.08 +0.145 (+15.32 %)	4.19 +0.08 (+2.03 %)	807.77 +19.11 (+2.43 %)	396.99 +31.32 (+8.56 %)	216.59 +6.39 (+3.04 %)	CPD: 288 (106–46) LC: 26 (10–41) Total: **314 (116–507)**	**1**	**–46**
4	**res_small** Observed lower bound limit size distribution for residential primary carbonaceous particles[c]	A	0.12 +0.028 (+29.20 %)	1.19 +0.22 (+22.59 %)	4.21 +0.09 (+2.25 %)	2593.62 +1612.46 (+164.34 %)	689.74 +253.37 (+58.06 %)	252.68 +42.48 (+20.21 %)	CPD: 270 (98–435) LC: 24 (9–38) Total: **294 (108–473)**	**63**	**–502**
5	**res_large** Observed upper bound limit size distribution for residential primary carbonaceous particles[d]	A	0.11 +0.024 (+25.38 %)	1.07 +0.133 (+14.07 %)	4.19 +0.08 (+1.99 %)	768.03 −17.68 (−2.25 %)	375.94 +11.73 (+3.22 %)	213.85 +3.65 (+1.74 %)	CPD: 290 000 (106–468) LC: 26 (10–41) Total: **316 (116–509)**	**–7**	**–16**
6	**res_ × 2** Primary residential BC and POM doubled globally[a]	A, BC / OC × 2	0.14 +0.047 (+49.90 %)	1.20 +0.263 (+27.90 %)	4.25 +0.14 (+3.48 %)	776.73 −9.76 (−1.24 %)	387.52 +22.90 (+6.28 %)	215.82 +5.62 (+2.67 %)	CPD: 477 (177–764) LC: 42 (16–66) Total: **519 (193–830)**	**21**	**–25**
7	**res_BC × 2** Primary residential BC doubled globally[a]	A, BC × 2	0.14 +0.051 (+53.81 %)	1.07 +0.134 (+14.21 %)	4.20 +0.06 (+2.24 %)	778.32 −8.18 (−1.04 %)	383.19 +18.58 (+5.09 %)	214.91 +4.71 (+2.24 %)	CPD: 320 (118–517) LC: 28 (11–46) Total: **348 (129–563)**	**85**	**–26**

Table 2. Continued.

Expt. no.	Description	Emissions	BC burden (Tg)	POM burden (Tg)	$PM_{2.5}$ ($\mu g\,m^{-3}$)	N_3 (cm^{-3})	N_{50} (cm^{-3})	CDNC (cm^{-3})	Mortality (000)	All-sky DRE ($mW\,m^{-2}$)	First AIE ($mW\,m^{-2}$)
8	**res_POM × 2** Primary residential POM doubled globally[a]	A, OC × 2	0.11 +0.022 (+23.06 %)	1.20 +0.264 (+28.01 %)	4.24 +0.14 (+3.25 %)	776.25 −10.25 (−1.30 %)	386.42 +21.81 (+5.98 %)	215.55 +5.35 (+2.55 %)	CPD: 433 (160–695) LC: 39 (15–62) Total: **472 (175–757)**	**–66**	**–23**
9	textbfres_SO2 **× 2** Primary residential SO_2 doubled globally[a]	A, SO_2 × 2	0.11 +0.024 (+25.19 %)	1.07 +0.122 (+14.11 %)	4.21 +0.06 (+2.52 %)	785.99 −0.51 (−0.06 %)	3 88.35 +23.74 (+6.51 %)	217.23 +7.03 (+3.34 %)	CPD: 306 (113–494) LC: 29 (11–46) Total: **336 (124–540)**	**–43**	**–45**
10	**res_BHN_off**	None	–	–	–	–	–	–	–	**–**	**–**
11	**res_BHN** Binary homogeneous nucleation only. Boundary layer activation nucleation switched off[a]	A	0.11 +0.023 (+25.46 %)	1.04 +0.131 (+14.33 %)	4.18 +0.08 (+2.01 %)	431.91 +23.41 (+5.73 %)	306.09 +18.73 (+6.52 %)	187.76 +5.7 (+3.13 %)	CPD: 289 (106–467) LC: 26 (10–41) Total: **315 (116–508 000)**	**–8**	**–52**
12	**res_monthly_off**	None	–	–	–	–	–	–	–	**–**	**–**
13	**res_monthly** Monthly varying anthropogenic emissions (including residential emissions)[a]	M	0.11 +0.024 (+25.38 %)	1.08 +0.135 (+14.37 %)	4.19 +0.08 (+2.07 %)	797.54 −12.23 (−1.51 %)	393.16 +18.17 (+4.84 %)	219.57 +5.09 (+2.37 %)	CPD: 283 (104–457) LC: 25 (9–40) Total: **308 (113–497)**	**–8**	**–20**
14	**res_monthly_ × 2** Primary residential BC and POM doubled globally[a]	M, BC / OC × 2	0.14 +0.047 (+49.76 %)	1.20 +0.265 (+27.99 %)	0.25 +0.15 (+3.62 %)	794.68 −15.09 (−1.86 %)	399.03 +24.04 (+6.41 %)	220.47 +5.99 (+2.79 %)	CPD: 475 (176–761) LC: 41 (16–66) Total: **517 (192–827)**	**10**	**–21**

[a] Stier et al. (2005) recommended residential (biomass/biofuel) primary carbonaceous particle sizes; $D = 150$ nm, $\sigma = 1.59$. [b] Aer0Com (Dentener et al., 2006) recommended residential (biomass/biofuel) primary carbonaceous particle sizes; $D = 80$ nm, $\sigma = 1.8$. [c] Observed lower bound limit for RSF primary carbonaceous particle sizes; $D = 20$ nm, $\sigma = 1.8$ (Bond et al., 2006). [d] Observed upper bound limit for RSF primary carbonaceous particle sizes; $D = 500$ nm, $\sigma = 1.8$ (Bond et al., 2006).

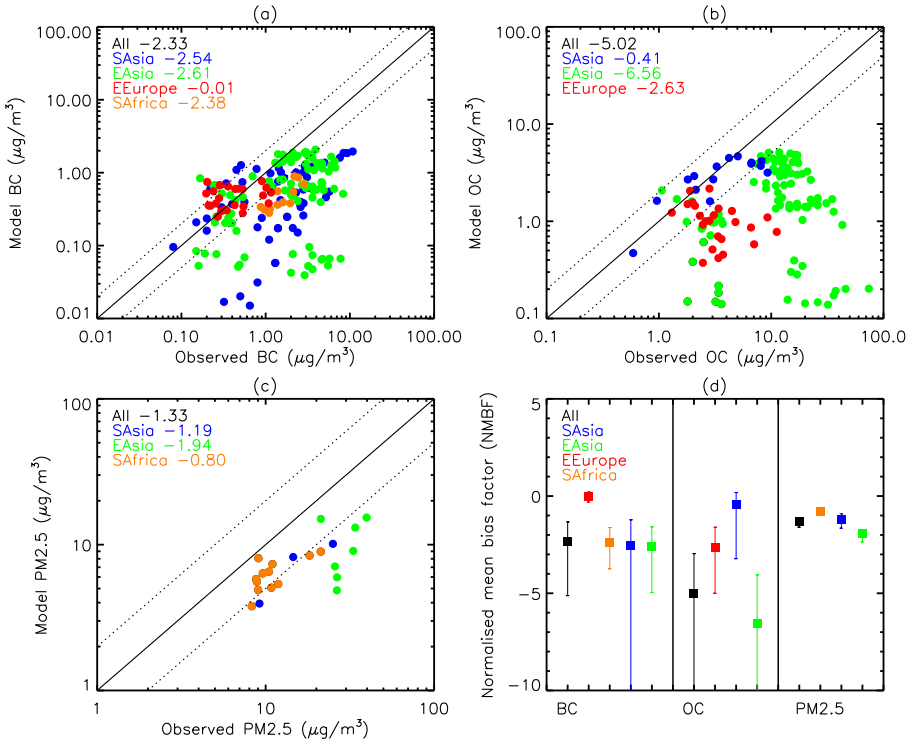

Figure 3. Observed and simulated monthly mean BC **(a)**, OC **(b)**, and $PM_{2.5}$ **(c)** concentrations for the baseline simulation (res_base) using ACCMIP emissions at each measurement location depicted in Table 1 and normalised mean bias factor (NMBF) for each region defined in Table 1. **(d)** NMBF where square shows the baseline simulation, bottom error bar shows the range for removed residential emissions (res_base_off), and top error bar shows residential carbonaceous emissions doubled (res_× 2) for each region defined in Table 1. Colours represent observed, simulated, and NMBF for measurement location regions defined in Table 1: all measurement locations (All: black), South Asian locations (SAsia: blue), East Asian locations (EAsia: green), Eastern European locations (EEurope: red), and South African locations (SAfrica: orange).

methods (Bond et al., 2004), which might explain the better agreement at Godavari and Hanimaadhoo. Doubling residential carbonaceous emissions improves the comparison against observations but leads to slight overestimation at Godavari and Hanimaadhoo. Pan et al. (2015) found that seven different global aerosol models underpredicted observed BC by up to a factor 10, suggesting that anthropogenic emissions are underestimated in these regions.

Observed BC and OC concentrations show strong seasonal variability, with lower concentrations during the summer monsoon period (June–September). The baseline simulation generally captures this seasonality relatively well (correlation coefficient between observed and simulated monthly mean concentrations $r > 0.5$ at most sites), with minimal improvement with monthly varying anthropogenic emissions. This suggests that meteorological conditions such as enhanced wet deposition during the summer monsoon period are the dominant drivers for the observed and simulated seasonal variability, consistent with other modelling studies for the same region (Adhikary et al., 2007; Moorthy et al., 2013). Model simulations where residential emissions have been switched off show that residential combustion contributes about two-thirds of simulated BC and OC at these locations. Figure 4k–l show a comparison of observed and simulated aerosol number concentrations at Hanimaadhoo. At this location, the baseline simulation simulates N_{20} (NMBF = 0.14), N_{50} (NMBF = 0.14) and N_{100} (NMBF = 0.24) concentrations well. Simulated number concentrations are sensitive to emitted particle size. Emitting residential primary carbonaceous emissions at very small sizes (res_small) results in an overestimation of N_{20} (NMBF = 1.84), N_{50} (NMBF = 1.28) and N_{100} (NMBF = 1.05), suggesting that this assumption is unrealistic.

Figure 5 compares observed and simulated surface monthly mean BC and OC concentrations for East Asian locations. Observed surface BC and OC concentrations are generally enhanced during winter (December–February) compared to the summer (June–August). At all locations, the model underestimates BC (except for Gosan) and OC concentrations. The baseline simulation underpredicts both BC (NMBF < -2) and OC (NMBF < -6) at Gaolan Shan and Longfengshan (as well as Akdala, Dunhuang, and Wusumu, which are not shown in Fig. 5), which is consistent with a previous model study at these locations (Fu et al., 2012).

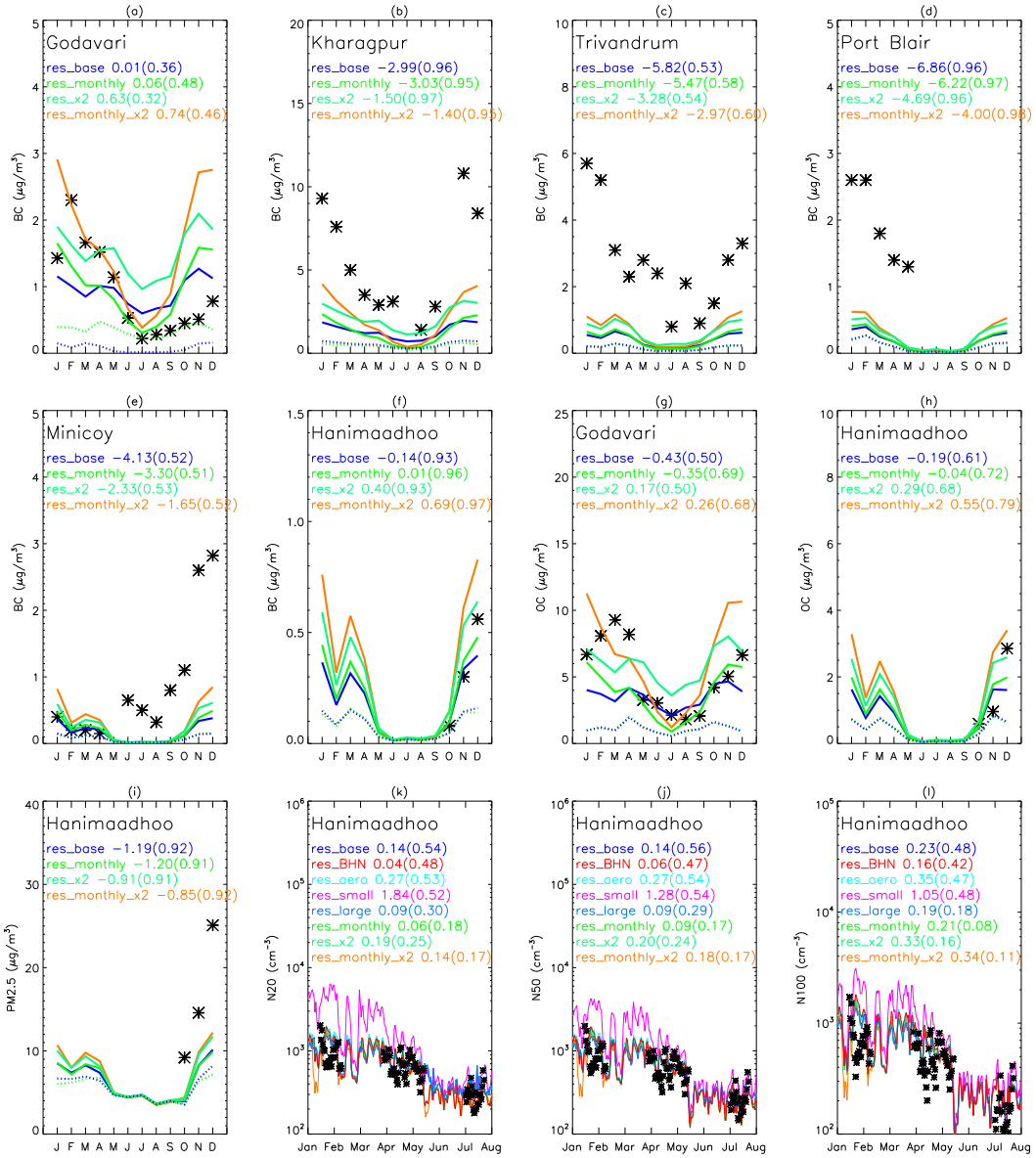

Figure 4. Observed (black stars) and simulated monthly mean BC **(a–f)**, OC **(g–h)**, $PM_{2.5}$ **(i)**, and daily mean N_{20} **(k)**, N_{50} **(j)**, and N_{100} **(l)** at South Asian locations. Normalised mean bias factor (NMBF) and correlation coefficient (r) are reported for each model simulation: NMBF(r). Experiments where residential emissions have been removed are represented by the blue (res_base_off) and green (res_monthly_off) dotted lines. Note that additional experiments (res_BHN, res_aero, res_small, and res_large) are included in **(k)**–**(i)** because these experiments have little impact on aerosol mass **(a–j)**.

The substantial underestimation at some locations (e.g. Dunhuang, Gaolan Shan, and Wusumu) may be due to local particulate sources that are not resolved by coarse model resolution. If we exclude these locations, NMBF improves for BC (-2.61 to -1.34) and OC (-4.43 to -3.29) for the East Asian region. The model better simulates BC (NMBF < -1) and OC (NMBF < -2) at Taiyangshan and Jinsha, although the model is still biased low. The baseline simulation, without seasonally varying emissions, fails to capture the observed seasonal variability in East Asia, with negative correlations between observed and simulated aerosol concentrations at a number of locations. Fu et al. (2012) suggests that residential emissions (most likely heating sources) were the principle driver of simulated seasonal variability of EC (BC) at these locations. Implementing monthly varying anthropogenic emissions (including residential emissions) generally improves the simulated seasonal variability ($r > 0.3$ at most sites) compared to using annual mean emissions. Doubling residential carbonaceous emissions also leads to improved NMBF at most locations. Residential emissions typi-

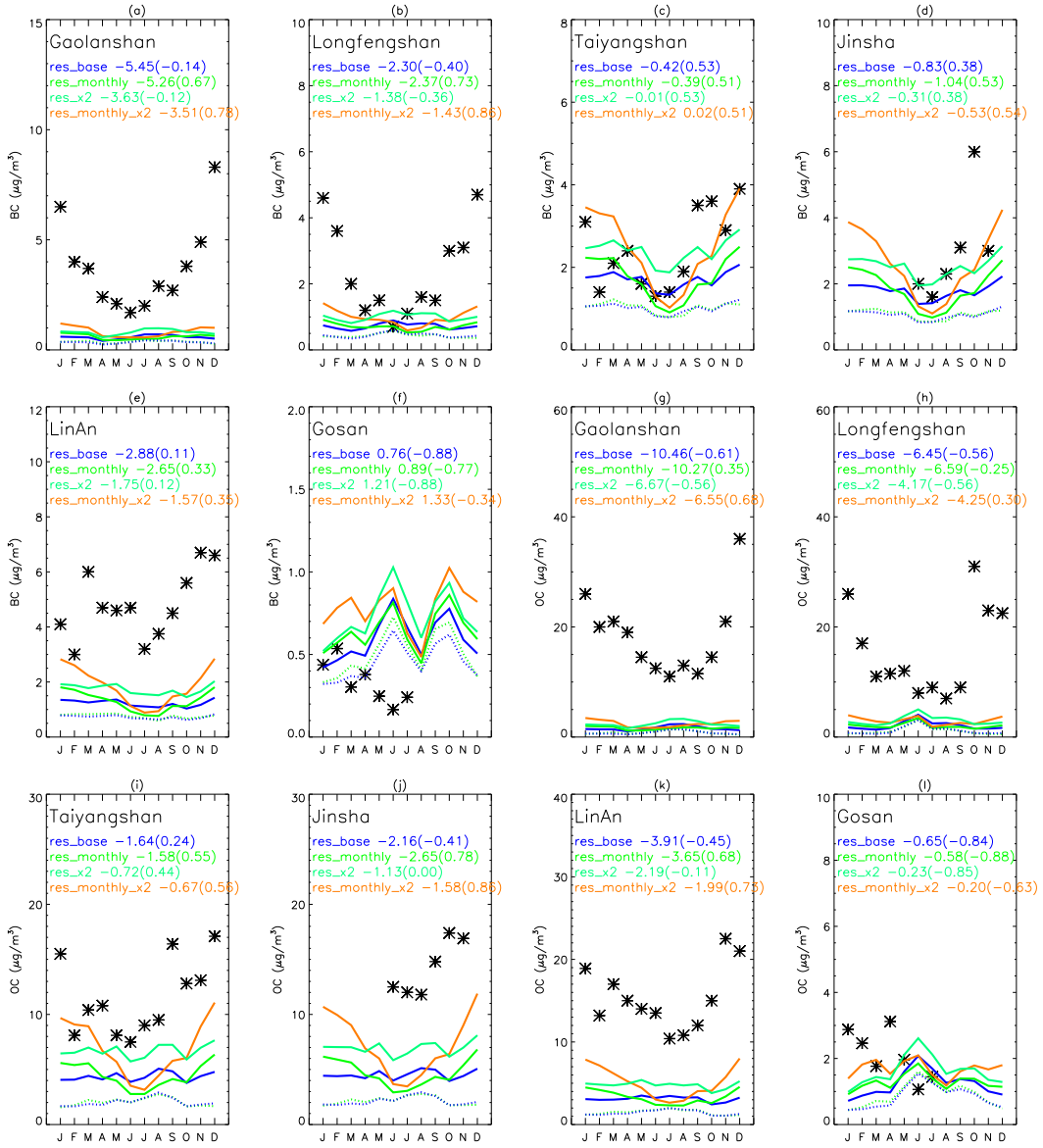

Figure 5. Observed (black stars) and simulated monthly mean BC **(a–f)** and OC **(g–l)** at East Asian locations. Normalised mean bias factor (NMBF) and correlation coefficient (r) are reported for each model simulation: NMBF(r). Experiments where residential emissions have been removed are represented by the blue (res_base_off) and green (res_monthly_off) dotted lines.

cally account for 50–65 % of simulated BC and OC concentrations at these locations.

Figure 6 compares simulated and observed aerosol at South African and Eastern European locations. Marikana, Botsalano, and Welgegund are all located within the same region of South Africa and are influenced by both residential emissions and open biomass burning during the dry season, of which open biomass burning savannah fire seasonality peaks in July–September (Venter et al., 2012; Vakkari et al., 2013). Simulated aerosol number concentrations (N_{20} and N_{100}) are underestimated at Marikana, consistent with the underprediction in BC at the same location, while number concentrations are better simulated at Botsalano and Welgegund. The model underprediction at Marikana is likely due to the location being closer to emission sources, compared to Botsalano and Welgegund. For N_{100} the model is generally good at simulating open biomass savannah burning seasonality (peaking in August–September), but increases in observed N_{100} earlier in the season (May–August at Marikana and July at Welgegund) are not simulated. At both locations this early season maxima is likely due to residential emissions (Vakkari et al., 2013), which suggests that residential emissions are underrepresented in the model possibly due to resolution effects.

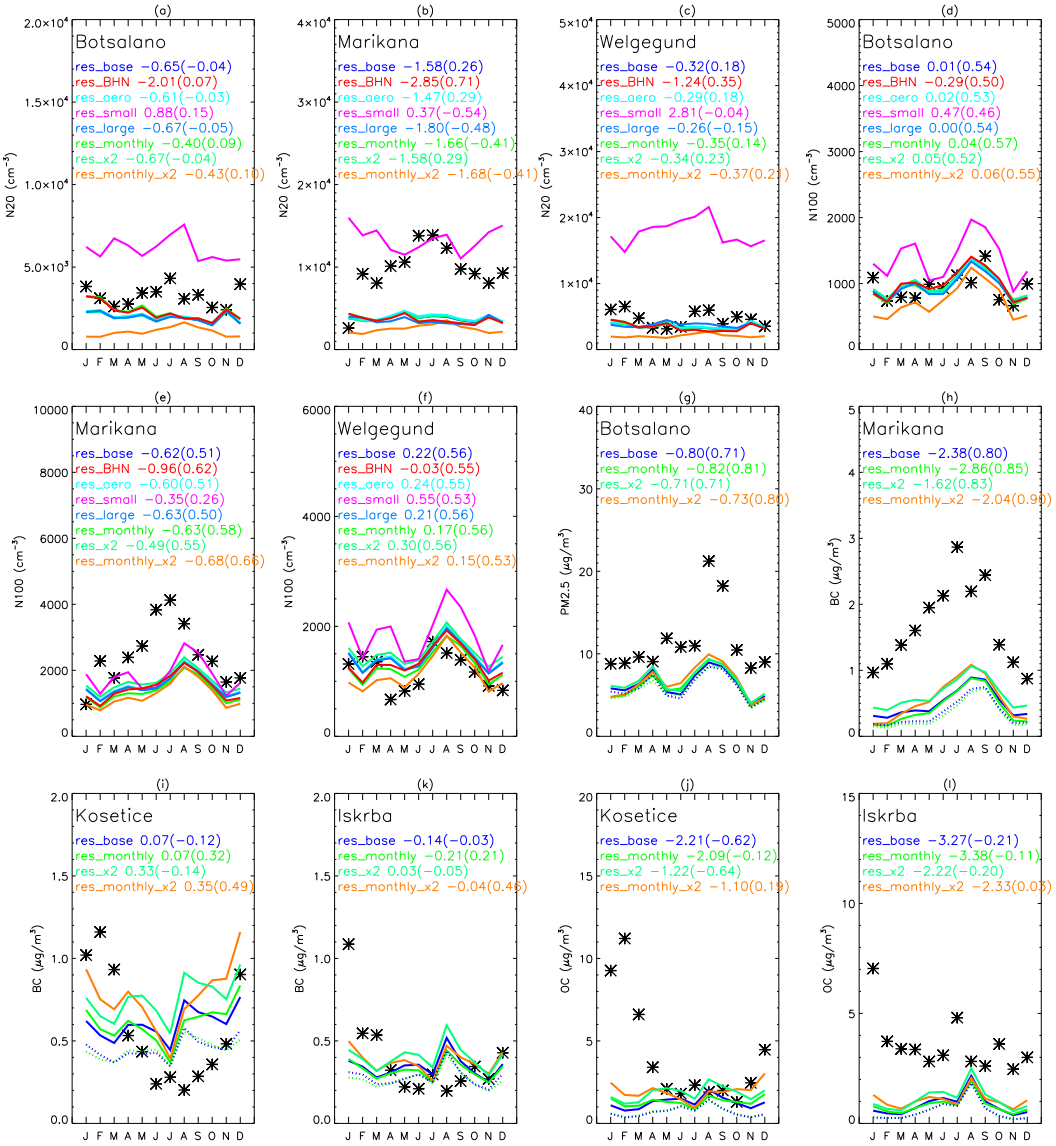

Figure 6. Observed (black stars) and simulated monthly mean N_{20} **(a–c)**, N_{100} **(d–f)**, $PM_{2.5}$ **(g)**, BC **(h–k)**, and OC **(j–l)** at South African and Eastern European locations. Normalised mean bias factor (NMBF) and correlation coefficient (r) are reported for each model simulation: NMBF(r). Experiments where residential emissions have been removed are represented by the blue (res_base_off) and green (res_monthly_off) dotted lines. Note that additional experiments (res_BHN, res_aero, res_small, and res_large) are included in **(a)–(f)** because these experiments have little impact on aerosol mass **(g–i)**.

Aerosol number concentrations at Botsalano (NMBF = 0.47 to 1.01) and Welgegund (NMBF = 0.55 to 2.81) are overestimated when primary carbonaceous particles are emitted at the smallest size (res_small), matching comparisons in South Asia and further suggesting that this assumption is unrealistic. The baseline simulation underestimates BC at Marikana (NMFB = −2.38) and $PM_{2.5}$ concentrations at Botsalano (NMBF = −0.88), with a reduction in BC bias when residential carbonaceous emissions are doubled (NMBF = −1.62). At both these locations the model simulates a reasonable seasonality even without monthly varying residential emissions ($r > 0.7$), possibly due to strong seasonality in open biomass savannah burning emissions.

Similar to other locations, observed BC and OC concentrations in Eastern Europe (Fig. 6i–l) are enhanced during winter (December–February). The baseline simulation performs well at simulating BC at Košetice (NMBF = +0.07) and Iskrba (NMBF = −0.14) but underestimates OC at Košetice (NMBF = −2.21) and Iskrba (NMBF = −3.27). Model agreement does not improve much when monthly varying anthropogenic emissions are used. The model performs bet-

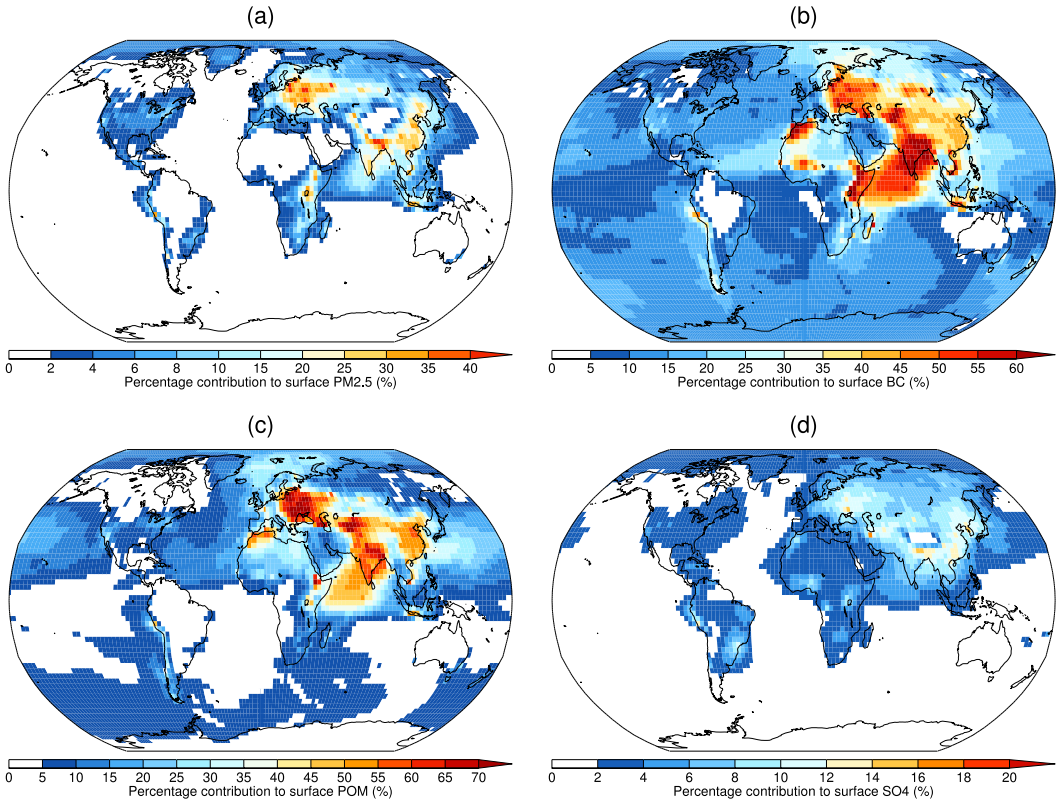

Figure 7. Percentage contribution of residential emissions to annual surface mean $PM_{2.5}$ **(a)**, BC **(b)**, POM **(c)**, and sulfate (SO_4) **(d)** concentrations (in size fraction $PM_{2.5}$) for the baseline simulation (res_base), relative to an equivalent simulation where residential emissions have been removed (res_base_off).

ter when residential carbonaceous emissions are doubled, but overestimates BC at Košetice.

In summary, we find the model typically underestimates observed BC and OC mass concentrations, which matches results from previous studies. Doubling residential emissions improves comparison against BC and OC observations, although the model is still typically biased low. To explore this further, we use ^{14}C analysis (Sect. 3.2) to evaluate the contribution of residential emissions to carbonaceous aerosol. In general, the model compares better against observations of particle number, except when carbonaceous particles are emitted at small sizes leading to large overestimates in particle number.

3.2 Contribution of residential emissions to PM concentrations

Figure 7 shows the fractional contribution of residential emissions to annual mean surface $PM_{2.5}$, BC, POM, and sulfate concentrations for the baseline simulation. Greatest fractional contributions (15 to > 40 %) to surface $PM_{2.5}$ are simulated over Eastern Europe (including parts of the Russian Federation), parts of East Africa, South Asia, and East Asia. Over these regions residential emissions contribute annual mean $PM_{2.5}$ concentrations of up to $6\,\mu g\,m^{-3}$, dominated by changes in POM concentrations of $2–5\,\mu g\,m^{-3}$, with BC and sulfate contributing up to $1\,\mu g\,m^{-3}$. Residential emissions contribute up to 60 % of simulated BC and POM over parts of Eastern Europe, Russian Federation, Asia, southeastern Africa, and northwestern Africa. Contribution of residential emissions to surface sulfate concentrations are typically smaller, with contributions of 10–14 % over parts of Asia, Eastern Europe, and the Russian Federation where residential coal emissions are more important (see Sect. 2.2). Over China, residential emissions account for 13 % of simulated annual mean $PM_{2.5}$, with larger contributions of 20–30 % in the eastern China. Over India, residential emissions account for 22 % of simulated annual mean $PM_{2.5}$, with contributions > 40 % over the Indo-Gangetic Plain. The contributions to $PM_{2.5}$ are increased to 21 % for China and 34 % for India, when residential carbonaceous emissions are doubled. The contribution of residential emissions to annual mean surface BC (POM) concentrations is ∼ 40 % (44 %) for China and ∼ 60 % (58 %) for India. When residential carbonaceous emissions are doubled, BC (POM) contributions are increased to 55 % (60 %) for China and 75 % (73 %) for India.

The absolute contribution of residential emissions to PM concentrations are greatest in the NH between 0 and 60° N below 500 hPa (not shown). The fractional contributions within this region are up to 16–24 % for both BC and POM and 1–4 % for sulfate. Residential emissions contribute ∼ 20 % of BC and ∼ 12–16 % of POM aloft (above 500 hPa) but cause small reductions in sulfate (−1 to −4 %) due to the suppression of nucleation and growth (see Sect. 3.4 for more details).

Table 2 reports the impact of residential emissions on simulated global annual mean BC and POM burden and continental surface $PM_{2.5}$ concentrations. In the baseline simulation, the global BC burden is 0.11 Tg with a global mean atmospheric BC lifetime of 4.95 days. This lifetime matches the 4.4 to 5.1 days reported by X. Wang et al. (2014), suggesting that our underestimation of observed BC is not due to fast deposition and short atmospheric lifetime, at least in comparison to other models. In the baseline simulation, residential emissions result in a global BC burden of 0.024 Tg, contributing 22 % of the global BC burden. Residential emissions contribute 12 % of global POM burden. When residential carbonaceous emissions are doubled, residential emissions contribute 33 % of the BC burden and 23 % of the POM burden. Changing from annual mean to monthly varying emissions results in little change to the global BC or POM burden. Emitting carbonaceous particles at very small sizes (res_small) results in a greater fractional contribution to global atmospheric BC (∼ 23 %) and POM (∼ 18 %) and longer BC lifetime (5.4 days) compared to the baseline simulation. Because the removal of carbonaceous particles in the model is size dependant (particularly for wet deposition), small particles below a critical size can escape removal, leading to enhanced lofting to the free troposphere (FT) where deposition rates are slow. In the res_small simulation, fractional changes in BC burden can be as large as 60–100 % in the FT, compared to 25–40 % in the baseline simulation. Continental surface $PM_{2.5}$ concentrations are increased by ∼ 2 % in the baseline simulation, which is increased to ∼ 3.6 % when carbonaceous residential emissions are doubled.

We further evaluate the simulated contribution of residential emissions to BC concentrations using ^{14}C source apportionment studies on the island of Hanimaadhoo (Gustafsson et al., 2009; Sheesley et al., 2012; Bosch et al., 2014), which is influenced by pollution transported from the Indian subcontinent. The model simulates well both BC and OC concentrations observed at this location (Sect. 3.1). Figure 8 compares simulated and observed biomass contributions to BC at Hanimaadhoo. The observed contribution depends on not only the time of year the measurements were taken but also the measurement technique used to derive BC (EC). For example, during the same measurement period Gustafsson et al. (2009) found that 46 ± 8 % of EC and 68 ± 6 % of BC originated from non-fossil biomass (January–March). Bosch et al. (2014) estimate that 59 ± 8 % of EC is from non-fossil biomass (February–March). Sheesley et al. (2012) estimated that 73 ± 6 % of EC originated from non-fossil biomass during the dry season (November–February). The observed contribution of non-fossil BC (EC) therefore spans a range of 46–73 %. Residential biofuel/biomass combustion dominates residential emissions in South Asia (Venkataraman et al., 2005). To estimate non-fossil values from the model, we assume that 90 % of residential BC transported to Hanimaadhoo originates from residential biofuel sources (consistent with ≥ 90 % estimates from the GAINS model), while the remaining non-fossil BC originates from open biomass burning (including agricultural waste and open waste/rubbish burning). We find a small contribution (< 10 % for all simulations) of open biomass burning to simulated BC at Hanimaadhoo, confirming that the non-fossil contribution at this location is likely dominated by residential biomass/biofuel sources, which is supported by the observed consistent con-

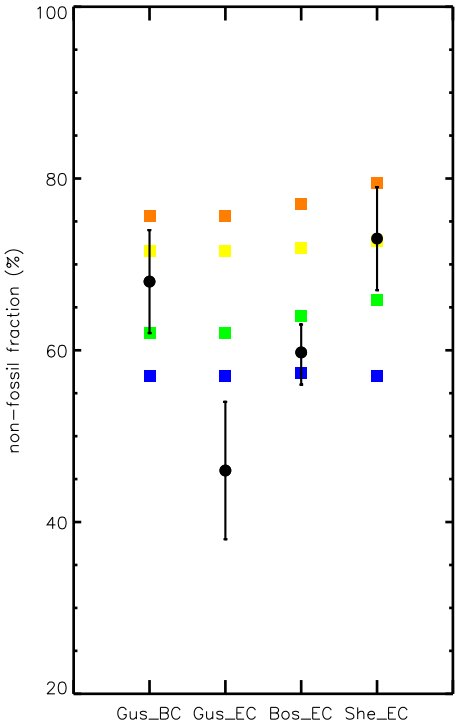

Figure 8. Comparison of simulated (squares) and observed (circles, error bars show uncertainty range) contributions of non-fossil (residential biofuel and open biomass burning) sources to BC concentrations in Hanimaadhoo, Indian Ocean. Observations are from Gustafsson et al. (2009) ("Gus EC" (thermo-optical) and "Gus BC" (optical) for January–March), Bosch et al. (2014) ("Bos EC" (thermo-optical) for February–March), and Sheesley et al. (2012) ("She EC" (thermo-optical) for November–February). Model simulations are represented by squares: standard emissions (blue: res_base; green: res_monthly) and where residential carbonaceous emissions have been doubled (yellow: res_× 2; orange: res_monthly_× 2). Simulated fractional contributions are averaged over the time of year that the observations were made.

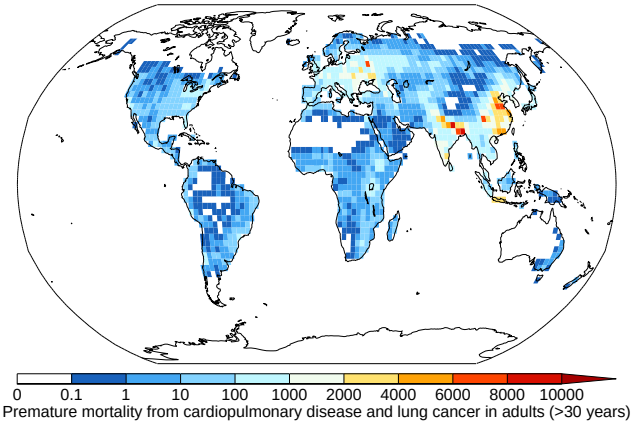

Figure 9. Simulated annual premature mortality (cardiopulmonary diseases and lung cancer) due to ambient exposure to ambient $PM_{2.5}$ from residential emissions (res_base – res_off).

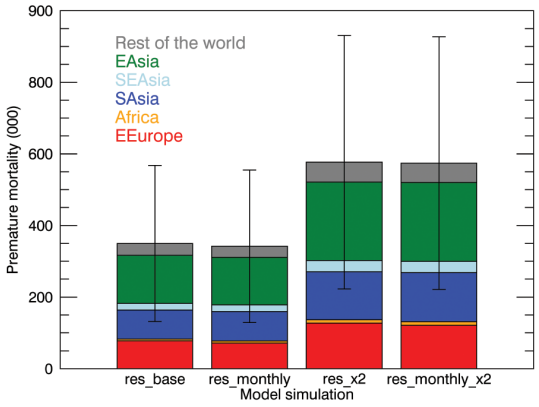

Figure 10. Simulated global annual premature mortality (cardiopulmonary diseases and lung cancer for persons over the age of 30 years) due to exposure to ambient $PM_{2.5}$ from residential emissions. Results are shown for standard emissions (res_base and res_monthly) and where residential emissions have been doubled (res_× 2 and res_monthly_× 2). Mortality is shown for Eastern Europe and the Russian Federation (EEurope), Africa (Africa), South Asia (SAsia), Southeast Asia (SEAsia), East Asia (EAsia), and the rest of the world (as defined by the coloured regions in Fig. 2).

tribution from a non-fossil source (Sheesley et al., 2012). The simulated contribution of non-fossil sources to total BC at this location is ∼ 57–79 %, depending on the time of year and model simulation. The baseline simulation has a 57 % contribution of non-fossil sources to simulated BC concentrations, with little variation between different times of year due to the annual mean emissions applied in this simulation. Model simulations with monthly varying emissions have a greater contribution of non-fossil sources to BC at this location, as well as greater variability between seasons with a contribution of 62–65 %. Doubling residential emissions increases the contribution of non-fossil sources to ∼ 72 % for annual mean emissions and ∼ 76–79 % for monthly varying emissions. The spread in observed EC contributions makes it difficult to constrain the contribution of residential emissions, with baseline and doubling of residential BC emissions bracketing the observed range. We do not analyse the non-fossil fraction of OC since OC arises from a larger range of sources including primary emissions and secondary organic aerosol (SOA). Nevertheless, non-fossil water-soluble organic carbon at Hanimaadhoo is dominated (∼ 80 %) by biomass and biogenic sources (Kirillova et al., 2013) but the relative enrichment in the stable (δ^{13}C) carbon isotope points largely to aged primary biomass emissions sources (Bosch et al., 2014). We estimate the simulated biomass contribution to OC at Hanimaadhoo to be ∼ 50–70 % for baseline simulations (res_base and res_monthly) and ∼ 70–80 % for simulations where residential carbonaceous emissions have been doubled.

3.3 Health impacts of residential emissions

Figure 9 shows the simulated annual excess premature mortality due to exposure to ambient $PM_{2.5}$ from residential emissions in the year 2000 for the baseline simulation. Greatest mortality is simulated over regions with substantial residential emissions and high population densities, notably parts of Eastern Europe, the Russian Federation, South Asia, and East Asia. Table 2 reports total global values for annual mortality due to residential emissions. For the baseline simulation, we estimate a total global annual mortality of 315 000 (132 000–508 000, 5th to 95th percentile uncertainty range). The simulation with monthly varying emissions (res_monthly) results in total global annual mortality of 308 000 (113 300–497 000), only a 2 % difference from the baseline estimate. Uncertainty in the magnitude of residential emissions causes substantial uncertainty in the simulated impact on human health. When residential carbonaceous emissions are doubled, annual premature mortality increases by 65 % to 519 000 (193 000–830 000) with annual mean emissions and by 68 % to 517 000 (192 000–827 000) with monthly varying emissions. Therefore, uncertainty in the emission budget and uncertainty in the health impacts of PM (as specified by 95 % confidence intervals in the cause-specific coefficients) result in similar uncertainties in estimated global mortality. The CRF function treats all aerosol components as equally harmful, so simulations where residential emissions of POM, BC, and SO_2 are increased individually show that health effects are most sensitive to uncertainty in POM emissions because this component dominates the total emission mass. Doubling POM emissions (res_POM× 2) increases estimated premature mortality by 50 %, whereas doubling BC emissions (res_BC× 2) results in an 11 % increase and doubling SO_2 emissions (res_SO2× 2) leads to a 6.5 % increase.

Figure 10 shows simulated annual total mortality by region. For the baseline simulation, we estimate that resi-

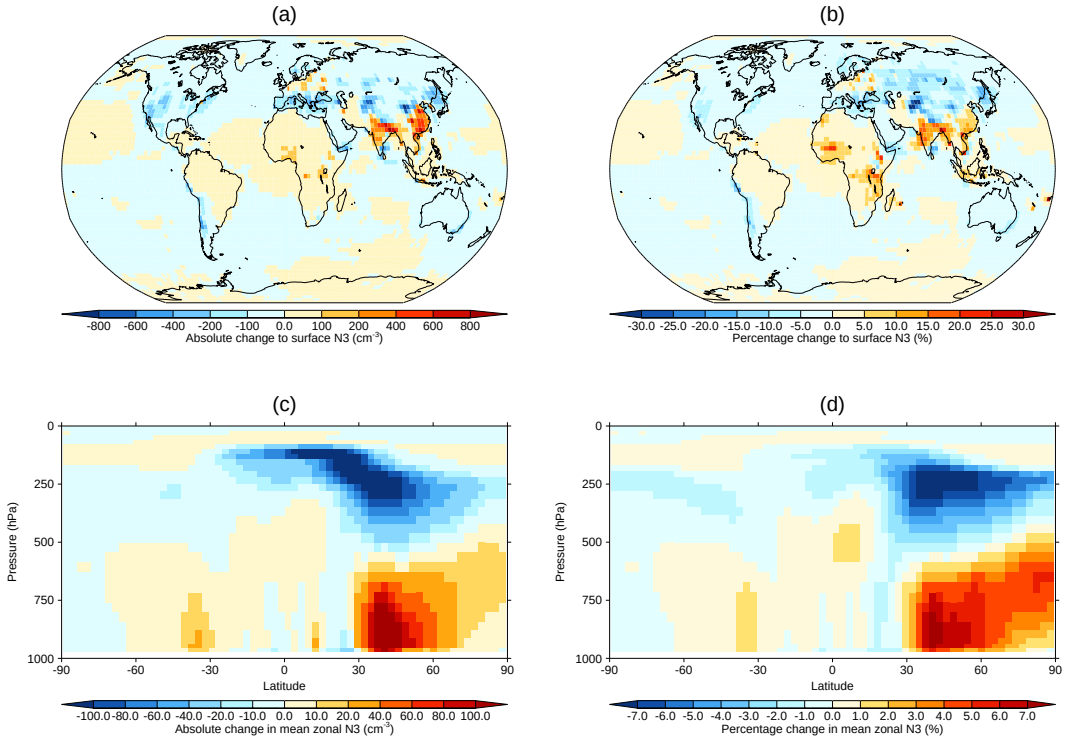

Figure 11. Simulated absolute and percentage change in annual mean surface **(a–b)** and zonal **(c–d)** number concentration (N_3; greater than 3 nm dry diameter) due to residential emissions (res_base), relative to an equivalent simulation where residential emissions have been removed (res_base_off).

dential emissions cause the greatest mortality in East Asia with 121 075 (44 596–195 443, 95 % confidence intervals) annual deaths – 38 % of global mortalities due to residential emissions. We also calculate substantial health effects in other regions, with 72 890 (26 891–117 360) annual deaths in South Asia (28 % of global mortalities) and 69 757 (25 714–112 447) in Eastern Europe and Russia (22 % of global mortalities). Elsewhere we estimate lower mortality with 16 723 (6152–27 018) annual deaths in Southeast Asia (5 %) and 4791 (1751–7784) in sub-Saharan Africa (2 %). Annual premature mortality in sub-Saharan Africa is less than in Asia due to a smaller contribution of residential emissions to $PM_{2.5}$ concentrations (Fig. 7), combined with typically lower population densities, lower baseline mortality rates for lung cancer and cardiopulmonary disease, and a smaller fraction of the population over 30 years of age.

To our knowledge, this is the first study of the global excess mortality due to ambient $PM_{2.5}$ from both residential cooking and heating emissions. A recent study by Chafe et al. (2014) concluded that ambient $PM_{2.5}$ from RSF cooking emissions resulted in 420 000 annual excess deaths in 2005 and 370 000 annual excess deaths in 2010. Chafe et al. (2014) also simulated lower mortality in sub-Saharan Africa (10 800 deaths in 2005) compared to Asia, consistent with our findings. The regions where we estimate the largest health impacts due to residential emissions are dominated by RSF emissions. In East Asia, residential emissions are dominated by both residential coal and biofuel sources whereas in South Asia emissions are dominated by biofuel sources (Bond et al., 2013).

3.4 Impact of residential emissions on total particle number and N_{50} concentrations

Figure 11 shows the change in annual mean surface and zonal mean particle number concentration (N_3; particles greater than 3 nm dry diameter) due to residential emissions for the baseline simulation. Residential emissions increase N_3 concentrations over source regions by up to 800 cm^{-3} due to primary emitted particles. Downwind of source regions, N_3 concentrations are reduced by up to $\sim$400 cm^{-3}. This reduction is caused by primary particles acting as a coagulation sink for nucleated particles and a condensation sink for nucleating and condensing vapours, suppressing new particle formation (Spracklen et al., 2006), which is broadly consistent with the findings of Kodros et al. (2015) for particle number concentrations due to the effect of biofuel emissions. Residential emissions decrease N_3 concentrations in the FT ($>$ 500 hPa) by up to 100 cm^{-3} (7 %) due to suppression of nucleation and growth from reduced availability of H_2SO_4 vapour due to increased condensation on primary particles.

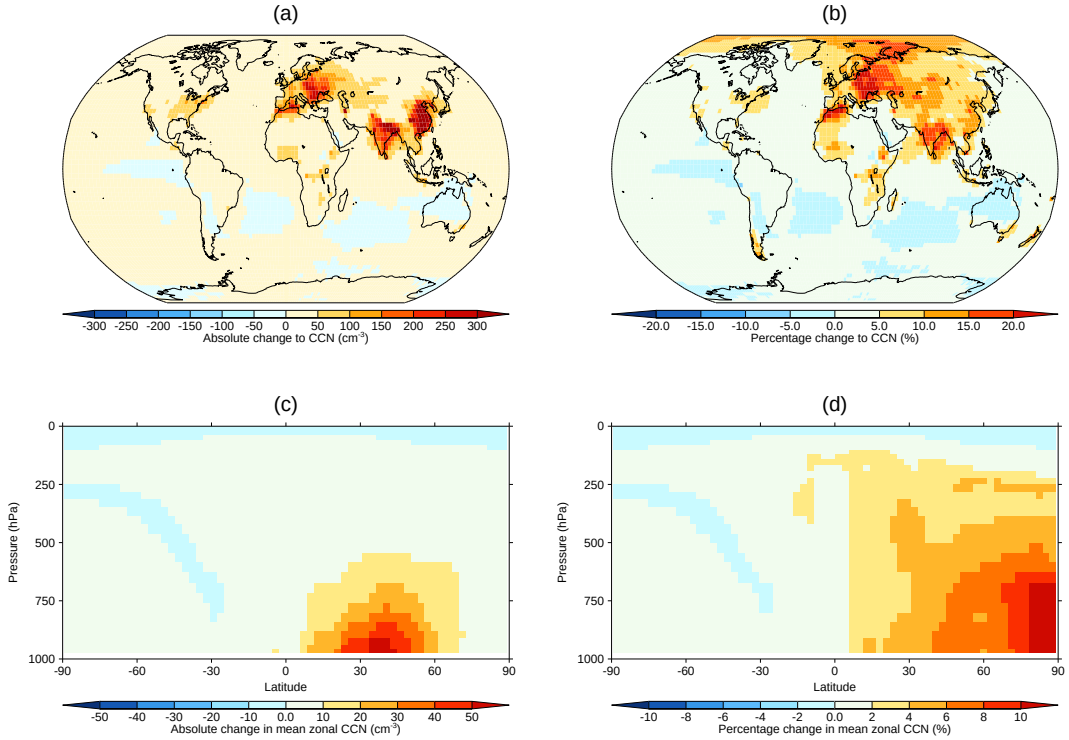

Figure 12. Simulated absolute and percentage change in annual mean surface **(a–b)** and zonal **(c–d)** soluble N_{50} concentrations due to residential emissions (res_base), relative to an equivalent simulation where residential emissions have been removed (res_base_off).

In the baseline simulation, residential emissions reduce annual global mean N_3 concentrations by 1.0 % (Table 2). When activation BLN is switched off (res_BHN), this suppression is no longer important, and residential emissions increase annual global mean N_3 concentrations by 5.7 %. The impact of residential emissions on global particle number depends on the assumed particle size of primary carbonaceous emissions. When residential carbonaceous emissions are emitted at smaller sizes (res_aero and res_small), global mean N_3 concentrations are increased by 2.4 and 164 % respectively. This is because a greater number of particles are being emitted per emission mass compared to the baseline simulation.

Figure 12 shows the impact of residential emissions on surface and zonal mean soluble N_{50} number concentrations for the baseline simulation. Residential emissions increase N_{50} concentrations over source regions of East Asia, South Asia, and Eastern Europe by up to 300–500 cm^{-3}. Simulated N_{50} concentrations are increased by up to 20 % in the Arctic, Eastern Europe, Russian Federation, North Africa, and South Asia. Despite high absolute changes, fractional changes in N_{50} concentration over East Asia (e.g. China) are smaller (< 15 %) because of higher baseline N_{50} in this region from other sector emissions (e.g. from industry). N_{50} concentrations increase globally due to residential emissions, but small reductions (< 5 %) are simulated in the remote Southern Ocean because of the reduction in the amount of H_2SO_4 and condensable vapour available for nucleation and growth in FT, which results in reduced entrainment of nucleated particles into the boundary layer. Absolute and fractional changes in zonal mean N_{50} are greatest between 0 and 60° N and below 500 hPa.

Table 2 reports the global annual mean change in N_{50} concentrations between different simulations. In the baseline simulation, residential emissions increase global mean surface N_{50} by ~ 5 %. When primary residential carbonaceous particles are emitted at smaller sizes, residential emissions cause a greater increase in N_{50} concentrations, with annual global mean N_{50} concentrations increasing by ~ 20 % in the simulation with smallest particle size (res_small). Emitting particles at larger sizes results in a smaller increase in global mean N_{50} (3.1 %) because large particles are more efficiently scavenged. The sensitivity of global mean N_{50} concentrations to assumptions about emitted particle size is consistent with previous studies (Adams and Seinfeld, 2003; Spracklen et al., 2005b, 2011a). When residential carbonaceous aerosol emissions are doubled, residential emissions increase global annual mean N_{50} by ~ 6.3 % (res_$\times$ 2). Simulations where individual carbonaceous components are doubled separately (res_BC$\times$ 2 and (res_POM$\times$ 2) show that N_{50} is mainly sensitive to change in OC emissions which dominate the carbonaceous aerosol mass. When residential SO_2 emissions are doubled, residential emissions increase global annual mean N_{50} by 6.5 %. When activation BLN is assumed not to oc-

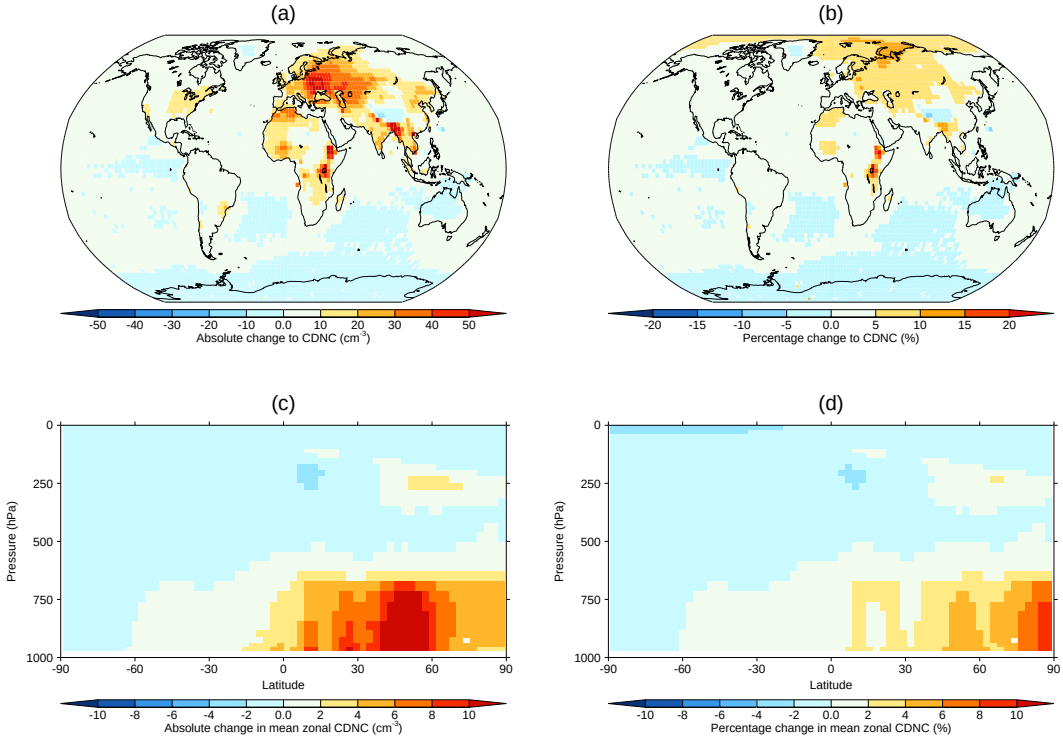

Figure 13. Simulated absolute and percentage change in annual mean at low cloud height (850–900 hPa) **(a–b)** and zonal **(c–d)** CDNC due to residential emissions (res_base), relative to an equivalent simulation where residential emissions have been removed (res_base_off).

cur, residential emissions increase global annual mean N_{50} by 6.5 % relative to the simulation with no residential emissions. This greater sensitivity is because the baseline N_{50} concentrations without BLN are lower (287.4 cm^{-3}) than the baseline simulation (364.6 cm^{-3}).

3.5 Impact of residential emissions on cloud droplet number concentrations

Figure 13 shows the impact of residential emissions on annual mean low-cloud level (850–900 hPa) and zonal mean CDNC for the baseline simulation. Residential emissions increase low-cloud level CDNCs by 20–100 cm^{-3} over source regions. Smaller absolute and percentage changes in CDNC are simulated over regions with greater baseline CDNCs due to CDNC saturation effects. In contrast, CDNCs increases of 20 % are simulated over regions with low simulated background CDNCs, including parts of East Africa. Simulated absolute increases in zonal mean CDNC are greatest between 0 and 60° N below 500 hPa, whereas greatest fractional changes occur in the Arctic (6–8 %) due to low background concentrations. Small reductions in CDNC are simulated in the FT (~ -2 %) and in the remote Southern Ocean (1–2 %) at cloud level. This is caused by suppressed nucleation in the FT.

In the baseline simulation, residential emissions increase global annual low-cloud level CDNC by 2.1 % (Table 2). Uncertainty in the emitted particle size of primary carbonaceous emissions causes most of the uncertainty in simulated CDNC. When residential carbonaceous particles are emitted at smaller sizes (res_small) emissions increase global annual mean CDNC by 20 %. Emitting particles at smaller sizes resulted in greater N_{50} concentrations, meaning more CCN-sized particles are available to activate. While larger particle sizes can active cloud drops more easily compared to smaller particles, large particles will deplete available water vapour more quickly, which will lower SS_{max}, leading to a suppression of small particles being activated. When activation BLN is switched off (res_BHN), residential emissions cause a greater increase in CDNC (3 %) compared to the baseline simulation, due to lower background CDNCs. Annual mean CDNC are increased by +2.7 % when primary carbonaceous emissions are doubled (res_$\times$ 2), but greater increases (+3.3 %) are simulated when residential SO_2 is doubled separately (res_SO2$\times$ 2). This suggests that residential SO_2 is having a greater effect on CDNC compared to carbonaceous emissions because the small size distribution of secondary sulfate is more efficient in the activation of cloud drops.

3.6 Radiative effects of residential emissions

Figure 14 shows annual mean all-sky TOA DRE and first AIE due to residential emissions for the baseline simulation.

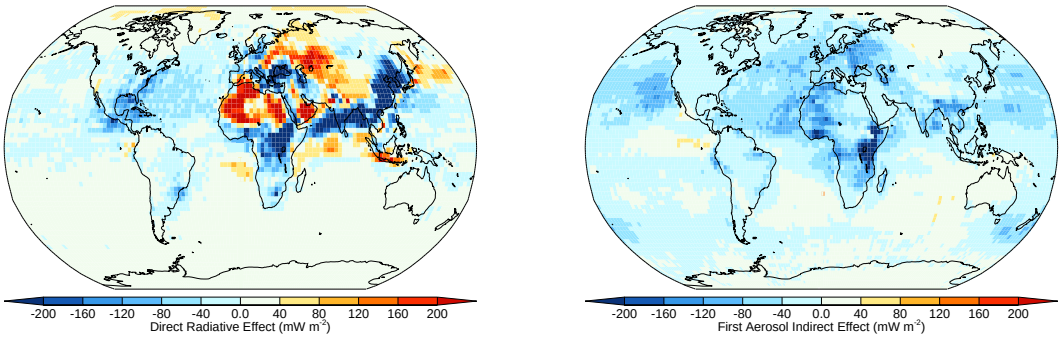

Figure 14. Annual mean all-sky direct radiative effect (DRE) (left panel) and first aerosol indirect effect (AIE) (right panel) due to residential emissions (res_base), relative to an equivalent simulation where residential emissions have been removed (res_base_off).

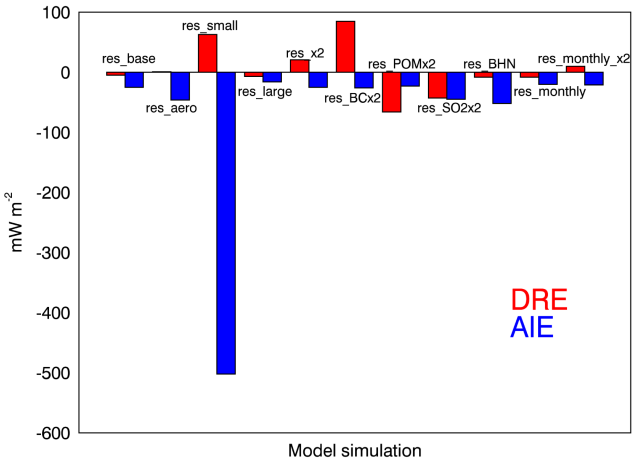

Figure 15. Global annual mean all-sky direct radiative effect (DRE) (red) and first aerosol indirect effect (AIE) (blue) for all model simulations due to the impact of residential combustion emission, relative to simulations where residential combustion emissions have been removed. DRE and AIE values for each simulation are detailed in Table 2.

Residential emissions result in a negative (cooling) annual mean DRE over large regions of South Asia, East Asia, sub-Saharan Africa, and parts of southern Europe, with values as large as $-200\,\mathrm{mW\,m^{-2}}$. The simulated net negative DRE in South Asia and East Asia is consistent with a previous study (Aunan et al., 2009). In contrast, over parts of Eastern Europe and the Russian Federation, North Africa, the Middle East, and Southeast Asia, residential emissions lead to a positive DRE. Residential emissions cause a negative first AIE over most regions, with values as large as $-200\,\mathrm{mW\,m^{-2}}$ over eastern Africa, Eastern Europe, and West Africa. Small positive AIE ($<40\,\mathrm{mW\,m^{-2}}$) is simulated in the remote Southern Ocean due to reductions in CDNC as mentioned in Sect. 3.5.

Figure 15 compares the annual mean all-sky DRE and first AIE across the different model simulations (also reported in Table 2). The simulated global annual mean DRE has an uncertain sign, with our estimates between -66 and $+85\,\mathrm{mW\,m^{-2}}$. The baseline simulation results in a global mean DRE of $-5\,\mathrm{mW\,m^{-2}}$, similar to the simulation using monthly varying emissions ($-8\,\mathrm{mW\,m^{-2}}$). Our estimates differ somewhat to Kodros et al. (2015), who found a homogeneous optical mixing state produced a positive DRE of $+15\,\mathrm{mW\,m^{-2}}$ for biofuel emissions; however, because residential emissions differ to biofuel emissions, comparisons become problematic. We therefore assume that differences in radiative effect compared to Kodros et al. (2015) are likely dominated by differences in emissions used and differences in the optical calculation. Doubling residential carbonaceous emissions, but keeping SO_2 emissions constant, results in a positive global annual mean DRE ($+21\,\mathrm{mW\,m^{-2}}$ for res_$\times$ 2 and $+10\,\mathrm{mW\,m^{-2}}$ for res_monthly_$\times$ 2). This suggests that the carbonaceous (BC and POM) component of residential aerosol in our model exerts a positive DRE, but this is offset by cooling from SO_2 emissions. Doubling only BC emissions leads to a stronger positive DRE ($+85\,\mathrm{mW\,m^{-2}}$), whereas negative DRE are simulated for doubling only POM ($-66\,\mathrm{mW\,m^{-2}}$) or SO_2 ($-43\,\mathrm{mW\,m^{-2}}$) emissions. The DRE is also sensitive to emitted particle size, resulting in positive global mean DRE of between $+1$ and $+63\,\mathrm{mW\,m^{-2}}$ when carbonaceous particles are emitted at smaller sizes (res_aero and res_small respectively). This change in sign to a positive DRE can be attributed to reduced removal rates for carbonaceous particles emitted at smaller sizes, which leads to larger BC burden, particularly in the FT where BC influence on DRE is most efficient. Residential emissions exert a negative (cooling) but uncertain global annual mean first AIE, estimated at between -502 and $-16\,\mathrm{mW\,m^{-2}}$. The baseline simulation results in a global mean first AIE of $-25\,\mathrm{mW\,m^{-2}}$, similar to the simulation using monthly varying emissions ($-20\,\mathrm{mW\,m^{-2}}$). Emitting residential carbonaceous aerosol at small sizes contributes most of the uncertainly to simulated first AIE, with estimates between $-46\,\mathrm{mW\,m^{-2}}$ (res_aero) and $-502\,\mathrm{mW\,m^{-2}}$ (res_small) due to a greater increase in global CDNC. We find little sensitivity of the AIE to changes in carbonaceous emission mass: doubling carbonaceous emissions (res_$\times$ 2) changes

AIE by less than 2 mW m^{-2} ($\sim$ 10 %) due to limited changes in CDNC. In contrast, doubling SO_2 emissions leads to the greater negative AIE (-45 mW m^{-2}) due to greater global contribution to CDNCs.

4 Discussion and conclusions

We used a global aerosol microphysics model (GLOMAP) to quantify the impacts of residential emissions on ambient aerosol, human health, and climate in the year 2000. We tested the sensitivity of simulated aerosol to uncertainty in emission amount and seasonal variability, emitted primary carbonaceous aerosol size distributions, and the impact of particle formation.

To evaluate model simulations we synthesised in situ observations of BC, OC, and $PM_{2.5}$ concentrations and aerosol number size distribution. The baseline simulation underestimated observed BC, OC, and $PM_{2.5}$ concentrations, with the largest underestimation over East Asia and South Asia, consistent with other modelling studies (Fu et al., 2012; Moorthy et al., 2013; Pan et al., 2015). Applying monthly varying emissions (MACCity emission data set), in place of annual mean emissions (ACCMIP emission), has little improvement on overall model bias but does improve the ability of the model to simulate the observed seasonal variability of aerosol. Doubling residential carbonaceous combustion emissions improved model agreement, but GLOMAP still underestimated BC, OC, and $PM_{2.5}$ concentrations. The model typically had a larger underestimation of OC compared to BC concentrations, possibly due to uncertainty in emission factors or potentially due to an underestimation of anthropogenic SOA (Spracklen et al., 2011b).

We used source apportionment studies using ^{14}C non-fossil BC analysis at the island site of Hanimaadhoo in the Indian Ocean as an additional constraint of the model. Non-fossil sources have been estimated to contribute 46–73 % at this location. This large range makes it difficult to constrain the model. With standard emissions (ACCMIP and MACCity), we estimate a non-fossil fraction of 57–65 %, whereas when residential BC emissions are doubled, we simulate a non-fossil fraction of 72–79 %.

Overall, our results suggest that residential emissions may be underestimated in the MACCity and ACCMIP data sets. Uncertainty in aerosol removal processes and transport and missing anthropogenic SOA and nitrate formation may all contribute to underestimation of aerosol mass. Nevertheless, previous modelling studies have also suggested that residential emission data sets underestimate emissions (Park et al., 2005; Koch et al., 2009; Ganguly et al., 2009; Menon et al., 2010; Bergström et al., 2012; Nair et al., 2012; Fu et al., 2012; Moorthy et al., 2013; Bond et al., 2013; Pan et al., 2015). The ACCMIP and MACCity emission data sets are constructed using national data on fuel use, which implies uniform per capita fuel consumption at the country level. Using subnational fuel use data, R. Wang et al. (2014) showed that the MACCity data set underestimated residential emissions over source regions in Asia. Other studies have also had to increase residential emissions over Europe in order to match source apportionment studies (Denier van der Gon et al., 2015). However, Wang et al. (2013) suggested that model bias over China could partly be attributed to coarse model resolution and comparison against urban data and monthly mean observations. Kumar et al. (2015) also showed that a high-resolution model was able simulate reasonable BC distributions in South Asian region. We have restricted our analysis to rural and background sites but use monthly mean BC and OC data and a relatively coarse-resolution global model. To help resolve uncertainties in residential emission budget, higher-resolution emission inventories (using subnational fuel use data) and higher-resolution model simulations evaluated against long-term and high temporal resolution data are required. In many regions, observational data are lacking; there is an urgent requirement for detailed characterisation of the chemical, physical, and optical properties of aerosol in regions impacted by residential emissions, particularly in the developing world.

Particle number concentrations are generally predicted within a factor of 2 at the limited number of locations where observations are available. Simulated particle number is very sensitive to emitted particle size, which has a large uncertainty. Emitting residential carbonaceous particles at the small end of the range reported by Bond et al. (2006) (geometric mean diameter = 20 nm) substantially overestimates observed particle number, suggesting this assumption is not appropriate for coarse-resolution global models.

Residential emissions contribute substantially to simulated annual mean surface PM concentrations. Greatest fractional contributions (15 to $>$ 40 %) to surface $PM_{2.5}$ concentrations are simulated over Eastern Europe (including parts of the Russian Federation), parts of East Africa, South Asia, and East Asia. In these regions residential emissions contribute $>$ 50 % to total simulated BC and POM concentrations. These findings support previous studies suggesting a large contribution of residential emissions to $PM_{2.5}$ concentrations over Asia (Venkataraman et al., 2005; Cao et al., 2006; Klimont et al., 2009; Lei et al., 2011; Cui et al., 2015; Fu et al., 2012; Gustafsson et al., 2009; B. Chen et al., 2013). Our findings suggest that reductions in residential emissions need to be considered alongside mitigation strategies for other PM sources (e.g. industry and transport) within Asia and in even more developed regions such as parts of Europe (Fountoukis et al., 2014).

We estimated the impact of residential emissions on human health due to increased ambient $PM_{2.5}$ concentrations and tested the sensitivity to the emission data set and emission budget. We used a log-linear model of relative risk from the epidemiological literature (Ostro, 2004) to relate simulated changes in ambient $PM_{2.5}$ concentrations to long-term excess premature mortality for cardiopulmonary dis-

ease and lung cancer for adults (> 30 years of age). In the baseline simulation, we estimate that residential emissions cause 315 000 (132 000–508 000, 5th to 95th percentile uncertainty range) premature mortalities each year. Applying a seasonal cycle to emissions changed our estimate by less than 2 %, with residential emissions resulting in 308 000 (113 300–497 000) premature mortalities each year. Our estimate for residential emissions is equivalent to 8 % of the total mortality attributed to exposure to ambient $PM_{2.5}$ from all anthropogenic sources (WHO, 2014b), although we note that methodologies in the two studies are different. Doubling residential carbonaceous emissions, which improved model comparison against observed BC and POM concentrations, increases simulated excess mortality by ~ 64 % to 516 600 (192 000–827 000). Simulated mortality is greatest over regions with large residential emissions and high population densities including East Asia, South Asia, Eastern Europe, and the Russian Federation. We find that half of simulated global excess mortality from residential emissions occurs in China and India alone. Our results are consistent with a previous estimate of RSF cooking emissions on premature mortality (Chafe et al., 2014). The CRFs that are used to estimate long-term premature mortality are uncertain. The log-linear function used here is based on epidemiological studies from North America (Pope III et al., 2002), resulting in greater uncertainty when these functions are extrapolated to other regions (Silva et al., 2013). However, epidemiological studies are not available for all regions, so global mortality estimates often use functions based on these North American studies. Overall, we find that uncertainty in the relationship between PM concentrations and health impacts (as quantified by the 95th percentile range given by the log-linear model) and our measure of uncertainty in emissions (estimated here as a factor of 2 uncertainty) result in comparable uncertainty in the estimated global number of premature mortalities. Future work therefore needs to improve both our understanding of residential emissions and the relationships between enhanced PM concentrations and human health impacts. We also note that the coarse resolution of our global model likely provides a conservative estimate of premature mortality due to residential emissions because it cannot simulate high concentrations associated with highly populated urban and semi-urban areas. Further simulations using higher-resolution models and emission inventories will be required to accurately simulate $PM_{2.5}$ concentrations in urban and semi-urban areas. Health effects using more recent CRFs that relate RR of disease to changes in $PM_{2.5}$ over a large range of concentration exposures (Burnett et al., 2014) will also be required. In addition, exposure functions, such as the one used in this study, treat all aerosol components as equally toxic, but carbonaceous aerosol, which dominate residential emissions, may be more toxic compared to inorganic or crustal PM (Tuomisto et al., 2008). New exposure response functions will therefore need to account for the different toxicity of chemical components present in atmospheric aerosols.

We used an offline radiative transfer model to estimate the radiative effect (RE) of aerosol from residential emissions. We estimate that residential emissions exert a global annual mean DRE of between -66 and $+85\,\mathrm{mW\,m^{-2}}$. The simulated global mean DRE is sensitive to the amount and ratio of BC, POM, and SO_2 in emissions. Doubling residential carbonaceous emissions, but keeping SO_2 emissions constant, results in a positive global annual mean DRE, suggesting that the carbonaceous component of residential aerosol exerts a net positive DRE in our simulations, offset by cooling from SO_2 emissions. We also find a positive DRE when primary carbonaceous emissions are emitted at smaller sizes, but this simulation overestimates observed aerosol number, suggesting it is unrealistic. Discounting this simulation, we provide a best estimate of global mean DRE due to residential combustion of between -66 and $+21\,\mathrm{mW\,m^{-2}}$ for the year 2000.

Residential emissions exert a simulated global annual mean first AIE of between -502 and $-16\,\mathrm{mW\,m^{-2}}$. Uncertainty in emitted primary carbonaceous particle size contributes most of the uncertainly to calculated AIE. Emitting carbonaceous aerosol at smaller sizes results in greater simulated N_{50} and CDNC and a strong negative AIE as well as in overestimation of observed particle number, suggesting that emission at very small sizes is not realistic. We find little sensitivity to annual mean first AIE due changes in carbonaceous emission mass compared to the baseline simulation. Doubling carbonaceous emissions changes AIE by less than $2\,\mathrm{mW\,m^{-2}}$ (~ 10 %), highlighting a non-linear relationship between magnitude of emission and first AIE. Our best estimate of the first AIE due to residential emissions is between -52 and $-16\,\mathrm{mW\,m^{-2}}$ in the year 2000.

We have restricted our analysis of the RE of residential emissions to the aerosol DRE and first AIE. We treat POM aerosol as scattering, although a fraction of POM aerosol may absorb radiation (Kirchstetter et al., 2004; Chen and Bond, 2010; Arola et al., 2011; X. Wang et al., 2014). Furthermore, our DRE analysis is limited because we do not fully explore the full range of optical mixing states for residential emissions. We assume that BC is mixed homogeneously with scattering species, which provides an upper limit for BC DRE (Jacobson, 2001). A full investigation of the different optical mixing states commonly used in global models, such as in Kodros et al. (2015), would yield a better understanding of DRE from residential emissions. Because we use an offline radiative transfer model, we also do not treat cloud lifetime (second indirect effect) or semi-direct effects (Koch and Del Genio, 2010) and cannot explore additional impacts such as the weakening of the South Asia monsoon, altering of precipitation patterns (Ramanathan et al., 2005), tropical cyclone intensification (Evan et al., 2011), and accelerated melting of glaciers in the Himalayas (Xu et al., 2009).

The introduction of cleaner and fuel efficient residential combustion technologies, processed solid fuels, and clean alternative energy (e.g. natural gas, electricity) has been sug-

gested as one of the fastest ways to reduce residential emissions (UNEP, 2011), thus slowing climate change and improving air quality and human health (WHO, 2009). Our study shows that the complete elimination of residential emissions would result in substantially improved PM air quality and human health across large regions of the world regardless of the uncertainties between the different model simulations explored here.

We have shown that residential combustion emissions exert an uncertain RE, which leads to uncertainties in predicting the climate impact of emission reductions. Our work suggests that residential emission flux, chemical composition, and carbonaceous size distributions need to be better characterised in order to constrain the likely climate impact. Given these uncertainties, the missing processes within our model framework (described above), and the use of an offline radiative transfer model, it is difficult asses the full climate impacts due to residential emissions. In addition, because we find residential emission amount and resulting RE (particularly aerosol–cloud effects) are not linearly related, our results cannot be used to estimate the impacts associated with smaller, realistic reductions in residential emissions. Future research is needed to explore the air quality and climate impact of realistic emission reductions scenarios that could potentially be achieved through the implementation of cleaner combustion technologies and clean alternative fuels.

More people are using RSF for cooking than at any other point in human history, even though the fraction of the population using these fuels is falling (Bonjour et al., 2013). Over the next few decades (2005–2030), combustion of RSF is projected to increase in South Asia and Africa due to increases in human population (UNEP, 2011). We have reported human health and climate impacts for the year 2000, but in China, residential emissions have increased 34 % during the period 2000–2012 due to the growth of coal consumption (Cui et al., 2015). The use of biomass for heating is also expected to increase in developed countries such as in Western Europe because of rising fossil fuel prices and use of renewable biomass under climate change mitigation policy (Denier van der Gon et al., 2015). The impact of residential emissions on human health and climate is, therefore, likely to persist in the future unless effective mitigation to address the dependence on RSFs is taken.

Appendix A

Table A1. Acronyms used in this study.

Acronym	Description
ACCMIP	Atmospheric Chemistry and Climate Model Intercomparison Project
AF	Attributable fraction
AIE	Aerosol indirect effect
BC	Black carbon
BHN	Binary homogenous nucleation
BLN	Boundary layer nucleation
CCN	Cloud condensation nuclei
CDNC	Cloud droplet number concentration
CPD	Cardiopulmonary disease
CRF	Concentration response functions
DRE	Direct radiative effect
EC	Elemental carbon
FT	Free troposphere
LC	Lung cancer
LPG	Liquefied petroleum gas
LW	Longwave
MACCity	MACC/CityZEN project
NH	Northern Hemisphere
N_3	Number of particles greater than 3 nm dry diameter
N_{50}	Number of particles greater than 50 nm dry diameter
N_{100}	Number of particles greater than 100 nm dry diameter
NMBF	Normalised mean bias factor
OC	Organic carbon
PM	Particulate matter
$PM_{2.5}$	Particulate matter with an aerodynamic dry diameter of < 2.5 µm
POM	Particulate organic matter
RE	Radiative effect
RR	Relative risk
RSF	Residential solid fuel
SOA	Secondary organic aerosol
SW	Shortwave
TOA	Top of atmosphere

Acknowledgements. E. W. Butt acknowledges support from the United Bank of Carbon and the University of Leeds. V. Vakkari acknowledges support from the Academy of Finland Finnish Center of Excellence program (grant no. 1118615). Ambient aerosol measurements obtained through the Atmospheric Brown Cloud project funded by the United Nations Environmental Programme and the National Oceanic and Atmospheric Administration. Particulate matter sample collection, analysis, and data validation was supported by James J. Schauer at the University of Wisconsin-Madison, Jeff DeMinter at the Wisconsin State Laboratory of Hygiene, Soon-Chang Yoon of Seoul National University, and Pradeep Dangol and Bidya Banmali Pradhan at the International Center for Integrated Mountain Development. H. Yang would like to thank the support from National Science Foundation for Young Scholars of China (grant no. 41205003). We acknowledge funding from the Natural Environment Research Council (NERC) (grant no. NE/K015966/1).

Edited by: S. S. Gunthe

References

Adams, P. and Seinfeld, J.: Disproportionate impact of particulate emissions on global cloud condensation nuclei concentrations, Geophys. Res. Lett., 30, 1239, doi:10.1029/2002GL016303, 2003.

Adhikary, B., Carmichael, G. R., Tang, Y., Leung, L. R., Qian, Y., Schauer, J. J., Stone, E. A., Ramanathan, V., and Ramana, M. V.: Characterization of the seasonal cycle of south Asian aerosols: a regional-scale modeling analysis, J. Geophys. Res.-Atmos., 112, D22S22, doi:10.1029/2006JD008143,2007.

Allen, R. W., Gombojav, E., Barkhasragchaa, B., Byambaa, T., Lkhasuren, O., Amram, O., Takaro, T. K., and Janes, C. R.: An assessment of air pollution and its attributable mortality in Ulaanbaatar, Mongolia, Air Qual. Atmos. Health, 6, 137–150, 2013.

Andres, R. and Kasgnoc, A.: A time-averaged inventory of subaerial volcanic sulfur emissions, J. Geophys. Res.-Atmos., 103, 25251–25261, 1998.

Anenberg, S. C., Horowitz, L. W., Tong, D. Q., and West, J.: An estimate of the global burden of anthropogenic ozone and fine particulate matter on premature human mortality using atmospheric modeling, Environ. Health Persp., 118, 1189–1195, 2010.

Arnold, S. R., Chipperfield, M. P., and Blitz, M. A.: A three-dimensional model study of the effect of new temperature dependent quantum yields for acetone photolysis, J. Geophys. Res., 110, D22305, doi:10.1029/2005jd005998, 2005.

Arola, A., Schuster, G., Myhre, G., Kazadzis, S., Dey, S., and Tripathi, S. N.: Inferring absorbing organic carbon content from AERONET data, Atmos. Chem. Phys., 11, 215–225, doi:10.5194/acp-11-215-2011, 2011.

Aunan, K., Berntsen, T. K., Myhre, G., Rypdal, K., Streets, D. G., Woo, J.-H., and Smith, K. R.: Radiative forcing from household fuel burning in Asia, Atmos. Environ., 43, 5674–5681, 2009.

Barahona, D., West, R. E. L., Stier, P., Romakkaniemi, S., Kokkola, H., and Nenes, A.: Comprehensively accounting for the effect of giant CCN in cloud activation parameterizations, Atmos. Chem. Phys., 10, 2467–2473, doi:10.5194/acp-10-2467-2010, 2010.

Bauer, S. E., Menon, S., Koch, D., Bond, T. C., and Tsigaridis, K.: A global modeling study on carbonaceous aerosol microphysical characteristics and radiative effects, Atmos. Chem. Phys., 10, 7439–7456, doi:10.5194/acp-10-7439-2010, 2010.

Bellouin, N., Rae, J., Jones, A., Johnson, C., Haywood, J., and Boucher, O.: Aerosol forcing in the Climate Model Intercomparison Project (CMIP5) simulations by HadGEM2-ES and the role of ammonium nitrate, J. Geophys. Res.-Atmos., 116, D20206, doi:10.1029/2011JD016074, 2011.

Bellouin, N., Mann, G. W., Woodhouse, M. T., Johnson, C., Carslaw, K. S., and Dalvi, M.: Impact of the modal aerosol scheme GLOMAP-mode on aerosol forcing in the Hadley Centre Global Environmental Model, Atmos. Chem. Phys., 13, 3027–3044, doi:10.5194/acp-13-3027-2013, 2013.

Bergström, R., Denier van der Gon, H. A. C., Prévôt, A. S. H., Yttri, K. E., and Simpson, D.: Modelling of organic aerosols over Europe (2002–2007) using a volatility basis set (VBS) framework: application of different assumptions regarding the formation of secondary organic aerosol, Atmos. Chem. Phys., 12, 8499–8527, doi:10.5194/acp-12-8499-2012, 2012.

Bond, T. C., Streets, D. G., Yarber, K. F., Nelson, S. M., Woo, J.-H., and Klimont, Z.: A technology-based global inventory of black and organic carbon emissions from combustion, J. Geophys. Res., 109, D14203, doi:10.1029/2003jd003697, 2004.

Bond, T. C., Habib, G., and Bergstrom, R. W.: Limitations in the enhancement of visible light absorption due to mixing state, J. Geophys. Res., 111, D20211, doi:10.1029/2006JD007315, 2006.

Bond, T. C., Bhardwaj, E., Dong, R., Jogani, R., Jung, S., Roden, C., Streets, D. G., and Trautmann, N. M.: Historical emissions of black and organic carbon aerosol from energy-related combustion, 1850–2000, Global Biogeochem. Cy., 21, GB2018, doi:10.1029/2006GB002840, 2007.

Bond, T. C., Doherty, S. J., Fahey, D., Forster, P., Berntsen, T., DeAngelo, B., Flanner, M., Ghan, S., Kärcher, B., and Koch, D.: Bounding the role of black carbon in the climate system: a scientific assessment, J. Geophys. Res.-Atmos., 118, 5380–5552, 2013.

Bonjour, S., Adair-Rohani, H., Wolf, J., Bruce, N. G., Mehta, S., Pruss-Ustun, A., Lahiff, M., Rehfuess, E. A., Mishra, V., and Smith, K. R.: Solid fuel use for household cooking: country and regional estimates for 1980–2010, Environ. Health Persp., 121, 784–790, 2013.

Bosch, C., Andersson, A., Kirillova, E. N., Budhavant, K., Tiwari, S., Praveen, P., Russell, L. M., Beres, N. D., Ramanathan, V., and Gustafsson, Ö.: Source-diagnostic dual-isotope composition and optical properties of water-soluble organic carbon and elemental carbon in the South Asian outflow intercepted over the Indian Ocean, J. Geophys. Res.-Atmos., 119, 11743–11759, 2014.

Boucher, O., Randall, D., Artaxo, P., Bretherton, C., Feingold, G., Forster, P., Kerminen, V.-M., Kondo, Y., Liao, H., and Lohmann, U.: Clouds and aerosols, in: Climate Change 2013: The Physical Science Basis, Contribution of working group I to the fifth assessment report of the intergovernmental panel on climate change, Cambridge University Press, Cambridge, UK, and New York, NY, USA, 571–657, 2013.

Brook, R. D., Rajagopalan, S., Pope, C. A., Brook, J. R., Bhatnagar, A., Diez-Roux, A. V., Holguin, F., Hong, Y., Luepker, R. V., and Mittleman, M. A.: Particulate matter air pollution and cardiovascular disease an update to the scientific statement from

the American Heart Association, Circulation, 121, 2331–2378, 2010.

Browse, J., Carslaw, K. S., Arnold, S. R., Pringle, K., and Boucher, O.: The scavenging processes controlling the seasonal cycle in Arctic sulphate and black carbon aerosol, Atmos. Chem. Phys., 12, 6775–6798, doi:10.5194/acp-12-6775-2012, 2012.

Burnett, R. T., Pope, C. A., Ezzati, M., Olives, C., Lim, S. S., Mehta, S., Shin, H. H., Singh, G., Hubbell, B., and Brauer, M.: An integrated risk function for estimating the global burden of disease attributable to ambient fine particulate matter exposure, Environ. Health Perspect., 122, 397–403, doi:10.1289/ehp.1307049, 2014.

Cao, G., Zhang, X., and Zheng, F.: Inventory of black carbon and organic carbon emissions from China, Atmos. Environ., 40, 6516–6527, 2006.

Chafe, Z. A., Brauer, M., Klimont, Z., Van Dingenen, R., Mehta, S., Rao, S., Riahi, K., Dentener, F., and Smith, K. R.: Household cooking with solid fuels contributes to ambient $PM_{2.5}$ air pollution and the Burden of Disease, Environ. Health Perspect., 122, 1314–1320, 2014.

Chen, B., Andersson, A., Lee, M., Kirillova, E. N., Xiao, Q., Kruså, M., Shi, M., Hu, K., Lu, Z., and Streets, D. G.: Source forensics of black carbon aerosols from China, Environ. Sci. Technol., 47, 9102–9108, 2013.

Chen, Y. and Bond, T. C.: Light absorption by organic carbon from wood combustion, Atmos. Chem. Phys., 10, 1773–1787, doi:10.5194/acp-10-1773-2010, 2010.

Chen, Y., Sheng, G., Bi, X., Feng, Y., Mai, B., and Fu, J.: Emission factors for carbonaceous particles and polycyclic aromatic hydrocarbons from residential coal combustion in China, Environ. Sci. Technol., 39, 1861–1867, 2005.

Chen, Y., Zhi, G., Feng, Y., Fu, J., Feng, J., Sheng, G., and Simoneit, B. R.: Measurements of emission factors for primary carbonaceous particles from residential raw-coal combustion in China, Geophys. Res. Lett., 33, L20815, doi:10.1029/2006GL026966, 2006.

Chen, Y., Ebenstein, A., Greenstone, M., and Li, H.: Evidence on the impact of sustained exposure to air pollution on life expectancy from China's Huai River policy, P. Natl. Acad. Sci. USA, 110, 12936–12941, 2013.

Chipperfield, M.: New version of the TOMCAT/SLIMCAT offline chemical transport model: intercomparison of stratospheric tracer experiments, Q. J. Roy. Meteorol. Soc., 132, 1179–1203, 2006.

Cohen, A. J., Anderson, H. R., Ostro, B., Pandey, K. D., Krzyzanowski, M., Künzli, N., Gutschmidt, K., Pope III, C. A., Romieu, I., and Samet, J. M.: Urban air pollution, Comparative Quantification of Health Risks, 2, 1353–1433, 2004.

Cohen, A. J., Anderson, H. R., Ostro, B., Pandey, K. D., Krzyzanowski, M., Künzli, N., Gutschmidt, K., Pope III, C. A., Romieu, I., and Samet, J. M.: The global burden of disease due to outdoor air pollution, J. Toxicol. Env. Heal. A, 68, 1301–1307, 2005.

Cui, H., Mao, P., Zhao, Y., Nielsen, C. P., and Zhang, J.: Patterns in atmospheric carbonaceous aerosols in China: emission estimates and observed concentrations, Atmos. Chem. Phys., 15, 8657–8678, doi:10.5194/acp-15-8657-2015, 2015.

Denier van der Gon, H. A. C., Bergström, R., Fountoukis, C., Johansson, C., Pandis, S. N., Simpson, D., and Visschedijk, A. J. H.: Particulate emissions from residential wood combustion in Europe – revised estimates and an evaluation, Atmos. Chem. Phys., 15, 6503–6519, doi:10.5194/acp-15-6503-2015, 2015.

Dentener, F., Kinne, S., Bond, T., Boucher, O., Cofala, J., Generoso, S., Ginoux, P., Gong, S., Hoelzemann, J. J., Ito, A., Marelli, L., Penner, J. E., Putaud, J.-P., Textor, C., Schulz, M., van der Werf, G. R., and Wilson, J.: Emissions of primary aerosol and precursor gases in the years 2000 and 1750 prescribed data-sets for AeroCom, Atmos. Chem. Phys., 6, 4321–4344, doi:10.5194/acp-6-4321-2006, 2006.

Dusek, U., Frank, G., Hildebrandt, L., Curtius, J., Schneider, J., Walter, S., Chand, D., Drewnick, F., Hings, S., and Jung, D.: Size matters more than chemistry for cloud-nucleating ability of aerosol particles, Science, 312, 1375–1378, 2006.

Edwards, J. and Slingo, A.: Studies with a flexible new radiation code. I: Choosing a configuration for a large-scale model, Q. J. Roy. Meteorol. Soc., 122, 689–719, 1996.

EEA: European Union emission inventory report, 1990–2012 under the UNECE Convention on Long-range Transboundary Air Pollution (LRTAP), EEA (European Environment Agency), Copenhagen, 2014.

Evan, A. T., Kossin, J. P., and Ramanathan, V.: Arabian Sea tropical cyclones intensified by emissions of black carbon and other aerosols, Nature, 479, 94–97, 2011.

Forster, P., Ramaswamy, V., Artaxo, P., Berntsen, T., Betts, R., Fahey, D. W., Haywood, J., Lean, J., Lowe, D. C., Myhre, G., Nganga, J., Prinn, R., Raga, G., Schulz, M., and Dorland, R. V.: Changes in Atmospheric Constituents and in Radiative Forcing, in: Climate Change 2007: The Physical Science Basis, Contribution of Working Group I to the Fourth Assessment Report of the Intergovernmental Panel on Climate Change, edited by: Solomon, S., Qin, D., Manning, M., Chen, Z., Marquis, M., Averyt, K. B., Tignor, M., and Miller, H. L., Cambridge University Press, Cambridge, UK, and New York, USA, 2007.

Fountoukis, C. and Nenes, A.: Continued development of a cloud droplet formation parameterization for global climate models, J. Geophys. Res.-Atmos., 110, D11212, doi:10.1029/2004jd005591, 2005.

Fountoukis, C., Butler, T., Lawrence, M., van der Gon, H. D., Visschedijk, A., Charalampidis, P., Pilinis, C., and Pandis, S.: Impacts of controlling biomass burning emissions on wintertime carbonaceous aerosol in Europe, Atmos. Environ., 87, 175–182, 2014.

Fu, T.-M., Cao, J. J., Zhang, X. Y., Lee, S. C., Zhang, Q., Han, Y. M., Qu, W. J., Han, Z., Zhang, R., Wang, Y. X., Chen, D., and Henze, D. K.: Carbonaceous aerosols in China: top-down constraints on primary sources and estimation of secondary contribution, Atmos. Chem. Phys., 12, 2725–2746, doi:10.5194/acp-12-2725-2012, 2012.

Fuller, K. A., Malm, W. C., and Kreidenweis, S. M.: Effects of mixing on extinction by carbonaceous particles, J. Geophys. Res.-Atmos., 104, 15941–15954, 1999.

Ganguly, D., Ginoux, P., Ramaswamy, V., Winker, D., Holben, B., and Tripathi, S.: Retrieving the composition and concentration of aerosols over the Indo-Gangetic basin using CALIOP and AERONET data, Geophys. Res. Lett., 36, L13806, doi:10.1029/2009GL038315, 2009.

Giannadaki, D., Pozzer, A., and Lelieveld, J.: Modeled global effects of airborne desert dust on air quality and premature mortal-

ity, Atmos. Chem. Phys., 14, 957–968, doi:10.5194/acp-14-957-2014, 2014.

Gong, S.: A parameterization of sea-salt aerosol source function for sub- and super-micron particles, Global Biogeochem. Cy., 17, 1097, doi:10.1029/2003gb002079, 2003.

Granier, C., Bessagnet, B., Bond, T., D'Angiola, A., Van Der Gon, H. D., Frost, G. J., Heil, A., Kaiser, J. W., Kinne, S., and Klimont, Z.: Evolution of anthropogenic and biomass burning emissions of air pollutants at global and regional scales during the 1980–2010 period, Climatic Change, 109, 163–190, 2011.

Guenther, A., Hewitt, C. N., Erickson, D., Fall, R., Geron, C., Graedel, T., Harley, P., Klinger, L., Lerdau, M., McKay, W. A., Pierce, T., Scholes, B., Steinbrecher, R., Tallamraju, R., Taylor, J., and Zimmerman, P.: A global model of natural volatile organic compound emissions, J. Geophys. Res., 100, 8873–8892, doi:10.1029/94jd02950, 1995.

Gustafsson, Ö., Kruså, M., Zencak, Z., Sheesley, R. J., Granat, L., Engström, E., Praveen, P., Rao, P., Leck, C., and Rodhe, H.: Brown clouds over South Asia: biomass or fossil fuel combustion?, Science, 323, 495–498, 2009.

Halmer, M. M., Schmincke, H. U., and Graf, H. F.: The annual volcanic gas input into the atmosphere, in particular into the stratosphere: a global data set for the past 100 years, J. Volcanol. Geoth. Res., 115, 511–528, doi:10.1016/s0377-0273(01)00318-3, 2002.

Han, Z., Zhang, R., Wang, Q. G., Wang, W., Cao, J., and Xu, J.: Regional modeling of organic aerosols over China in summertime, J. Geophys. Res.-Atmos., 113, D11202, doi:10.1029/2007JD009436, 2008.

Jacobson, M. Z.: Strong radiative heating due to the mixing state of black carbon in atmospheric aerosols, Nature, 409, 695–697, 2001.

Jacobson, M. Z.: Short-term effects of controlling fossil-fuel soot, biofuel soot and gases, and methane on climate, Arctic ice, and air pollution health, J. Geophys. Res.-Atmos., 115, D14209, doi:10.1029/2009JD013795, 2010.

Johnson, M., Edwards, R., Alatorre Frenk, C., and Masera, O.: In-field greenhouse gas emissions from cookstoves in rural Mexican households, Atmos. Environ., 42, 1206–1222, 2008.

Johnston, F. H., Henderson, S. B., Chen, Y., Randerson, J. T., Marlier, M., DeFries, R. S., Kinney, P., Bowman, D. M., and Brauer, M.: Estimated global mortality attributable to smoke from landscape fires, Environ. Health Persp., 120, 695–701, 2012.

Johnston, F. H., Hanigan, I. C., Henderson, S. B., and Morgan, G. G.: Evaluation of interventions to reduce air pollution from biomass smoke on mortality in Launceston, Australia: retrospective analysis of daily mortality, 1994–2007, Brit. Med. J., 346, e8446, doi:10.1136/bmj.e8446, 2013.

Kettle, A. and Andreae, M.: Flux of dimethylsulfide from the oceans: a comparison of updated data sets and flux models, J. Geophys. Res.-Atmos., 105, 26793–26808, 2000.

Kirchstetter, T. W., Novakov, T., and Hobbs, P. V.: Evidence that the spectral dependence of light absorption by aerosols is affected by organic carbon, J. Geophys. Res.-Atmos., 109, D21208, doi:10.1029/2004JD004999, 2004.

Kirillova, E. N., Andersson, A., Sheesley, R. J., Kruså, M., Praveen, P., Budhavant, K., Safai, P., Rao, P., and Gustafsson, Ö.: 13C- and, 14C-based study of sources and atmospheric processing of water-soluble organic carbon (WSOC) in South Asian aerosols, J. Geophys. Res.-Atmos., 118, 614–626, 2013.

Klimont, Z., Cofala, J., Xing, J., Wei, W., Zhang, C., Wang, S., Kejun, J., Bhandari, P., Mathur, R., and Purohit, P.: Projections of SO_2, NO_x and carbonaceous aerosols emissions in Asia, Tellus B, 61, 602–617, 2009.

Koch, D. and Del Genio, A. D.: Black carbon semi-direct effects on cloud cover: review and synthesis, Atmos. Chem. Phys., 10, 7685–7696, doi:10.5194/acp-10-7685-2010, 2010.

Koch, D., Schulz, M., Kinne, S., McNaughton, C., Spackman, J. R., Balkanski, Y., Bauer, S., Berntsen, T., Bond, T. C., Boucher, O., Chin, M., Clarke, A., De Luca, N., Dentener, F., Diehl, T., Dubovik, O., Easter, R., Fahey, D. W., Feichter, J., Fillmore, D., Freitag, S., Ghan, S., Ginoux, P., Gong, S., Horowitz, L., Iversen, T., Kirkevåg, A., Klimont, Z., Kondo, Y., Krol, M., Liu, X., Miller, R., Montanaro, V., Moteki, N., Myhre, G., Penner, J. E., Perlwitz, J., Pitari, G., Reddy, S., Sahu, L., Sakamoto, H., Schuster, G., Schwarz, J. P., Seland, Ø., Stier, P., Takegawa, N., Takemura, T., Textor, C., van Aardenne, J. A., and Zhao, Y.: Evaluation of black carbon estimations in global aerosol models, Atmos. Chem. Phys., 9, 9001–9026, doi:10.5194/acp-9-9001-2009, 2009.

Kodros, J. K., Scott, C. E., Farina, S. C., Lee, Y. H., L'Orange, C., Volckens, J., and Pierce, J. R.: Uncertainties in global aerosols and climate effects due to biofuel emissions, Atmos. Chem. Phys., 15, 8577–8596, doi:10.5194/acp-15-8577-2015, 2015.

Kulmala, M., Laaksonen, A., and Pirjola, L.: Parameterizations for sulfuric acid/water nucleation rates, J. Geophys. Res.-Atmos., 103, 8301–8307, 1998.

Kulmala, M., Lehtinen, K. E. J., and Laaksonen, A.: Cluster activation theory as an explanation of the linear dependence between formation rate of 3nm particles and sulphuric acid concentration, Atmos. Chem. Phys., 6, 787–793, doi:10.5194/acp-6-787-2006, 2006.

Kumar, R., Barth, M. C., Nair, V. S., Pfister, G. G., Suresh Babu, S., Satheesh, S. K., Krishna Moorthy, K., Carmichael, G. R., Lu, Z., and Streets, D. G.: Sources of black carbon aerosols in South Asia and surrounding regions during the Integrated Campaign for Aerosols, Gases and Radiation Budget (ICARB), Atmos. Chem. Phys., 15, 5415–5428, doi:10.5194/acp-15-5415-2015, 2015.

Lam, N. L., Chen, Y., Weyant, C., Venkataraman, C., Sadavarte, P., Johnson, M. A., Smith, K. R., Brem, B. T., Arineitwe, J., and Ellis, J. E.: Household light makes global heat: high black carbon emissions from kerosene wick lamps, Environ. Sci. Technol., 46, 13531–13538, 2012.

Lamarque, J.-F., Bond, T. C., Eyring, V., Granier, C., Heil, A., Klimont, Z., Lee, D., Liousse, C., Mieville, A., Owen, B., Schultz, M. G., Shindell, D., Smith, S. J., Stehfest, E., Van Aardenne, J., Cooper, O. R., Kainuma, M., Mahowald, N., McConnell, J. R., Naik, V., Riahi, K., and van Vuuren, D. P.: Historical (1850–2000) gridded anthropogenic and biomass burning emissions of reactive gases and aerosols: methodology and application, Atmos. Chem. Phys., 10, 7017–7039, doi:10.5194/acp-10-7017-2010, 2010.

Lei, Y., Zhang, Q., He, K. B., and Streets, D. G.: Primary anthropogenic aerosol emission trends for China, 1990–2005, Atmos. Chem. Phys., 11, 931–954, doi:10.5194/acp-11-931-2011, 2011.

Li, X., Wang, S., Duan, L., Hao, J., and Nie, Y.: Carbonaceous aerosol emissions from household biofuel combustion in China, Environ. Sci. Technol., 43, 6076–6081, 2009.

Lim, S. S., Vos, T., Flaxman, A. D., et al.: A comparative risk assessment of burden of disease and injury attributable to 67 risk factors and risk factor clusters in, 21 regions, 1990–2010: a systematic analysis for the Global Burden of Disease Study 2010, Lancet, 380, 2224–2260, 2012.

Lu, Z., Zhang, Q., and Streets, D. G.: Sulfur dioxide and primary carbonaceous aerosol emissions in China and India, 1996–2010, Atmos. Chem. Phys., 11, 9839–9864, doi:10.5194/acp-11-9839-2011, 2011.

Mann, G. W., Carslaw, K. S., Spracklen, D. V., Ridley, D. A., Manktelow, P. T., Chipperfield, M. P., Pickering, S. J., and Johnson, C. E.: Description and evaluation of GLOMAP-mode: a modal global aerosol microphysics model for the UKCA composition-climate model, Geosci. Model Dev., 3, 519–551, doi:10.5194/gmd-3-519-2010, 2010.

Marlier, M. E., DeFries, R. S., Voulgarakis, A., Kinney, P. L., Randerson, J. T., Shindell, D. T., Chen, Y., and Faluvegi, G.: El Nino and health risks from landscape fire emissions in southeast Asia, Nat. Clim. Change, 3, 131–136, 2013.

Mathers, C., Fat, D. M., and Boerma, J.: The Global Burden of Disease: 2004 Update, World Health Organization, Switzerland, 2008.

Menon, S., Koch, D., Beig, G., Sahu, S., Fasullo, J., and Orlikowski, D.: Black carbon aerosols and the third polar ice cap, Atmos. Chem. Phys., 10, 4559–4571, doi:10.5194/acp-10-4559-2010, 2010.

Merikanto, J., Spracklen, D. V., Pringle, K. J., and Carslaw, K. S.: Effects of boundary layer particle formation on cloud droplet number and changes in cloud albedo from 1850 to 2000, Atmos. Chem. Phys., 10, 695–705, doi:10.5194/acp-10-695-2010, 2010.

Moorthy, K. K., Beegum, S. N., Srivastava, N., Satheesh, S., Chin, M., Blond, N., Babu, S. S., and Singh, S.: Performance evaluation of chemistry transport models over India, Atmos. Environ., 71, 210–225, 2013.

Nair, V. S., Solmon, F., Giorgi, F., Mariotti, L., Babu, S. S., and Moorthy, K. K.: Simulation of South Asian aerosols for regional climate studies, J. Geophys. Res.-Atmos., 117, D04209, doi:10.1029/2011JD016711, 2012.

Nenes, A. and Seinfeld, J. H.: Parameterization of cloud droplet formation in global climate models, J. Geophys. Res.-Atmos., 108, 4415, doi:10.1029/2002JD002911, 2003.

Nightingale, P. D., Malin, G., Law, C. S., Watson, A. J., Liss, P. S., Liddicoat, M. I., Boutin, J., and Upstill-Goddard, R. C.: In situ evaluation of air–sea gas exchange parameterizations using novel conservative and volatile tracers, Global Biogeochem. Cy., 14, 373–387, 2000.

Ostro, B.: Outdoor air pollution: Assessing the environmental burden of disease at national and local levels, WHO Environmental Burden of Disease Series No. 5, WHO, Geneva, 2004.

Pagels, J., Dutcher, D. D., Stolzenburg, M. R., McMurry, P. H., Gälli, M. E., and Gross, D. S.: Fine-particle emissions from solid biofuel combustion studied with single-particle mass spectrometry: identification of markers for organics, soot, and ash components, J. Geophys. Res.-Atmos., 118, 859–870, 2013.

Pan, X., Chin, M., Gautam, R., Bian, H., Kim, D., Colarco, P. R., Diehl, T. L., Takemura, T., Pozzoli, L., Tsigaridis, K., Bauer, S., and Bellouin, N.: A multi-model evaluation of aerosols over South Asia: common problems and possible causes, Atmos. Chem. Phys., 15, 5903–5928, doi:10.5194/acp-15-5903-2015, 2015.

Parashar, D., Gadi, R., Mandal, T., and Mitra, A.: Carbonaceous aerosol emissions from India, Atmos. Environ., 39, 7861–7871, 2005.

Park, R. J., Jacob, D. J., Palmer, P. I., Clarke, A. D., Weber, R. J., Zondlo, M. A., Eisele, F. L., Bandy, A. R., Thornton, D. C., and Sachse, G. W.: Export efficiency of black carbon aerosol in continental outflow: global implications, J. Geophys. Res.-Atmos., 110, D11205, doi:10.1029/2004JD005432, 2005.

Partanen, A. I., Laakso, A., Schmidt, A., Kokkola, H., Kuokkanen, T., Pietikäinen, J.-P., Kerminen, V.-M., Lehtinen, K. E. J., Laakso, L., and Korhonen, H.: Climate and air quality trade-offs in altering ship fuel sulfur content, Atmos. Chem. Phys., 13, 12059–12071, doi:10.5194/acp-13-12059-2013, 2013.

Penner, J. E., Andreae, M., Annegarn, H., Barrie, L., Feichter, J., Hegg, D., Jayaraman, A., Leaitch, R., Murphy, D., Nganga, J., and Pitari, G.: Aerosols, their Direct and Indirect Effects, in: Climate Change 2001: The Physical Science Basis, Contribution of Working Group I to the Third Assessment Report of the Intergovernmental Panel on Climate Change, edited by: Houghton, J. T., Ding, Y., Griggs, D. J., Noguer, M., van der Linden, P. J., Dai, X., Maskell, K., and Johnson, C. A., Cambridge University Press, Cambridge, UK, and New York, USA, 2001.

Pierce, J. R. and Adams, P. J.: Uncertainty in global CCN concentrations from uncertain aerosol nucleation and primary emission rates, Atmos. Chem. Phys., 9, 1339–1356, doi:10.5194/acp-9-1339-2009, 2009.

Pierce, J. R., Chen, K., and Adams, P. J.: Contribution of primary carbonaceous aerosol to cloud condensation nuclei: processes and uncertainties evaluated with a global aerosol microphysics model, Atmos. Chem. Phys., 7, 5447–5466, doi:10.5194/acp-7-5447-2007, 2007.

Pierce, J. R., Theodoritsi, G., Adams, P., and Pandis, S.: Parameterization of the effect of sub-grid scale aerosol dynamics on aerosol number emission rates, J. Aerosol Sci., 40, 385–393, 2009.

Pope III, C. A. and Dockery, D. W.: Health effects of fine particulate air pollution: lines that connect, JAPCA J. Air Waste Manage., 56, 709–742, 2006.

Pope III, C. A., Burnett, R. T., Thun, M. J., Calle, E. E., Krewski, D., Ito, K., and Thurston, G. D.: Lung cancer, cardiopulmonary mortality, and long-term exposure to fine particulate air pollution, Jama, 287, 1132–1141, 2002.

Pringle, K. J., Carslaw, K. S., Spracklen, D. V., Mann, G. M., and Chipperfield, M. P.: The relationship between aerosol and cloud drop number concentrations in a global aerosol microphysics model, Atmos. Chem. Phys., 9, 4131–4144, doi:10.5194/acp-9-4131-2009, 2009.

Pringle, K. J., Carslaw, K. S., Fan, T., Mann, G. W., Hill, A., Stier, P., Zhang, K., and Tost, H.: A multi-model assessment of the impact of sea spray geoengineering on cloud droplet number, Atmos. Chem. Phys., 12, 11647–11663, doi:10.5194/acp-12-11647-2012, 2012.

Qu, W. J., Zhang, X. Y., Arimoto, R., Wang, D., Wang, Y. Q., Yan, L. W., and Li, Y.: Chemical composition of the background aerosol at two sites in southwestern and northwestern China: po-

tential influences of regional transport, Tellus B, 60, 657–673, 2008.

Ramanathan, V. and Carmichael, G.: Global and regional climate changes due to black carbon, Nat. Geosci., 1, 221–227, 2008.

Ramanathan, V., Chung, C., Kim, D., Bettge, T., Buja, L., Kiehl, J., Washington, W., Fu, Q., Sikka, D., and Wild, M.: Atmospheric brown clouds: impacts on South Asian climate and hydrological cycle, P. Natl. Acad. Sci. USA, 102, 5326–5333, 2005.

Rap, A., Scott, C. E., Spracklen, D. V., Bellouin, N., Forster, P. M., Carslaw, K. S., Schmidt, A., and Mann, G.: Natural aerosol direct and indirect radiative effects, Geophys. Res. Lett., 40, 3297–3301, 2013.

Reddington, C. L., Carslaw, K. S., Spracklen, D. V., Frontoso, M. G., Collins, L., Merikanto, J., Minikin, A., Hamburger, T., Coe, H., Kulmala, M., Aalto, P., Flentje, H., Plass-Dülmer, C., Birmili, W., Wiedensohler, A., Wehner, B., Tuch, T., Sonntag, A., O'Dowd, C. D., Jennings, S. G., Dupuy, R., Baltensperger, U., Weingartner, E., Hansson, H.-C., Tunved, P., Laj, P., Sellegri, K., Boulon, J., Putaud, J.-P., Gruening, C., Swietlicki, E., Roldin, P., Henzing, J. S., Moerman, M., Mihalopoulos, N., Kouvarakis, G., Ždímal, V., Zíková, N., Marinoni, A., Bonasoni, P., and Duchi, R.: Primary versus secondary contributions to particle number concentrations in the European boundary layer, Atmos. Chem. Phys., 11, 12007–12036, doi:10.5194/acp-11-12007-2011, 2011.

Reddington, C. L., McMeeking, G., Mann, G. W., Coe, H., Frontoso, M. G., Liu, D., Flynn, M., Spracklen, D. V., and Carslaw, K. S.: The mass and number size distributions of black carbon aerosol over Europe, Atmos. Chem. Phys., 13, 4917–4939, doi:10.5194/acp-13-4917-2013, 2013.

Reddington, C. L., Butt, E. W., Ridley, D. A., Artaxo, P., Morgan, W. T., Coe, H., and Spracklen, D. V.: Air quality and human health improvements from reductions in deforestation-related fire in Brazil, Nat. Geosci., 8, 768–771, 2015.

Roden, C. A., Bond, T. C., Conway, S., and Pinel, A. B. O.: Emission factors and real-time optical properties of particles emitted from traditional wood burning cookstoves, Environ. Sci. Technol., 40, 6750–6757, 2006.

Roden, C. A., Bond, T. C., Conway, S., Osorto Pinel, A. B., MacCarty, N., and Still, D.: Laboratory and field investigations of particulate and carbon monoxide emissions from traditional and improved cookstoves, Atmos. Environ., 43, 1170–1181, 2009.

Rossow, W. B. and Schiffer, R. A.: Advances in understanding clouds from ISCCP, B. Am. Meteorol. Soc., 80, 2261–2287, 1999.

Schlesinger, R., Kunzli, N., Hidy, G., Gotschi, T., and Jerrett, M.: The health relevance of ambient particulate matter characteristics: coherence of toxicological and epidemiological inferences, Inhal. Toxicol., 18, 95–125, 2006.

Schmidt, A., Ostro, B., Carslaw, K. S., Wilson, M., Thordarson, T., Mann, G. W., and Simmons, A. J.: Excess mortality in Europe following a future Laki-style Icelandic eruption, P. Natl. Acad. Sci. USA, 108, 15710–15715, 2011.

Schmidt, A., Carslaw, K. S., Mann, G. W., Rap, A., Pringle, K. J., Spracklen, D. V., Wilson, M., and Forster, P. M.: Importance of tropospheric volcanic aerosol for indirect radiative forcing of climate, Atmos. Chem. Phys., 12, 7321–7339, doi:10.5194/acp-12-7321-2012, 2012.

Scott, C. E., Rap, A., Spracklen, D. V., Forster, P. M., Carslaw, K. S., Mann, G. W., Pringle, K. J., Kivekäs, N., Kulmala, M., Lihavainen, H., and Tunved, P.: The direct and indirect radiative effects of biogenic secondary organic aerosol, Atmos. Chem. Phys., 14, 447–470, doi:10.5194/acp-14-447-2014, 2014.

SEDAC: Sociodemographic Data and Applications Centre, Gridded Population of the World (GPW), v3., available at: http://sedac.ciesin.columbia.edu/data/collection/gpw-v3 (last acces: 1 November 2013), 2004.

Sheesley, R. J., Kirillova, E., Andersson, A., Kruså, M., Praveen, P., Budhavant, K., Safai, P. D., Rao, P., and Gustafsson, Ö.: Year-round radiocarbon-based source apportionment of carbonaceous aerosols at two background sites in South Asia. J. Geophys. Res.-Atmos., 117, D10202, doi:10.1029/2011JD017161, 2012.

Shen, G., Wang, W., Yang, Y., Zhu, C., Min, Y., Xue, M., Ding, J., Li, W., Wang, B., and Shen, H.: Emission factors and particulate matter size distribution of polycyclic aromatic hydrocarbons from residential coal combustions in rural Northern China, Atmos. Environ., 44, 5237–5243, 2010.

Sihto, S.-L., Kulmala, M., Kerminen, V.-M., Dal Maso, M., Petäjä, T., Riipinen, I., Korhonen, H., Arnold, F., Janson, R., Boy, M., Laaksonen, A., and Lehtinen, K. E. J.: Atmospheric sulphuric acid and aerosol formation: implications from atmospheric measurements for nucleation and early growth mechanisms, Atmos. Chem. Phys., 6, 4079–4091, doi:10.5194/acp-6-4079-2006, 2006.

Silva, R. A., West, J. J., Zhang, Y., Anenberg, S. C., Lamarque, J.-F., Shindell, D. T., Collins, W. J., Dalsoren, S., Faluvegi, G., and Folberth, G.: Global premature mortality due to anthropogenic outdoor air pollution and the contribution of past climate change, Environ. Res. Lett., 8, 034005, doi:10.1088/1748-9326/8/3/034005, 2013.

Smith, K. R., Bruce, N., Balakrishnan, K., Adair-Rohani, H., Balmes, J., Chafe, Z., Dherani, M., Hosgood, H. D., Mehta, S., and Pope, D.: Millions dead: how do we know and what does it mean? Methods used in the comparative risk assessment of household air pollution, Annu. Rev. Publ. Health, 35, 185–206, 2014.

Spracklen, D. V., Pringle, K. J., Carslaw, K. S., Chipperfield, M. P., and Mann, G. W.: A global off-line model of size-resolved aerosol microphysics: I. Model development and prediction of aerosol properties, Atmos. Chem. Phys., 5, 2227–2252, doi:10.5194/acp-5-2227-2005, 2005a.

Spracklen, D. V., Pringle, K. J., Carslaw, K. S., Chipperfield, M. P., and Mann, G. W.: A global off-line model of size-resolved aerosol microphysics: II. Identification of key uncertainties, Atmos. Chem. Phys., 5, 3233–3250, doi:10.5194/acp-5-3233-2005, 2005b.

Spracklen, D. V., Carslaw, K. S., Kulmala, M., Kerminen, V.-M., Mann, G. W., and Sihto, S.-L.: The contribution of boundary layer nucleation events to total particle concentrations on regional and global scales, Atmos. Chem. Phys., 6, 5631–5648, doi:10.5194/acp-6-5631-2006, 2006.

Spracklen, D. V., Carslaw, K. S., Pöschl, U., Rap, A., and Forster, P. M.: Global cloud condensation nuclei influenced by carbonaceous combustion aerosol, Atmos. Chem. Phys., 11, 9067–9087, doi:10.5194/acp-11-9067-2011, 2011a.

Spracklen, D. V., Jimenez, J. L., Carslaw, K. S., Worsnop, D. R., Evans, M. J., Mann, G. W., Zhang, Q., Canagaratna, M. R.,

Allan, J., Coe, H., McFiggans, G., Rap, A., and Forster, P.: Aerosol mass spectrometer constraint on the global secondary organic aerosol budget, Atmos. Chem. Phys., 11, 12109–12136, doi:10.5194/acp-11-12109-2011, 2011b.

Stier, P., Feichter, J., Kinne, S., Kloster, S., Vignati, E., Wilson, J., Ganzeveld, L., Tegen, I., Werner, M., Balkanski, Y., Schulz, M., Boucher, O., Minikin, A., and Petzold, A.: The aerosol-climate model ECHAM5-HAM, Atmos. Chem. Phys., 5, 1125–1156, doi:10.5194/acp-5-1125-2005, 2005.

Stohl, A., Klimont, Z., Eckhardt, S., Kupiainen, K., Shevchenko, V. P., Kopeikin, V. M., and Novigatsky, A. N.: Black carbon in the Arctic: the underestimated role of gas flaring and residential combustion emissions, Atmos. Chem. Phys., 13, 8833–8855, doi:10.5194/acp-13-8833-2013, 2013.

Stone, E. A., Lough, G. C., Schauer, J. J., Praveen, P., Corrigan, C., and Ramanathan, V.: Understanding the origin of black carbon in the atmospheric brown cloud over the Indian Ocean, J. Geophys. Res.-Atmos., 112, D22S23, doi:10.1029/2006JD008118, 2007.

Stone, E. A., Schauer, J. J., Pradhan, B. B., Dangol, P. M., Habib, G., Venkataraman, C., and Ramanathan, V.: Characterization of emissions from South Asian biofuels and application to source apportionment of carbonaceous aerosol in the Himalayas, J. Geophys. Res.-Atmos., 115, D06301, doi:10.1029/2009JD011881, 2010.

Stone, E. A., Yoon, S.-C., and Schauer, J. J.: Chemical characterization of fine and coarse particles in Gosan, Korea during springtime dust events, Aerosol Air Qual. Res., 11, 31–43, 2011.

Tiitta, P., Vakkari, V., Croteau, P., Beukes, J. P., van Zyl, P. G., Josipovic, M., Venter, A. D., Jaars, K., Pienaar, J. J., Ng, N. L., Canagaratna, M. R., Jayne, J. T., Kerminen, V.-M., Kokkola, H., Kulmala, M., Laaksonen, A., Worsnop, D. R., and Laakso, L.: Chemical composition, main sources and temporal variability of PM_1 aerosols in southern African grassland, Atmos. Chem. Phys., 14, 1909–1927, doi:10.5194/acp-14-1909-2014, 2014.

Tuomisto, J. T., Wilson, A., Evans, J. S., and Tainio, M.: Uncertainty in mortality response to airborne fine particulate matter: Combining European air pollution experts, Reliabil. Eng. Syst. Saf., 93, 732–744, 2008.

UNEP: Near-term Climate Protection and Clean Air Benefits: Actions for Controlling Short-Lived Climate Forcers, United Nations Environment Programme (UNEP), Nairobi, Kenya, 78 pp., 2011.

Unger, N., Bond, T. C., Wang, J. S., Koch, D. M., Menon, S., Shindell, D. T., and Bauer, S.: Attribution of climate forcing to economic sectors, P. Natl. Acad. Sci. USA, 107, 3382–3387, 2010.

Vakkari, V., Beukes, J. P., Laakso, H., Mabaso, D., Pienaar, J. J., Kulmala, M., and Laakso, L.: Long-term observations of aerosol size distributions in semi-clean and polluted savannah in South Africa, Atmos. Chem. Phys., 13, 1751–1770, doi:10.5194/acp-13-1751-2013, 2013.

van der Werf, G. R., Randerson, J. T., Collatz, G. J., Giglio, L., Kasibhatla, P. S., Arellano, A. F., Olsen, S. C., and Kasischke, E. S.: Continental-scale partitioning of fire emissions during the 1997 to 2001 El Nino/La Nina period, Science, 303, 73–76, 2004.

Venkataraman, C. and Rao, G. U. M.: Emission factors of carbon monoxide and size-resolved aerosols from biofuel combustion, Environ. Sci. Technol., 35, 2100–2107, 2001.

Venkataraman, C., Habib, G., Eiguren-Fernandez, A., Miguel, A., and Friedlander, S.: Residential biofuels in South Asia: carbonaceous aerosol emissions and climate impacts, Science, 307, 1454–1456, 2005.

Venter, A. D., Vakkari, V., Beukes, J. P., Van Zyl, P. G., Laakso, H., Mabaso, D., Tiitta, P., Josipovic, M., Kulmala, M., and Pienaar, J. J.: An air quality assessment in the industrialised western Bushveld Igneous Complex, South Africa, S. Afr. J. Sci., 108, 1–10, 2012.

Wang, R., Tao, S., Balkanski, Y., Ciais, P., Boucher, O., Liu, J., Piao, S., Shen, H., Vuolo, M. R., and Valari, M.: Exposure to ambient black carbon derived from a unique inventory and high-resolution model, P. Natl. Acad. Sci. USA, 111, 2459–2463, 2014.

Wang, X., Wang, Y., Hao, J., Kondo, Y., Irwin, M., Munger, J. W., and Zhao, Y.: Top-down estimate of China's black carbon emissions using surface observations: sensitivity to observation representativeness and transport model error, J. Geophys. Res.-Atmos., 118, 5781–5795, 2013.

Wang, X., Heald, C. L., Ridley, D. A., Schwarz, J. P., Spackman, J. R., Perring, A. E., Coe, H., Liu, D., and Clarke, A. D.: Exploiting simultaneous observational constraints on mass and absorption to estimate the global direct radiative forcing of black carbon and brown carbon, Atmos. Chem. Phys., 14, 10989–11010, doi:10.5194/acp-14-10989-2014, 2014.

WHO: The Energy Access Situation in Developing Countries, World Health Organization and United Nations Development Programme, New York, USA, 2009.

WHO: Burden of Disease from Household Air Pollution for 2012, World Health Organisation, Geneva, Switzerland, 2014a.

WHO: Burden of Disease from Ambient Air pollution for 2012, World Health Organisation, Geneva, Switzerland, 2014b.

Xu, B., Cao, J., Hansen, J., Yao, T., Joswia, D. R., Wang, N., Wu, G., Wang, M., Zhao, H., and Yang, W.: Black soot and the survival of Tibetan glaciers, P. Natl. Acad. Sci. USA, 106, 22114–22118, 2009.

Yu, S., Eder, B., Dennis, R., Chu, S. H., and Schwartz, S. E.: New unbiased symmetric metrics for evaluation of air quality models, Atmos. Sci. Lett., 7, 26–34, 2006.

Zhang, X., Wang, Y., Zhang, X., Guo, W., and Gong, S.: Carbonaceous aerosol composition over various regions of China during 2006, J. Geophys. Res.-Atmos., 113, D14111, doi:10.1029/2007JD009525, 2008.

Zhi, G., Chen, Y., Feng, Y., Xiong, S., Li, J., Zhang, G., Sheng, G., and Fu, J.: Emission characteristics of carbonaceous particles from various residential coal-stoves in China, Environ. Sci. Technol., 42, 3310–3315, 2008.

Chapter 5

Near-term global and regional air quality and health benefits in 2050 due to widespread adoption of clean residential combustion technologies

Edward W Butt[1],Hana Pearce[1], Zbigniew Klimont[2], Chris Heyes[2], Joe McNorton[1,3],Luke Conibear[1], Carly L Reddington[1], Stephen R Arnold[1], Dominick V Spracklen[1]

[1]*Institute of Climate and Atmospheric Science (ICAS), School of Earth and Environment, University of Leeds, Leeds, UK*

[2]*International Institute for Applied Systems Analysis (IIASA), 2361 Laxenburg, Austria*

[3]*European Centre for Medium-Range Weather Forecasts (ECMWF), Reading, UK*

Abstract

Long-term exposure to ambient particulate matter ($PM_{2.5}$, mass of particles with an aerodynamic dry diameter of < 2.5 μm) is causally associated with respiratory and cardiovascular disease mortality and is a major risk factor to the global burden of disease. Residential combustion of solid fuel for cooking and heating contributes up to one-third of global deaths attributable to ambient $PM_{2.5}$. Despite this, few studies have examined the potential near-term air quality and associated health burden benefits of clean residential combustion technologies. We used a global chemistry-transport model coupled to a global aerosol model together with exposure-response relationships, to examine the extent of near-term changes in ambient $PM_{2.5}$ concentrations and associated health burden impacts by 2050 under different emission scenarios. Under a 2050 reference scenario, we found that global annual mean population-weighted $PM_{2.5}$ concentrations increased by 12.3%, relative to 2015. Under the this same scenario, global mortality attributable to ambient $PM_{2.5}$ increased by 72.8%, corresponding to 7.1 [3.9-10.7] million deaths in 2050. We found that population growth and ageing overwhelmingly contributed to increases in mortality in 2050, even in some regions where $PM_{2.5}$ concentrations declined, such as across East Asia. We examined an additional scenario in 2050 assuming the widespread implementation of best available clean combustion technologies across the residential sector, including adoption of clean cookstoves. We further compared this clean residential scenario to a maximum anthropogenic emission reduction scenario, where clean technologies and measures were implemented in all anthropogenic emission sectors, to assess the important of clean residential combustion in 2050. We found that clean residential combustion alone avoids 26.7% of the maximum preventable mean population-weighted $PM_{2.5}$ concentration (4.9 μg m^{-3}) globally by 2050 and 0.34 [0.28-0.4] million deaths or 20% of the maximum possible global avoidable mortality. Air quality and associated mortality benefits are highlighted across regions where residential

emissions contribute to anthropogenic ambient $PM_{2.5}$, such as across Sub-Saharan Africa where half to two thirds of the maximum possible avoidable $PM_{2.5}$ and mortality benefits, can be achieved by clean residential control technologies alone. However, in general, we found that the greater avoidable $PM_{2.5}$ and mortalities in 2050 under the maximum possible anthropogenic reduction scenario in most regions highlights the priority for reducing all anthropogenic emissions collectively. Nevertheless, clean residential combustion technologies can provide substantial global and regional ambient air quality and public health benefits by 2050, with total avoidable mortalities being nearly 100% greater if considered under newly available health exposure-response relationships. We hope that our findings can be used to help inform ambient clean air quality policy management strategies, particularly across low-income regions where legislation is lacking and residential combustion emissions are important.

5.1 Introduction

Nearly 40% of the world's population, overwhelmingly in low and middle-income countries, rely on solid fuels for basic household tasks such as cooking, space heating and lighting (Bonjour et al., 2013). The incomplete combustion of these residential solid fuels, often referred to as household or domestic solid fuels (e.g., wood, coal, agricultural and animal waste) in traditional open fires (e.g., 3-stone fires) or simple cooking or heating stoves results in the emission of large amounts of particulate matter (PM) into household and ambient environments (Jetter and Kariher, 2009; Bond et al., 2013; Winijkul, Fierce, and Bond, 2016).

Long-term exposure to PM with a median aerodynamic dry diameter of $< 2.5\ \mu m$ ($PM_{2.5}$) is causally associated with respiratory and cardiovascular disease mortality (Dockery et al., 1993; Pope et al., 1995; Pope III and Dockery,

2006; Krewski et al., 2009). The Global Burden of Disease's (GBD) Comparative Risk Assessment (CRA) places both ambient and household exposure to $PM_{2.5}$ within the top ten risk factors affecting global health in the present-day (Gakidou et al., 2017). Long-term exposure to ambient $PM_{2.5}$ is the fifth largest risk factor, causing 4.1 million deaths annually in 2016, while exposure to household air pollution (HAP) is the tenth largest risk factor, contributing to 2.6 million deaths in the same year (Gakidou et al., 2017; Smith et al., 2014a).

Emissions from residential solid fuel combustion contribute to ambient $PM_{2.5}$ concentrations and thus directly contribute to the burden of disease attributable to ambient $PM_{2.5}$ exposure. (Chafe et al., 2014; Butt et al., 2016). In the present-day, residential emissions contribute to about one-third of the attributable deaths due to ambient $PM_{2.5}$ globally (Lelieveld et al., 2015). Regionally, they contribute to one-third of the attributable deaths in China (Archer-Nicholls et al., 2016) and Africa (Lacey et al., 2017a), and one-third to one-half attributable deaths in India (Conibear et al., 2018a; GBD MAPS Working Group, 2018). Even among high-income countries (e.g., North America and Europe), residential space heating emissions contribute about one-tenth the attributable deaths due to ambient $PM_{2.5}$ (Chafe et al., 2015). Given these large contributions, understanding future impacts to changes in residential emissions is vital for informing air quality management.

Use of residential solid fuels has undergone regional changes in the past few decades. For low and middle-income regions, while urbanisation, income and development transitions have led to a relative reduction in households using solid fuels (Smith and Ezzati, 2005; Wilkinson et al., 2009; Shen et al., 2017), the absolute number of people relying on solid fuels has remained relatively stable due to population growth (Bonjour et al., 2013). For high-income regions, such as those across Europe, while the relative contribution of residential space heating $PM_{2.5}$ may be increasing, absolute emissions are generally declining due to energy diversification and air quality regulation

(Chafe et al., 2015).

The issue of solid fuel use in low and middle-income countries has been a focal point of international development for many decades. Since the 1980s, household energy interventions targeting the adoption of fuel efficient or so called 'improved' biomass cookstoves, were part of efforts to alleviate environmental impacts associated with unsustainable firewood collection (Anenberg et al., 2012). However, while achieving mixed results in terms of scale, these early interventions did not necessarily reduce heath relevant PM emissions or HAP exposures (Anenberg et al., 2012). Moreover, emissions and health goals were often not considered part of an intervention's aims.

More recently, intervention policy has shifted towards public health favouring the use of advanced 'clean' solid fuel stove technologies and/or use of cleaner fuels (e.g., liquefied petroleum gas (LPG) and electricity) (Goldemberg et al., 2018). However, while the replacement of solid fuels with cleaner fuels is seen as the most desirable for public heath goals (Goldemberg et al., 2018; Steenland et al., 2018; Smith and Sagar, 2014; Lacey et al., 2017a), such fuels remain elusive for many across low and middle-income regions as a result of accessibility and affordability barriers (Anenberg et al., 2013; Rehfuess et al., 2014). This suggests a transitional or interim role for clean combustion technologies using solid fuels, such as clean cookstoves.

Relative to traditional three-stone fires, advanced clean cookstove technologies can achieve up to 50% reductions in PM emissions, and forced draft (fan assisted) stoves can achieve up to 90% reductions under controlled conditions (Jetter and Kariher, 2009; Jetter et al., 2012). However, successful large-scale implementation means that such technologies need to replace traditional polluting methods and be an attractive option for users. The widespread adoption of these technologies are also attractive because they potentially not only deliver improved air quality (both ambient and HAP), but also multiple co-benefits, including climate change mitigation to other socio-economic

benefits, such as reduced fuel collection or expenditure for poor households, and business for stove manufacturers distributors (Grieshop, Marshall, and Kandlikar, 2011; Bond et al., 2013; Anenberg et al., 2013; Amann, Klimont, and Kupiainen, 2011). Nevertheless, few studies have examined the obvious global and regional ambient air quality and associated health burden potential of such technologies, particularly when considering near-term future transitions in residential fuel use, as well as demographic and epidemiological transitions (Kuhn et al., 2016).

In this study, we investigate changes in ambient $PM_{2.5}$ concentrations and associated public health impacts between 2015 and 2050. We use a global chemistry-transport model coupled to a modal aerosol model with estimated changes in anthropogenic emissions, demographics and disease epidemiology. We estimate ambient air quality and health impacts in a 2050 reference scenario and compare it to a scenario where the widespread adoption of clean residential combustion technologies has taken place. We further examine these potential benefits against an additional 2050 scenario where available clean combustion technologies are widely adopted in all anthropogenic sectors. In examining such scenarios, we hope to identify regions where clean residential combustion might be important for near-term ambient air quality management.

5.2 Methods

5.2.1 TOMCAT-GLOMAP description

We use the offline 3-D global chemical-transport model (CTM) TOMCAT (Chipperfield, 2006; Monks et al., 2017), with a horizontal resolution of 2.8° $\times$ 2.8° and 31 hybrid vertical σ–p levels extending from the surface to 10 hPa. Vertical σlevels are terrain-following below about 100 hPa above which they are purely pressure levels. Model transport and meteorology is driven by

winds, temperature and humidity fields from the ECMWF (European Centre for Medium-Range Weather Forecasts) ERA-Interim (Dee et al., 2011) reanalyses.

The TOMCAT chemistry scheme includes detailed tropospheric gas-phase chemistry inclusive of reactions of odd oxygen (O_x), nitrogen (NO_y), hydrogen (HO_x = OH + HO_2), as well as carbon monoxide (CO), methane (CH_4) and short chain non-methane volatile organic compounds (VOCs) (Chipperfield, 2006; Monks et al., 2017). We use a version of TOMCAT that is fully coupled to the aerosol microphysics model, the GLObal Model of Aerosol Processes (GLOMAP) (Spracklen et al., 2005b). Coupling to GLOMAP allows for the interaction and feedback of atmospheric chemistry and aerosol, such as the changes in oxidant concentrations due to changes in gas-phase aerosol precursor emissions. We use the modal version of GLOMAP (GLOMAP-mode) where aerosol mass and number concentrations are carried in seven log-normal size modes: four hydrophilic (nucleation (diameter (D) $<$ 10 nm), Aitken (D 10-100 nm), accumulation (D 100 nm - 1 µm), and coarse (D $>$ 1 µm)), and three non-hydrophilic (Aitken, accumulation, and coarse) modes (Mann et al., 2010). Size-resolved aerosol microphysical processes in GLOMAP-mode include primary emissions, secondary particle formation, particle growth through coagulation, condensation, and cloud-processing and removal by dry and wet deposition.

GLOMAP-mode simulates aerosol components: sulfate (SO_4^{2-}), mineral dust, black carbon (BC), particulate organic matter (POM), and sea salt (NaCl). Secondary organic aerosol (SOA) is formed from products of monoterpene oxidation, generated at a 13% yield and assumed to be involatile (Spracklen et al., 2006; Scott et al., 2014). We also assume a global organic carbon (OC) to POM ratio of 2.1 as based on an upper regional estimate (Philip et al., 2014). There is no representation of anthropogenic SOA or ammonium nitrate in this version of GLOMAP-mode (Mann et al., 2010). This version of

the model also does not include mineral dust, instead we used a 10-year average $PM_{2.5}$ dust climatology (Reddington et al., 2015; Butt et al., 2017) and add it to simulated $PM_{2.5}$ fields.

5.2.2 Emission scenarios

Table 5.1 summaries emission scenarios used in this study. Anthropogenic gas-phase and primary aerosol emissions are taken from the ECLIPSE (Evaluating the Climate and Air Quality Impacts of Short-Lived Pollutants) emission inventory (see Section A.1.1). We include anthropogenic emissions in 2015 (present-day) and in a 2050 reference scenario. Emissions in the reference scenario are based on International Energy Agency (IEA) energy projections under an assumption of full implementation and enforcement of current and planned national air quality legislation as of 2013 (refereed to by ECLIPSE as CLE or 'current legislation') (Stohl et al., 2015; IEA, 2012). In terms of carbon dioxide (CO_2) concentrations, the reference scenario is compatible with the representative concentration pathway scenario (RCP6.0).

Scenario name	Year	Emission description
2015 present-day	2015	Anthropogenic emissions in 2015.
2050 reference	2050	Anthropogenic emissions in 2050 based on IEA energy projections under the assumption of full implementation and enforcement of current and planned national air quality legislation as of 2013.
2050 clean residential	2050	Same anthropogenic emissions as in the reference scenario but with penetration of best available emission control technologies in the residential sector only.
2050 MTFR (maximum technically feasible reduction)	2050	Same as the clean residential scenario but with penetration of best available emission control technologies in all anthropogenic emission sectors, including some non-technical measures.

TABLE 5.1: Air quality emission scenarios used. All scenarios include natural emissions consistent with present-day meteorology.

We apply two additional 2050 scenarios to which we compare the reference: a clean residential and maximum technically feasible reduction (MTFR) scenario. The MTRF scenario is provided separately by the ECLIPSE inventory, which starts at the level of the reference scenario, but instead allocates best available emission control technologies in all anthropogenic sectors, regardless of implementation costs, barriers and institutional issues, but with some technological, geophysical, and cultural limitations. The MTFR scenario accounts for very limited fuel transitions (e.g., solid fuels to LPG or electricity)

as these are accounted for in the reference scenario, but it does include some non-technical measures, such as the elimination of highly emitting vehicles, agricultural waste burning, and reduced gas flaring. Further details of control options used in the MTFR can be found elsewhere (Stohl et al., 2015; Klimont et al., 2017).

To isolate the effects of clean residential combustion technologies only, we created the hybrid 2050 'clean residential' scenario, which is identical to the reference scenario, but instead allocates MTFR best available control technologies in the residential sector only. Because the MTFR scenario represents the maximum possible anthropogenic emission reduction in 2050, comparing it to the clean residential scenario will identify the relative importance of near-term clean residential emission controls for improving regional air quality and associated public health impacts.

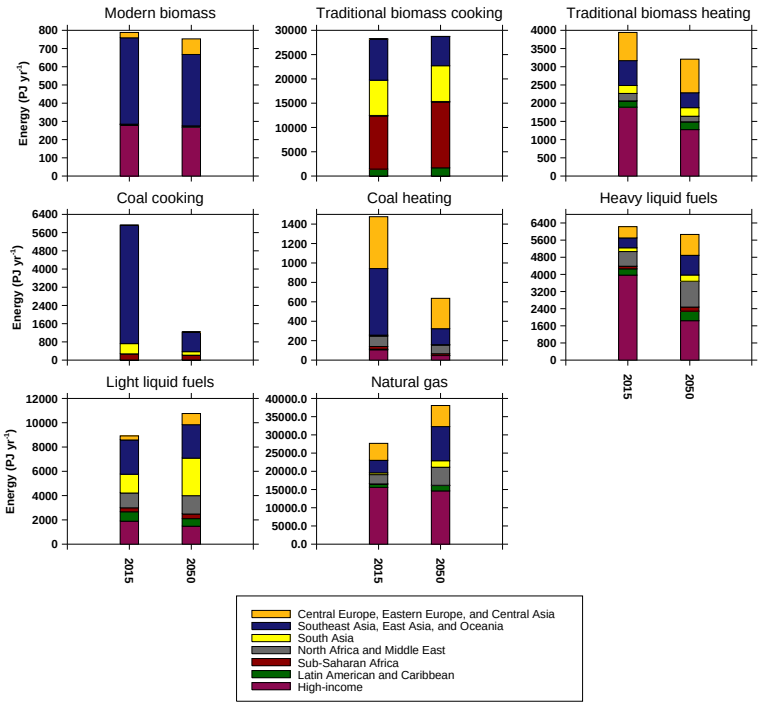

FIGURE 5.1: Energy consumption of combustible fuels in the residential sector in 2015 and 2050, split by geographical super region (see Figure A.1 for super region breakdown). Projected energy use estimates for consumption in 2050 are based on IEA forecasts (IEA, 2012) consistent with 2050 ECLIPSE reference (i.e., CLE) and MTFR scenarios.

Figure 5.1 shows residential sector energy use per combustible fuel in 2015 and 2050, split by geographical super region (see Figure A.1 for super region breakdown). Energy consumption of solid fuel biomass remains important in 2050, despite global reductions in modern biomass (5%) and traditional biomass heating (19%), driven largely by reductions across the super region of Southeast Asia, East Asia, and Oceania (i.e., primarily East Asia), and across high-income regions. Relative to 2015, global consumption of traditional biomass increases slightly by 2% in 2050, driven largely by a 25% increases across Sub-Saharan African regions, despite reductions across East Asia. Global coal consumption for cooking and heating experienced considerable reductions in 2050 (79% and 57% respectively), particularly driven by reductions across East Asia (83% and 76% respectively), due to planned limits imposed by China. For non-solid residential fuels, global consumption of heavy liquid fuels (e.g., oil) are expected to decrease by 6% in 2050, whereas consumption of liquid light fuels and national gas are predicted to increase by 21% and 38% respectively globally.

Table 5.2 summarises the emission control technologies used in the 2050 clean residential scenario in fuel sectors reported in Figure 5.1, where reduced emissions through more efficient and optimised combustion are achieved. Here, traditional cookstoves or three-stone fires using solid fuel biomass are replaced with best available forced-air (fan assisted) cookstoves across middle and low-income countries, while the penetration of coal briquettes and appropriate clean stoves are assumed for cooking with coal. For space heating in high-income regions, penetration of biomass pellet stoves and single house boilers, and coal briquette stoves are assumed, while best available log stoves and boilers, and coal briquette heating stoves are assumed across low and middle-income regions. For lighting in low and middle-income countries, kerosene lamps are replaced with light-emitting diode (LED) lamps, which is also largely accounted for in the reference scenario based on ambitious national electrification projections.

To isolate the effects of changes in anthropogenic emissions only, all scenarios include natural emissions (see Section A.1.2) consistent with present-day meteorology. Annual mean $PM_{2.5}$ concentrations for each scenario are calculated as a 5-year average using meteorology for the period 2011-2015. Finally, we remove residential emissions in all scenarios to examine residential emission contributions under each scenario.

Control option	Non-specific	Lighting	Fireplace	Stove	Household boiler	Medium boiler
Improved	×		×	× (Cooking and Heating)	×	
New			×	× (Cooking and Heating)	×	
Fan Stove				× (Cooking)		
Coal briquette				× (Cooking and Heating)		
Hurricane lamp		×				
LED lamp		×				
Pellets				× (Heating)	×	×
Cyclone						×
ESP				× (Heating)	×	×

TABLE 5.2: Residential control technology options used in the clean residential scenario. Control options are based on laboratory and field emission factors using best available control technologies. Table data adapted from Klimont et al., 2017.

Future emission changes

Figure 5.2 shows anthropogenic emissions for each scenario by super region. Regional changes in emissions between 2015 and the 2050 reference scenario generally reflect differences in energy use and current and planned air quality management or lack of. Relative to 2015, global BC and OC emissions decreased in the reference scenario by 6% and 4% respectively, due to reductions in East Asia, and high-income regions, despite increases in South Asia, North Africa and Middle East and, Sub-Saharan Africa. Large emission reductions in BC and OC in the super region of Southeast Asia, East Asian and Oceania were largely a result of legislation controlling the use of residential coal for cooking and space heating in China. The contribution of residential combustion to global BC and OC emission is large relative to the other air pollutants, and remains a significant contributor in the 2050 reference scenario, despite falling 12.4 and 3.6 percentage points to 45.2% and 61.1%, respectively. Relative to the reference scenario, global BC and OC emissions are reduced by 33.7% and 48.4%, respectively under the 2050 clean residential

scenario, with considerable decreases predicted across Sub-Saharan Africa (64.9% and 68.4%, respectively) and South Asia (33.1% and 57.7%, respectively), as well as reducing the global residential combustion contribution to 17.3% and 24.6%, respectively. However, larger reductions in global BC and OC emissions are predicted in the MTFR scenario (82.8% and 82.1%, respectively), with regional reductions typically above 70%.

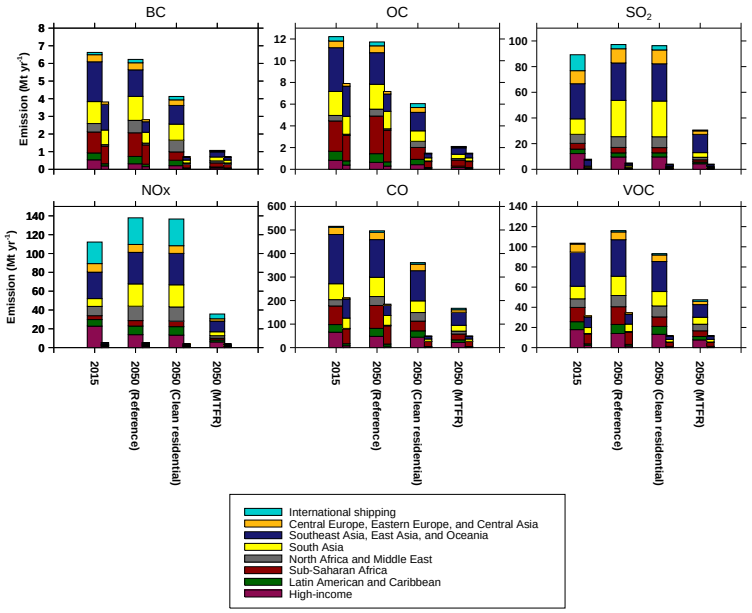

FIGURE 5.2: Anthropogenic air pollutant emissions (million tonnes (Mt) for individual scenarios split by broad geographical super region as identified in Figure A.1, including international shipping. Air pollutants include, BC (black carbon), OC (organic carbon), SO_2 (sulfur dioxide), NO_x (nitrogen oxides), CO (carbon monoxide), and VOCs (volatile organic compounds). Total residential sector emissions for each scenario are also included and represented by the smaller bar to the right.

Relative to 2015, global sulphur dioxide (SO_2) emissions increased 8.9% in the 2050 reference scenario, despite reductions across high-income and East Asian regions, and low sulphur fuel transitions in international shipping. This global increase was driven mainly by a large 134% increase in South Asian (mostly in India) SO_2 emissions, due to poor legislation in the power and industrial sectors in the face of rapid population growth and energy consumption (Stohl et al., 2015). Residential combustion contributes only 5% of global SO_2 emissions in the 2050 reference scenario, down 4 percentage

points from 2015 largely due to residential coal controls in China. Therefore, relative to the reference scenario, global SO_2 emissions are only reduced by 1% in the clean residential scenario compared to the much larger reduction under the MTFR scenario (68.5%). Similarly, global emissions of nitrogen oxides (NO_x) also increase in the 2050 reference scenario (22.9%), but because of the small contribution of residential combustion to global NO_x emissions (4%), global emissions are reduced by only 0.9% in the clean residential scenario, relative to the reference, which is compared to the much larger reduction in the MTFR scenario (74.1%).

Global carbon monoxide (CO) emissions decrease by 3.6% in the 2050 reference scenario, relative to 2015, which was largely due to emission controls in high-income regions and East Asia. The contribution to residential combustion to global CO emissions is 37.2% in the reference scenario. Relative to the reference, global CO emissions decrease by 27.3% under the clean residential scenario, which is less than half the reduction under the MTFR scenario (66.3%).

Relative to 2015, global volatile organic compound (VOC) emissions increase by 12% in 2050 under the reference scenario. Residential emissions increase under the reference scenario, but with little change between the relative contribution to global emissions between 2015 (30.5%) and 2050 (29.9%). Relative to the reference, global VOC emissions decrease by 19.7% in 2050 under the clean residential scenario, which is less than half the reduction in the MTFR (59.1%).

5.2.3 Evaluating simulated $PM_{2.5}$ concentrations

We compare 2015 annual mean simulated $PM_{2.5}$ concentrations with measurements collected across multiple locations and regions (see Section A.2). In general, simulated $PM_{2.5}$ concentrations are underestimated compared to

measurements (Figure A.2), with the exception across North America (normalised mean bias factor (NMBF) = 0.29). The model underestimates by a similar magnitude across Europe (NMBF = -0.22) and Southeast Asia (NMBF = -0.29), as well as across Africa (NMBF = -0.24), but with a greater spread. However, large underestimates of a factor 2 and 3 are estimated across China and India, respectively.

$PM_{2.5}$ measurements are taken from a mix of urban, semi-urban, rural, and remote locations. For example, measurements across North America and Europe are almost exclusively from rural or remote locations, whereas all measurements in India are from urban locations, as are many of the measurements in China. These differences may partly explain the very low bias in India and China as the relatively coarse spatial resolution of TOMCAT struggles to resolve urban concentration gradients. Low PM bias has been shown in previous studies using the global aerosol model GLOMAP-mode, each citing missing or uncertain emission sources, model processes, and spatial resolution as possible contributing factors (Butt et al., 2016; Butt et al., 2017; Turnock et al., 2015). Nevertheless, a Pearson's correlation coefficient (r) = 0.87 suggests that the model is well able to simulate the overall spatial distribution of the observations, but not necessarily the magnitude in them.

To account for the low model bias, we use a 'semi-observational' gridded dataset of ambient $PM_{2.5}$ concentration applied in recent GBD CRA, the DIMAQ (Data Integration Model for Air Quality) (Shaddick et al., 2018) (Section A.3.1). We averaged DIMAQ from its original resolution of $0.1^\circ \times 0.1^\circ$ (11 km $\times$ 11 km at the equator) to the TOMCAT resolution ($2.8^\circ \times 2.8^\circ$) and made a comparison (Figure A.3). Similar to the comparison with surface measurements, we found that while the model underestimates compared to DIMAQ in most regions (NMBF of between 0 and -1), TOMCAT is well able to simulate the overall spatial distribution of DIMAQ $PM_{2.5}$ estimates (r = 0.80) (Figure A.3 **b**). Supported by this good spatial correlation, we regionally scaled 2015 simulated concentrations as described in Section A.3.2.

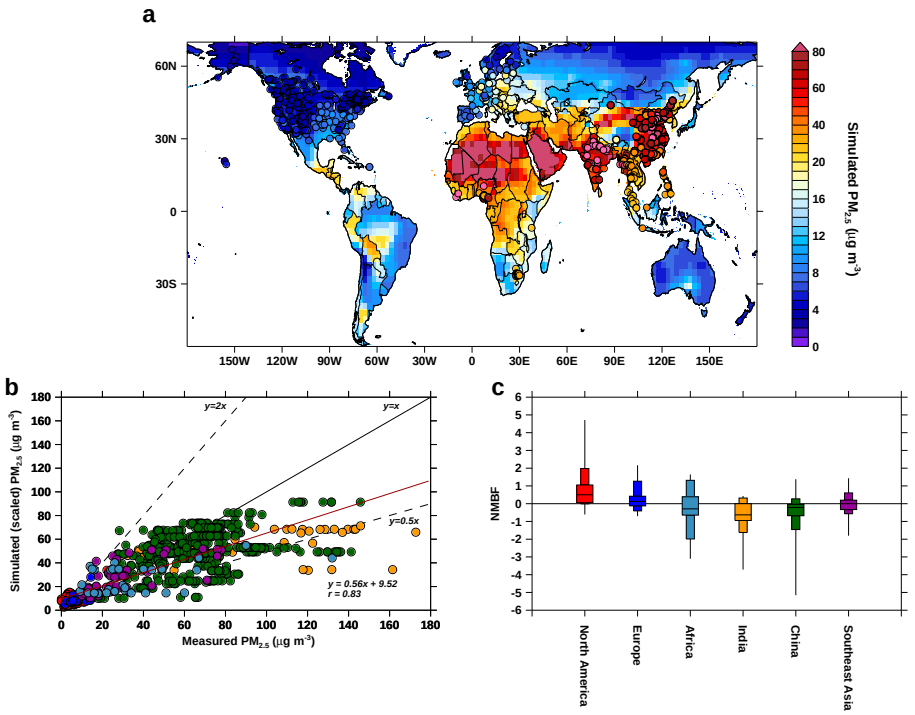

FIGURE 5.3: Comparison of simulated (scaled) $PM_{2.5}$ concentrations with measurements collected across multiple locations and regions. **a** 2015 TOMCAT simulated surface annual mean $PM_{2.5}$ concentrations (background) compared to measurements (filled circles). **b** Comparison of $PM_{2.5}$ concentrations, best fit line (red line), 1:1 (solid black line), 2:1 and 1:2 (dashed black lines). Best fit line has slope = 0.32 and Pearson's correlation coefficient (r) = 0.87. **c** Normalised mean bias factor (NMBF) box and whisker by sub-region, showing the minimum, maximum and median distribution values, as well as the 10^{th}, 25^{th}, 75^{th}, and 90^{th} percentiles.

Figure 5.3 shows the comparison of the scaled TOMCAT 2015 $PM_{2.5}$ concentrations to surface measurements (see also scaled comparison to DIMAQ, Figure A.4). After scaling, we find an overall reduction in the regional low bias compared to surface measurements, although low biases still persist across China and India, but to a lesser extent. In addition, we find that scaling also leads to a slightly greater overestimation across North America. Nevertheless, we apply the same scaling methodology to all 2050 scenarios and use these scaled estimates to report impacts on ambient $PM_{2.5}$ and associated health burdens in the current study.

5.2.4 Health impact assessment

We use integrated exposure-response (IER) relationships (Burnett et al., 2014) to estimate mortality burdens attributable to ambient $PM_{2.5}$ exposure, which have been used extensively for health assessments over the past few years. Using epidemiological risk estimates from different combustion sources, the IER is used to predict relative risk of mortality for cause-specific diseases over the global range of $PM_{2.5}$ exposure. Cause-specific diseases that have been deemed consistent with causal relationships are predicted, ischaemic heart disease (IHD), cerebrovascular disease (ischaemic stroke and haemorrhagic stroke; CEV), lung cancer, chronic obstructive pulmonary disease (COPD), and lower respiratory infections (LRI). Employing updates described in (Cohen et al., 2017), the IER takes the form:

$$RR(c) = 1 + \alpha \times (1 - e^{\beta(c - c_{cf})^{\gamma +}})$$

$$RR(c) = 1 \quad \text{for} \quad c \leq c_{cf}$$

where *RR(c)* is the relative risk at $PM_{2.5}$ concentration, and c_{cf} is the theoretical minimum risk exposure level (TMREL), below which is no risk is assumed. The TMREL is determined by a uniform distribution representing the minimum and 5^{th} percentiles of exposure distributions estimated in ambient air pollution prospective cohort studies (2.4-5.9 µg m^{-3}). The grouping $1 + \alpha$ is the maximum risk, β is the ratio of the IER at low to high $PM_{2.5}$ concentrations, and γ is the power of $PM_{2.5}$ concentration (Cohen et al., 2017). Using 1000 parameter sets of c_{cf}, α, β, and γ, we calculate the mean of the IER at each $PM_{2.5}$ concentration as a central estimate, with the uncertainty range defined by the 5^{th} and 95^{th} percentiles.

The IER curves are generally non-linear, with reduced sensitivity to changes

in $PM_{2.5}$ at higher exposure distributions, particularly for cardiovascular diseases (IHD and CEV) (Figure A.5). Age-specific RRs are also fitted for cardiovascular diseases as risk factors for these diseases decline with age (Singh et al., 2013; Burnett et al., 2014).

We calculate attributable mortality due to long-term ambient $PM_{2.5}$ exposure at the country-level following similar methods to the GBD CRA. For a given year, country and sex, total attributable mortality ($Mort_{PM_{2.5}}$) can be calculated by multiplying the population attributable fraction (PAF), representing the country-level proportional reduction in population mortality that would occur if $PM_{2.5}$ exposures were reduced to the TMREL, with the total age-cause-specific background disease mortality $Mort_{background_{age}}$:

$$Mort_{PM_{2.5}} = \left[PAF = \frac{P_{fage}(RR_{age} - 1)}{P_{fage}(RR_{age})} \right] \times Mort_{background_{age}}$$

where RR_{age} is the all-age or age-specific IER estimate derived from a annual mean population-weighted $PM_{2.5}$ concentration in a given country, and P_{fage} is the fraction of the population age-group of interest. To estimate the contribution of mortality due to residential emissions, we estimate attributable mortality and averted mortality due to the removal of residential emissions as described in Section A.4.

Calculating attributable mortality for the period 2015 to 2050 requires forecasts on background disease and demographic characteristics. Following previous studies (Silva et al., 2016; Silva et al., 2017; West et al., 2013), we use forecast data in 2050 from the International Futures (IFs) socioeconomic modelling system (Hughes et al., 2011) described in Section A.5.

Understanding future changes in total attributable mortality requires knowledge of the contribution from four different factors: $PM_{2.5}$ exposure, population growth, population ageing, and rates in background disease mortality. As these factors change over time, so does their contribution to the

change in total attributable mortality. To examine factor change contributions to changes in attributable mortality between 2015 and 2050 (reference), we use a decomposition analysis described in Cohen et al., 2017, where the difference between factors incrementally is used as a measure of their contribution.

5.3 Results and Discussion

5.3.1 Impacts in the future reference scenario

Figure 5.4 shows the change in annual mean surface $PM_{2.5}$ concentrations in 2050 under reference scenario, relative to 2015 present-day. Large changes in $PM_{2.5}$ concentrations are simulated across regions, which is result of anthropogenic emission changes alone consistent with present-day natural emissions and meteorology. Distinct reductions in $PM_{2.5}$ concentrations are simulated across North America, Europe, and East Asia, with increases in concentrations simulated across Sub-Saharan Africa, North Africa and the Middle East, South Asia, and Southeast Asia.

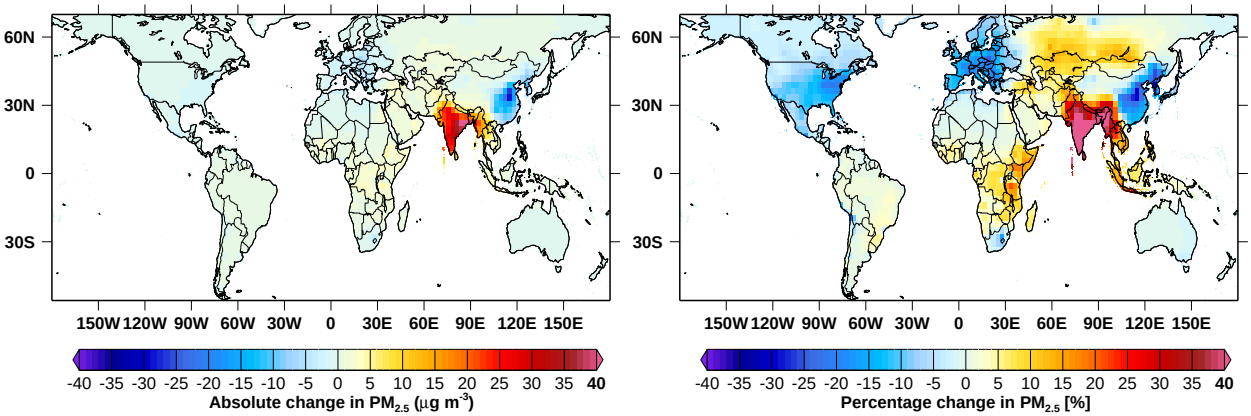

FIGURE 5.4: Absolute (left) and percentage (right) change in annual mean surface $PM_{2.5}$ concentrations in the 2050 reference scenario, relative to the present-day 2015.

Figure 5.5 shows annual mean population-weighted $PM_{2.5}$ concentrations

across different regions in 2015 and in the 2050 reference scenario, including fractional contributions from residential emissions and fractions of populations exposed to WHO annual standards (see also Table A.1). Relative to 2015, global mean population-weighted $PM_{2.5}$ concentrations increased by 12.3% in the 2050 reference scenario, exposing nearly half of the global population to levels above the WHO annual interim target 1 (IT-1) of 35 μg m^{-3} or exposing 90% to levels above the WHO annual air quality guidelines (AQG) of 10 μg m^{-3}. Global increase in mean population-weighted $PM_{2.5}$ concentrations are largely driven by the substantial increases across populated South Asia (39.7%), despite reductions across North America (13.6%), Western and Central Europe (13% and 18.5%, respectively), and East Asia (18.7%). Small to modest increases in mean population-weighted $PM_{2.5}$ concentrations were also simulated in many other regions, notably across Central Asia (9.5%) and Southeast Asia (15.5%), with smaller increases estimated across North Africa and Middle East (4%) and regions of Sub-Saharan Africa.

The considerable increases in the $PM_{2.5}$ concentrations simulated across South Asia were dominated by sulfate PM (not shown), largely due to increases in SO_2 emissions associated with growth in the power generation and industrial sectors. In the 2050 reference scenario, 91.3% of South Asian population are exposed to ambient $PM_{2.5}$ levels above the WHO IT-1 standard, the largest population exposure fraction of any region. Despite a 10 μg m^{-3} reduction in mean population-weighted $PM_{2.5}$ concentrations in the 2050 reference scenario, relative to 2015, 79.3% of the population across East Asia are also exposed to unhealthy levels above the WHO IT-1 standard, presenting the second largest population exposure fraction of any region. In contrast, high-income regions have the lowest population exposure fractions to WHO standards in 2050, with typically less than half of their populations exposed to above the AQG and virtually zero exposed to above the IT-1.

Reflecting both changes in residential emissions and other anthropogenic

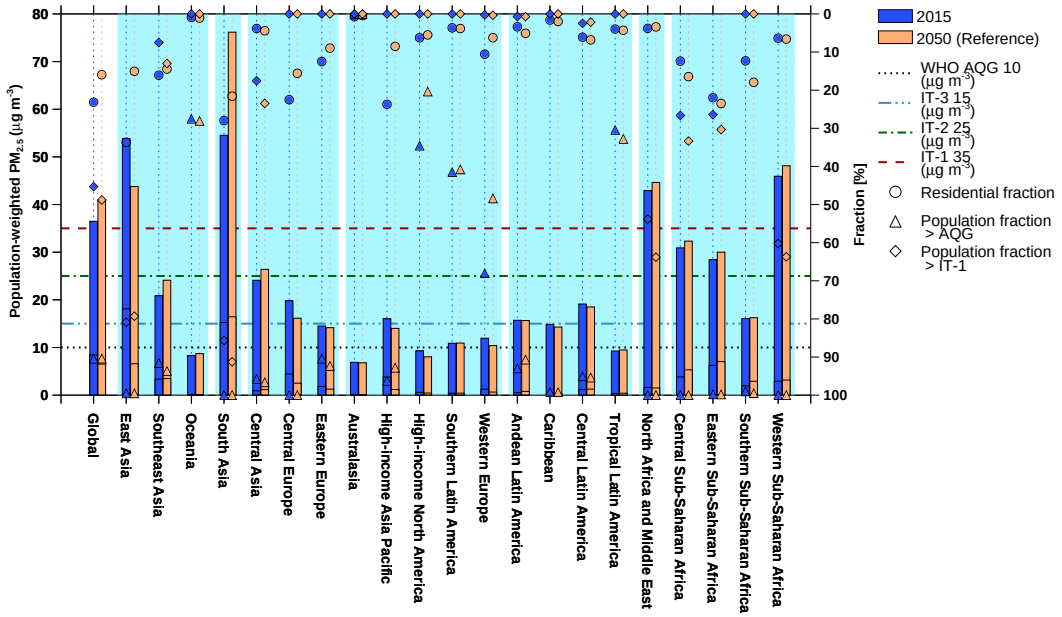

FIGURE 5.5: Annual mean population-weighted $PM_{2.5}$ concentrations in 2015 and the 2050 reference scenario per sub region (bars). Horizontal lines in bars represent the absolute population-weighted $PM_{2.5}$ concentrations due to residential combustion emissions (left axis). Also shown is the fraction or relative contribution of residential emissions to population-weighted $PM_{2.5}$ concentrations, and fraction of the population in each region exposed to $PM_{2.5}$ concentration levels above the WHO annual mean standards including the air quality guideline (AQG) (10 µg m^{-3}) and interim target 1 (IT-1) (35 µg m^{-3}) (right axis).

emission sources, the absolute and relative contribution of residential emissions to $PM_{2.5}$ concentrations also changed regionally in 2050 under the reference scenario (see Figure 5.5 and Figure A.8). Globally, absolute and relative residential contribution to mean population-weighted $PM_{2.5}$ concentrations decreased from 8.5 µ g m^{-3} to 6.5 µ g m^{-3} and 23% to 16% respectively from 2015 to 2050. Absolute and relative contributions also decreased in many other regions, such as in East Asia, where controls on residential sources largely contributed to a 63.6% absolute and 18.6 percentage point relative reduction in residential contribution. In contrast, residential contribution to $PM_{2.5}$ concentrations increased across South Asia and Sub-Saharan Africa, where modest increases in residential emissions led to absolute and relative increases in Sub-Saharan Africa, but only absolute increases in South Asia, due to growth in other anthropogenic emissions (see also Figure A.8).

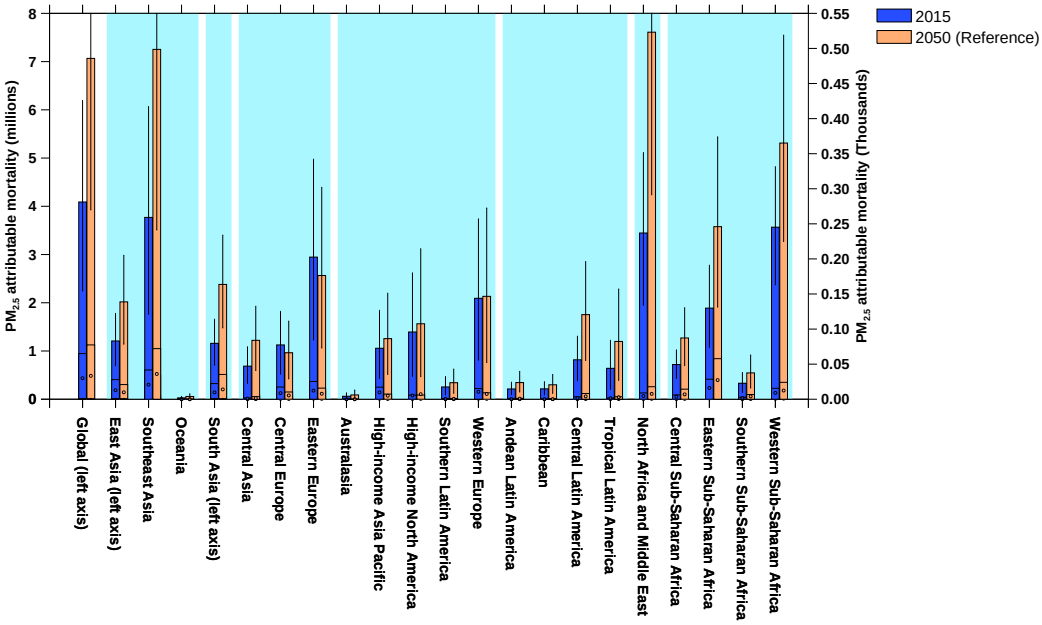

FIGURE 5.6: Mortality attributable (millions) to long-term ambient $PM_{2.5}$ exposure in 2015 and 2050 reference per sub region (bars). Horizontal lines in bars represent mortality attributable to residential emissions (attribution method), while small circles in bars represent averted mortality due to the removal of residential emissions (subtraction method) (see Section A.4). Note that the left axis is used for global, East Asia and South Asia, while the right axis is for all other regions.

Figure 5.6 shows total mortality attributable to long-term ambient $PM_{2.5}$ exposure in 2015 and the 2050 reference scenario, including mortality due to residential emissions. Globally, mortality is estimated to increase by 72.8% to 7.1 [3.9-10.7] million deaths in 2050, with East Asia and South Asia contributing 63% (up 4.8 percentage points), representing 2 [1.1-3.0] and 2.4 [1.5-3.4] million deaths, respectively. Mortality is estimated to increase in most regions in 2050, even in regions where $PM_{2.5}$ concentrations have declined, such as across East Asia. In such cases, we find that while changes in $PM_{2.5}$ exposure contribute to changes in mortality, demographic transitions of population growth and ageing dominate the magnitude in the overall mortality change among regions (Figure A.9), which is consistent with previous studies (Cohen et al., 2017; Wang et al., 2017; Butt et al., 2017; GBD MAPS Working Group, 2016; GBD MAPS Working Group, 2018). For example, 2050 mortality increases across East Asia are driven exclusively by population ageing,

despite declining $PM_{2.5}$, total population, and background disease. Similarly, population growth and ageing increased mortality across high-income North America despite declining $PM_{2.5}$ concentrations. We find that population ageing tends to be more important in high and middle-income regions, whereas population growth is more important among low-income regions (e.g., Sub-Saharan Africa) as a result of high birth and death rates (Figure A.9).

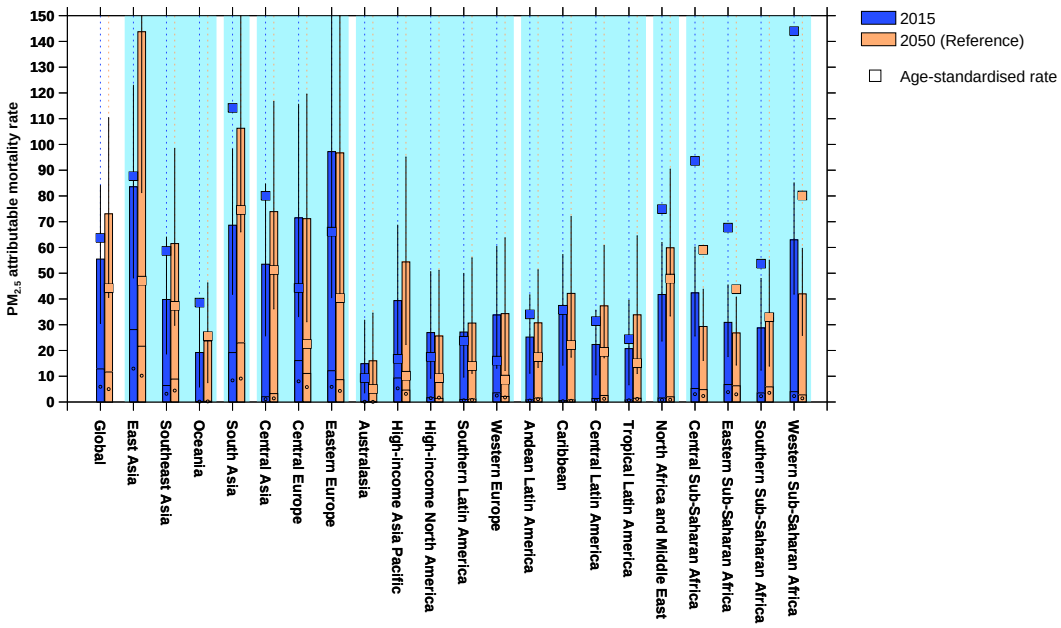

FIGURE 5.7: Attributable mortality rates (deaths per 10^5) due to long-term ambient $PM_{2.5}$ exposure in 2015 and 2050. Bars show per capita (e.g., crude) mortality rates while squares show age-standardised mortality rates. Horizontal lines in bars represent mortality attributable to residential emissions (attribution method), while small circles in bars represent averted mortality due to the removal residential emissions (subtraction method) (see Section A.4).

Unlike changes in total mortality, attributable per capita (e.g., crude) mortality rates (deaths per 10^5) adjust for population size, while age-standardised mortality rates also adjust for age profiles allowing comparisons across regions with different population structures (Figure 5.7). Relative to 2015, global attributable per capita and age-standardised mortality rates increase and decrease respectively in 2050. Global and regional declines in age-standardised mortality rates reflect declines in background disease rates (Figure A.6), with

the highest attributable rates found across regions with appreciably high ambient $PM_{2.5}$ and high background disease rates (e.g., Sub-Saharan Africa and South Asia) (Figure 5.7). In contrast, global per capita rates increase by 31.6% in 2050, and largely dominated by changes in background COPD mortality, whereas declines in background LRI dominated attributable per capita mortality rate reductions across Sub-Saharan African regions (Figure A.10).

The contribution of mortality from residential emissions are also shown in Figures 5.6 and 5.7. Globally, mortality attributable to residential emissions increase in the 2050 reference scenario by 20% to 1.1 [0.6-1.7] million deaths and 7 [3.9-10.6] age-standardised death per 10^5 (attribution method), relative to 2015. Similarly, averted mortality from the complete removal of residential emissions increases in 2050 by 11% to 0.49 [0.4-0.6] million deaths and 3 [2.5-3.6] age-standardised deaths per 10^5 (subtraction method), relative to emission removal in 2015. Attributable residential mortality is estimated be greater than the mortality averted from residential emission removal in 2050, simply because of non-linear IER effects influencing their methods of estimation (Section A.4).

Assuming residential attributable mortality (attribution method, as recommended by the GBD in the context of the policy making community), sizeable residential mortalities are located across regions with appreciatively large attributable mortality in 2050, such in South Asia (0.5 [0.3-0.7] million deaths and 16.1 [10-23] age-standardised deaths per 10^5) and East Asia (0.3 [0.2-0.5] million deaths and 7.1 [4-10.5] age-standardised deaths per 10^5). Relative to 2015, residential attributable mortality increased across South Asia by 59% in 2050, owing to increasing residential emissions and large mortality burdens. In contrast, East Asia saw an estimated 25.2% decline in residential attributable mortality, a result of policies targeting residential emission sources. Despite lower mortality compared to Asian regions, residential attributable mortality increased across Sub-Saharan African regions in 2050, with residential age-standardised mortality rates comparable to those in Asian regions

(e.g., 10.3 [5.4-15.8] deaths per 10^5 in Eastern Sub-Saharan Africa).

5.3.2 Benefits of the clean residential scenario

Figure 5.8 shows the estimated change in annual mean $PM_{2.5}$ concentrations in 2050 under the clean residential scenario, where relative to the 2050 reference scenario, mean $PM_{2.5}$ concentrations decrease in all regions. Notable reductions in $PM_{2.5}$ concentrations of up to 35% are estimated across populated regions of South Asia and Sub-Saharan Africa where combustion of residential biomass solid fuels for cooking is common. However, if concentrations in the clean residential scenario are compared relative to the present-day 2015, increases of up to 40% are estimated across South Asia, despite reductions across most regions (Figure A.11). For South Asia, this suggests that the considerable growth in other anthropogenic emissions in the 2050 reference scenario may limit the potential of residential emission control technologies to deliver reductions in $PM_{2.5}$ concentrations from present-day levels.

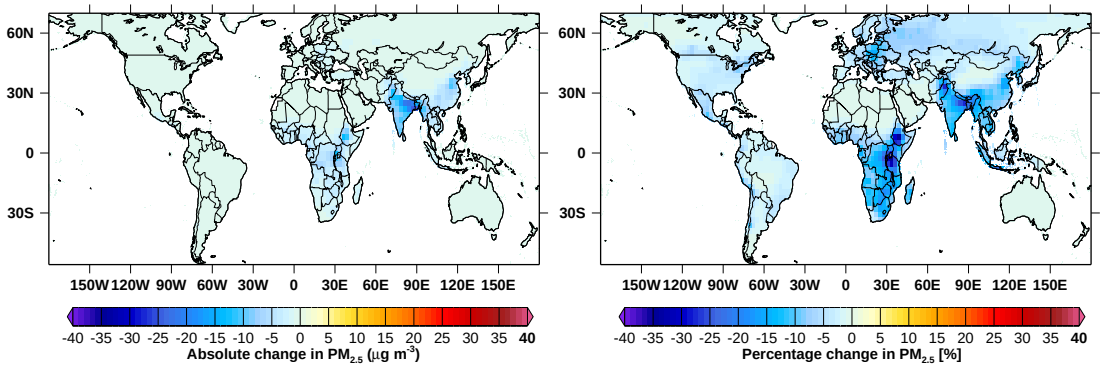

FIGURE 5.8: Absolute (left) and percentage (right) change in annual mean surface $PM_{2.5}$ concentrations in 2050 under the clean residential scenario relative to the 2050 reference scenario.

Figure 5.9 shows the avoided population-weighted $PM_{2.5}$ concentration due to the clean residential scenario in 2050, including as a proportion of the maximum possible avoided in the MTFR scenario. Relative to the reference scenario, the clean residential scenario reduces global mean population-weighted $PM_{2.5}$ concentrations by 11.9% and avoids 4.9 µg m^{-3}, accounting for 26.7% of the maximum avoided under the MTFR scenario (18.3 µg m^{-3}).

The largest avoidable concentrations are estimated across South Asia where 12.6 μg m^{-3} of mean population-weighted $PM_{2.5}$ are avoided, representing 24.8% of the maximum avoided in the MTFR (50.9 μg m^{-3} avoided). Moderately large avoidable concentrations from the clean residential scenario are also estimated across East Asia (4.3 μg m^{-3} and 23.3% of MTFR) and regions of Sub-Saharan Africa. Relative to the MTFR scenario, Sub-Saharan African regions are estimated to gain the most from clean residential combustion technologies, where moderately large avoidable concentrations (e.g., 5.6 and 4.2 μg m^{-3} in Eastern and Central Sub-Saharan Africa, respectively) typically represent 50% to 70% of the maximum avoidable concentrations in the MTFR. Despite lower avoidable concentrations, technology measures under the clean residential scenario also account for up to one third of the maximum avoidable concentrations in the MTFR across Central Europe (33.8%), Andean (35.5%) and Central (32%) Latin America.

The near-term $PM_{2.5}$ air quality benefits from technological controls in the clean residential scenario, particularly across Sub-Saharan Africa, highlights the potential interim role for technologies such as cookstoves to improve ambient air quality. Potential for improved heating stoves and boiler technologies across regions such as Europe are also highlighted. However, while these benefits may be considerable, perhaps larger than any one anthropogenic emission sector in terms of mitigation potential, larger avoidable $PM_{2.5}$ concentrations in the MTFR scenario (maximum reduction) across regions, highlights the priority for reducing all anthropogenic emissions collectively by 2050.

The clean residential scenario also reduces the global contribution of residential mean population-weighted $PM_{2.5}$ in 2050 by 11.4 percentage points to 4.5% (1.7 μg m^{-3}), but also reduces the fraction of the global population exposed to $PM_{2.5}$ levels above the WHO IT-1 (35 μg m^{-3}) (see Figure A.12). However, in some regions (e.g., South Asia, North Africa and Middle East, and Sub-Saharan Africa), fractional exposure to levels above the WHO AQG

(10 µg m^{-3}) remain at or very near 100%, under either the clean residential or MTFR scenarios (Figure A.12). In such cases, relatively high levels of $PM_{2.5}$ persist due to the failure of clean combustion technologies to eliminate all PM emissions in the face of rapid energy demand and population growth (e.g., South Asia), as well as due to contributions from natural sources, such as mineral dust (e.g., North Africa and Middle East) and wildfires (e.g., parts of Sub-Saharan Africa).

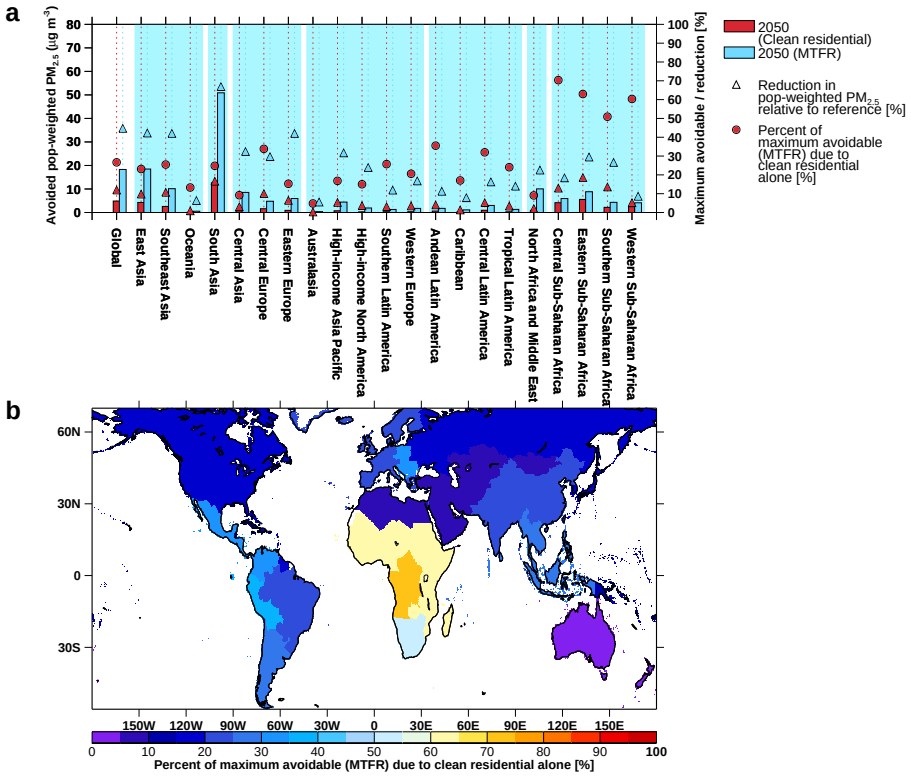

FIGURE 5.9: Avoided population-weighted $PM_{2.5}$ concentrations in 2050 due to the clean residential scenario and maximum feasible reduction (MTFR) scenario (bars, left axis), and change (reduction) in population-weighted $PM_{2.5}$ concentrations in 2050 due to both scenarios, relative to the reference scenario (right axis) **a**. Also shown is the maximum avoidable population-weighted $PM_{2.5}$ concentration potential due to the clean residential scenario (i.e., clean residential avoided / MTFR avoided) (**a** (left axis) and **b**).

Figure 5.10 shows the avoided mortality as a result of the clean residential scenario in 2050, including as a proportion of the maximum possible avoided in the MTFR scenario. Relative to the reference scenario, the clean residential scenario reduces global mortality by 5% and avoids 0.34 [0.28-0.4] million deaths, accounting for 19.4% of the maximum avoided mortality in

the MTFR (1.8 [1.4-2.1] million deaths avoided). This suggests that nearly 20% of global maximum avoided $PM_{2.5}$ mortality can be achieved by 2050 through the widespread use of clean residential combustion technologies alone. However, despite lower $PM_{2.5}$ concentrations, global attributable mortality in 2050 under either the clean residential (6.7 [3.6-10.3] million deaths) or MTFR (5.3 [2.5-8.6] million deaths) scenarios are larger than what is estimated in the present-day 2015 (4.1 [2.3-6.2] million deaths), as is the case for most regions (Figure A.13). This is largely because of demographic transitions of population growth and ageing in 2050. In fact, we find that $PM_{2.5}$ concentrations would have to be reduced to levels at or below 15 μg m^{-3} (IT-3) across all regions before global attributable mortality levels in 2050 approached that of levels in 2015 (not shown).

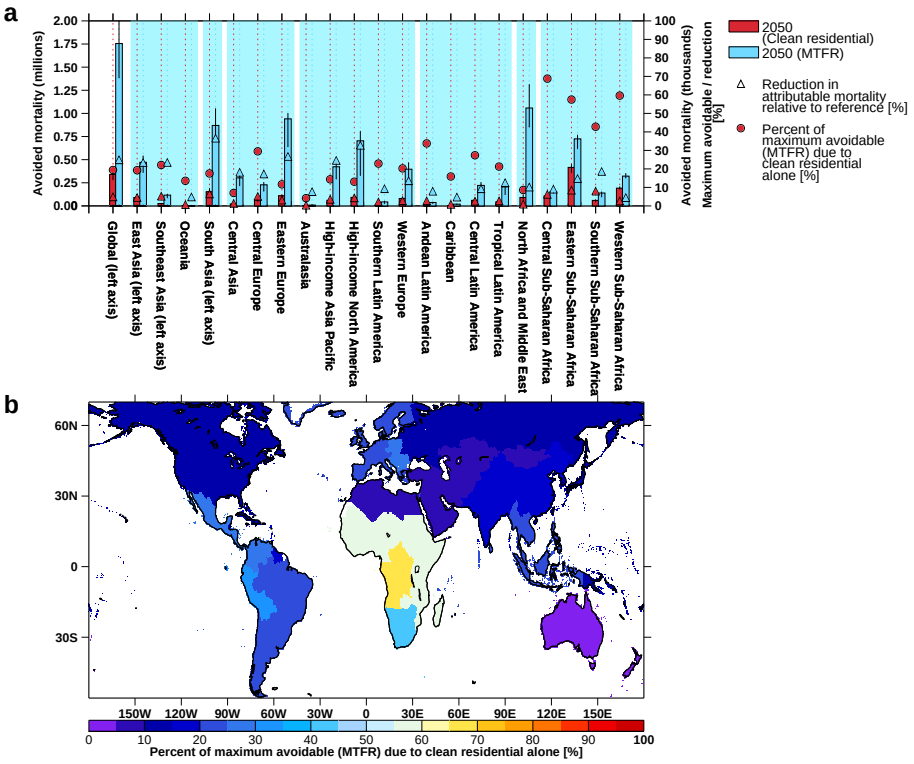

FIGURE 5.10: Avoided attributable mortality in 2050 due to clean residential scenario maximum feasible reduction (MTFR) scenario (bars, left and right axis), and change (reduction) in attributable mortality in 2050 due to both scenarios, relative to the reference scenario (left axis) **a**. Also shown is the maximum avoidable mortality potential due to the clean residential scenario (i.e., clean residential avoided / MTFR avoided) (**a** (left axis) and **b**).

The greatest numbers of avoidable mortalities as a result of the clean residential scenario are estimated across regions with appreciably large mortality burdens in the reference scenario, such as across South Asia (0.15 [0.1-0.2] million deaths, 17.5% of avoided in MTFR) and East Asia (0.1 [0.07-0.11] million deaths), both of which contribute to 17.5% and 19% of that avoided in the MTFR, respectively. Both of these regions contribute 72% to the total global mortality avoided in the clean residential scenario. Removing the influence of total population, we find that clean residential scenario avoids 3.5 [2.9-5.2] per capita deaths per 10^5 globally, with reasonably sizeable avoidable per capita mortality rates estimated across Asian, Central and Eastern European and Sub-Saharan African regions (Figure A.14). For age standardised deaths rates (deaths per 10^5), the clean residential scenario avoids 2.1 [1.8-2.5] deaths globally, with sizeable deaths rates generally limited to South Asian (4.8 [4.1-5.9] deaths) and Sub-Saharan African regions (e.g., 3.7 [3.2-4] deaths in Eastern Sub-Saharan Africa) (Figure A.14).

Similar to avoidable $PM_{2.5}$ concentrations reported in Figure 5.9, Sub-Saharan African regions are estimated to gain the most from clean residential combustion technologies, where sizeable avoided mortalities (e.g., 21,000 [18,000-22,000] deaths avoided in Eastern Sub-Saharan Africa) represent greater than half the maximum avoidable mortalities in the MTFR (e.g., 69%, 60% and 57% in Central, Western and Eastern Sub-Saharan Africa regions) (Figure 5.10 and Figure A.14). Similarly, avoided mortalities in the clean residential scenario contribute a sizeable proportion of MTFR avoided across Central and Western European regions (29.5% (3000 [2500-4000] deaths avoided) and 20.3% (4000 [3000-5000] deaths avoided), respectively), and Andean and Central Latin American regions (32% (600 [500-700] death avoided) and 27.4% (3000 [2000-3400] deaths avoided), respectively), also highlighting the potential near-term public health benefits from clean residential combustion technologies in these regions. However, as for $PM_{2.5}$ concentrations, the considerably large avoided mortalities in the MTFR scenario, particularly across South and

East Asia, also highlights a priority for reducing all anthropogenic emissions collectively.

We find that, mortality averted from the removal of residential emissions in 2050 under the reference scenario (e.g., 0.49 [0.4-0.6] million deaths using the subtraction method) is greater than mortality avoided from the clean residential scenario (e.g., 0.34 [0.28-0.4] million deaths). This is because not all residential emissions are removed in the clean residential scenario, highlighting the limitation of clean residential combustion technologies to remove all residential emissions (Figure A.13). However, reduced residential emissions substantially reduces residential mortality in the clean residential scenario (73% for attributable and 70.3% for averted mortality) relative to the reference scenario. That being said, residential mortality slightly increases under the MTFR scenario relative to the clean residential scenario, due to the larger relative contribution of residential emissions to $PM_{2.5}$ concentrations and non-linear IER effects at lower $PM_{2.5}$ concentrations in the MTFR scenario (Figure A.13).

5.3.3 Comparison to previous work

Our global estimate of attributable mortality due to ambient $PM_{2.5}$ in the present-day 2015 is very close to the 4.1 million deaths estimated by recent GBD studies (Gakidou et al., 2017; Cohen et al., 2017), with similar regional estimates. This places confidence in our mortality estimates by which to compare our scenarios in 2050. Our estimated $PM_{2.5}$ attributable to residential emissions in the present-day (attribution method) is also similar to that reported by Lelieveld et al., 2015 at 1 million deaths in 2010. However, our global averted mortality due to the removal of residential emissions (0.44 million deaths, subtraction method) is larger than that estimated by Butt et

al., 2016 (0.31 million deaths), which is likely a result of a different exposure-response relationship used in that study. Comparing to studies reporting attributable residential mortality using the IER, our present-day estimates for China (0.39 million deaths) are similar to Archer-Nicholls et al., 2016 (0.31 million deaths), but are mixed for India (0.27 million deaths) being lower compared to Conibear et al., 2018a (0.51 million deaths) but similar to GBD MAPS Working Group, 2018 (0.27 million deaths). These three studies use much higher spatial resolution models, suggesting that our model (with additional scaling) is broadly able to simulated relatively similar population exposure distributions from residential combustion. For high-income regions, such as Europe and North America, we find that our present-day residential attributable mortality of 58,000 and 6,000 deaths respectively, are similar to those estimated by Chafe et al., 2015 (61,000 and 10,000 deaths respectively), which were largely reported to be attributable to residential space heating emissions.

Comparing our estimated attributable mortalities in 2050 in the context of the reference scenario is difficult given the different assumptions controlling future emission scenarios used across studies. We used a 'semi' business-as-usual 2050 reference scenario in which current and planned environmental policies are assumed. Using the same reference scenario, Stohl et al., 2015 estimated global mortality to increase by 335% to 3.7 million deaths by 2050 (relative to present-day), which is much larger than the increase predicted here, but with a much lower overall mortality estimate. We attribute this difference to the use of a different exposure-response relationship. In that same study, Stohl et al., 2015 also used the same MTFR scenario and estimated 0.7 million avoided deaths in 2050 (relative to 2050 reference), lower to what we found (1.8 million deaths avoided), again attributed largely to the different exposure-response relationship used.

The authors are aware of only one other study that has examined ambient air quality mortality due to residential emission controls by 2050. In that

study, Lacey et al., 2017b reported 0.26 million deaths avoided in 2050 from to a linear elimination of cookstove emissions. This estimate is similar to the avoided mortality estimated reported from our clean residential scenario (0.34 [0.28-0.4] million deaths avoided), despite the differences between the scenarios (e.g., emission removal versus emission control through technology used here).

5.3.4 Implications for policy

Our findings suggest that global total mortality attributable to ambient $PM_{2.5}$ will be greater in 2050 compared to present-day 2015 levels, even when ambient $PM_{2.5}$ concentrations are reduced below present-day levels. Demographic transitions in 2050, and to some extent non-linear exposure-response (IER) relationships, are the main reason for this. This suggests that policy makers implementing air quality management strategies, particularly across many low and middle-come countries, will need to substantially reduce levels of ambient $PM_{2.5}$.

Examining avoidable mortality burdens (relative to the reference) provides important insights on how improvements in air quality through near-term emission controls can reduce attributable health burdens in 2050. In general, our analysis shows that the very considerable maximum anthropogenic ambient air quality and public health benefits in the MTFR scenario highlights the regional priority for reducing anthropogenic emissions collectively between now and 2050. However, targeting residential emissions alone through the implementation of clean combustion technologies (e.g., clean cooking and heating stoves) under the clean residential scenario can provide sizeable near-term air quality and public health benefits, contributing nearly 20% of maximum preventable attributable mortality in 2050 globally, as well as across polluted regions of South Asia (e.g., India) and East Asia (e.g., China).

This is especially true among regions where residential combustion emissions are an important component of anthropogenic $PM_{2.5}$ concentrations, such those across low and middle-income regions. In these regions, particularly across Sub-Saharan Africa, the widespread adoption of clean cookstove technologies provides up to half to two thirds of the maximum anthropogenic ambient air quality and attributable health burden benefits. In these regions, implementation of such technologies (or alternative clean fuels) can also be considered alongside the additional, presumably substantial, public health benefits associated with alleviating HAP, due to interconnection of residential combustion emissions on ambient and household environments. This suggests that mitigation efforts of ambient and household air pollution, in such regions, should be closely linked. However, since many middle and low-income regions do not have established ambient air quality management strategies (Giannadaki, Lelieveld, and Pozzer, 2016), we hope our findings can be used as a first step to help guide new policy.

Our findings also highlight air quality and health benefits across some high to middle-income regions in the clean residential scenario. In these regions, such as in Europe and high-income Latin America, penetration of pellet heating stoves potentially offsets emissions from low performing wood burning stoves or open fires, contributing up to one-third of the maximum anthropogenic avoidable benefits in some regions. While emissions from, and consumption of, solid fuels for space heating is generally predicted to decline across such regions by 2050, its contribution to poor winter time air quality, for example across Europe, has been highlighted recently. This has been blamed on a number of reasons, including climate change policies favouring 'renewable' biomass over fossil-fuels, rising fossil-fuel prices, recreational popularity, and lack of enforcement across smoke control areas (Ots et al., 2017; Denier Van Der Gon et al., 2015; Fuller et al., 2013; Chafe et al., 2015; Mitchell et al., 2017). Inaction across these regions may potentially lead to persistent or increasing air quality issues from this emission source in the

near-term. We hope our findings can help guide policy regarding the benefits of space heating emission controls.

We caution the widespread adoption of clean residential combustion technologies using solid fuels (e.g., as is the case in the clean residential scenario) only in situations where they are used to partly offset substantial PM emissions associated with combustion of traditional solid fuels, and where it is not possible to use alternative cleaner residential fuels (e.g., gas and electricity). As shown from the greater avoidable health burden from the removal of residential emissions in 2050 (0.49 [0.4-0.6] million deaths, subtraction method), compared to the clean residential scenario (0.34 [0.28-0.4] million deaths), removal of emissions through, for example the use of alternative clean fuels would provide larger public health benefits. Similarly, it is important that decision makers be made aware of potential undesirable consequences related to residential energy, especially when considering climate change mitigation co-benefits. For example, climate policy favouring a shift from light fossil fuels (e.g., gas) to 'carbon-neutral' biomass (wood) for space heating may worsen PM air pollution (e.g. Haluza et al., 2012). Alternatively, a climate compatible development agenda favouring clean cookstoves burning 'carbon-neutral' biomass solid fuel may offset air quality improvements (both ambient and HAP) from the use of light fossil-fuel alternative fuels (e.g., LPG) if they are available (Goldemberg et al., 2018; Smith and Sagar, 2014).

Other policy relevant conclusions can be drawn from our analysis. For example, we find that large population fractions exposed to ambient $PM_{2.5}$ levels above WHO AQG and IT-3 standards under both the clean residential and MTFR scenarios persist across some regions (e.g., Sub-Saharan Africa). The contribution of wildfires may be partly responsible for this, suggesting that reductions in open burning will likely complement air quality and health improvements, as has been shown previously (e.g. Reddington et al., 2015).

5.3.5 Additional uncertainties and sensitivities

There are many limitations and sources of uncertainties that are beyond the scope of this study to address in full. Common sources of uncertainty regarding low model bias in simulated $PM_{2.5}$ include missing or underrepresented model processes (e.g., deposition rates), missing PM components (e.g. nitrite and anthropogenic SOA), relatively coarse spatial resolution, as well as uncertainties in emissions inventories.

Nitrate is an important aerosol component that is missing in the model, which may be partly contribute to the overall low model bias. Low model bias could also be partly explained by the fact that TOMCAT also does not account for SOA formation from anthropogenic sources, which could be important for residential combustion as this source includes significant SOA precursor VOCs (Bruns et al., 2016; Ciarelli et al., 2017). Computational constraints of multi-year, multi-scenario global simulations also limit us to a relatively coarse model spatial resolution. We report health impacts from nation-level population-weighted $PM_{2.5}$ concentrations calculated at the original model resolution of $2.8^\circ \times 2.8^\circ$, with additional national scaling using the satellite-derived DIMAQ averaged to $2.8^\circ \times 2.8^\circ$ (see Section A.3). However, noting the uncertainty in $PM_{2.5}$ exposure distribution at coarse spatial resolutions of a global model, we conducted a sensitivity where the satellite-derived DIMAQ was used to downscale TOMCAT simulated $PM_{2.5}$ from $2.8^\circ \times 2.8^\circ$ to $0.1^\circ \times 0.1^\circ$ following a widely used approach (Lacey et al., 2017b; Chowdhury, Dey, and Smith, 2018; GBD MAPS Working Group, 2016; GBD MAPS Working Group, 2018; Archer-Nicholls et al., 2016; Weagle et al., 2018) (see Section A.3). We found that while mean population-weighted $PM_{2.5}$ concentrations were greater across some regions under the higher resolution downscaled concentrations (e.g., South Asia), due to averaging effects in the coarse resolution concentrations, these same effects also slightly increased concentrations across some regions as a result of concentration redistribution to

more populated areas in the coarse resolution concentrations estimates (Figure A.15). In any case, differences in mean population-weighted $PM_{2.5}$ concentrations between resolutions differ by only up to 20%, with a small overall difference in calculated global mortality of a only a few percent (not shown). As a result, we conclude that while the downscaling approach may reproduce a slightly better representation of exposure distributions, our estimated exposure distributions at the original global model resolution (with additional national scaling) does not lead to very large differences in estimated mortality, and thus does not change the overall study conclusions.

Understanding how changes in $PM_{2.5}$ concentrations will unfold in the context of a future 2050 reference scenario is uncertain. We used a reference scenario employing energy projections based under the assumption that pollutants are limited by the full implementation and enforcement of current and planned national environmental legislations to 2050. While this scenario can be interpreted as a business-as-usual scenario, it may in fact, be optimistic given that it does not assume failure or delays in planned enforcement (Stohl et al., 2015). However, we note that future anthropogenic emission changes will be a result of complex interactions across different variables, including socio-economic development, technological change, improved efficiency, environment and health policies directed at pollution control (e.g. Rao et al., 2017). Thus, the reference scenario used here, is one on many possible emission pathways.

Climate change can also affect future changes in $PM_{2.5}$ concentrations through numerous pathways, such as changes in meteorology (e.g. precipitation, stagnation events, ventilation, dilution, humidity, clouds etc.), temperature, and natural emissions (Von Schneidemesser et al., 2015; Fiore, Naik, and Leibensperger, 2015; Jacob and Winner, 2009), all of which are not accounted for under our 2050 scenarios. However, while there is general agreement among climate models for an increase in ambient $PM_{2.5}$ by 2050 as a result of climate change (Silva et al., 2017; Allen, Landuyt, and Rumbold, 2016),

changes in concentrations will most likely be dominated by future changes in anthropogenic emissions (e.g. West et al., 2013). Changes in natural emissions as a result of climate change, including of that of wildfire emissions (e.g. Spracklen et al., 2009), are also not accounted for under our 2050 scenarios.

Specific uncertainties related to the 2050 clean residential scenario, include the use of emissions factors (e.g., for clean cookstoves) based on a mixture of laboratory and field measurements. However, laboratory emission factors are often lower than reported in field studies (Wathore, Mortimer, and Grieshop, 2017; Roden et al., 2009; Sambandam et al., 2015; Lozier et al., 2016; Aung et al., 2016; Grieshop et al., 2017), suggesting that emission reductions estimated in this scenario may be an upper limit in some cases. Additionally, the clean residential scenario is based on the assumption that clean combustion technologies are widely implemented, adopted and completely displace traditional combustion of solid fuels. However, evidence from cookstove intervention studies conducted across low income countries, report modest adoption and user rates, as well as 'stove stacking', where intervention clean stoves fail to replace traditional stoves, potentially offsetting air quality and health benefits (Clark et al., 2017; Pillarisetti et al., 2014; Lozier et al., 2016). These undesirable outcomes are caused by interaction of multiple implementation barriers, including the failure of intervention stoves to meet user needs and preferences, supply chain distribution challenges, lack of monitoring, training and maintenance, and financial constraints (Rehfuess et al., 2014; Lewis and Pattanayak, 2012), all of which are not accounted for under our residential scenario. Thus, our estimated near-term benefits in the clean residential scenario represent a best case scenario, where solutions to critical implementation barriers are in place.

Additionally, we report $PM_{2.5}$ and mortality impacts at the national level but cannot account for transboundary contributions from non-national sources. Such information is important for national or sub-national authorities to help

implement sound air quality management strategies. As a result, our analysis could be greatly improved under a receptor or adjoint modelling approach (Lacey et al., 2017b; Lee et al., 2015).

We note uncertainties in the shape of the IER, and whether it is appropriate to apply such functions to all global populations under an additional assumption of treating all $PM_{2.5}$ components as equally toxic, regardless of composition and source. We use the IER because of its extensive use over the past few years, by which to compare to other studies. A leading assumption underpinning the IER is the use of disease risks from other combustion sources (e.g., active and passive tobacco smoking) to partly determine the shape of the exposure-response relationship at high $PM_{2.5}$ exposure distributions, a direct consequence of the limited number of ambient air pollution cohort studies in polluted regions. However, using a newly available exposure-response relationship based entirely on ambient air pollution cohort studies, including evidence from a cohort across polluted areas of China (Burnett et al., 2018), we find that mortality burdens are increased quite substantially (see Section A.6 and Figure A.15). For example, under this alternative relationship, global attributable mortality in 2015 and the 2050 reference scenario are nearly 100% greater than reported here using the IER (7.9 [6.6-9.2] and 15.4 [12.8-17.8] million deaths, respectively), with the clean residential scenario avoiding 0.52 million more deaths in 2050 (0.86 [0.73-1] million deaths avoided). This highlights large sensitivity to the use of different relationships. However, while the health burden estimates are greater using this alternative relationship, they do not change the overall message of our findings using the IER, but instead highlight the uncertainty and fast pace of scientific understanding regarding the shape of the exposure-response from ambient $PM_{2.5}$ exposure.

5.4 Conclusions

We used the TOMCAT global chemistry-transport model coupled to an aerosol model to examine near-term changes in ambient $PM_{2.5}$ concentrations and associated health burden impacts by 2050. We found that simulated $PM_{2.5}$ concentrations typically underestimated measurements at surface locations in the present-day 2015, particularly across China and India. However, this low model bias was reduced after scaling concentrations using a separate satellite-derived $PM_{2.5}$ dataset.

Under a 2050 reference scenario employing energy projections based under the assumption that pollutants are limited by the full implementation and enforcement of current and planned environmental legislations, we found that global annual mean population-weighted $PM_{2.5}$ concentrations would increase by 12.3% in 2050, driven largely be increases across South Asia and Sub-Saharan Africa, despite reductions across East Asia, Europe and North America. Additionally, we found that while the relative contribution of residential emissions to global mean population-weighted $PM_{2.5}$ concentrations decreased in 2050 by 7 percentage points, the contribution of residential emissions to population-weighted $PM_{2.5}$ is still expected to be considerable by 2050 at 16%. Global mortality attributable to ambient $PM_{2.5}$ exposure is also predicted to increase by 72.8% to 7.1 [3.9-10.7] million deaths in 2050 under the reference scenario, a result of regional changes in $PM_{2.5}$ concentrations, demographic transitions of population growth and ageing. Demographic transitions overwhelming contributed to increases in attributable mortality by 2050 even in regions where ambient $PM_{2.5}$ concentrations have declined, such across East Asia. Additionally, we found that global attributable mortality from residential emissions increased in 2050 by 20% to 1.1 [0.6-1.7] million deaths, representing 0.49 [0.4-0.6] million deaths averted if residential emissions are removed by 2050.

We examined an alternative scenario in 2050 based on the reference scenario,

but instead assuming the widespread implementation and adoption of best available clean combustion technologies in the residential emission sector, including the use of clean cooking and heating stoves. This clean residential scenario was then compared to a maximum possible anthropogenic reduction scenario, where best available emission control technologies were installed in all anthropogenic emission sectors by 2050 (maximum technological feasible reduction, MTFR scenario). By comparing both the clean residential and MTFR scenarios, we identified the relative importance of near-term clean residential emission controls for improving regional ambient air quality and associated public healths by 2050.

In general, we found that the very large avoidable ambient $PM_{2.5}$ and attributable mortality in 2050 under the MTFR scenario (relative to reference) highlighted the regional priority for reducing all anthropogenic emissions collectively. However, targeting residential emissions alone through the clean residential scenario can provide large near-term air quality and public health benefits, especially in regions where residential emissions are important for ambient $PM_{2.5}$ concentrations. Regions of Sub-Saharan Africa are expected to benefit the most, where half to two thirds of the maximum anthropogenic avoidable $PM_{2.5}$ and mortality in the MTFR scenario can be achieved by clean combustion technology measures under the clean residential scenario alone. Clean residential combustion technologies are also found to be important across other regions, including Europe and Latin America, where up to one third of the avoidable $PM_{2.5}$ and mortality benefits in the MTFR are achieved. Globally, the clean residential scenario avoids 0.34 [0.28-0.4] million deaths in 2050 (relative to reference), suggesting that nearly 20% of maximum global avoidable mortality (e.g., in MTFR) can be achieved through clean residential combustion technologies. However, exploring new developments in the $PM_{2.5}$ health exposure-response relationship, we found that the global avoidable mortality under the clean residential scenario could be nearly 100% larger. We hope that our findings can be used to help inform

ambient clean air quality management strategies, particularly among low-income regions (e.g., Sub-Saharan Africa) where legislation in this area are lacking and residential emissions are important.

Chapter 6

Discussion and Conclusions

The last 50 years have seen considerable regional changes in anthropogenic emissions. declining emissions across high-income regions due to the implementation of air quality and emission control regulations have coincided with a large rise in economic-related emissions across parts of Asia. This has resulted in regional changes in ambient $PM_{2.5}$ concentrations and associated public health impacts, the understanding of which is important for future air quality management strategies. Residential combustion of solid fuels for heating and cooking also contributes a considerable amount to the global burden of primary aerosol emissions in the present-day, especially across many low and middle-income countries. Understanding this source contribution to ambient air quality, and its associated public health impacts is important for understanding the potential of emission mitigation measures. Similarly, it is also important to understand the air quality and health potential of emission mitigation measures across the residential sector in the context of near-term changes in other anthropogenic emissions.

Using a global composition-climate model (CCM) and a global chemistry-transport model (CTM) coupled (or uncoupled) to a global aerosol model, this thesis examined the impacts of changing anthropogenic emissions on ambient air quality and associated health impacts covering the past, present and future. Additionally, it focused on the role of the residential emission

sector to understand air quality and health impacts in the present-day and its potential role for reducing impacts into the near-term future.

The following sections provide a summary of the results found in this thesis and refer to the aims presented in Chapter 1.

6.1 Chapter 3: Global and regional trends in particulate air pollution and attributable health burden over the past 50 years

The HadGEM3-UKCA CCM, together with exposure-response relationships, was used to simulate global and regional changes in ambient $PM_{2.5}$ concentrations and associated health burden impacts over the period 1960 to 2009. Simulated $PM_{2.5}$ concentrations were also compared to available long-term observations and satellite-derived estimates of $PM_{2.5}$ to evaluate model performance. A summary of the findings from this study in relation to the posed research questions is reported below:

(a) **Can simulated changes in regional $PM_{2.5}$ concentrations reproduce long-term observed changes?** The model is generally well able to simulate observed regional changes in annual mean ambient $PM_{2.5}$ concentrations at long-term measurement locations in the United States (IMPROVE, Interagency Monitoring of Protected Visual Environments) and Europe (EMEP, European Monitoring and Evaluation Programme). The baseline model simulated a 20% and 23% reduction in annual mean ambient $PM_{2.5}$ concentrations at both IMPROVE (1992 to 2009) and EMEP (1999 to 2009) locations respectively, which was similar to the observed 25% and 14% reduction, respectively. However, the baseline model consistently underestimated annual mean $PM_{2.5}$ concentrations across both IMPROVE (NMBF = -0.54) and EMEP (NMBF = -1.2) locations. Scaling the baseline model to the median distribution of a perturbed parameter

ensemble (PPE) improved the comparison at IMPROVE (NMBF = 0.11) and EMEP (NMBF = -0.47) locations, with the PPE 5th and 95th percentile incremented baseline range bracketing the observations. Comparing annual mean population-weighted $PM_{2.5}$ concentrations from the baseline (plus median PPE) to satellite-derived $PM_{2.5}$ estimates over the period 1990 to 2009, showed that the model was broadly able to simulate changes across the US and Europe, but with smaller changes simulated at the global level and across polluted regions of China and India. However, the baseline (plus median PPE) underestimated the magnitude in satellite-derived population-weighted $PM_{2.5}$ concentrations in all regions, with the PPE 5th and 95th percentile incremented baseline range bracketing the satellite-derived estimates.

(b) **What are main sources of uncertainty in the model that are influencing the comparison to long-term measurements?** There are a number of possible reasons for the low observed bias in the baseline model. These included complex interaction of uncertain model processes, missing aerosol components (e.g., nitrite and anthropogenic SOA), and uncertainties in the mass flux in emission inventories, and water content. Attribution of individual uncertain model parameters to the variance in the PPE identified the contribution of key uncertain parameters in the model. These included large uncertainties associated with dry deposition of accumulation mode particles in all regions, and the mass flux of residential combustion carbonaceous emissions, particularly across Asian regions. The relatively coarse spatial resolution of the model was also examined as a possible large contributor to the low model bias. However, averaging the satellite-derived $PM_{2.5}$ estimates (assumed to be 'semi-observational') to the same spatial resolution of the model, resulted in less than expected reductions in regional population-weighted $PM_{2.5}$ concentrations, suggesting that other uncertain or missing processes (described above) may be playing dominant roles.

(c) **How have global and regional simulated $PM_{2.5}$ concentrations changed over the period 1960 to 2009?** Over the period 1960 to 2009, the model predicted that global population-weighted $PM_{2.5}$ concentrations increased by 37.5%. This global increase was dominated by the regional increase across China (52.7%) and India (69.8%), despite declines in concentrations across the US (55.3%) and European Union (EU) (38%). Growth in ambient population-weighted $PM_{2.5}$ concentrations across China and India were found to be a result of anthropogenic emission rises related to economic growth at the expense of environmental and public health degradation, whereas the implementation of air quality regulation and emission controls resulted in an overall reduction in population-weighted $PM_{2.5}$ concentrations across the US and EU.

(d) **How has the global and regional burden of disease attributable to long-term exposure to ambient $PM_{2.5}$ changed over the period 1960 to 2009?** Using integrated exposure-response (IER) relationships, global deaths attributable to long-term ambient $PM_{2.5}$ exposure increased by 89% to 124% over the period 1960 to 2009, suggesting that the global attributable burden of disease is now larger in the present-day than at any other point since 1960. This global mortality increase was found to be dominated by large increases across China (194.5 to 238%) and India (166.7% to 194%), despite declines across the US (47.9% to 58.9%) and EU (65.7% to 71.9%). In contrast, global attributable per capita mortality rates (deaths per 10^5) decrease slightly by about 1% over the same period, which was due to reduce overall background disease rates and improved air quality across North American and European regions.

(e) **What factors have dominated the contribution to the change in total $PM_{2.5}$ mortality over the period 1960 to 2009?** Changes in total attributable mortality were found to be a result of changes in contributing factors. Over the period 1960 to 2006, it was estimated that population

growth and ageing, and to a lesser extent increasing $PM_{2.5}$ concentrations, dominated the increases in mortality globally, driven mostly by changes across China and India. In contrast, regional reductions in ambient $PM_{2.5}$, and to a lesser extent reductions in background disease rates, were the dominant contributors to reduced mortality across the US and EU.

(f) **How can trends in historical $PM_{2.5}$ concentrations help inform policy makers about the impacts of future changes in $PM_{2.5}$ mortality?** The results from this study highlight the historical benefits of clean air policy in improving air quality and public health across North America and Europe. This provides evidence for the benefits of clean air policy which will be useful for policy makers in polluted low and middle-income regions. However, given the non-linear exposure-responses in highly polluted regions together with projected demographic transitions, low and middle-income countries may need to introduce very stringent ambient air pollution standards in order to replicate the declines in total attributable health burdens seen across high-income regions.

6.2 Chapter 4: The impact of residential combustion emissions on atmospheric aerosol, human health, and climate

The TOMCAT-GLOMAP configuration with prescribed offline oxidants was used to make an integrated assessment of the impact of residential combustion emissions in the present-day (or near present-day year 2000) on atmospheric aerosol, radiative effect, and human health. The use of exposure-response relationships and an offline radiative transfer model were used to estimate the impact of residential-derived aerosol on the radiative effect and human health, respectively. In order to evaluate the model, simulated aerosol mass and number concentrations were compared to observations at locations

where residential combustion was thought to be important. Sensitivity experiments examining the uncertainty in emission mass flux, seasonal emission variability, carbonaceous composition, and emitted primary carbonaceous aerosol size distributions were conducted to test simulated uncertainty on observational comparison, radiative effect and human health. A summary of the findings from this study in relation to the posed research questions is reported below:

(a) **Can a global model simulate observed aerosol mass and number concentrations at locations where influence of residential combustion on atmospheric aerosol are thought to be important?** The baseline model simulation was found to underestimate observed black carbon (BC), organic carbon (OC) and $PM_{2.5}$ mass concentrations at measurement locations across South Asia and East Asia, by greater than a factor of 2. Applying monthly varying emissions in the model did little to improve the low bias but did improve the simulated to observed seasonal variability in aerosol mass. The doubling of residential carbonaceous emissions did improve the overall model agreement with observations, but the low bias in simulated mass still persisted, particularly for organic aerosol. This low bias was due possibly to uncertainties in emission inventories and/or treatment of organic aerosol such as missing secondary organic aerosol (SOA) from anthropogenic sources. In agreement with other studies, the sensitivity simulations indicated that residential emissions may be underestimated in the model. A combination of uncertainties in model processes, missing aerosol mass from anthropogenic SOA and nitrate, relatively coarse model spatial resolution, and emission inventory uncertainties, were all postulated as potential contributing factors to low model bias. Observed particle number concentrations were generally better predicted by the model compare to

aerosol mass and were typically within a factor of 2 at the limited number of locations where observations were available. Simulated particle number concentrations were estimated to be very sensitive to emitted particle size range of primary residential carbonaceous emissions, which have a large uncertainty. Emitting residential carbonaceous particles at the small end of size ranges substantially overestimated the observed particle number concentrations suggesting that this was an unrealistic assumption.

(b) **What are the global regional contributions of residential combustion emissions to atmospheric aerosol mass in the near present-day?** Residential combustion emissions were estimated to contribute substantially to regional annual mean surface $PM_{2.5}$ concentrations. The largest relative contributions (15 to $>$ 40 %) to mean $PM_{2.5}$ concentrations were estimated across Eastern Europe (including parts of the Russian Federation), parts of East Africa, South Asia, and East Asia. In these regions, the residential emission contribution to annual mean simulated BC and particulate organic matter (POM) concentrations can reach up to 60%. In the baseline model, residential combustion emissions were estimated to contribute to 22% of the total global BC burden and 12% of the global POM burden. When residential carbonaceous emissions were doubled, residential emissions contributed to 33% and 32% of the total global BC and POM burden, respectively.

(c) **What is the near present-day global and regional burden of disease attributable residential combustion emissions on ambient $PM_{2.5}$ concentrations?** In the baseline model simulation, it was estimated that a total of 315,000 (132,000-508,000) deaths could have been averted in the year 2000 if $PM_{2.5}$ concentrations associated with residential combustion emissions were removed. This averted mortality burden increased by 64% to 516,600 (192,000-827,000) if residential $PM_{2.5}$ concentrations were removed based on the simulation where residential emission were

doubled. It was found that estimated averted mortalities were greatest across regions with large residential emissions and high population densities, including East Asia, South Asia, Eastern Europe, and the Russian Federation, but with half of total averted mortality occurring in just China and India. Estimated health impacts are sensitive to the exposure-response relationship used, suggesting that the magnitude of the health impact from residential combustion emissions may vary depending on the relationship used, but is likely to be considerable.

(d) **What is the near present-day direct and first indirect radiative effect of residential combustion aerosol on the Earth's radiation budget?** Using an offline radiative transfer model, it was found that residential combustion emissions exerted an uncertain global annual mean direct radiative effect (DRE) of between -66 and $+85$ mW m^{-2} across all simulations, with a best estimate of between -66 and $+21$ mW m^{-2} after discounting the unrealistic simulation emitting very small carbonaceous particles. Simulated DRE was estimated to be sensitive to the amount and ratio of residential BC, POM, and SO_2, with the carbonaceous component of residential-derived aerosol exerting an overall net positive DRE in the simulations, offset by cooling from SO_2 residential emissions. It was found that residential combustion emissions exerted a negative but uncertain global annual mean first aerosol indirect effect (AIE) of between -502 and -16 mW m^{-2} across all simulations, with a best estimated range of -52 and -16 mW m^{-2} after discounting the unrealistic simulation emitting very small residential carbonaceous particles. Uncertainty in the emitted primary carbonaceous particle size range was found to be the largest contributor of uncertainly to simulated AIE, due to residential combustion emissions. Many limitations exist in the methods used to estimate the radiative effect. These include the use of an offline radiative transfer model that cannot examine other

climate effects and interactions, as well as simplistic assumptions regarding the optical properties of POM and optical mixing states of BC.

(e) **What might the uncertainties in residential combustion emission mass flux and emitted size distributions mean for quantifying residential impacts on air quality, human health and radiative effect?** This study highlighted that the removal of residential combustion emissions would substantially improve particulate matter air quality and human health across many regions, even when considering the uncertainties between the different model simulations explored. However, residential combustion emissions exert an uncertain radiative effect, with a DRE spanning both positive and negative signs. Better characterisation of residential emission mass flux, chemical composition, and carbonaceous size distributions, together with a more detailed optical treatment of aerosol mixing states within a climate composition model, are needed to assess the full climate impacts due to residential emissions.

6.3 Chapter 5: Near-term global and regional air quality and health benefits due to widespread adoption of clean residential combustion technologies

The TOMCAT-GLOMAP configuration with coupled chemistry was used to simulate changes in ambient $PM_{2.5}$ concentrations and associated public health burden impacts between 2015 and 2050. Estimated impacts in 2050 were first examined under a reference scenario using projected energy consumption data from the International Energy Agency based under an assumption of present-day current and planned environmental legislation, and secondly under a similar scenario where widespread adoption of clean residential combustion technologies (e.g., implementation of clean cooking and

heating stoves) had taken place. An additional 2050 scenario was also examined impacts after available clean combustion technologies were widely adopted in all anthropogenic sectors. A summary of the findings from this study in relation to the posed research questions is reported below:

(a) **To what extent can a global chemical-transport model reproduce annual mean observed $PM_{2.5}$ concentrations across multiple global regions?** In general, the model underestimated annual mean ambient $PM_{2.5}$ concentration when compared to regional measurements in the present-day (year 2015). Significant low biases were predicted across measurement locations in China and India by a factor 2 and 3, respectively. However, many of the measurements used for the evaluation were taken from urban or semi-urban locations, which may largely explain the low model bias due to the relatively coarse spatial resolution of the model. To account for the low model bias, simulated $PM_{2.5}$ were scaled nationally using a satellite-derived 'semi-observational' $PM_{2.5}$ dataset, which largely improved the model performance. The same scaling factors were then applied to the simulated $PM_{2.5}$ concentrations in the 2050 scenarios, which were then used to estimate air quality and health burden impacts.

(b) **How do annual mean ambient $PM_{2.5}$ concentrations change regionally under a reference scenario in the year 2050?** In the 2050 reference scenario, estimated reductions in annual mean $PM_{2.5}$ concentrations were simulated across North America, Europe, and East Asia, with estimated increases simulated across Sub-Saharan Africa, North Africa and the Middle East, South Asia, and Southeast Asia. Relative to 2015, global population-weighted $PM_{2.5}$ concentrations were found to increase by 12.3% under the 2050 reference scenario, which were largely driven by large increases across South Asia (39.7%), despite reductions across East Asia (18.7%). Reductions in ambient $PM_{2.5}$ concentrations across East Asia were estimated largely to be a result of current and

planned residential emission controls, whereas increases across South Asia were a result of weak regulation and emission increases in the power and industrial sectors in the face of rapid population growth and subsequent growth in energy demand.

(c) **How does the disease burden attributable to ambient $PM_{2.5}$ exposure change in the year 2050 under the reference scenario?** Relative to 2015, global mortality attributable to ambient $PM_{2.5}$ exposure was found to increase by 72.8% in 2050 under the reference scenario to 7.1 [3.9-10.7] million deaths. Mortality increases are predicted in most regions in 2050 and driven largely by demographic transitions represented by total population growth and population ageing, and to a lesser extent by regional changes in ambient $PM_{2.5}$ concentrations. Even in regions where ambient $PM_{2.5}$ concentrations are estimated to decline in 2050, demographic transitions such as population ageing result in attributable mortality increases (e.g., East Asia). $PM_{2.5}$ mortality due to residential emissions were also estimated to increase by 20% to 1.1 [0.6-1.7] million deaths, representing 0.49 [0.4-0.6] million deaths averted if residential emissions were removed in 2050.

(d) **How does the widespread adoption and sustained use of clean residential combustion technologies improve ambient $PM_{2.5}$ air quality relative to a reference scenario and a maximum anthropogenic emission reduction scenario?** Relative to the reference 2050 scenario, the widespread implementation of clean residential combustion technologies, is estimated to reduce global mean population-weighted $PM_{2.5}$ concentrations by 11.9% and avoid 4.9 $\mu g\ m^{-3}$ in 2050. The largest $PM_{2.5}$ air quality improvements are estimated across South Asia where the implementation of clean residential combustion technologies can avoid

18.3 μ g m^{-3} of mean population-weighted $PM_{2.5}$ concentrations. However, in other regions, particularly across Sub-Saharan Africa, the implementation of clean residential combustion technologies alone can contribute one half to two thirds of the maximum anthropogenic avoidable reduction in population-weighted $PM_{2.5}$ concentrations.

(e) **How does the widespread adoption and sustained use of clean residential combustion technologies improve the $PM_{2.5}$ mortality burden relative to a reference scenario and a maximum anthropogenic emission reduction scenario?** Relative to the reference 2050 scenario, the widespread implementation of clean residential combustion technologies, is estimated to reduce global attributable mortality by 5% and avoid 0.34 [0.28-0.4] million deaths in 2050, which was estimated to be nearly 20% of the maximum preventable mortality in same year. However, despite lower $PM_{2.5}$ concentrations, demographic transitions in 2050 result in greater attributable mortality in 2050 under either the clean residential and maximum reduction scenarios, relative to the present-day 2015. The largest avoidable mortalities as a result of clean residential combustion technologies were estimated across South Asia (0.15 [0.1-0.2] million deaths) and East Asia (0.1 [0.07-0.11] million deaths), with additionally relatively large age-standardised mortalities avoided across South Asia (4.8 [4.1-5.9] deaths per 10^5 people) but also across Sub-Saharan African regions (e.g., 3.7 [3.2-4] deaths per 10^5 people in Eastern Sub-Saharan Africa). However, half to two thirds of the maximum avoidable mortality across Sub-Saharan Africa in 2050 were estimated to be achievable through residential emission controls alone, representing the largest contributor to maximum preventable mortality of any region.

(f) **How can near-term scenarios of clean residential emission controls inform ambient air quality management strategies?** In general, this study highlighted the regional priority for reducing all anthropogenic

emissions collectively. However, targeting residential emissions alone through clean combustion technologies or clean fuels can provide large near-term air quality and public health benefits, especially across many low and middle-income regions where residential emissions are important to anthropogenic $PM_{2.5}$ concentrations. Since many middle and low-income regions do not have established ambient air quality management strategies, it is hoped that the findings of this study can help guide new policy designed to protect public health and the environment.

6.4 Summary and synthesis

Anthropogenic emission trends in aerosol primary and precursors during the last 50 years has resulted in considerable regional changes in ambient $PM_{2.5}$ air quality. Findings reported in Chapter 3 showed that simulated changes in ambient $PM_{2.5}$, using the HadGEM3-UKCA CCM, generally followed that of long-term regional observations highlighting pronounced declines across high-income regions of North America and Western Europe with associated growth across many low and middle-income regions, particular across Asian countries. These findings are consistent with declining emissions associated with air quality regulation and emission control technology implementation in high-income regions to that of emission growth associated with population and economic expansion at the expense of equivalent regulation and control in many low and middle-income regions over the past 50 years. Regional disease burdens attributable to ambient $PM_{2.5}$ exposure generally followed that of regional changes in ambient $PM_{2.5}$, with an estimated increase in global burden of disease of between 89% to 124% in 2009, relative to 1960. This global attributable mortality increase which was largely driven by mortality growth in Asia, the growth of which was strongly influenced by demographic transitions (i.e., population growth and ageing), highlighting the

importance of this transition when considering future near-term disease burden trends. However, more importantly, the results reported in Chapter 3 highlight the advantages of clean air policy for improving air quality and public health in North American and European regions. This provides the evidence base needed for policy makers across polluted low and middle-income regions can learn from and replicate. However, given the non-linear disease exposure-responses relationships associated with highly polluted regions (i.e., high exposure distributions) and near-term projected transitions in demography, low and middle-income countries may need to introduce very stringent ambient air pollution standards in order to replicate similar public health benefits experienced by high-income regions since the 1960s.

Although not specifically addressed in Chapter 3, much of the anthropogenic emission declines experienced across high-income regions, particularly Western Europe, were a result of declines in residential solid fuel combustion, typically coal for heating. This use and reduction in use of solid fuels, in part due to combined air quality policy, economic and energy transitions, shares some parallels with energy poverty and transitions facing many low and middle-income countries today. For example, while combustion of solid fuels are generally less important for anthropogenic emissions in high-income countries today, they remain an important fuel source across many low and middle-income regions, where 3 billion poor people still rely on such fuels (e.g., biomass and coal) to meet basic energy demands (e.g., cooking, heating and lighting). At the same time, although the global number of poor households using solid fuels has decreased over the last few decades, population growth has kept the total number of users at relatively stable levels. As a result, the residential sector remains an important anthropogenic emission source in the present-day, undoubtedly leading to large global and regional negative impacts on public health and the wider environment. For poor communities in low and middle-income, the use solid fuel clean cookstoves or

clean fuels, such as LPG, is considered one of the best ways to reduce emissions from residential solid fuel combustion, potentially leading to large public health benefits through improved household and ambient air quality, and additional climate and socio-economic co-benefits. However, until relatively recently, little was known about the overall impact of residential emissions on air quality, health and climate in the present-day. Understanding these impacts are a vita first step in identifying where clean cookstoves and fuels will have the most benefit, and was the focus of Chapter 4 of this thesis. Using the TOMCAT-GLOMAP CTM, results reported in Chapter 4 showed that residential emissions contributed substantially to regional annual mean surface $PM_{2.5}$, BC and POM concentrations in the present-day, with significant contributions across regions of Asia and Sub-Saharan Africa, as well as many Eastern European countries of the former Soviet Union. The disease burden due to the removal of residential emissions was estimated to be considerable (3.0 to 0.5 million deaths globally), highlighting the potentially large public health benefits of residential emission controls, even when considering a number of key emission uncertainties. Understanding the present-day radiative impacts due to residential emissions, however, was shown to be uncertain and sometimes of opposite sign. This uncertainty was in part due to the limitations of using a offline radiative transfer model together with uncertainties associated with residential emission mass flux, size and composition, and other uncertain model parameters, highlighting the need for more advanced modelling approaches and measurements.

The last chapter of this thesis (Chapter 5) was designed in such away that would naturally lead on from Chapters 3 and 4. In particular, it focused on understanding the possible impact of changes in anthropogenic emissions on future near-term air quality and disease burdens in 2050, with an additional focus on clean emission technologies, particularly residential clean

cookstoves, as a means of reducing impacts by 2050. Using the TOMCAT-GLOMAP CTM, Chapter 5 showed that despite ambient $PM_{2.5}$ concentrations declining many regions (apart from South Asia and to some extent Sub-Saharan Africa) under a reference scenario, the attributable global burden of disease increased by 73% in 2050 (relative to 2015). Similar to the findings reported in Chapter 3, the growth in the mortality burden was significantly influenced by demographic transitions, so much so that disease burden increases were estimated in regions where ambient $PM_{2.5}$ concentrations had declined relative to 2015 (e.g., China). This finding further highlights a real need for polluted regions to adopt stringent limits on ambient $PM_{2.5}$ in order to reduce disease burdens in the near-term. Relative to this reference scenario, the widespread implementation of clean residential combustion technologies (i.e., clean cookstove) was found to improve near-term air quality and public health benefits in 2050, especially for many low and middle-income countries, such as Sub-Saharan Africa. The adoption of clean cookstove technologies alone was found to represent one half to two thirds of the maximum preventable ambient $PM_{2.5}$ and mortality estimated across Sub-Saharan African countries in 2050. At the global level, clean residential technologies were found to represent 20% of global the preventable $PM_{2.5}$ mortality in 2050. The findings reported in Chapter 5 thus highlight the potential effectiveness of residential emission controls and technologies for improving near-term ambient air quality and public health, particularly among many low and middle-income regions, where they can also help towards alleviating many other environmental and socio-economic problems.

While the results reported in thesis represent a first step in identifying impacts and potential areas of interested for policy, the section below provides a discussion on additional work that could be undertaken to build on what is reported here. Additionally, a further discussion is also provided below on research priorities for the wider research community.

6.5 Implications for Future Work

6.5.1 Priorities relating to my research

Reducing model biases

The evaluation of the different models used in each Chapter highlight a consistent low bias, particularly when comparing to aerosol mass concentration measurements. This suggests a contribution from missing and/or uncertain model processes, aerosol components and emission sources. It is therefore important that future model developments focus on key areas of uncertainty in order to address model biases.

Nitrate is an important aerosol component missing in the model configurations used in this thesis, which may partly contribute to low simulated biases. Accounting for nitrate formation may be important for understanding historical and future aerosol changes, particularly where SO_2 emissions (and sulfate) have declined and are expected to decline in the future. For example, because the formation pathway for ammonium nitrate requires an excess of ammonia, beyond that required for sulfate formation, reductions in SO_2 emissions with constant or increasing ammonia emissions may mean that nitrate concentrations do not respond linearly to changes in NO_x emissions. Historical reductions in SO_2 emissions together with increasing agricultural-related ammonia emissions since the 1960s over North America and European regions (Hoesly et al., 2018) may have limited the effects of NO_x reductions on nitrate and increased the relative importance of nitrate PM fraction (Erisman and Schaap, 2004; Fagerli and Aas, 2008). Similarly, nitrate concentrations may not respond linearly to future declines in NO_x emissions across regions where SO_2 emissions are also declining (e.g., parts of Asia such as China), but where ammonia concentrations remain level or are predicted to increase (Bellouin et al., 2011; Hauglustaine, Balkanski, and Schulz, 2014).

The implementation of nitrate formation in atmospheric models is challenging given the volatile nature of nitrate aerosol, however its implementation and evaluation should be a priority.

Another missing aerosol component common in the model configurations used in this thesis is the representation of SOA formation beyond that of biogenic origin, which may in part explain the low bias in organic aerosol reported in Chapter 4. The quantification of SOA from biogenic and anthropogenic sources is a large source of uncertainty to the global burden of organic aerosol (Spracklen et al., 2011a; Tsigaridis et al., 2014). Additionally, the global model configurations used in this thesis treat biogenic SOA formation in a relatively simplistic way, via the oxidation of biogenic monoterpene that condense irreversibly onto existing aerosol under an assumption of zero vapour pressure. Recent developments in the representation of organic aerosol under different volatilities as part of the volatility basis set (VBS) provide a framework in which the evolution of organic aerosol can be simulated in more physically-based way (Donahue et al., 2011). However, while the implementation of VBS schemes is challenging in global models (Tsigaridis et al., 2014), its implementation and evaluation should be a priority for the future. This could be particularly important for estimating organic aerosol contribution from residential combustion as emissions from this source include significant SOA precursor VOCs that are not well characterised (e.g. Bruns et al., 2016; Ciarelli et al., 2017).

The PPE analysis reported in Chapter 3 (see Appendix A Figure S2) highlighted key uncertain model parameters responsible for uncertainties in simulated $PM_{2.5}$ concentrations in the HadGEM3-UKCA model. Because GLOMAP-mode was used in all the model configurations in this thesis, I assume that the common parameter uncertainties highlighted in the PPE for HadGEM3-UKCA also apply for TOMCAT-GLOMAP model variants used in Chapters 4 and 5. While the PPE sensitivity analysis in Chapter 3 provides a first step in identifying the parameter uncertainty space in the model, identifying high

skilled model variants with commonalities is the next step towards constraining uncertainty in model parameters (i.e., do PPE model variants capable of reproducing observations have anything in common with each other?). Since the writing (and publication) of Chapter 3, further analysis of PPEs using GLOMAP-mode simulated aerosols have been conducted to identify skilled model variants through comparison to aerosol observations. While these analyses suggest that PPE model variants can be constrained to a high degree, discounting up to 60% of model variants as implausible, the parametric range of the 'best' model variants are very wide with the same model skill arising from multiple parameter settings (Browse, 2019). Nevertheless, some important uncertain parameters have been constrained through these analyses, including dry deposition rate of accumulation mode (a large uncertainty source identified in Chapter 3), boundary layer nucleation rate, anthropogenic SO_2 emissions, sea salt emissions, biogenic VOCs emissions, and monolayers (of secondary organic and sulphate) required for a insoluble particle to be soluble (Browse, 2019; Regayre et al., 2018; Johnson et al., 2018). As a result, future model simulations including some of these constrained parameters would likely improve low simulated to observed biases.

The relatively large spatial resolution of the global models used in this thesis may also have contributed to low simulated to observed biases, particularly when evaluating against urban or semi-urban aerosol measurements such as $PM_{2.5}$. However, computational constraints needed to perform multi-year and multi-sensitivity simulations, currently limit the global models used here to relatively coarse spatial resolutions. Nevertheless, similar research questions to those examined in this thesis could be examined using nested regional simulations over a particular region of interest (e.g. Gordon et al., 2018). Such a model setup would allow for comparisons between the coarse spatial resolution of the global model to that of the regional nest, where the high spatial resolution might resolve air pollutant concentration gradients allowing for better simulated to observed comparisons.

Representing uncertainty in future impacts

Understanding how emissions will change and evolve into the future is vital for understanding the mitigation potential of certain policy measures. The air quality and health benefits as a result of the emission scenarios reported in Chapter 5 (i.e., clean residential and MTFR scenarios) were based by comparing to the baseline reference scenario in 2050. This approach for measuring the potential of the clean residential and MTFR scenarios is thus based under assumptions in the reference scenario. While the emissions in the reference scenario are based under the assumption that pollutants are limited by the full implementation and enforcement of current and planned national environmental legislation, they could be also be optimistic based on the fact that they cannot possibly predict failures and/or delays in planned enforcement. Nevertheless, future emission pathways may be more diverse, with anthropogenic emissions being controlled by complex forces governing projected changes in socio-economic development, technological change, improved efficiency, environment and health policies directed at pollution control. As such, additional simulations exploring a range of possible pathways such as those employed by the 'Shared Socio-economic Pathways' (Rao et al., 2017) would have benefited the analysis in Chapter 5.

Climate change will also likely affect air pollutant concentrations in the future. Climate change affects air pollution through numerous pathways (Von Schneidemesser et al., 2015; Fiore, Naik, and Leibensperger, 2015; Jacob and Winner, 2009), such as changes in meteorology, temperature, and natural emissions, as well as the frequency of wildfire events. In the case of $PM_{2.5}$ concentrations, the ability to predict a robust response due to changes in meteorology is uncertain because of the uncertainty among climate models to predict meteorological changes in a future climate. For relatively extreme climate change scenarios (i.e., RCP8.5), there is considerable agreement among climate model ensemble members for regional enhancements

in $PM_{2.5}$ concentrations by 2100, when emissions are fixed at present-day levels (Silva et al., 2017; Allen, Landuyt, and Rumbold, 2016). These enhancements are generally attributed to a decrease in wet deposition associated with reduced large-scale precipitation over continental regions. In general, the magnitude and sign of the $PM_{2.5}$ response due to climate change is a result of differences among climate models to predict large-scale meteorological changes, treatments of atmospheric chemistry, and feedbacks such as the response of natural emissions (Silva et al., 2017). However, while a changing climate will likely affect air quality levels, future changes are likely to be dominated by changes in future anthropogenic emissions West et al., 2013. Nevertheless, the $PM_{2.5}$ concentration changes reported for 2050 in Chapter 5 (i.e., under the reference scenario) were forced with present-day meteorology and so neglect additional impacts associated with climate change. Using a climate composition model would provide the necessary setup to examine how climate change might affect ambient $PM_{2.5}$ concentrations, but also how climate might respond to different emission scenarios. In the case of Chapter 5, understanding the climate implications due to the widespread adoption of clean cookstoves might be of particular importance considering that emissions from these technologies likely contain a higher proportion of BC containing particles relative to traditional combustion (Aung et al., 2016; Grieshop et al., 2017; Winijkul, Fierce, and Bond, 2016). Additionally, using an earth-system model fully coupled to the land-surface may also provide insights into whether widespread adoption of clean cookstoves would result in energy efficiency leading to reduced pressures on woodfuel resources or whether cookstoves overstate carbon savings (e.g. Bailis et al., 2015; Bailis et al., 2017). Considering that many clean cookstove intervention programmes are being implemented under climate compatible development goals and are funded through carbon financing, having a complete understanding of their overall climate impact is essential.

In addition, calculating mortality in 2050 as part of the analysis in Chapter 5

were based on base case forecasts of underlying disease rates following other modelling studies using the International Futures model (Silva et al., 2016; Silva et al., 2017; West et al., 2013). However, as with future anthropogenic emission pathways, underlying health pathways may be more diverse than what is predicted in the base case scenario alone, with similar socio-economic and environment variables driving uncertainties in health forecasts. As such, additional simulations exploring a range of possible future health pathways such as those employed by recent GBD studies (Foreman et al., 2018) would have benefited the analysis in Chapter 5.

Finally, the clean residential scenario examined in Chapter 5 were based under the assumption of widespread adoption and sustained use of clean residential combustion technologies by the year 2050. However, evidence from historical and present-day cookstove interventions, report modest adoption and user rates among communities and/or 'stove stacking', where intervention stoves fail to replace traditional stoves completely, potentially offsetting air quality and health benefits (Clark et al., 2017; Pillarisetti et al., 2014; Lozier et al., 2016). Such undesirable outcomes are caused by multiple implementation barriers, including the failure of intervention stoves to meet user needs and preferences, supply chain distribution challenges, lack of monitoring, training and maintenance, and financial constraints (Rehfuess et al., 2014; Lewis and Pattanayak, 2012). These important implementation barriers are not considered in Chapter 5, thus the introduction of additional scenarios examining the variability in adoption and user rates would provide additional information to fully evaluate the potential impact of clean stove technologies on air quality and health. Similarly, the emission factors used in Chapter 5 for clean residential combustion technologies are largely taken from controlled laboratory measurements, which are often lower than reported from field studies (Wathore, Mortimer, and Grieshop, 2017; Roden et al., 2009; Sambandam et al., 2015; Lozier et al., 2016). Thus the inclusion of emission factors exclusively from field measurements in the analysis reported in Chapter 5

would be ideal.

Health impacts

Mortality reported in this thesis are based on long-term exposure to ambient $PM_{2.5}$ only. As a result, the residential mortality estimates reported in Chapter 4 and Chapter 5, exclude the considerable loss of life due to residential combustion adversely affecting household air pollution (HAP). The disease burden from HAP is considerable in the present-day, causing 2.6 million deaths globally in 2016 (Gakidou et al., 2017; Smith et al., 2014a). However, while approximate joint health burden estimates for ambient and HAP are estimated by the Global Burden of Disease project under an assumption of independence, with little correlation and/or interaction (Gakidou et al., 2017), new methodologies seeking to combine the exposure distributions from both ambient and HAP $PM_{2.5}$ can be useful in wanting to examine the combined disease burden effect (e.g. Kodros et al., 2017). The additional use of this integrated methodology in Chapters 4 5, could provide a more comprehensive understanding of the disease burden associated with residential combustion.

There are large uncertainties relating to exposure-response relationships used in health impact assessments, including those used in this thesis. The integrated exposure-response (IER) relationship used in both Chapters 3 and 5 was, until relatively recently, the most up-to-date relationship used by the health assessment community. The strength of the IER was its use of disease risks from other combustion sources (e.g., active and passive tobacco smoking) to determine the shape of the exposure-response at high $PM_{2.5}$ exposure distributions in the absence of observed risk estimates from ambient air pollution prospective cohort studies. However, new relationships have emerged recently that are based entirely on observed risk estimates from ambient air pollution cohort studies (Burnett et al., 2018), including recent observations from China. A sensitivity analysis conducted in Chapter 5 showed that the

use of these new exposure-response relationships increased attributable mortality by nearly 100% compared to the IER. Considering that these new relationships are based on the most recent epidemiological evidence, employing their use in future health burden assessments would be ideal.

Exposure to $PM_{2.5}$ is not the only ambient air pollutant known to cause adverse health outcomes (Table 1.4). However, exposure to ozone (O_3) is the only other pollutant that has enough evidence to justify its use in health impact assessments. Ambient O_3 is an important global pollutant, contributing to between 233.6 (90.1-385.3) thousand to 1.04-1.23 million global deaths in the present-day (Gakidou et al., 2017; Malley et al., 2017). Considering that the model configurations used in both Chapters 3 and 5 provide changes in O_3, its health impact could also be considered under the same scenarios.

6.5.2 Research priorities for the wider community

The of value of PPEs in directing research priorities

The complexity of interacting uncertain parameters related to aerosol and physical atmosphere processes, emissions and other assumptions within CCMs and CTMs, means that traditional sensitivity experiments where uncertain parameters are perturbed in isolation (e.g., what was done in Chapter 4), cannot possibly be used to constrain model uncertainty. As a result, the use of PPEs and associated emulation provide a useful tool for the modelling community, in which modellers can explore the entire model parametric uncertainty space to measure total uncertainty, as well as attribute individual parameter contributions to uncertainty (e.g. Lee et al., 2013; Regayre et al., 2014; Regayre et al., 2018; Johnson et al., 2018). As previously mentioned, analysis of PPE simulations (using GLOMAP-mode simulated aerosol) with large datasets of in-situ aerosol observations, including aerosol number, mass

concentrations, and CDNC, can be used to remove implausible model variants, leaving only the 'best' model variants (Browse, 2019). However, while such analysis can remove a large proportion of implausible model variants, and in the process constraining some important uncertain model parameters (reported above), the parametric range of the 'best' model variants remains very wide with the same model skill being obtained from multiple parameter settings (Browse, 2019). This principle of eqifinality (i.e., the same simulated outcome from multiple pathways) means that many key uncertain parameters, including Aitken mode width, assumed activation diameter for in-cloud scavenging, biomass burning and residential emissions, remain unconstrained. This suggests that existing in-situ aerosol measurements may not be insufficient alone to constrain parametric uncertainty in complex models (Browse, 2019; Regayre et al., 2018). This type of analysis using PPEs therefore not only has important implications for future modelling approaches, but also identifies the need for future observational approaches. In particular, it identifies the need for processed-lead observations which are designed to test the plausibility of uncertain model parameters rather than just model simulated output (e.g. Browse, 2019).

Need for more air quality epidemiology

There are large uncertainties associated with exposure-response relationships used to assess the health impacts due to $PM_{2.5}$ exposure. Much of this uncertainty stems from a lack of epidemiology evidence across highly polluted regions such as Asia. For example, currently there has only been one cohort study conducted in a highly polluted region, with that study only considering adult men in various locations across China (Yin et al., 2017). As such, many more epidemiology studies are required across polluted regions in order to corroborate or refute current tools such as the IER used in most current $PM_{2.5}$ health impact assessments (e.g. Burnett et al., 2018). Additionally, the installation of surface air quality measurement networks across

highly polluted regions, such as recently developed across China (e.g. Silver et al., 2018), would also greatly benefit epidemiology studies, as well as the air quality modelling community. At the same time, a greater amount epidemiology research should also be focused in very clean regions, so that a greater understanding of the theoretical minimum risk exposure level (TEMREL) can be obtained (e.g. Shi et al., 2016). A greater understanding of the TEMREL is vital particularly when considering the establishment and setting of air quality standards designed to protect human health.

Health impact assessments currently assume that all $PM_{2.5}$ mass as equally toxic, regardless of composition and emission source. However, this is unlikely given that differences in composition and emission sources will certainly affect the levels of toxicity present in $PM_{2.5}$ (e.g. Thurston et al., 2016). However, there is not enough current evidence to draw conclusive associations between the biological effects of $PM_{2.5}$ composition at the population level (e.g. Burnett et al., 2014). Such caveats support the need for greater understanding in this area of toxicology and epidemiology, but also point to additional routine measurements of air pollutant composition (e.g., $PM_{2.5}$ speciation) so that specific health associations can be investigated.

Health impact assessments conducted in this thesis only consider five diseases associated with $PM_{2.5}$ exposure. However, while there is enough evidence for a causal relation with these five cardiovascular and respiratory diseases, evidence exists for other diseases, including Alzheimer's disease (e.g., Cacciottolo et al., 2017), Parkison's disease (e.g., Ritz et al., 2016), premature birth and low birth weight (e.g. Fleischer et al., 2014; Pedersen et al., 2013), mental health (e.g., Oudin et al., 2016), impaired cognitive function (e.g., Ailshire and Crimmins, 2014), and type 2 diabetes (e.g., He et al., 2017) (Table 1.4). However, as of yet, there is not enough evidence for their inclusion in impact assessments, suggesting more research is needed. In addition, there is suggestive health evidence for other air pollutants (Table 1.4). It is therefore

important that sufficient research be conducted to identify the range of disease associated with various air pollutants in order to build the health impact evidence base needed for proper and swift policy action.

Appendix A

Appendix A Supplementary material for Chapter 3

Global and regional trends in particulate air pollution and attributable health burden over the past 50 years

E W Butt[1*], S T Turnock[2], R Rigby[1], C L Reddington[1], M Yoshioka[1], J S Johnson[1], L A Regayre[1], K J Pringle[1], G W Mann[3] and D V Spracklen[1]

[1] School of Earth and Environment, University of Leeds, Leeds, UK

[2] Met Office Hadley Centre, Fitzroy Road, Exeter, Devon, UK

[3]National Centre for Atmosphere Science, University of Leeds, Leeds, UK

*Correspondence E-mail: e.butt@leeds.ac.uk

Supplementary information (SI)

1 Methods

1.1 Simulated $PM_{2.5}$ concentrations

HadGEM3-UKCA uses GLOMAP-mode to simulate aerosol processes (Mann et al., 2010). GLOMAP-mode uses log-normal modes to represent the aerosol size distribution and simulates the evolution of the size-resolved number and mass of aerosol particles with different compositions. GLOMAP-mode simulates the interaction of various aerosol processes including primary emissions, cloud processing, new particle formation, hygroscopic growth, coagulation, condensation, deposition and scavenging. Log-normal modes are used to represent aerosols in the nucleation (diameter (D) < 10 nm), Aitken (D 10–100 nm), accumulation (D 100 nm–1 µm) and coarse (D > 1 µm) modes.

1.2 $PM_{2.5}$ observations

We use measurements of $PM_{2.5}$ mass concentration at remote surface sites in the United States and Europe (Fig.S1). In Europe we use observations from the European Monitoring and Evaluation Programme (EMEP) network (http:// www.emep.int). The measurements were made using a range of techniques and time frequencies (hourly and daily). The data were screened to remove any anomalous data points according to flags in the original data records. For the United States we use observations from the Interagency Monitoring of Protected Visual Environments (IMPROVE) database. The IMPROVE network makes observations of $PM_{2.5}$ over a 24-hour period every 3 days (Malm et al., 1994). We calculate annual mean concentrations for locations with >75 measurements

within a given year. We quantify the comparison between simulated and observed $PM_{2.5}$ as the mean bias (MB) and the normalised mean bias factor (NMBF) as defined in Yu et al. (2006):

$$\mathrm{MB} = \sum (M_i - O_i) = \bar{M} - \bar{O} \tag{S1}$$

$$\mathrm{NMBF} = \frac{\sum (M_i - O_i)}{\sum O_i} \; if \; \bar{M} \geq \bar{O}$$

$$= \frac{\sum (M_i - O_i)}{\sum M_i} \; if \; \bar{M} \leq \bar{O} \tag{S2}$$

Where M_i and O_i are the model and observation values at measurement site and/or year *i*, and $\bar{M}$ and $\bar{O}$ are the annual mean model and observation values, respectively. MB shows the mean deviation of the model compared to observations in the units of the original data (i.e., μg m^{-3}), while NMBF is unitless and is interpreted as a factor+1 by which the model under or overestimates the observation value. For example, a NMBF of -1.0, implies the model underestimates the observation value by a factor of 2.

1.3 UKCA perturbed parameter ensemble (PPE)

We use a perturbed parameter ensemble (PPE) of 235 UKCA simulations for the year 2008 where 26-related parameters are perturbed simultaneously (Yoshioka et al., 2017) to explore uncertainty in simulated PM2.5 concentrations. The PPE encompasses the parametric uncertainty with respect to aerosols in the model. Using variance-based sensitivity analysis techniques we can decompose the overall variance in $PM_{2.5}$ concentration across the PPE into individual parameter contributions. Figure S2 shows the percentage contribution of individual model parameters to the variance of estimated $PM_{2.5}$ concentrations both regionally and globally. Globally, dry deposition of accumulation mode size particles represents the largest uncertainty in model processes, accounting for approx. 50% of the uncertainty. Smaller, but important contributions to the uncertainty come from the perturbations in the biogenic secondary organic aerosol formation, sea spray aerosol emissions flux and the carbonaceous emission mass flux of biomass burning and small scale residential combustion. Regionally, the same parameters dominate the uncertainty in $PM_{2.5}$ concentrations, with the largest contribution over the US and Europe also from processes relating to the dry deposition of accumulation mode size particles. However, for India and East China, it is the uncertainty relating to carbonaceous emission mass flux of small scale residential combustion that dominates the uncertainty in simulated $PM_{2.5}$ concentrations, which is an important emission source in these regions (Butt et al., 2016).

Figure S3 shows that the simulated population-weighted $PM_{2.5}$ concentrations in the baseline of the UKCA model ($UKCA_{\_base}$) is towards to the bottom end of the PPE uncertainty range in all regions, which may be partly responsible for the low bias to observations seen in the US and Europe (Fig. 2).

We use the uncertainty range provided by the UKCA PPE and apply it to the baseline of the UKCA model. We use the median of the PPE to increment the baseline model ($UKCA_{\_base}$): in each surface grid cell, we calculate the median $PM_{2.5}$ concentration across the entire PPE and then apply the absolute difference between the median and $UKCA_{\_base}$ in the year 2008. We then applied this difference throughout the entire UKCA simulation period (1960 to 2009). We use the same approach for two additional sensitivity simulations to explore the lower and upper bound range of the PPE using the 5^{th} ($UKCA_{\_ppe\text{-}05}$) and 95^{th} ($UKCA_{\_ppe\text{-}95}$) percentile range of the PPE represented by the error bars in Fig. S3.

1.4 Background disease and demographic data

National level population and age group distribution data are taken from the United Nations (UN) Population Division (UN, 2015) [https://esa.un.org/unpd/wpp/], which are available for the period 1960 to 2010 at 5 year intervals. We linearly interpolated between these data to obtain values for all years over the period (see Fig. S5). We used gridded population count data from the Gridded Population of the World v3 (GPWv3) [http://sedac.ciesin.columbia.edu/data/collection/gpw-v3/sets/browse] (CIESIN, 2015), available at a resolution of 2.5 arc-minutes for the period 1990 to 2010 at 5 year intervals. We extrapolated the GPWv3 to 1960 applying the rate of change in the UN national level data. When the GPWv3 is summed to national level values are typically within ~0.1-2% of UN national totals as shown in Fig. S6. This method does not account for changes in spatial distributions of population at the subnational level over the period 1960 to 1990.

Uncertainty bounds for the GPWv3 and UN national level population total and age group structure are not provided and so we assume no uncertainty in these datasets, although sources of error are documented elsewhere for GPWv3 (e.g., Deichmann et al., 2001).

Age and cause-specific background disease endpoint data for the period 1980 to 2010 are taken from the cause of disease visualisation tool hosted by Health Metrics and Evaluation [https://vizhub.healthdata.org/cod/] (IHME, 2014). The IHME uses statistical and analytical methods to redistribute modelled or reported deaths by their probable underlying causes. The dataset provides national level background disease endpoint data for cardiovascular ischemic heart disease (IHD) and stroke, lung cancer (LungC), chronic obstructive pulmonary disease (COPD) and lower respiratory infections (LRI). We also use the reported upper and lower uncertainty bounds to explore uncertainty in background disease. The dataset provides national level data, which is an over simplification as it does not account for variation in background disease rates such as differences between urban, sub-urban, and rural settings (Cossman et al., 2010), which can be influenced by differences in demographic characteristics, income and access to healthcare.

Background disease rates are not available prior to 1980, so we assume that rates remain constant at year 1980 levels for the period 1960 to 1979 (for example, see Fig. S7 for LRI in infants). To explore how sensitive the attributable health burden is using fixed rates prior to 1980, we conduct an additional sensitivity study and instead assume that background disease rates follow the same trend to that between 1980 and 1990 and apply it to the period prior to 1980. We calculate the rate of

change between 1980 and 1990 and multiply the fixed prescribed 1980 rate in the year 1960 for each country. Finally, we linearly interpolated between 1960 and 1980 to obtain new disease rates for all years between the period 1961 to 1979 (for example, see Fig. S7 for LRI in infants).

1.5 Attributable health burden calculation

We use the integrated exposure-response (IER) relationship (Burnett et al., 2014) to calculate the relative risk (RR) (equation S3). The IER compiles epidemiological evidence from different combustion sources to cover the range of exposures experienced by populations in all parts of the world (Burnett et al., 2014; Pope et al., 2009; Pope et al., 2011). The IER has been used in a number of recent studies (Apte et al., 2015; Chowdhury and Dey, 2016; Cohen et al., 2017; Ford and Heald, 2015; Lelieveld et al., 2015; Wang et al., 2016; Xie et al., 2016; Zheng et al., 2015) including recent Global Burden of Disease (GBD) assessments (Forouzanfar et al., 2016; Forouzanfar et al., 2015; Lim et al., 2013). We use IER developed for the GBD2013 (Forouzanfar et al., 2015), which differs from the previous version developed for GBD2010 (Lim et al., 2013) and the most recent developed for GBD2015 (Forouzanfar et al., 2016). The IER allows for age-dependent (i.e. ≥ 25 years of age at 5 year intervals to age 80+) calculation of RR for IHD and stroke, adult (≥ 25 years of age) for LC and COPD, and all ages for lower respiratory infections (LRI). The IER parameterises RR based on the $PM_{2.5}$ concentration, C:

$$RR(c) = 1+\propto \left(1 - \exp\left\{\beta\left(\frac{C - C_0}{1e10}\right)^{\gamma}\right\}\right)$$

$$RR = 1 \quad for\ C \leq C_o$$

(S3)

The theoretical minimum risk exposure level (TMREL), $C_{0,}$ is determined by the minimum (5.8 μg m^{-3}) and 5% quantile (8.8 μg m^{-3}) from the exposure distribution estimated from the aggregate of cohort studies used (Forouzanfar et al., 2015; Lim et al., 2013). We use 1000 combination of parameters of C_0, α, β and γ used in the GBD2013 [http://cloud.ihme.washington.edu/index.php/s/lXFBFXizUrOKXyS]. As in Apte et al. (2015), we developed an updated lookup table, compatible for GBD2013, for each disease endpoint using the mean of the estimated RRs at each $PM_{2.5}$ concentration spanning a range 0−300 μg m^{-3} at 0.1 μg m^{-3} increments. This lookup table is reported in the supplementary data 1. We also produce the 5th and 95th percentile of the estimated RR ranges to explore upper and lower uncertainty bounds of the IER relationship. The IER relationships are non-linear (Fig. S4), with reduced sensitivity of RR to changes in $PM_{2.5}$ at higher concentrations (Pope et al., 2009; Pope et al., 2011), particularly for cardiovascular IHD, stroke and LRI.

To calculate attributable premature deaths in grid cell i for disease endpoint *j* and population age group structure *z* ($M_{i,j,z}$), we apply the attributable fraction type relationship (Apte et al., 2015):

$$M_{i,j,z} = P_{i,z} \times \hat{I}_{j,z,k} \times \left(RR_{j,z}(C_i) - 1\right)$$

$$where\ \hat{I}_{j,z,k} = \frac{I_{j,z,k}}{\overline{RR}_{j,z,k}}\ \ and\ \ \overline{RR}_{j,z,k} = \frac{\sum_{i=1}^{N} P_{i,z} \times RR_{j,z}(C_i)}{\sum_{i=1}^{N} P_{i,z}} \quad \text{(S4)}$$

where $P_{i,z}$ is population in each age group z in cell *i,* $RR_{j,z}(C_i)$ is RR for disease endpoint *j* for age group *z* at annual mean $PM_{2.5}$ concentration C_i, $I_{i,k,z}$ is the background disease rate for endpoint *j* in age *z* stratum in country *k.* $P_{i,z}$ is calculated by multiplying the population in each grid cell by the age group fraction. $\overline{RR}_{i,z,k}$ represents the average population-weighted RR for each disease endpoint *j* for population age group *z* in country *k.* Attributable deaths are calculated at the spatial resolution of the gridded population data. We estimate the uncertainty range using the upper and lower uncertainty bounds of the IER relationship and background disease data. We assume no uncertainty in demographic data.

We also estimate years of life lost (YLLs), which is an estimate of the average years a person would have lived had they not died prematurely from long-term exposure ambient $PM_{2.5}$. YLLs are calculated by summing attributable deaths within each age group and multiplying it by the associated expected life expectancy taken from the standard life table provided by Murray et al. (2013).

1.6 Relative contribution to attributable mortality

We explored the relative contribution of estimated attributable deaths over the period 1980 to 2009 to changing $PM_{2.5}$ concentrations, population demographics (total population growth and ageing) and background disease characteristic. In order to explore the relative contribution to changes in these four variables, we calculate new baseline estimates by holding each variable constant at 1980 levels one at a time. We then explored the relative contribution to changes in each individual variable by comparing the difference between the new baseline estimates to the original baseline estimates. This analysis was restricted to the period 1980 to 2009 when most data were available.

References

Apte, J. S., Marshall, J. D., Cohen, A. J., and Brauer, M.: Addressing Global Mortality from Ambient PM2. 5, Environmental science & technology, 49, 8057-8066, 2015.

Burnett, R. T., Pope, C. A., Ezzati, M., Olives, C., Lim, S. S., Mehta, S., Shin, H. H., Singh, G., Hubbell, B., and Brauer, M.: An integrated risk function for estimating the global burden of disease attributable to ambient fine particulate matter exposure, 2014. 2014.

Butt, E. W., Rap, A., Schmidt, A., Scott, C. E., Pringle, K. J., Reddington, C. L., Richards, N. A. D., Woodhouse, M. T., Ramirez-Villegas, J., Yang, H., Vakkari, V., Stone, E. A., Rupakheti, M., S. Praveen, P., G. van Zyl, P., P. Beukes, J., Josipovic, M., Mitchell, E. J. S., Sallu, S. M., Forster, P. M., and Spracklen, D. V.: The impact of residential combustion emissions on atmospheric aerosol, human health, and climate, Atmos. Chem. Phys., 16, 873-905, 2016.

Chowdhury, S. and Dey, S.: Cause-specific premature death from ambient PM 2.5 exposure in India: Estimate adjusted for baseline mortality, Environment international, 91, 283-290, 2016.

CIESIN: Gridded Population of the World, Version 3 (GPWv3) Data Collection. 2015.

Cohen, A. J., Brauer, M., Burnett, R., Anderson, H. R., Frostad, J., Estep, K., Balakrishnan, K., Brunekreef, B., Dandona, L., and Dandona, R.: Estimates and 25-year trends of the global burden of disease attributable to ambient air pollution: an analysis of data from the Global Burden of Diseases Study 2015, The Lancet, 389, 1907-1918, 2017.

Cossman, J. S., James, W. L., Cosby, A. G., and Cossman, R. E.: Underlying causes of the emerging nonmetropolitan mortality penalty, American journal of public health, 100, 1417-1419, 2010.

Deichmann, U., Balk, D., and Yetman, G.: Transforming population data for interdisciplinary usages: from census to grid, Washington (DC): Center for International Earth Science Information Network, 200, 2001.

Ford, B. and Heald, C.: Exploring the uncertainty associated with satellite-based estimates of premature mortality due to exposure to fine particulate matter, Atmospheric Chemistry and Physics Discussions, 15, 25329-25380, 2015.

Forouzanfar, M. H., Afshin, A., Alexander, L. T., Anderson, H. R., Bhutta, Z. A., Biryukov, S., Brauer, M., Burnett, R., Cercy, K., Charlson, F. J., and Cohen, A. J.: Global, regional, and national comparative risk assessment of 79 behavioural, environmental and occupational, and metabolic risks or clusters of risks, 1990-2013: a systematic analysis for the Global Burden of Disease Study 2015, The Lancet, 388, 1659-1724, 2016.

Forouzanfar, M. H., Alexander, L., Anderson, H. R., Bachman, V. F., Biryukov, S., Brauer, M., Burnett, R., Casey, D., Coates, M. M., and Cohen, A.: Global, regional, and national comparative risk assessment of 79 behavioural, environmental and occupational, and metabolic risks or clusters of risks in 188 countries, 1990-2013: a systematic analysis for the Global Burden of Disease Study 2013, The Lancet, 386, 2287-2323, 2015.

IHME: http://vizhub.healthdata.org/cod/, last access: 30th September 2015, 2014.

Lelieveld, J., Evans, J., Fnais, M., Giannadaki, D., and Pozzer, A.: The contribution of outdoor air pollution sources to premature mortality on a global scale, Nature, 525, 367-371, 2015.

Lim, S. S., Vos, T., Flaxman, A. D., Danaei, G., Shibuya, K., Adair-Rohani, H., AlMazroa, M. A., Amann, M., Anderson, H. R., and Andrews, K. G.: A comparative risk assessment of burden of disease and injury attributable to 67 risk factors and risk factor clusters in 21 regions, 1990–2010: a systematic analysis for the Global Burden of Disease Study 2010, The lancet, 380, 2224-2260, 2013.

Malm, W. C., Sisler, J. F., Huffman, D., Eldred, R. A., and Cahill, T. A.: Spatial and seasonal trends in particle concentration and optical extinction in the United States, Journal of Geophysical Research: Atmospheres, 99, 1347-1370, 1994.

Mann, G., Carslaw, K., Spracklen, D., Ridley, D., Manktelow, P., Chipperfield, M., Pickering, S., and Johnson, C.: Description and evaluation of GLOMAP-mode: a modal global aerosol microphysics model for the UKCA composition-climate model, Geoscientific Model Development, 3, 519-551, 2010.

Murray, C. J., Vos, T., Lozano, R., Naghavi, M., Flaxman, A. D., Michaud, C., Ezzati, M., Shibuya, K., Salomon, J. A., and Abdalla, S.: Disability-adjusted life years (DALYs) for 291 diseases and injuries in

21 regions, 1990–2010: a systematic analysis for the Global Burden of Disease Study 2010, The lancet, 380, 2197-2223, 2013.

Pope, C. A., Burnett, R. T., Krewski, D., Jerrett, M., Shi, Y., Calle, E. E., and Thun, M. J.: Cardiovascular mortality and exposure to airborne fine particulate matter and cigarette smoke shape of the exposure-response relationship, Circulation, 120, 941-948, 2009.

Pope, C. A., Burnett, R. T., Turner, M. C., Cohen, A., Krewski, D., Jerrett, M., Gapstur, S. M., and Thun, M. J.: Lung cancer and cardiovascular disease mortality associated with ambient air pollution and cigarette smoke: shape of the exposure-response relationships, Environmental health perspectives, 119, 1616, 2011.

UN: World Population Prospects: The 2015 Revision, United Nations, Department of Economic and Social Affairs, Population Division, New York, USA, 2015.

Wang, J., Xing, J., Mathur, R., Pleim, J., Wang, S., Hogrefe, C., Gan, C., Wong, D., and Hao, J.: Historical Trends in PM 2.5-Related Premature Mortality during 1990-2010 across the Northern Hemisphere, Environ Health Perspect, 2016. 2016.

Xie, Y., Dai, H., Dong, H., Hanaoka, T., and Masui, T.: Economic impacts from PM2. 5 pollution-related health effects in China: A provincial-level analysis, Environmental Science & Technology, 2016. 2016.

Yoshioka et al.: Ensembles of global climate model simulations to explore uncertainty in global aerosols and radiative forcing, in-prep, 2017. 2017.

Yu, S., Eder, B., Dennis, R., Chu, S. H., and Schwartz, S. E.: New unbiased symmetric metrics for evaluation of air quality models, Atmospheric Science Letters, 7, 26-34, 2006.

Zheng, S., Pozzer, A., Cao, C., and Lelieveld, J.: Long-term (2001–2012) concentrations of fine particulate matter (PM 2.5) and the impact on human health in Beijing, China, Atmospheric Chemistry and Physics, 15, 5715-5725, 2015.

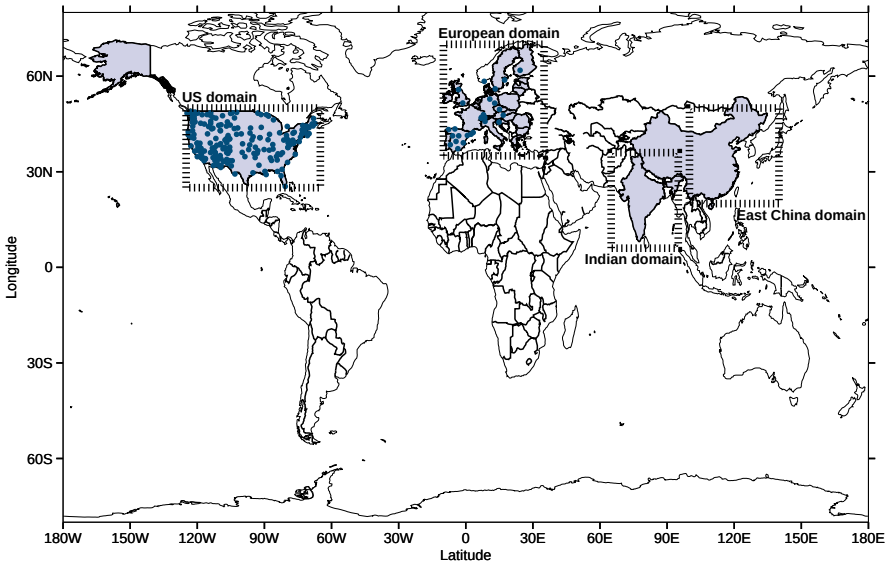

Figure S1: Location of IMPROVE in the US (United States) and EMEP in EU (comprising current 28 member states of the European Union) measurement sites (filled circles) and regional domains used in Fig 1. Shaded regions comprising China, India, EU and the US are where health burden estimates are reported for.

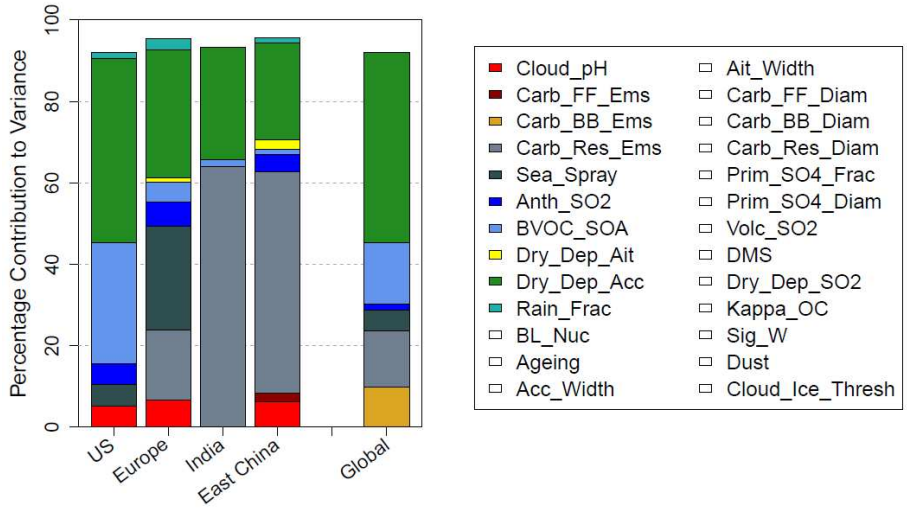

Figure S2: Percentage contribution of individual UKCA model parameters to the variance of estimated $PM_{2.5}$ concentrations in perturbed parameter ensemble (PPE). Note only includes contributions to uncertainty greater than 1% . Regional domains identified in Fig S1.

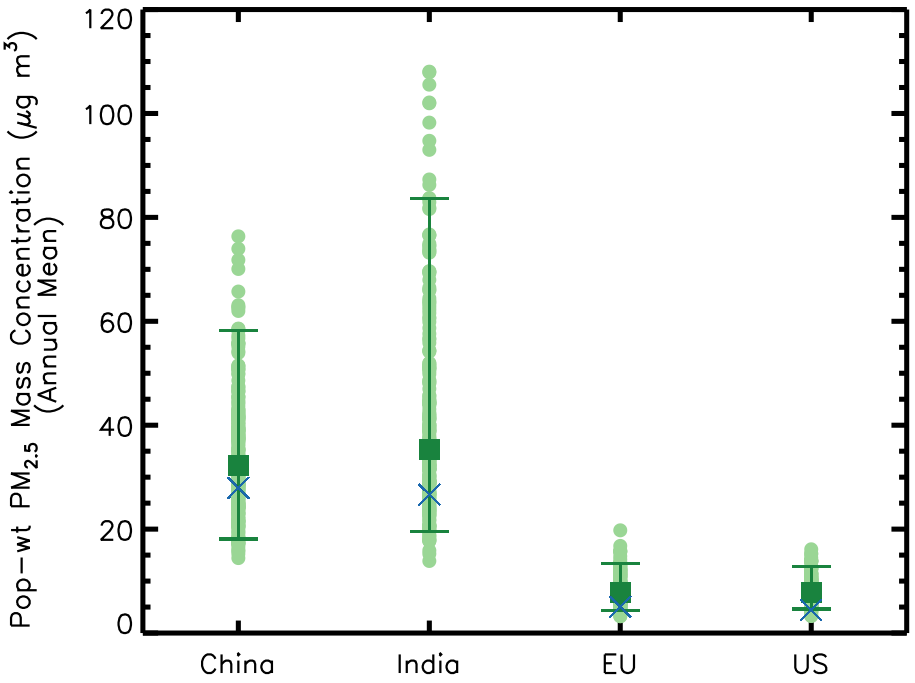

Figure S3: Annual mean surface population-weighted $PM_{2.5}$ concentration for UKCA-PPE (light green squares) in the year 2008. Dark green squares represent the median of the PPE ($UKCA_{\text{-ppe-med}}$), error bars represent the 5^{th} ($UKCA_{\text{-ppe05}}$) and 95^{th} ($UKCA_{\text{-ppe95}}$) percentile range of the PPE. Blue crosses represent mean surface population-weighted $PM_{2.5}$ concentration from the UKCA base model ($UKCA_{\text{-base}}$) .

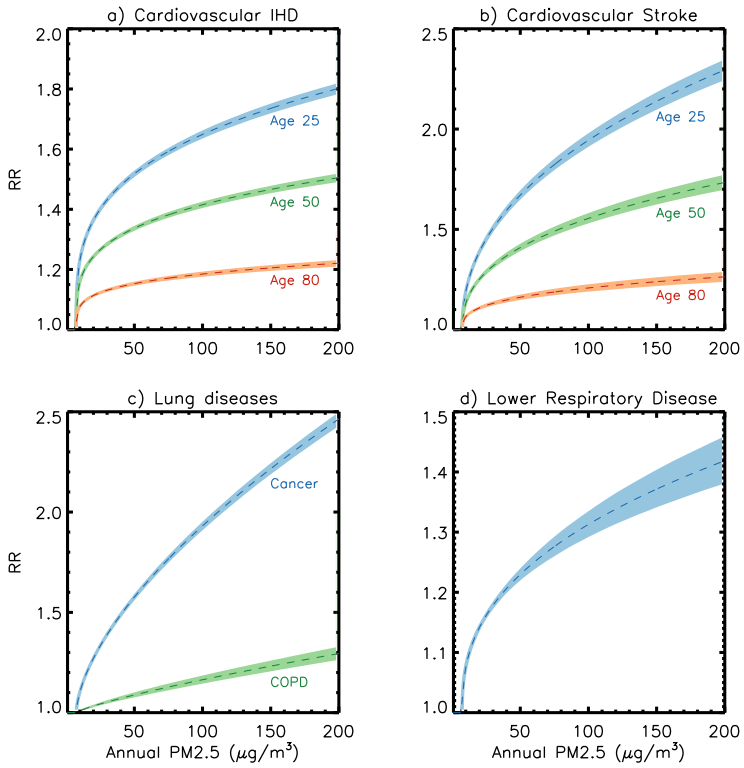

Figure S4: GBD2103 integrated exposure-response (IER) relationships for disease endpoints associated with long-term exposure to ambient $PM_{2.5}$ a) ischemic heart disease (IHD) and b) Stoke, c) lung diseases lung cancer and chronic obstructive pulmonary disease (COPD), and d) lower respiratory disease. Shaded areas represents the upper and lower uncertainty bound of the IER relationship. See supplementary data 1 for the IER lookup table.

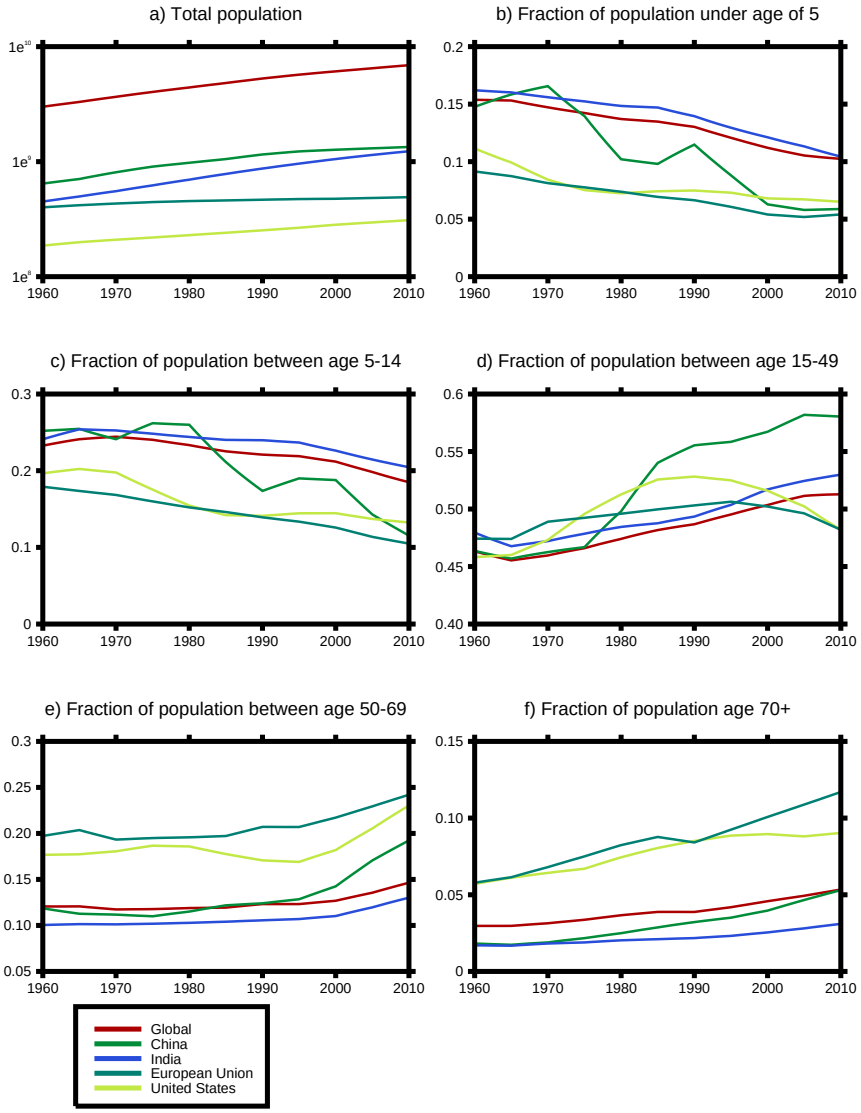

Figure S5: National level a) total population and b) fraction of population in age groups < 5, c) 5-15, d) 15-49, e) 50-69 and f) 70 plus years in China, India, EU and the US.

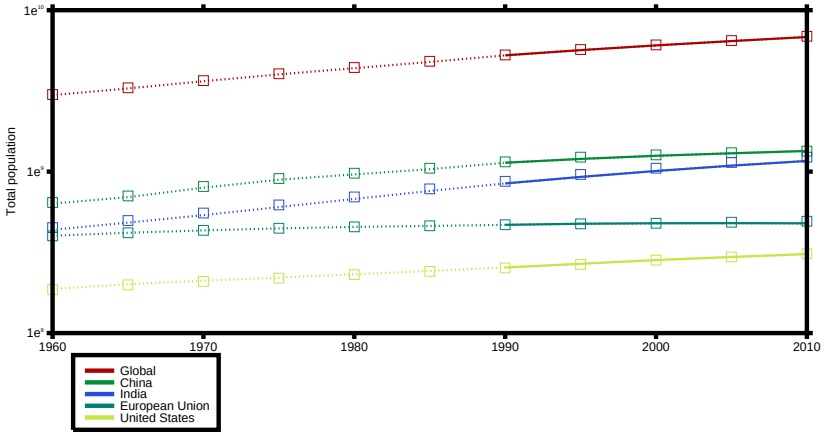

Figure S6: National level total population. Country level UN population estimates (open squares) (UN, 2015) and gridded population from GWPv3 dataset (CIESIN, 2015) summed to the national level (solid line). Extrapolated summed gridded population count data at the national level (dotted lines) based on the rate of change of official national level.

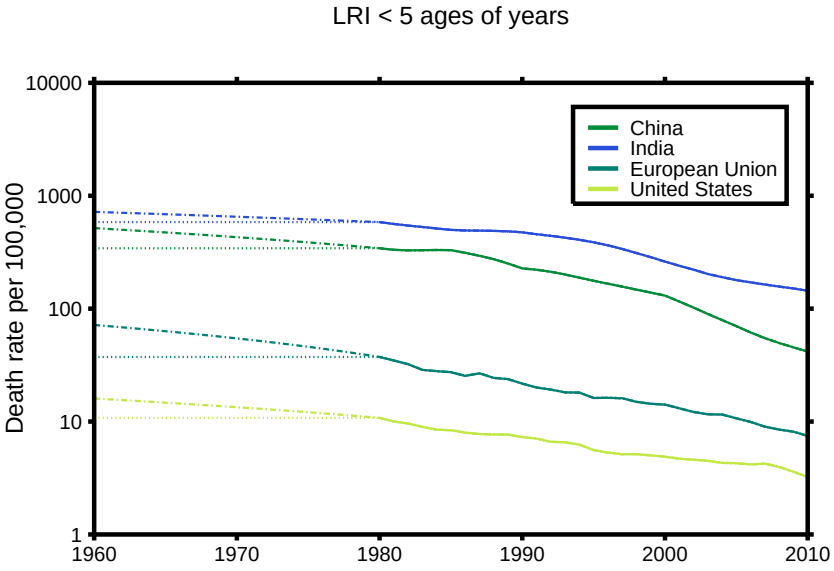

Figure S7: Background disease rates for lower respiratory infection (LRI) disease (per 100 000) in age group < 5 years for China, India, EU and the US. Dotted line represents fixed 1980 disease rates prior to 1980, while dotted and dashed lines represents to rate of change between 1980 and 1990 used prior to 1980.

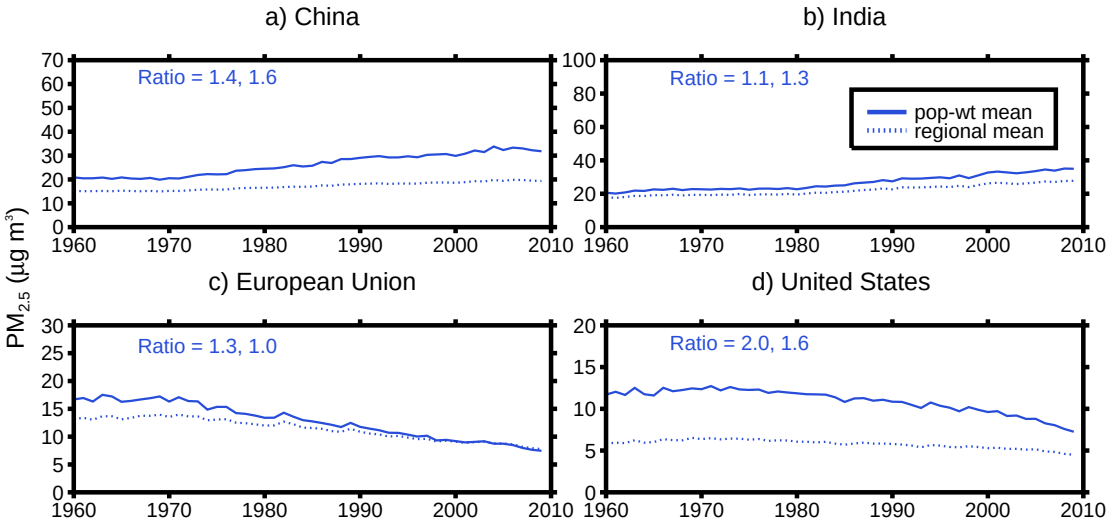

Figure S8: Annual mean population-weighted (pop-wt mean) and regional average (regional mean) $PM_{2.5}$ concentrations for a) China, b) India, b) European Union and d) United States. Results are shown for $UKCA_{\_ppe\text{-}med}$. Ratio between pop-wt mean and regional mean are shown (Ratio=(pop-wt_{1960}/$regional_{1960}$), (pop-wt_{2009}/$regional_{2009}$)).

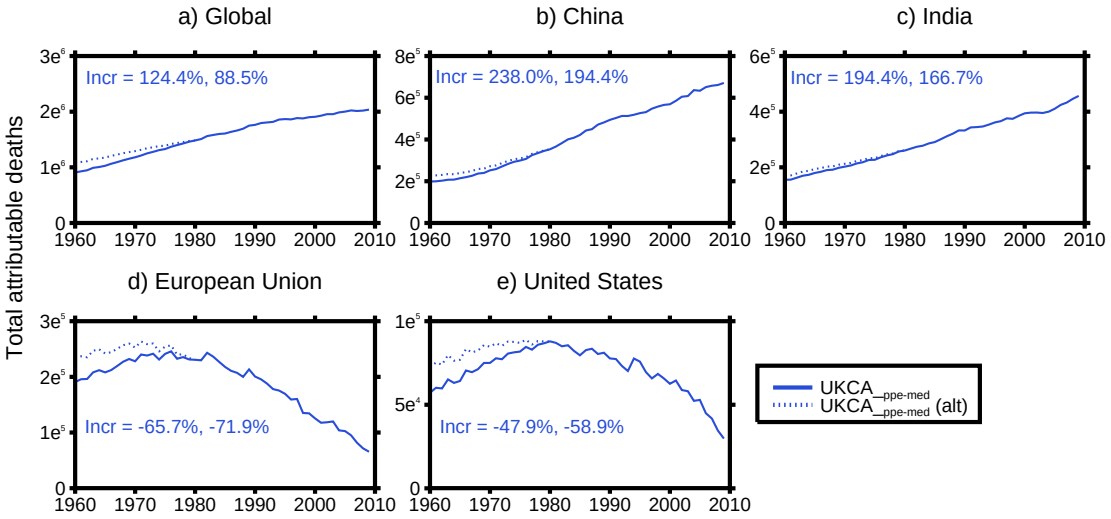

Figure S9: Attributable deaths for using a fixed background disease prior to 1980 (solid line) compared to using an alternative background disease rate prior to 1980 based on the rate of change between 1980 and 1990 (UKCA (alt)). Percentage changes (Incr = (2009-1960)/1960) are shown for $\text{UKCA}_{\text{-ppe-med}}$ using both a fixed background disease rate prior to 1980 and the alternative varying disease rate prior to 1980, respectively

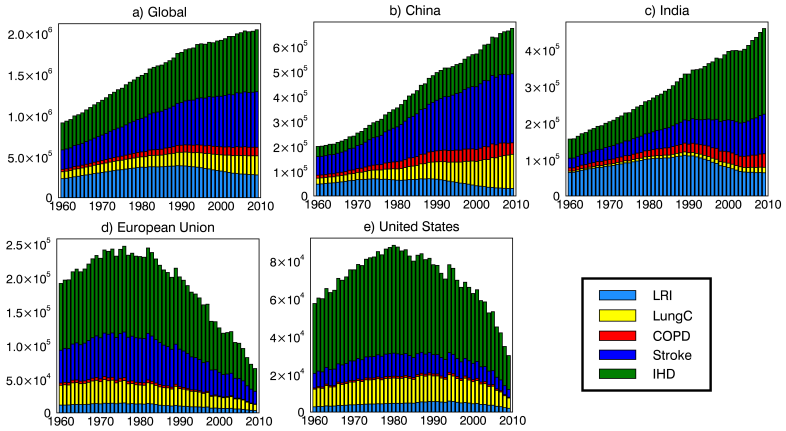

Figure S10: Contribution of different diseases to attributable deaths: cardiovascular ischemic heart disease (IHD) and Stroke, and lung diseases including lung cancer (LungC) and chronic obstructive pulmonary disease (COPD), and lower respiratory infection disease (LRI). Results are shown for UKCA$_{\text{-ppe-med}}$ using a fixed background disease rate prior to 1980.

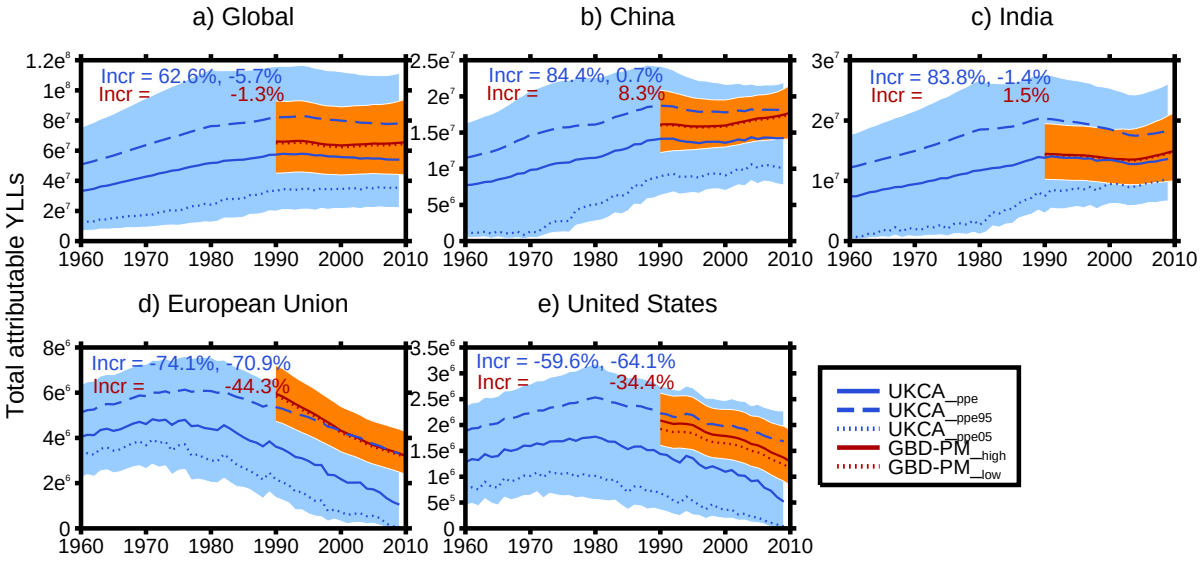

Figure S11: Years of life lost (YLLs) a) globally and b-e) regionally. Note that attributable YLLs use a fixed background disease rate prior to 1980. Shading, percentage changes, regions and key as for Fig 3.

Appendix B

Appendix B Supplementary material for Chapter 5

Supplementary information

A.1 Emissions

A.1.1 Anthropogenic emissions

Anthropogenic gas-phase and primary aerosol emissions of black carbon (BC), organic carbon (OC), sulphur dioxide (SO_2), nitrogen oxides (NO_x), carbon monoxide (CO), non-methane volatile organic compounds (VOCs) and methane (CH_4 are taken from the ECLIPSE (Evaluating the Climate and Air Quality Impacts of Short-Lived Pollutants) project version v5a (http://www.iiasa.ac.at/web/home/research/researchPrograms/air/ECLIPSEv5a.html). Anthropogenic emissions are provided for the following sectors: energy (including flaring), industry, solvent use, transport, residential and commercial, agriculture, agricultural waste burning, waste treatment and international shipping. Monthly variability in emissions was applied off-line using sector specific monthly varying weights provided separately by ECLIPSE. Lumped anthropogenic VOCs from ECLIPSE were separated according to TOMCAT species (Monks et al., 2017) using anthropogenic sector ratios provided by the RETRO (REanalysis of the TROposhperic chemical composition) project for the reference year 2000.

ECLIPSE emissions are created by the GAINS (Greenhouse gas–Air pollution Interactions and Synergies;http://www.iiasa.ac.at/web/home/research/researchPrograms/GAINS.en.html) model (Amann et al., 2011), which holds key information about emission sources, environmental legislation and mitigation opportunities for multiple country regions, including 2000 technologies to control air pollutant emissions and at least 500 options to control green-house-gas (GHG) emissions (Stohl et al., 2015).

A.1.2 Natural emissions

Natural gas-phase emissions of biogenics are taken from the MACC (Monitoring Atmospheric Composition and Climate) project (MACCity), which provides simulated VOCs by MEGAN (Model of Emissions of Gases and Aerosols from Nature) v2.0 for the reference year 2000 (Guenther et al., 2006). Oceanic CO and VOC emissions and soil NO_x are taken from the POET inventory. Lightning emissions of NO_x are coupled to convection activity in TOMCAT and thus vary in space and time (Stockwell et al., 1999). Volcanic emissions of SO_2 are based on both continuous (Andres and Kasgnoc, 1998) and explosive (Halmer, Schmincke, and Graf, 2002) volcanic eruptions. Open biomass burning emissions are taken from GFED (Global Fire Emission Database) v3 (Van Der Werf et al., 2004) and are based on a 1997-2010 average. Emissions of Oceanic dimethylsulfide (DMS) are calculated using an ocean surface concentration database

(Kettle and Andreae, 2000). Gridded surface CH_4 emission are read into TOMCAT then scaled to a suitable global mean surface concentration given the year under investigation (e.g., present-day 2015 or future 2050) based on a box model steady-state calculation (McNorton et al., 2016).

A.2 $PM_{2.5}$ surface measurements

We collected a global dataset of surface $PM_{2.5}$ concentration measurements at remote, rural, semi-urban and urban locations across multiple countries and regions.

For measurements across Europe, we used measurements from the EMEP network (European Monitoring and Evaluation Programme; http://www.emep.int). Measurements were made using a range of techniques and time frequencies (hourly and daily). For measurements across North America, we IMPROVE (Interagency Monitoring of Protected Visual Environments) network. The IMPROVE network makes observations of $PM_{2.5}$ over a 24-hour period every 3 days (Malm et al., 1994). Measurements taken from EMEP and IMPROVE were screened to remove flagged points, then annually averaged at locations with the closest year of measurement to 2015, excluding locations with measurements before the year 2010.

For measurements across China, we use hourly $PM_{2.5}$ observations published in real time by CNEMC (China National Environmental Monitoring Center; http://www.cnemc.cn/). Measurements for 2014 were downloaded from PM25.in (http://pm25.in/), a direct mirror of CNEMC. Repeated identical measurements for three or more continuous hours were removed due to instrument malfunction. Measurements less than 1 μg m^{-3} were also removed due to instrument detection limits. Daily average measurements were calculated from hourly concentrations during 0:00-23:59 local time if 18 or more hourly measurements were available.

For India, hourly measurements were taken from the Central Pollution Control Board (CPCB), Ministry of Environment and Forests, Government of India (http://www.cpcb.gov.in/CAAQM/). We use the same measurements as described in Conibear et al., 2018 for the year 2016. For Africa and Southeast Asia, we manually selected measurements collected between 2015 and 2010 as part of the WHO Air Pollution in Cities report (WHO, 2016) at individual monitoring locations via the ambient air pollution interactive map (http://maps.who.int/airpollution/), some of which are estimated from PM_{10} measurements.

We quantify the comparison between TOMCAT simulated and measured $PM_{2.5}$ concentrations as the mean bias (MB) and the normalised mean bias factor (NMBF), defined by Yu et al., 2006:

$$MB = \sum(M_i - O_i) = \bar{M} - \bar{O}$$

$$NMBF = \frac{\sum(M_i - O_i)}{\sum(O_i)} \quad \text{if} \quad \bar{M} \geq \bar{O}$$

$$= \frac{\sum(M_i - O_i)}{\sum(M_i)} \quad \text{if} \quad \bar{M} \leq \bar{O}$$

Where M_i and O_i are the simulated and measured values at station and/or year i, and $\bar{M}$ and $\bar{O}$ are the annual mean simulated and measured values,respectively. MB shows the mean deviation of the simulated value compared to the measured value in the original units (µg m $^{-3}$). The NMBF is unitless and is interpreted as a factor+1 by which the simulated value under or overestimates the measured value.

A.3 Scaling simulated $PM_{2.5}$ concentrations

A.3.1 The DIMAQ dataset

The Data Integration Model for Air Quality (DIMAQ) is a high-resolution spatially extensive 'semi-observational' gridded dataset of ambient $PM_{2.5}$ concentrations at a resolution of 0.1° × 0.1° (11km × 11km at the equator) (Shaddick et al., 2018). DIMAQ estimates $PM_{2.5}$ concentrations by combining satellite retrievals of aerosol optical depth (AOD), 6003 ground measurements with simulated relationships between $PM_{2.5}$ concentrations and AOD as prescribed by the GEOS-Chem chemical transport model (CTM). A CSV file containing column information longitude, latitude and ambient $PM_{2.5}$ estimates for the year 2014 was downloaded from the World Health Organisation (WHO) website (http://www.who.int/phe/health_topics/outdoorair/databases/modelled-estimates/en/).

A.3.2 $PM_{2.5}$ scaling methodology

We scaled TOMCAT 2015 $PM_{2.5}$ concentrations at the country level using DIMAQ at 2.8° × 2.8° using a country scale factor $SFac$:

$$SFac = \left[\frac{PM_{2.5DIMAQ_{ctry}}}{PM_{2.5_{2015unscaled_{cctry}}}} \right]$$

where $PM_{2.5DIMAQ_{ctry}}$ and $PM_{2.5_{2015unscaled_{cctry}}}$ are the country-level concentration average of DIMAQ (at 2.8° × 2.8°) and TOMCAT 2015 for a given county $ctry$, respectively at the TOMCAT grid. Unscaled TOMCAT 2015 concentrations are then multiplied by the scaling factor $SFac$ per grid cell for a given country $cctry$:

$$PM_{2.5_{2015scaled_{cctry}}} = PM_{2.5_{2015unscaled_{cctry}}} \times SFac$$

where $PM_{2.5_{2015scaled_{cctry}}}$ is the scaled $PM_{2.5}$ concentration in 2015 for grid cells in a given country $cctry$, and $PM_{2.5_{2015unscaled_{cctry}}}$ are the unscaled TOMCAT 2015 grid cell concentrations. To estimate scaled $PM_{2.5}$ concentrations for 2050 scenarios, we multiply by the same scaling factor:

$$PM_{2.5_{2050scaled_{cctry}}} = PM_{2.5_{2050unscaled_{cctry}}} \times SFac$$

As a sensitivity, we also use DIMAQ to downscale TOMCAT simulated $PM_{2.5}$ concentrations from 2.8° × 2.8° to 0.1° × 0.1° following a widely used approach (Lacey et al., 2017; Chowdhury, Dey, and Smith, 2018; GBD MAPS Working Group, 2016; GBD MAPS Working Group, 2018; Archer-Nicholls et al., 2016; Weagle et al., 2018) to test sensitivity of spatial resolution to mortality estimation. The approach is similar

to the one described above but uses a spatial map of the annual mean ratio of DIMAQ at $0.1^\circ \times 0.1^\circ$ to simulated TOMCAT $PM_{2.5}$ re-gridded on a $0.1^\circ \times 0.1^\circ$ grid.

A.4 Mortality attributable to residential combustion emissions

We estimate mortality due to residential emissions using two different methods used widely (Kodros et al., 2016; Conibear et al., 2018). The first method estimates mortality attributable to residential emissions $Mort_{residential\_attribute}$ (attribution method) based on a linear relationship where the total $PM_{2.5}$ attributable mortality from all sources $Mort_{PM_{2.5}}$ is scaled by the $PM_{2.5}$ fraction due to residential emissions (e.g., estimated from simulations where residential combustion emissions have been removed) Res_{frac}:

$$Mort_{residential\_attribute} = Res_{frac} \times Mort_{PM_{2.5}}$$

This attribution method is also considered by the GBD to be the most favourable method for attributing emission sources to $PM_{2.5}$ mortality in a manor that is understood by the policy making community.

The second method estimates the number of averted mortality due to a complete removal of residential of emissions in isolation $Mort_{residential\_averted}$ (subtraction method). Here the averted mortality is estimated by subtracting the total number of $PM_{2.5}$ attributable mortality in a simulation where residential emissions are present ($Mort_{PM_{2.5}}$) from a simulation where residential emissions have been removed ($Mort_{residential\_off}$):

$$Mort_{residential\_averted} = Mort_{PM_{2.5}} - Mort_{residential\_off}$$

Residential mortality estimates using the two different methods described above will result in different mortality estimates, which can be largely explained by the non-linearity of the IER (Kodros et al., 2016).

A.5 Data from International Futures

We use forecast data on background disease and demographic characteristics for the period 2015 to 2050 from the International Futures (IFs) socioeconomic modelling system (Hughes et al., 2011), which draw drivers of health and population outcomes, including demographic, economic, educational, socio-political, agricultural and environmental. IFs forecasts were taken through the downloadable model version v7.31 (`https://pardee.du.edu/access-ifs`), under a base case scenario where present-day dynamic patterns and relationships continue to unfold and evolve to 2050. IFs model does not provide confidence intervals for forecast data, thus we assume all uncertainty in attributable mortality from exposure-response relationship.

Following similar methods (Silva et al., 2016; Silva et al., 2017; West et al., 2013), IFs country-level lumped cardiovascular diseases are used to estimate ischaemic heart disease (IHD) and cerebrovascular (CEV) disease given their present-day proportion in cardiovascular disease (e.g. using GBD proportions in 2015), as are respiratory disease for chronic obstructive pulmonary disease (COPD), malignant neoplasms for

lung cancers and respiratory infections for lower respiratory infections (LRI). For regional background disease, age-cause-specific mortality rates are expected to decrease across all diseases by 2050 (Figure A.6), however, with two exceptions (LRI, CEV), total cause-specific mortality is predicted to increase due to population growth and ageing.

IFs country-level 2015 population data are gridded to a 15 arc-minute grid and spatially distributed using the fraction of the total population per country for each grid cell using 2015 UN-adjusted Gridded Population of the World version 4 (GPWv4) estimates (http://sedac.ciesin.columbia.edu/data/collection/gpw-v4) (Doxsey-Whitfield et al., 2015). IFs Population forecasts for 2050 are gridded in a similar way, assuming that the spatial distribution of the fraction of the total population per country is unchanged from 2020 UN-adjusted GPWv4 estimates. As shown in Figure A.7, IFs national-level estimates closely match summed national-level GPWv4 in 2015, as well as closely matching UN 2050 projections used to construct ECLIPSE 2050 emission scenarios (UN, 2011; IEA, 2012). IFs forecasts predict that global population will increase to nearly 10 billion in 2050, with an increasing ageing population relative to 2015.

A.6 Exposure-response relationship sensitivity

We conduct a brief sensitivity and estimate attributable mortality from our air quality scenarios using a newly alternative exposure-response relationship. We used the Global Exposure Mortality Model (GEMM), which was used recently to estimate global burden of disease attributable to long-term ambient $PM_{2.5}$ exposure (Burnett et al., 2018). Unlike the IER (Burnett et al., 2014), hazard ratios estimated from GEMM are based entirely on 41 ambient air pollution cohort risks. The development of the GEMM attempts to address some of the limitations associated with the IER (e.g., using risks from different combustion sources to infer risks at high exposure distributions) by combining limited results from ambient air pollution cohort studies conducted in polluted regions, including one from China.

We use parameters provided by Burnett et al., 2018 and estimate GEMM hazard ratios through a log-linear relationship for non-accidental non-communicable plus lower respiratory infection endpoints. We use GEMM parameters that include the Chinese cohort study and fix the maximum $PM_{2.5}$ concentration risk estimate to 84 μg m^{-3} to match the maximum exposure distribution measured in the single Chinese cohort study. Figure A.16 shows attributable mortality using GEMM compared to that using the IER. We find that while the estimated health burden are larger using the GEMM, relative to the IER, they do not change the overall message we convey regarding the health impacts and benefits of our air quality scenarios using the IER.

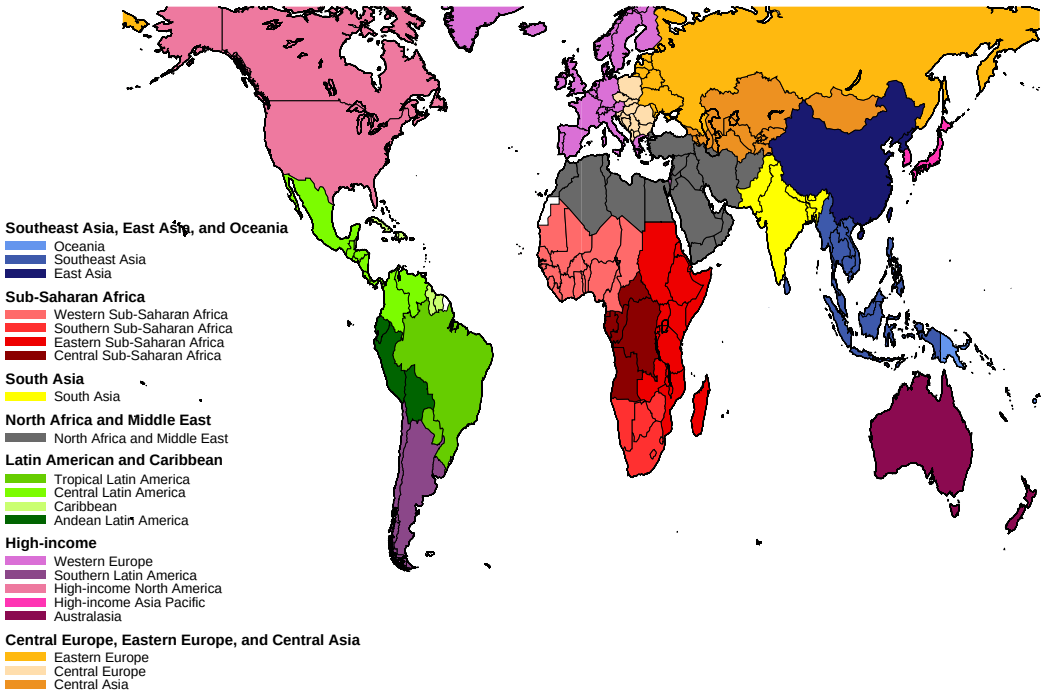

FIGURE A.1: GBD super regions.

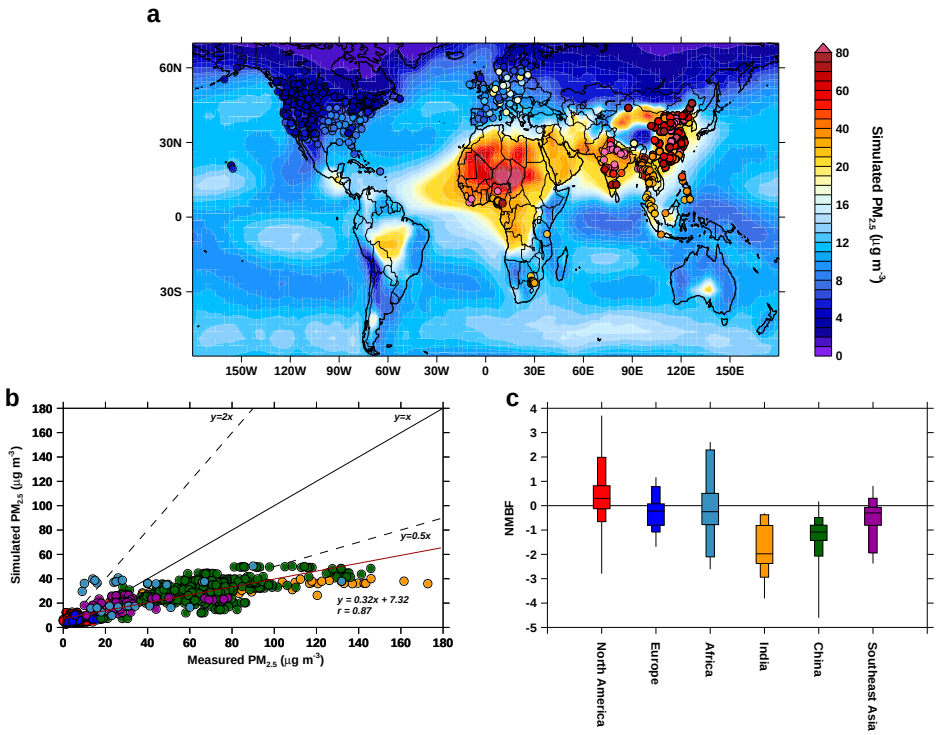

FIGURE A.2: Comparison of simulated $PM_{2.5}$ concentrations with measurements collected across multiple locations and regions. **a** 2015 TOMCAT simulated surface annual mean $PM_{2.5}$ concentrations (background) compared to measurements (filled circles). **b** Comparison of $PM_{2.5}$ concentrations, best fit line (red line), 1:1 (solid black line), 2:1 and 1:2 (dashed black lines). Best fit line has slope = 0.32 and Pearson's correlation coefficient (r) = 0.87. **c** Normalised mean bias factor (NMBF) box and whisker by sub-region, showing the minimum, maximum and median distribution values, as well as the 10^{th}, 25^{th}, 75^{th}, and 90^{th} percentiles.

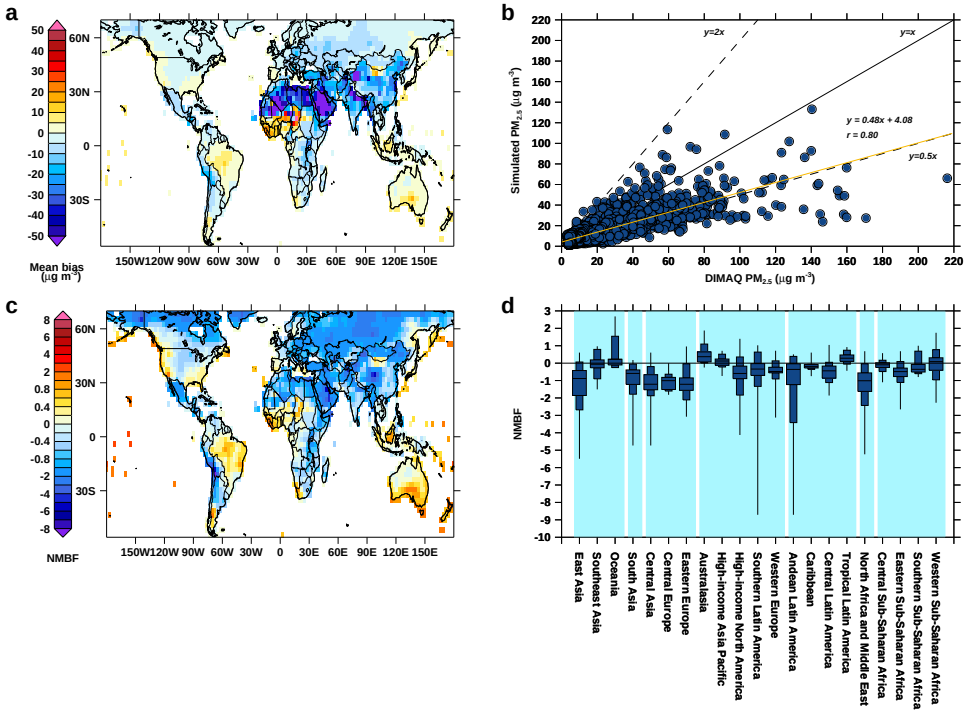

FIGURE A.3: Comparison of TOMCAT 2015 simulated $PM_{2.5}$ concentrations with DIMAQ gridded estimate (averaged to the TOMCAT resolution). **a** Mean bias in the spatial distribution of annual mean surface $PM_{2.5}$ concentrations. **b** Comparison of $PM_{2.5}$ concentrations, best fit line (yellow line), 1:1 (solid black line), 2:1 and 1:2 (dashed black lines). Best fit line has slope = 0.48 and Pearson's correlation coefficient (r) = 0.80. **c** Spatial distribution of Normalised mean bias factor (NMBF), and **c** NMBF box and whisker by sub-region, showing the minimum, maximum and median distribution values, as well as the 10^{th}, 25^{th}, 75^{th}, and 90^{th} percentiles.

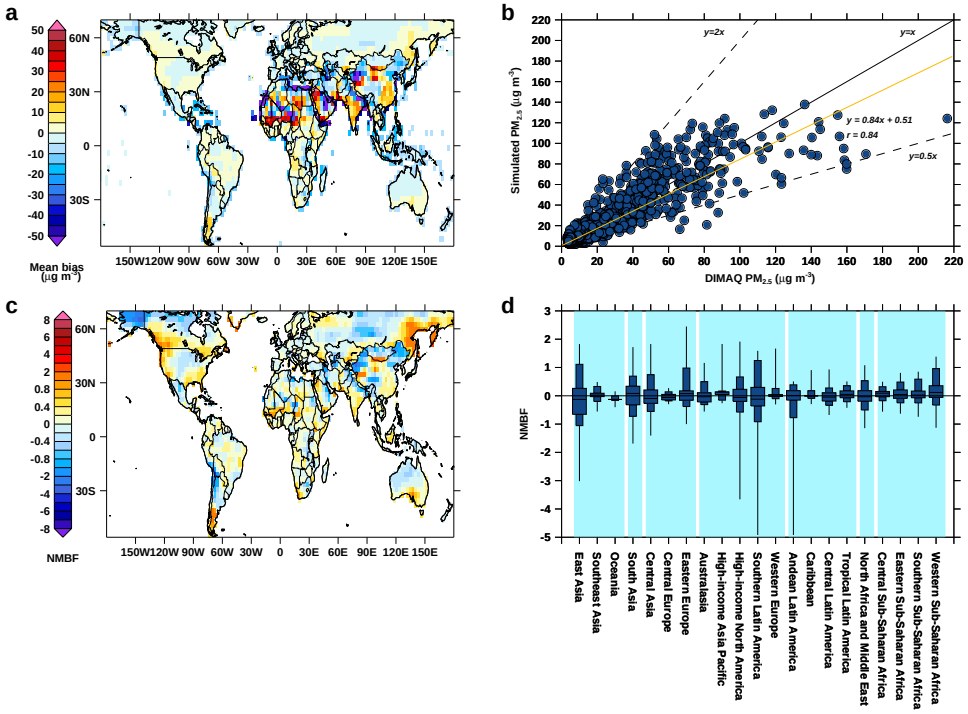

FIGURE A.4: Comparison of scaled TOMCAT 2015 simulated $PM_{2.5}$ concentrations with DIMAQ gridded estimate (averaged to the TOMCAT resolution). **a** Mean bias in the spatial distribution of annual mean surface $PM_{2.5}$ concentrations. **b** Comparison of $PM_{2.5}$ concentrations, best fit line (yellow line), 1:1 (solid black line), 2:1 and 1:2 (dashed black lines). Best fit line has slope = 0.56 and Pearson's correlation coefficient (r) = 0.83. **c** Spatial distribution of Normalised mean bias factor (NMBF), and **c** NMBF box and whisker by sub-region, showing the minimum, maximum and median distribution values, as well as the 10^{th}, 25^{th}, 75^{th}, and 90^{th} percentiles.

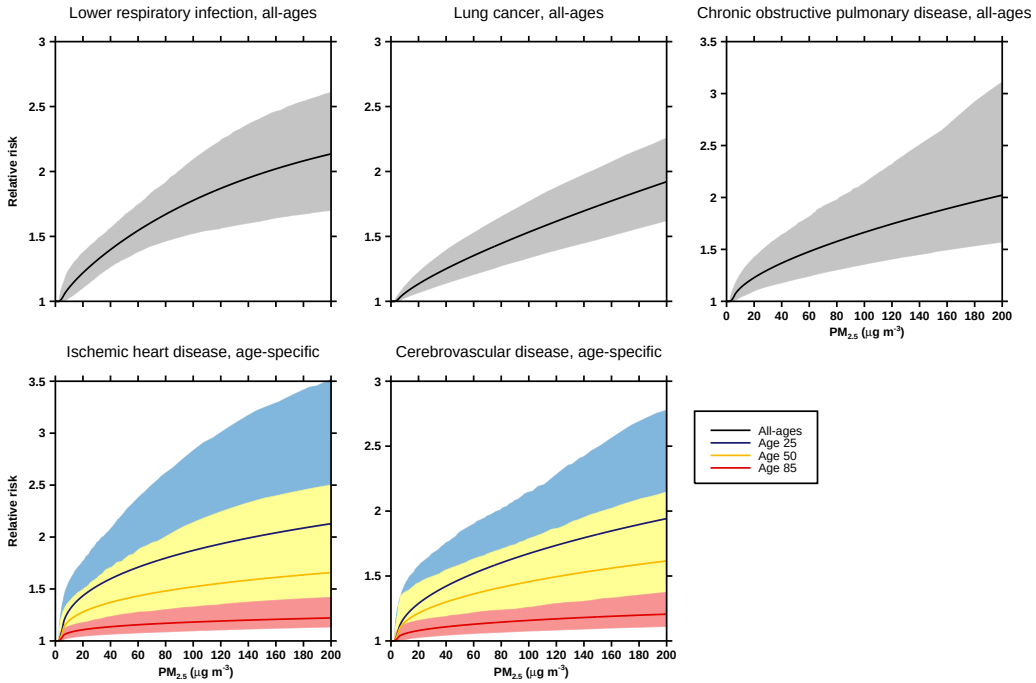

FIGURE A.5: Integrated-exposure response (IER) relationships used to relate long-term $PM_{2.5}$ exposure to mortality to cause-specific disease in the form of relative risk (RR) estimates. Cause-specific disease RR estimates include all-ages lower respiratory infections, lung cancer, chronic obstructive pulmonary disease, and age-specific ischaemic heart disease and cerebrovascular disease (ischaemic stroke and haemorrhagic stroke). The 95% confidence interval is represented by the coloured shading.

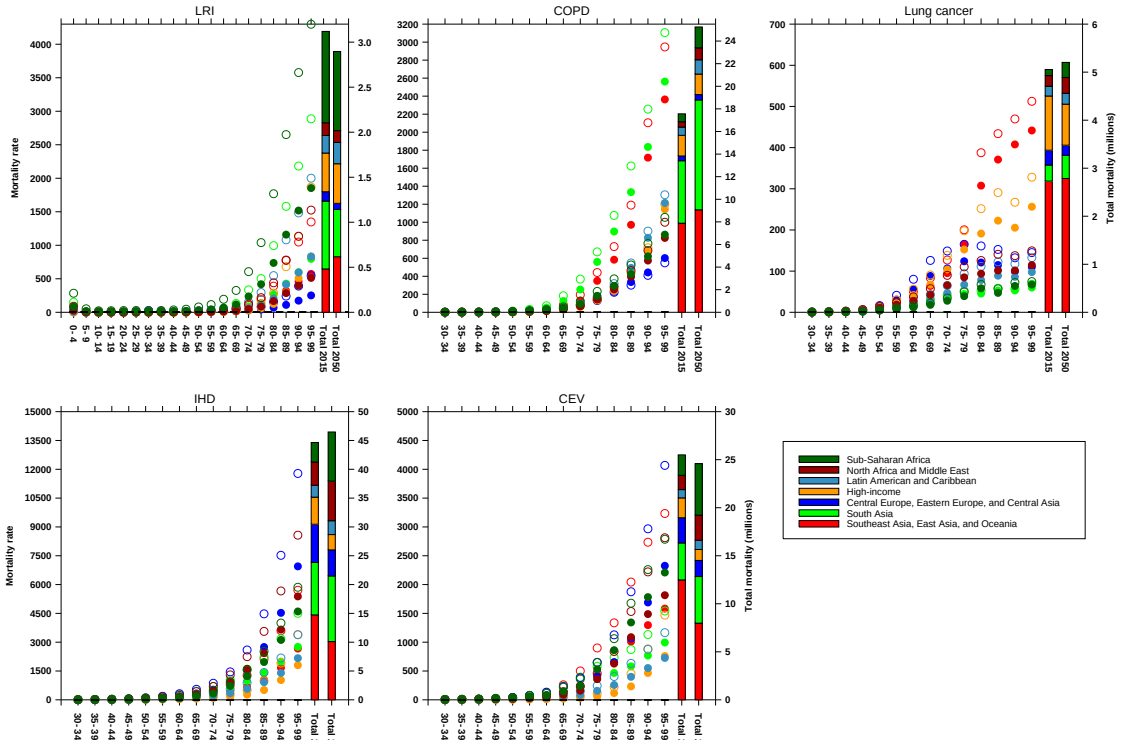

FIGURE A.6: Cause-specific diseases per age group in the base case of the International Futures model per super regions defined in (Figure A.1) including lower respiratory infections (LRI), chronic obstructive pulmonary disease (COPD), Lung cancer, and cardiovascular diseases: ischaemic heart disease (IHD) and cerebrovascular disease (CEV; ischaemic stroke and haemorrhagic stroke). Filled and open circles represent background disease mortality rate (per 100,000 deaths) in 2015 and 2050, respectively (left axis). Stacked bars represent total deaths per cause-specific diseases in 2015 and 2050 (right axis).

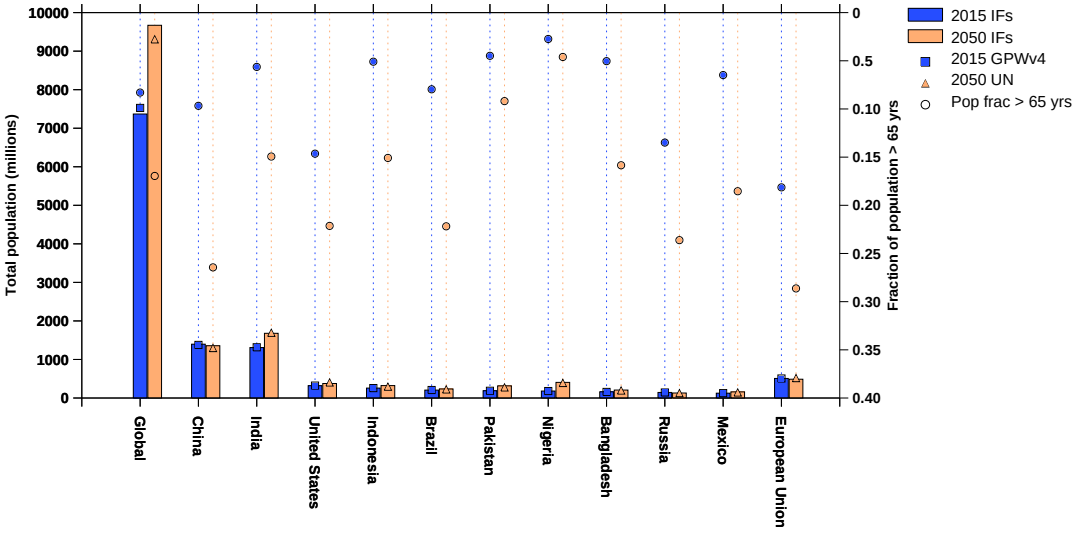

FIGURE A.7: Population estimates in the base case of the International Futures (IFs) model. Bars show IFs total population for ten populous countries, while square and triangle symbols represent UN-adjusted GPWv4 (2015) and UN projections (2050). Filled circles represent fraction of IFs population over 65 years of age.

Region	Population-weighted $PM_{2.5}$			Fraction of population	
	2050	Residential	Residential fraction (%)	> AQG (%)	> IT-1 (%)
Global	41 (4.5,12.3%)	6.5(-1.9,-22.7%)	15.9(-7.2)	90.4(-0.0)	48.8(3.5)
East and Southeast Asia, and Oceania					
East Asia	43.8 (-10,-18.7%)	6.6(-11.5,-63.6%)	15.1(-18.6)	99.6(0.0)	79.3(-1.6)
Southeast Asia	24.1 (3.2,15.5%)	3.5(0.1,3.9%)	14.5(-1.6)	93.7(2.1)	13.0(5.5)
Oceania	8.7 (0.4,4.7%)	0.1(0.01,27.5%)	1.1(0.2)	28.1(0.6)	0.0(0.0)
South Asia					
South Asia	76.2 (21.6,39.7%)	16.4(1.2,7.8%)	21.6(-6.4)	100.0(0.0)	91.3(5.6)
Central and Eastern Europe, and Central Asia					
Central Asia	26.4 (2.3,9.5%)	1.2(0.2,26.6%)	4.4(0.6)	96.7(0.9)	23.5(5.9)
Central Europe	16.1 (-3.7,-18.5%)	2.5(-1.9,-43.6%)	15.6(-6.9)	100(0.0)	0.0(0.0)
Eastern Europe	14.2 (-0.4,-2.4%)	1.3(-0.5,-29.9%)	9.0(-3.5)	92.4(1.9)	0.0(-0.0)
High-income					
Australasia	6.8 (-0.1,-1.4%)	0.01(-0.01,-41.6%)	0.4(-0.3)	0.1(0.0)	0.0(0.0)
High-income Asia Pacific	14.0 (-2.0,-12.5%)	1.2(-2.6,-68.6%)	8.5(-15.2)	92.8(-3.5)	0.0(0.0)
High-income North America	8.0 (-1.3,-13.6%)	0.4(-0.1,-24.0%)	5.5(-0.8)	20.4(-14.2)	0.0(0.0)
Southern Latin America	10.9 (0,0.3%)	0.4(0.01,5.7%)	3.8(0.2)	40.8(-0.7)	0.0(0.0)
Western Europe	10.4 (-1.5,-13.0%)	0.6(-0.6,-48.6%)	6.2(-4.3)	48.4(-19.6)	0.3(0.1)
Latin America and Caribbean					
Andean Latin America	15.7 (-0.1,-0.4%)	0.8(0.3,49.7%)	5.1(1.7)	90.7(-2.3)	0.7(0.0)
Caribbean	14.3 (-0.5,-3.6%)	0.3(0.0,18.2%)	2.0(0.4)	99.3(0.1)	0.0(0.0)
Central Latin America	18.5 (-0.6,-3.2%)	1.3(0.1,7.8%)	6.8(0.7)	95.4(0.3)	2.2(-0.3)
Tropical Latin America	9.5 (0.2,2.3%)	0.4(0.0,10.6%)	4.3(0.3)	32.8(2.4)	0.0(0.0)
North Africa and Middle East					
North Africa and Middle East	44.6 (1.7,4%)	1.5(-0.1,-6.6%)	3.4(-0.4)	100(0.0)	63.8(10.0)
Sub-Saharan Africa					
Central Sub-Saharan Africa	32.3 (1.4,4.6%)	5.3(1.5,38.9%)	16.4(4.1)	100(0.0)	33.3(6.7)
Eastern Sub-Saharan Africa	30.0 (1.6,5.5%)	7.1(0.8,12.9%)	23.5(1.5)	99.8(0.0)	30.3(3.9)
Southern Sub-Saharan Africa	16.2 (0.2,1.2%)	2.9(0.9,47.6%)	17.9(5.6)	99.5(0.5)	0.0(0.0)
Western Sub-Saharan Africa	48.1 (2.2,4.8%)	3.2(0.3,8.7%)	6.6(0.2)	100(0.0)	63.7(3.5)

TABLE A.1: Simulated values in 2050 under the reference scenario with associated changes (in parenthesis), relative to 2015. Second column: population-weighted $PM_{2.5}$ (μg m^{-3}) with associated changes (absolute and percentage, respectively). Third column: population-weighted $PM_{2.5}$ due to residential emissions (μg m^{-3}) with associated changes (absolute and percentage, respectively). Fourth column: percentage of mean population-weighted $PM_{2.5}$ concentrations due to residential emissions with associated changes (percentage point). Fifth column: percentage of regional population exposed to levels above the WHO air quality guideline (AQG) standard of annual mean $PM_{2.5}$ (10 μg m^{-3}) with associated changes (percentage point). Sixth column: percentage of regional population exposed to levels above the WHO interim target 1 (IT-1) standard of annual mean $PM_{2.5}$ (35 μg m^{-3}) with associated changes (percentage point).

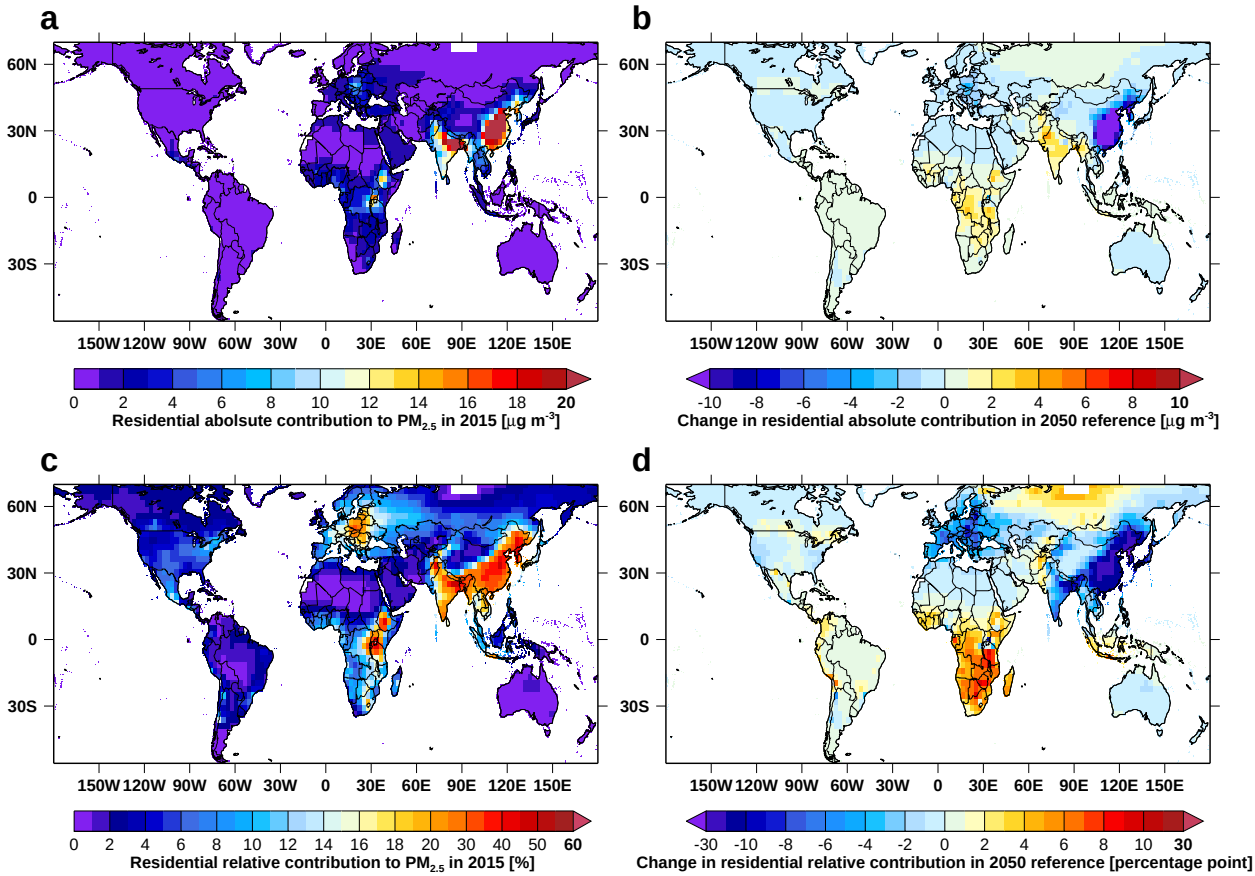

FIGURE A.8: Absolute and relative contribution of residential combustion emissions to annual mean surface $PM_{2.5}$ concentrations in 2015 **a** and **c** respectively, and change in the 2050 reference scenario **b** and **d**, relative to 2015, respectively.

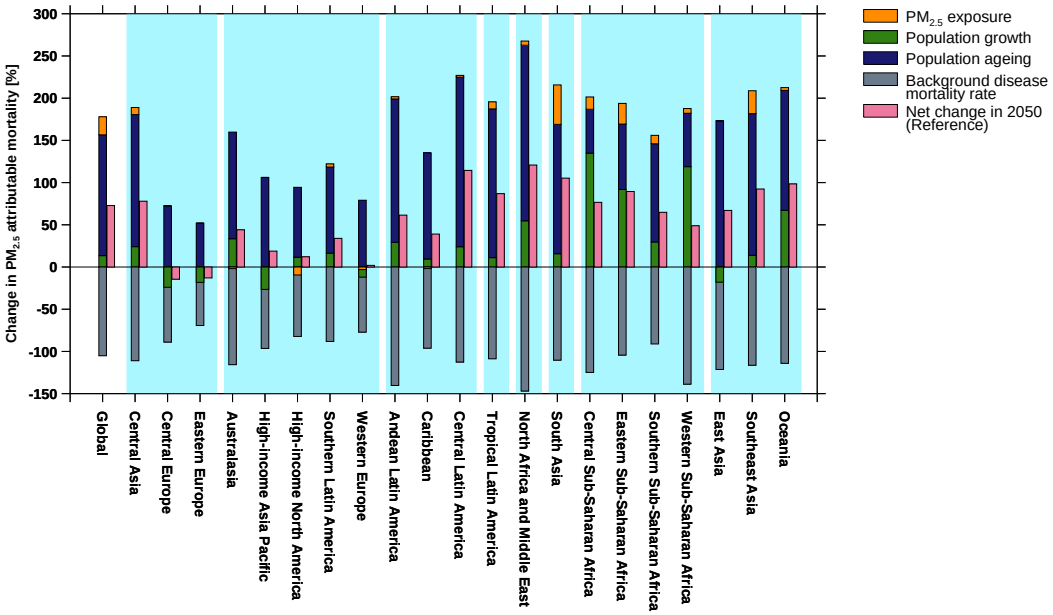

FIGURE A.9: Change in attributable mortality in the 2050 reference scenario (relative to 2015) with corresponding change in factor contributions that influence the overall change in attributable mortality.

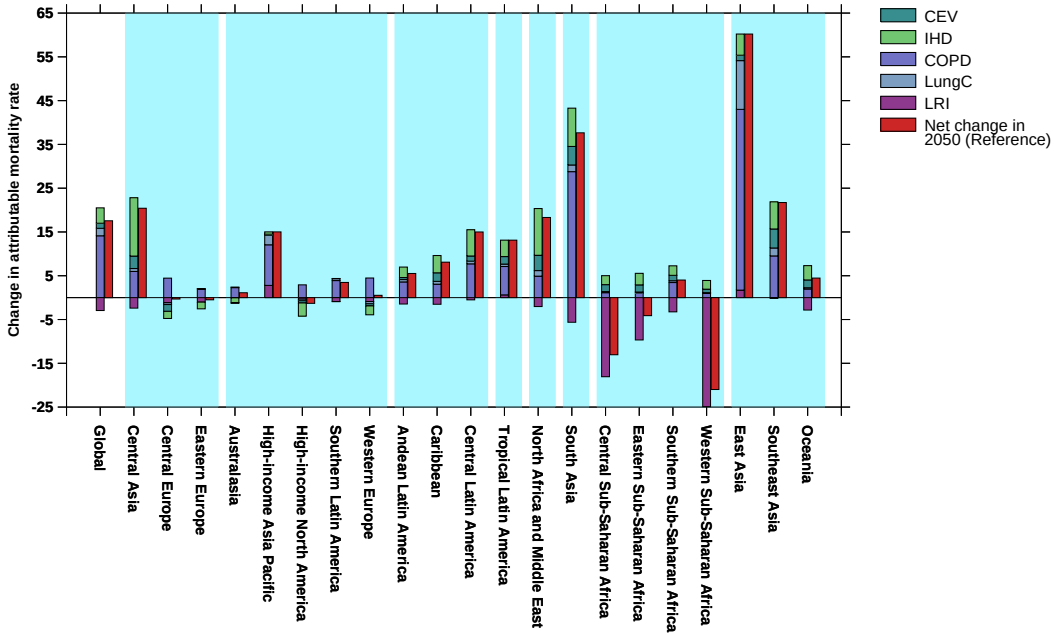

FIGURE A.10: Change in attributable per capita (e.g., crude) mortality rates (deaths per 10^5) in the 2050 reference per cause-specific disease: lower respiratory infections (LRI), chronic obstructive pulmonary disease (COPD), Lung cancer, and cardiovascular diseases: ischaemic heart disease (IHD) and cerebrovascular disease (CEV; ischaemic stroke and haemorrhagic stroke).

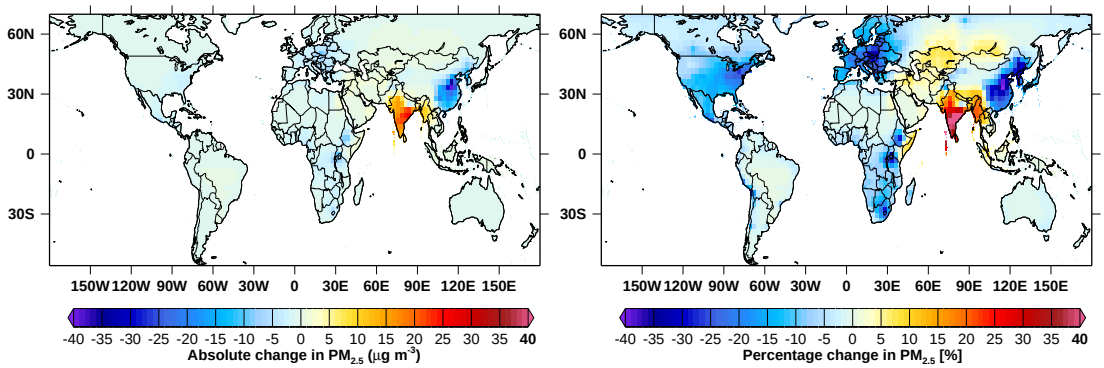

FIGURE A.11: Absolute (left) and percentage (right) change in annual mean surface $PM_{2.5}$ concentrations in 2050 under the clean residential scenario relative to the present-day 2015.

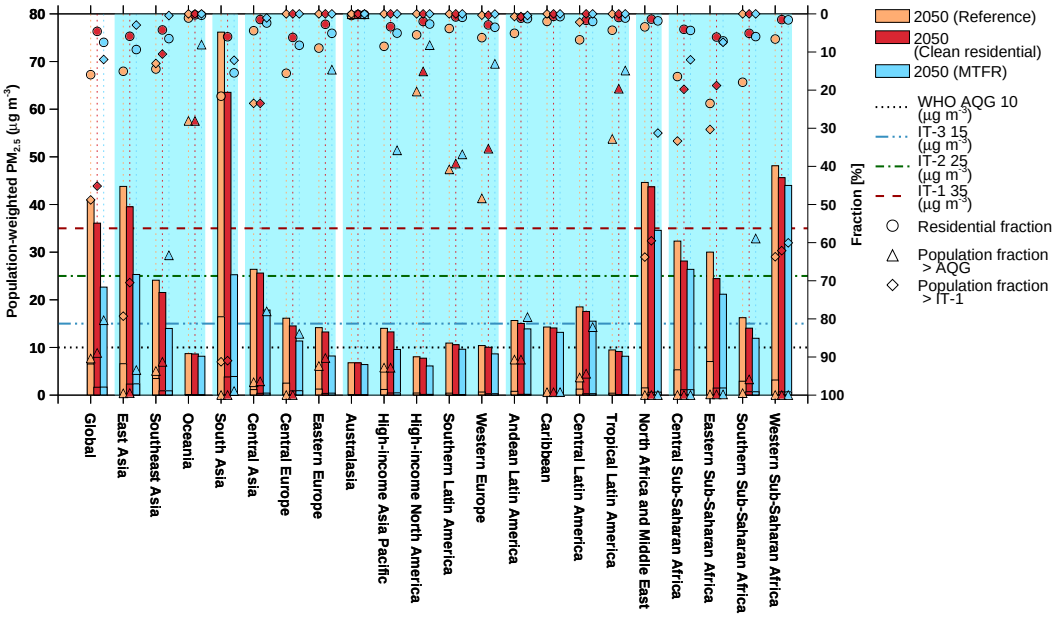

FIGURE A.12: Annual mean population-weighted $PM_{2.5}$ concentrations in 2050 under the reference, clean residential and maximum technical feasible reduction (MTFR) scenarios per sub region (bars). Horizontal lines in bars represent population-weighted $PM_{2.5}$ concentrations due to residential combustion emissions (left axis). Also shown is the fraction or relative contribution of residential emissions to population-weighted $PM_{2.5}$ concentrations, and fraction of the population in each region exposed to $PM_{2.5}$ concentration levels above the WHO annual mean standards including the air quality guideline (AQG) (10 µg m^{-3}) and interim target 1 (IT-1) (35 µg m^{-3}) (right axis).

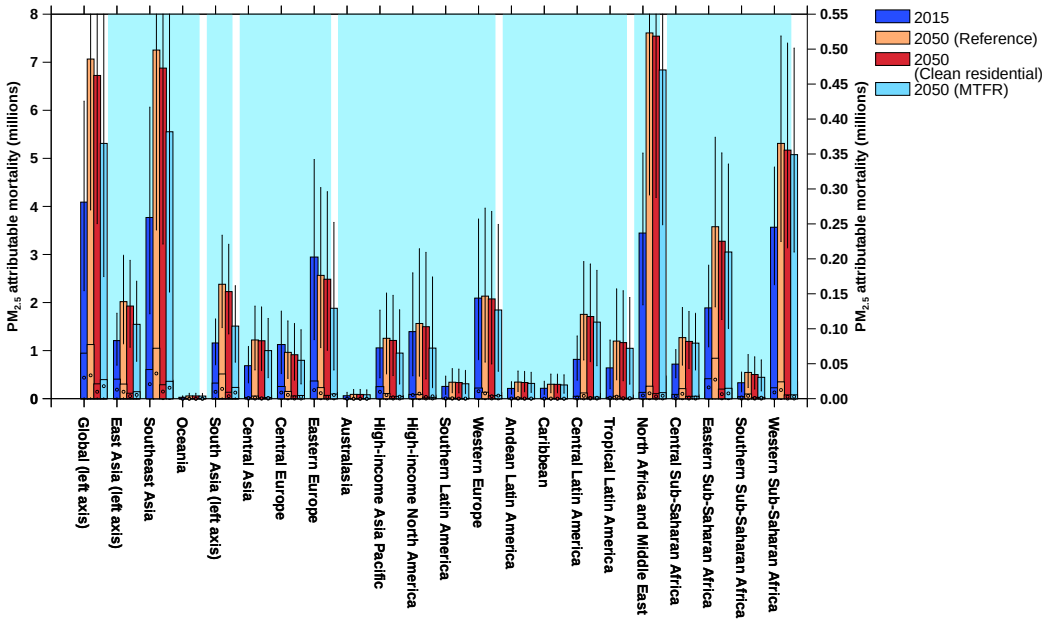

FIGURE A.13: Mortality attributable (millions) to long-term ambient $PM_{2.5}$ exposure in 2015 and 2050 under the reference, clean residential and MTFR scenarios (bars). Horizontal lines in bars represent mortality attributable to residential emissions (attribution method), while small circles in bars represent averted mortality due to the removal residential emissions (subtraction method) (see Section A.4). Note that the left axis is used for global, East Asia and South Asia, while the right axis is for all other regions.

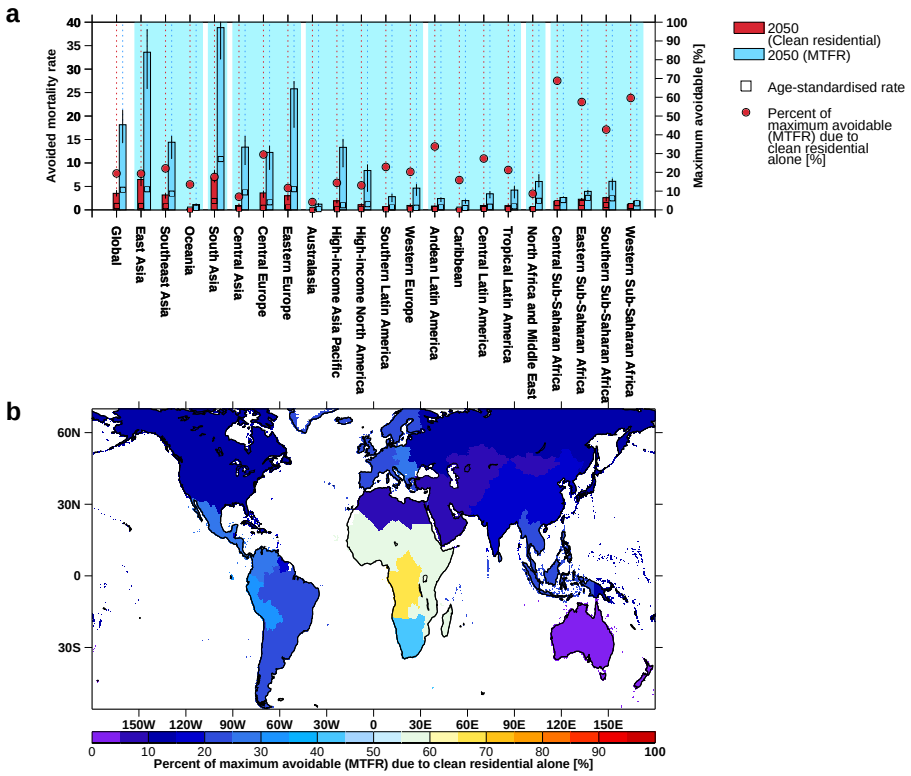

FIGURE A.14: Avoided attributable mortality rates (deaths per 10^5) in 2050 due to clean residential scenario maximum feasible reduction (MTFR) scenario for per capita (bars) and age-standardised **a**. Also shown is the maximum avoidable mortality rate potential due to the clean residential scenario (i.e., clean residential avoided / MTFR avoided) (**a** (left axis) and **b**).

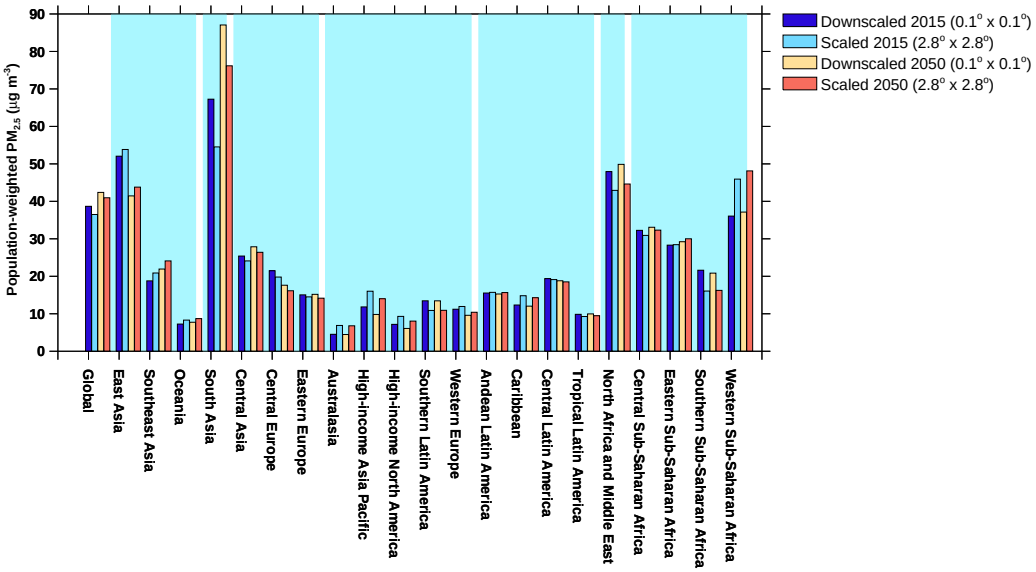

FIGURE A.15: Annual mean population-weighted $PM_{2.5}$ concentrations in 2015 and 2050 reference using the national scaling approach at $2.8^\circ \times 2.8^\circ$ reported in the main paper and a widely used downscaling approach at $0.1^\circ \times 0.1^\circ$ (see Section A.3 for both approaches)

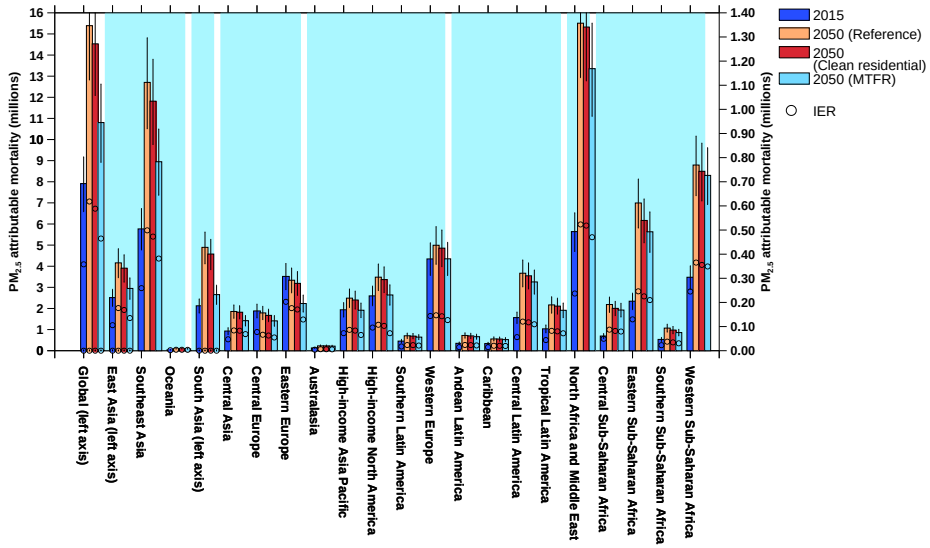

FIGURE A.16: Mortality attributable (millions) to long-term ambient $PM_{2.5}$ exposure using the alternative exposure-response relationship the Global Mortality Exposure Mortality Model (GEMM) (bars), mortality provided by the integrated exposure-response (IER) for comparison (circles). Attributable mortality estimates are shown from 2015 and 2050 scenarios: reference, clean residential and MTFR scenarios (bars). Horizontal lines in bars represent residential mortality using the 'attribution' method. Note that the left axis is used for global, East Asia and South Asia, while the right axis is for all other regions.

Bibliography

Amann, Markus et al. (2011). "Cost-effective control of air quality and greenhouse gases in Europe: Modeling and policy applications". In: *Environmental Modelling & Software* 26.12, pp. 1489–1501.

Andres, RJ and AD Kasgnoc (1998). "A time-averaged inventory of subaerial volcanic sulfur emissions". In: *Journal of Geophysical Research: Atmospheres* 103.D19, pp. 25251–25261.

Archer-Nicholls, Scott et al. (2016). "The regional impacts of cooking and heating emissions on ambient air quality and disease burden in China". In: *Environmental science & technology* 50.17, pp. 9416–9423.

Burnett, Richard et al. (2018). "Global estimates of mortality associated with long-term exposure to outdoor fine particulate matter". In: *Proceedings of the National Academy of Sciences*, p. 201803222.

Burnett, Richard T et al. (2014). "An integrated risk function for estimating the global burden of disease attributable to ambient fine particulate matter exposure". In: *Environmental health perspectives* 122.4, p. 397.

Chowdhury, Sourangsu, Sagnik Dey, and Kirk R Smith (2018). "Ambient PM 2.5 exposure and expected premature mortality to 2100 in India under climate change scenarios". In: *Nature Communications* 9.1, p. 318.

Conibear, Luke et al. (2018). "Residential energy use emissions dominate health impacts from exposure to ambient particulate matter in India". In: *Nature communications* 9.1, p. 617.

Doxsey-Whitfield, Erin et al. (2015). "Taking advantage of the improved availability of census data: a first look at the gridded population of the world, version 4". In: *Papers in Applied Geography* 1.3, pp. 226–234.

GBD MAPS Working Group (2016). "Burden of Disease Attributable to Coal-Burning and Other Major Sources of Air Pollution in China". In: 21.

— (2018). "Burden of Disease Attributable to Major Air Pollution Sources in India". In: 20.

Guenther, A et al. (2006). "Estimates of global terrestrial isoprene emissions using MEGAN (Model of Emissions of Gases and Aerosols from Nature)". In: *Atmospheric Chemistry and Physics* 6.11, pp. 3181–3210.

Halmer, Martina M, H-U Schmincke, and H-F Graf (2002). "The annual volcanic gas input into the atmosphere, in particular into the stratosphere: a global data set for the past 100 years". In: *Journal of Volcanology and Geothermal Research* 115.3-4, pp. 511–528.

Hughes, Barry B et al. (2011). "Projections of global health outcomes from 2005 to 2060 using the International Futures integrated forecasting model". In: *Bulletin of the World Health Organization* 89.7, pp. 478–486.

IEA (2012). *Energy technology perspectives*. Tech. rep.

Kettle, AJ and MO Andreae (2000). "Flux of dimethylsulfide from the oceans: A comparison of updated data sets and flux models". In: *Journal of Geophysical Research: Atmospheres* 105.D22, pp. 26793–26808.

Kodros, John K et al. (2016). "Global burden of mortalities due to chronic exposure to ambient PM2. 5 from open combustion of domestic waste". In: *Environmental Research Letters* 11.12, p. 124022.

Lacey, Forrest G et al. (2017). "Transient climate and ambient health impacts due to national solid fuel cookstove emissions". In: *Proceedings of the National Academy of Sciences* 114.6, pp. 1269–1274.

Malm, William C et al. (1994). "Spatial and seasonal trends in particle concentration and optical extinction in the United States". In: *Journal of Geophysical Research: Atmospheres* 99.D1, pp. 1347–1370.

McNorton, Joe et al. (2016). "Role of OH variability in the stalling of the global atmospheric CH 4 growth rate from 1999 to 2006". In: *Atmospheric Chemistry and Physics* 16.12, pp. 7943–7956.

Monks, Sarah A et al. (2017). "The TOMCAT global chemical transport model v1. 6: description of chemical mechanism and model evaluation". In: *Geoscientific Model Development* 10.8, p. 3025.

Shaddick, Gavin et al. (2018). "Data integration model for air quality: a hierarchical approach to the global estimation of exposures to ambient air pollution". In: *Journal of the Royal Statistical Society: Series C (Applied Statistics)* 67.1, pp. 231–253.

Silva, Raquel A et al. (2016). "The effect of future ambient air pollution on human premature mortality to 2100 using output from the ACCMIP model ensemble". In: *Atmospheric chemistry and physics* 16.15, pp. 9847–9862.

Silva, Raquel A et al. (2017). "Future global mortality from changes in air pollution attributable to climate change". In: *Nature Climate Change* 7.9, p. 647.

Stockwell, DZ et al. (1999). "Modelling NOx from lightning and its impact on global chemical fields". In: *Atmospheric Environment* 33.27, pp. 4477–4493.

Stohl, Andreas et al. (2015). "Evaluating the climate and air quality impacts of short-lived pollutants". In: *Atmospheric Chemistry and Physics* 15.18, pp. 10529–10566.

UN (2011). "World Population Prospects: The 2010 Revision". In: *New York: United Nations Population Division, Department of Economic and Social Affairs*.

Van Der Werf, Guido R et al. (2004). "Continental-scale partitioning of fire emissions during the 1997 to 2001 El Nino/La Nina period". In: *Science* 303.5654, pp. 73–76.

Weagle, Crystal L et al. (2018). "Global Sources of Fine Particulate Matter: Interpretation of PM2. 5 Chemical Composition Observed by SPARTAN using a Global Chemical Transport Model". In: *Environmental science & technology*.

West, J Jason et al. (2013). "Co-benefits of mitigating global greenhouse gas emissions for future air quality and human health". In: *Nature climate change* 3.10, p. 885.

WHO (2016). "WHO global urban ambient air pollution database (update 2016)". In: *Geneva. Diunduh*.

Yu, Shaocai et al. (2006). "New unbiased symmetric metrics for evaluation of air quality models". In: *Atmospheric Science Letters* 7.1, pp. 26–34.

References

Ailshire, Jennifer A and Eileen M Crimmins (2014). "Fine particulate matter air pollution and cognitive function among older US adults". In: *American journal of epidemiology* 180.4, pp. 359–366.

Albrecht, Bruce A (1989). "Aerosols, cloud microphysics, and fractional cloudiness". In: *Science* 245.4923, pp. 1227–1230.

Allen, Robert J, William Landuyt, and Steven T Rumbold (2016). "An increase in aerosol burden and radiative effects in a warmer world". In: *Nature Climate Change* 6.3, p. 269.

Amann, M, Z Klimont, and K Kupiainen (2011). *Integrated assessment of black carbon and tropospheric ozone*.

Amann, Markus, Zbigniew Klimont, and Fabian Wagner (2013). "Regional and global emissions of air pollutants: recent trends and future scenarios". In: *Annual Review of Environment and Resources* 38, pp. 31–55.

Andres, RJ and AD Kasgnoc (1998). "A time-averaged inventory of subaerial volcanic sulfur emissions". In: *Journal of Geophysical Research: Atmospheres* 103.D19, pp. 25251–25261.

Anenberg, Susan C et al. (2012). "Global air quality and health co-benefits of mitigating near-term climate change through methane and black carbon emission controls". In: *Environmental Health Perspectives* 120.6, p. 831.

Anenberg, Susan C et al. (2013). *Cleaner cooking solutions to achieve health, climate, and economic cobenefits*.

Archer-Nicholls, Scott et al. (2016). "The regional impacts of cooking and heating emissions on ambient air quality and disease burden in China". In: *Environmental science & technology* 50.17, pp. 9416–9423.

Arnold, SR, MP Chipperfield, and MA Blitz (2005). "A three-dimensional model study of the effect of new temperature-dependent quantum yields for acetone photolysis". In: *Journal of Geophysical Research: Atmospheres* 110.D22.

Atkinson, R et al. (1992). "Evaluated kinetic and photochemical data for atmospheric chemistry". In: *Journal of Physical and Chemical Reference Data;(United States)* 21.6.

Atkinson, RW et al. (2014). "Epidemiological time series studies of PM2. 5 and daily mortality and hospital admissions: a systematic review and meta-analysis". In: *Thorax*, thoraxjnl–2013.

Atkinson, RW et al. (2016). "Long-term exposure to ambient ozone and mortality: a quantitative systematic review and meta-analysis of evidence from cohort studies". In: *BMJ open* 6.2, e009493.

Aung, Ther W et al. (2016). "Health and climate-relevant pollutant concentrations from a carbon-finance approved cookstove intervention in rural India". In: *Environmental science & technology* 50.13, pp. 7228–7238.

Bailis, Rob et al. (2017). "Getting the numbers right: revisiting woodfuel sustainability in the developing world". In: *Environmental Research Letters* 12.11, p. 115002.

Bailis, Robert et al. (2015). "The carbon footprint of traditional woodfuels". In: *Nature Climate Change* 5.3, p. 266.

Bellouin, Nicolas et al. (2011). "Aerosol forcing in the Climate Model Intercomparison Project (CMIP5) simulations by HadGEM2-ES and the role of ammonium nitrate". In: *Journal of Geophysical Research: Atmospheres* 116.D20.

Bellouin, Nicolas et al. (2013). "Impact of the modal aerosol scheme GLOMAP-mode on aerosol forcing in the Hadley Centre Global Environmental Model". In: *Atmospheric Chemistry and Physics* 13.6, pp. 3027–3044.

Beverland, Iain J et al. (2012). "A comparison of short-term and long-term air pollution exposure associations with mortality in two cohorts in Scotland". In: *Environmental health perspectives* 120.9, p. 1280.

Bond, Tami C et al. (2013). "Bounding the role of black carbon in the climate system: A scientific assessment". In: *Journal of Geophysical Research: Atmospheres* 118.11, pp. 5380–5552.

Bonjour, Sophie et al. (2013). "Solid fuel use for household cooking: country and regional estimates for 1980–2010". In: *Environmental health perspectives* 121.7, p. 784.

Boucher, Olivier et al. (2013). "Clouds and aerosols". In: *Climate change 2013: the physical science basis. Contribution of Working Group I to the Fifth Assessment Report of the Intergovernmental Panel on Climate Change*. Cambridge University Press, pp. 571–657.

Brauer, Michael et al. (2015). "Ambient air pollution exposure estimation for the global burden of disease 2013". In: *Environmental science & technology* 50.1, pp. 79–88.

Brown, Timothy J, Beth L Hall, and Anthony L Westerling (2004). "The impact of twenty-first century climate change on wildland fire danger in the western United States: an applications perspective". In: *Climatic change* 62.1-3, pp. 365–388.

Browse Jo, Ken Carslaw Lindsay Lee Carly Reddington Leighton Regayre Kirsty Pringle Jill Johnson S. Sangeeta J. Ogren J.Sherman C. Labuschagne O. L. Mayol-Bracero N. Mihalopoulos G. Kouvarakis R. Hillamo K. Sang-Woo R. Harrison U. Kaminski M. Kulmala S. Rodriguez U. Baltensperger P. Sherrer C. Monahan A. Marinoni P. Bonasoni R. Weller N. Kivekas J. Andriejauskiene K. Sellegri A. Gannett-Hallar P. Tunved David Cohen Ville Vakkari Richard Leaitch Tuumas Laurila A. Hyvarien C. Lunder M. Fiebig A. Asmi Patricia Quinn J. Johnson Anthony Clarke Timothy Bates Ernie Lewis Caroline Leck (2019). "Evaluating a Perturbed Parameter Ensemble against global aerosol observations to constrain parametric uncertainty: Is there an ideal aerosol model?" In: *In prep*.

Bruns, Emily A et al. (2016). "Identification of significant precursor gases of secondary organic aerosols from residential wood combustion". In: *Scientific reports* 6, p. 27881.

Burnett, Richard et al. (2018). "Global estimates of mortality associated with long-term exposure to outdoor fine particulate matter". In: *Proceedings of the National Academy of Sciences*, p. 201803222.

Burnett, Richard T et al. (2014). "An integrated risk function for estimating the global burden of disease attributable to ambient fine particulate matter exposure". In: *Environmental health perspectives* 122.4, p. 397.

Butt, EW et al. (2016). "The impact of residential combustion emissions on atmospheric aerosol, human health, and climate". In: *Atmospheric Chemistry and Physics* 16.2, pp. 873–905.

Butt, EW et al. (2017). "Global and regional trends in particulate air pollution and attributable health burden over the past 50 years". In: *Environmental Research Letters* 12.10, p. 104017.

Cacciottolo, M et al. (2017). "Particulate air pollutants, APOE alleles and their contributions to cognitive impairment in older women and to amyloidogenesis in experimental models". In: *Translational psychiatry* 7.1, e1022.

Cappa, Christopher D et al. (2012). "Radiative absorption enhancements due to the mixing state of atmospheric black carbon". In: *Science* 337.6098, pp. 1078–1081.

Chafe, Zoë et al. (2015). "Residential heating with wood and coal: health impacts and policy options in Europe and North America". In:

Chafe, Zoë A et al. (2014). "Household cooking with solid fuels contributes to ambient PM2. 5 air pollution and the burden of disease". In: *Environmental health perspectives* 122.12, p. 1314.

Chipperfield, MP (2006). "New version of the TOMCAT/SLIMCAT off-line chemical transport model: Intercomparison of stratospheric tracer experiments". In: *Quarterly Journal of the Royal Meteorological Society* 132.617, pp. 1179–1203.

Chowdhury, Sourangsu, Sagnik Dey, and Kirk R Smith (2018). "Ambient PM 2.5 exposure and expected premature mortality to 2100 in India under climate change scenarios". In: *Nature Communications* 9.1, p. 318.

Ciarelli, Giancarlo et al. (2017). "Constraining a hybrid volatility basis-set model for aging of wood-burning emissions using smog chamber experiments: a box-model study based on the VBS scheme of the CAMx model (v5. 40)". In: *Geoscientific Model Development* 10.6, p. 2303.

CIESIN (2005). *Gridded population of the world, version 3 (GPWv3): population density grid*.

Clark, S et al. (2017). "Adoption and use of a semi-gasifier cooking and water heating stove and fuel intervention in the Tibetan Plateau, China". In: *Environmental Research Letters* 12.7, p. 075004.

Cohen, Aaron J et al. (2004). "Urban air pollution". In: *Comparative quantification of health risks: global and regional burden of disease attributable to selected major risk factors* 2, pp. 1353–1433.

Cohen, Aaron J et al. (2017). "Estimates and 25-year trends of the global burden of disease attributable to ambient air pollution: an analysis of data from the Global Burden of Diseases Study 2015". In: *The Lancet* 389.10082, pp. 1907–1918.

Conibear, Luke et al. (2018a). "Residential energy use emissions dominate health impacts from exposure to ambient particulate matter in India". In: *Nature communications* 9.1, p. 617.

— (2018b). "Stringent emission control policies can provide large improvements in air quality and public health in India". In: *GeoHealth*.

Davies, Terry et al. (2005). "A new dynamical core for the Met Office's global and regional modelling of the atmosphere". In: *Quarterly Journal of the Royal Meteorological Society* 131.608, pp. 1759–1782.

Dee, Dick P et al. (2011). "The ERA-Interim reanalysis: Configuration and performance of the data assimilation system". In: *Quarterly Journal of the royal meteorological society* 137.656, pp. 553–597.

Denier Van Der Gon, HAC et al. (2015). "Particulate emissions from residential wood combustion in Europe–revised estimates and an evaluation". In: *Atmospheric Chemistry and Physics* 15.11, pp. 6503–6519.

Dentener, F et al. (2006). "Emissions of primary aerosol and precursor gases in the years 2000 and 1750 prescribed data-sets for AeroCom". In: *Atmospheric Chemistry and Physics* 6.12, pp. 4321–4344.

Dockery, Douglas W et al. (1993). "An association between air pollution and mortality in six US cities". In: *New England journal of medicine* 329.24, pp. 1753–1759.

Donahue, Neil M et al. (2011). "A two-dimensional volatility basis set: 1. organic-aerosol mixing thermodynamics". In: *Atmospheric Chemistry and Physics* 11.7, pp. 3303–3318.

Doxsey-Whitfield, Erin et al. (2015). "Taking advantage of the improved availability of census data: a first look at the gridded population of the world, version 4". In: *Papers in Applied Geography* 1.3, pp. 226–234.

Du, Yixing et al. (2016). "Air particulate matter and cardiovascular disease: the epidemiological, biomedical and clinical evidence". In: *Journal of thoracic disease* 8.1, E8.

Edwards, JM and A Slingo (1996). "Studies with a flexible new radiation code. I: Choosing a configuration for a large-scale model". In: *Quarterly Journal of the Royal Meteorological Society* 122.531, pp. 689–719.

Erisman, Jan Willem et al. (2008). "How a century of ammonia synthesis changed the world". In: *Nature Geoscience* 1.10, p. 636.

Erisman, JW and M Schaap (2004). "The need for ammonia abatement with respect to secondary PM reductions in Europe". In: *Environmental Pollution* 129.1, pp. 159–163.

Essery, RLH et al. (2003). "Explicit representation of subgrid heterogeneity in a GCM land surface scheme". In: *Journal of Hydrometeorology* 4.3, pp. 530–543.

EU, PEAN et al. (2008). "Directive 2008/50/EC of the European Parliament and of the Council of 21 May 2008 on ambient air quality and cleaner air for Europe". In: *Official Journal of the European Union*.

Ezzati, Majid et al. (2003). "Estimates of global and regional potentil health gains from reducing muliple major risk factors". In: *The Lancet* 362.9380, pp. 271–280.

Fagerli, Hilde and Wenche Aas (2008). "Trends of nitrogen in air and precipitation: Model results and observations at EMEP sites in Europe, 1980–2003". In: *Environmental Pollution* 154.3, pp. 448–461.

Feigin, V et al. (2016). "Global, regional, and national comparative risk assessment of 79 behavioural, environmental and occupational, and metabolic risks or clusters of risks, 1990-2015: a systematic analysis for the Global Burden of Disease Study 2015". In: *The Lancet* 388.10053, pp. 1659–1724.

Fiore, Arlene M, Vaishali Naik, and Eric M Leibensperger (2015). "Air quality and climate connections". In: *Journal of the Air & Waste Management Association* 65.6, pp. 645–685.

Fleischer, Nancy L et al. (2014). "Outdoor air pollution, preterm birth, and low birth weight: analysis of the world health organization global survey on maternal and perinatal health". In: *Environmental health perspectives* 122.4, p. 425.

Foreman, Kyle J et al. (2018). "Forecasting life expectancy, years of life lost, and all-cause and cause-specific mortality for 250 causes of death: reference and alternative scenarios for 2016–40 for 195 countries and territories". In: *The Lancet* 392.10159, pp. 2052–2090.

Forouzanfar, Mohammad H et al. (2015). "Global, regional, and national comparative risk assessment of 79 behavioural, environmental and occupational, and metabolic risks or clusters of risks in 188 countries, 1990–2013: a systematic analysis for the Global Burden of Disease Study 2013". In: *The Lancet* 386.10010, pp. 2287–2323.

Fuller, Gary W et al. (2013). "New Directions: Time to tackle urban wood burning?" In: *Atmospheric Environment* 68, pp. 295–296.

Gakidou, Emmanuela et al. (2017). "Global, regional, and national comparative risk assessment of 84 behavioural, environmental and occupational, and metabolic risks or clusters of risks, 1990–2016: a systematic analysis for the Global Burden of Disease Study 2016". In: *Lancet* 390.10100, pp. 1345–1422.

GBD MAPS Working Group (2016). "Burden of Disease Attributable to Coal-Burning and Other Major Sources of Air Pollution in China". In: 21.

— (2018). "Burden of Disease Attributable to Major Air Pollution Sources in India". In: 20.

Giannadaki, Despina, Jos Lelieveld, and Andrea Pozzer (2016). "Implementing the US air quality standard for PM 2.5 worldwide can prevent millions of premature deaths per year". In: *Environmental Health* 15.1, p. 88.

Goldemberg, Jose et al. (2018). "Household air pollution, health, and climate change–clearing the air". In: *Environmental Research Letters*.

Gong, SL (2003). "A parameterization of sea-salt aerosol source function for sub-and super-micron particles". In: *Global biogeochemical cycles* 17.4.

Gordon, Hamish et al. (2017). "Causes and importance of new particle formation in the present-day and pre-industrial atmospheres". In: *Journal of Geophysical Research: Atmospheres*.

Gordon, Hamish et al. (2018). "Large simulated radiative effects of smoke in the south-east Atlantic". In: *Atmospheric Chemistry and Physics* 18.20, pp. 15261–15289.

Granier, Claire et al. (2011). "Evolution of anthropogenic and biomass burning emissions of air pollutants at global and regional scales during the 1980–2010 period". In: *Climatic Change* 109.1-2, p. 163.

Grieshop, Andrew P, Julian D Marshall, and Milind Kandlikar (2011). "Health and climate benefits of cookstove replacement options". In: *Energy Policy* 39.12, pp. 7530–7542.

Grieshop, Andrew P et al. (2017). "Emission factors of health-and climate-relevant pollutants measured in home during a carbon-finance-approved cookstove intervention in rural India". In: *GeoHealth* 1.5, pp. 222–236.

Guenther, Alex et al. (1995). "A global model of natural volatile organic compound emissions". In: *Journal of Geophysical Research: Atmospheres* 100.D5, pp. 8873–8892.

Halmer, Martina M, H-U Schmincke, and H-F Graf (2002). "The annual volcanic gas input into the atmosphere, in particular into the stratosphere: a global data set for the past 100 years". In: *Journal of Volcanology and Geothermal Research* 115.3-4, pp. 511–528.

Haluza, Daniela et al. (2012). "Estimated health impact of a shift from light fuel to residential wood-burning in Upper Austria". In: *Journal of Exposure Science and Environmental Epidemiology* 22.4, p. 339.

Hauglustaine, DA, Y Balkanski, and M Schulz (2014). "A global model simulation of present and future nitrate aerosols and their direct radiative forcing of climate". In: *Atmos. Chem. Phys* 14.20, pp. 11031–11063.

He, Dian et al. (2017). "Association between particulate matter 2.5 and diabetes mellitus: A meta-analysis of cohort studies". In: *Journal of diabetes investigation* 8.5, pp. 687–696.

Health Metrics, Institute for and Evaluation (IHME) (2015). *GBD compare*.

Hewitt, HT et al. (2011). "Design and implementation of the infrastructure of HadGEM3: The next-generation Met Office climate modelling system". In: *Geoscientific Model Development* 4.2, pp. 223–253.

Hoesly, Rachel M et al. (2018). "Historical (1750–2014) anthropogenic emissions of reactive gases and aerosols from the Community Emissions Data System (CEDS)". In: *Geoscientific Model Development* 11.1, pp. 369–408.

Holtslag, AAM and BA Boville (1993). "Local versus nonlocal boundary-layer diffusion in a global climate model". In: *Journal of Climate* 6.10, pp. 1825–1842.

Hoppel, WA et al. (1994). "Marine boundary layer measurements of new particle formation and the effects nonprecipitating clouds have on aerosol size distribution". In: *Journal of Geophysical Research: Atmospheres* 99.D7, pp. 14443–14459.

Hughes, Barry B et al. (2011). "Projections of global health outcomes from 2005 to 2060 using the International Futures integrated forecasting model". In: *Bulletin of the World Health Organization* 89.7, pp. 478–486.

Hurrell, James W et al. (2008). "A new sea surface temperature and sea ice boundary dataset for the Community Atmosphere Model". In: *Journal of Climate* 21.19, pp. 5145–5153.

IEA (2012). *Energy technology perspectives*. Tech. rep.

— (2016). "World Energy Outlook Special Report". In:

Jacob, Daniel J and Darrell A Winner (2009). "Effect of climate change on air quality". In: *Atmospheric environment* 43.1, pp. 51–63.

Jacobson, Mark Z (2001). "Strong radiative heating due to the mixing state of black carbon in atmospheric aerosols". In: *Nature* 409.6821, p. 695.

Jerrett, Michael et al. (2009). "Long-term ozone exposure and mortality". In: *New England Journal of Medicine* 360.11, pp. 1085–1095.

Jetter, James et al. (2012). "Pollutant emissions and energy efficiency under controlled conditions for household biomass cookstoves and implications for metrics useful in setting international test standards". In: *Environmental science & technology* 46.19, pp. 10827–10834.

Jetter, James J and Peter Kariher (2009). "Solid-fuel household cook stoves: characterization of performance and emissions". In: *Biomass and Bioenergy* 33.2, pp. 294–305.

Johnson, Jill S et al. (2018). "The importance of comprehensive parameter sampling and multiple observations for robust constraint of aerosol radiative forcing". In: *Atmospheric Chemistry and Physics* 18.17, pp. 13031–13053.

Jones, Andy et al. (2001). "Indirect sulphate aerosol forcing in a climate model with an interactive sulphur cycle". In: *Journal of Geophysical Research: Atmospheres* 106.D17, pp. 20293–20310.

Jonson, Jan E et al. (2017). "Impact of excess NOx emissions from diesel cars on air quality, public health and eutrophication in Europe". In: *Environmental Research Letters* 12.9, p. 094017.

Kettle, AJ and MO Andreae (2000). "Flux of dimethylsulfide from the oceans: A comparison of updated data sets and flux models". In: *Journal of Geophysical Research: Atmospheres* 105.D22, pp. 26793–26808.

Kipling, Zak et al. (2016). "What controls the vertical distribution of aerosol? Relationships between process sensitivity in HadGEM3–UKCA and inter-model variation from AeroCom Phase II". In: *Atmospheric Chemistry and Physics* 16.4, pp. 2221–2241.

Klimont, Zbigniew et al. (2017). "Global anthropogenic emissions of particulate matter including black carbon". In: *Atmospheric Chemistry and Physics* 17.14, pp. 8681–8723.

Kodros, JK et al. (2017). "Quantifying the contribution to uncertainty in mortality attributed to household, ambient, and joint exposure to PM2. 5 from residential solid-fuel use". In: *GeoHealth*.

Kodros, John Kelly et al. (2015). "Uncertainties in global aerosols and climate effects due to biofuel emissions". In: *Atmospheric Chemistry and Physics* 15.15, pp. 8577–8596.

Krewski, D et al. (2000). *others: Reanalysis of the Harvard Six Cities Study and the American Cancer Society Study of Particulate Air Pollution and Mortality: Special Report*.

Krewski, Daniel et al. (2009). *Extended follow-up and spatial analysis of the American Cancer Society study linking particulate air pollution and mortality*. 140. Health Effects Institute Boston, MA.

Kuhn, Randall et al. (2016). "Beyond attributable burden: estimating the avoidable burden of disease associated with household air pollution". In: *PloS one* 11.3, e0149669.

Kulmala, M, KEJ Lehtinen, and A Laaksonen (2006). "Cluster activation theory as an explanation of the linear dependence between formation rate of 3nm particles and sulphuric acid concentration". In: *Atmospheric Chemistry and Physics* 6.3, pp. 787–793.

Kulmala, Markka, Ari Laaksonen, and Liisa Pirjola (1998). "Parameterizations for sulfuric acid/water nucleation rates". In: *Journal of Geophysical Research: Atmospheres* 103.D7, pp. 8301–8307.

Lacey, Forrest G et al. (2017a). "Improving present day and future estimates of anthropogenic sectoral emissions and the resulting air quality impacts in Africa". In: *Faraday discussions* 200, pp. 397–412.

Lacey, Forrest G et al. (2017b). "Transient climate and ambient health impacts due to national solid fuel cookstove emissions". In: *Proceedings of the National Academy of Sciences* 114.6, pp. 1269–1274.

Laden, Francine et al. (2006). "Reduction in fine particulate air pollution and mortality: extended follow-up of the Harvard Six Cities study". In: *American journal of respiratory and critical care medicine* 173.6, pp. 667–672.

Lamarque, J-F et al. (2010). "Historical (1850–2000) gridded anthropogenic and biomass burning emissions of reactive gases and aerosols: methodology and application". In: *Atmospheric Chemistry and Physics* 10.15, pp. 7017–7039.

Lee, Colin J et al. (2015). "Response of global particulate-matter-related mortality to changes in local precursor emissions". In: *Environmental science & technology* 49.7, pp. 4335–4344.

Lee, LA et al. (2011). "Emulation of a complex global aerosol model to quantify sensitivity to uncertain parameters". In: *Atmospheric Chemistry and Physics* 11.23, pp. 12253–12273.

Lee, LA et al. (2013). "The magnitude and causes of uncertainty in global model simulations of cloud condensation nuclei." In: *Atmospheric Chemistry & Physics Discussions* 13.3.

Lelieveld, Jos et al. (2015). "The contribution of outdoor air pollution sources to premature mortality on a global scale". In: *Nature* 525.7569, p. 367.

Lewis, Jessica J and Subhrendu K Pattanayak (2012). "Who adopts improved fuels and cookstoves? A systematic review". In: *Environmental health perspectives* 120.5, p. 637.

Lim, Stephen S et al. (2012). "A comparative risk assessment of burden of disease and injury attributable to 67 risk factors and risk factor clusters in 21 regions,

1990–2010: a systematic analysis for the Global Burden of Disease Study 2010". In: *The lancet* 380.9859, pp. 2224–2260.

Liss, Peter S and Liliane Merlivat (1986). "Air-sea gas exchange rates: Introduction and synthesis". In: *The role of air-sea exchange in geochemical cycling*. Springer, pp. 113–127.

Liu, Yang et al. (2004). "Mapping annual mean ground-level PM2. 5 concentrations using Multiangle Imaging Spectroradiometer aerosol optical thickness over the contiguous United States". In: *Journal of Geophysical Research: Atmospheres* 109.D22.

Lohmann, Ulrike and Johann Feichter (2005). "Global indirect aerosol effects: a review". In: *Atmospheric Chemistry and Physics* 5.3, pp. 715–737.

Lozier, Matthew J et al. (2016). "Use of Temperature Sensors to Determine Exclusivity of Improved Stove Use and Associated Household Air Pollution Reductions in Kenya". In: *Environmental science & technology* 50.8, pp. 4564–4571.

Malley, Christopher S et al. (2017). "Updated global estimates of respiratory mortality in adults>/= 30Years of age attributable to long-term ozone exposure". In: *Environmental Health Perspectives, 2017, vol. 125, num. 8, p. 087021*.

Malm, William C et al. (1994). "Spatial and seasonal trends in particle concentration and optical extinction in the United States". In: *Journal of Geophysical Research: Atmospheres* 99.D1, pp. 1347–1370.

Manktelow, PT et al. (2007). "Regional and global trends in sulfate aerosol since the 1980s". In: *Geophysical Research Letters* 34.14.

Mann, GW et al. (2010). "Description and evaluation of GLOMAP-mode: A modal global aerosol microphysics model for the UKCA composition-climate model". In: *Geoscientific Model Development* 3.2, pp. 519–551.

Mårtensson, EM et al. (2003). "Laboratory simulations and parameterization of the primary marine aerosol production". In: *Journal of Geophysical Research: Atmospheres* 108.D9.

Merikanto, J et al. (2010). "Effects of boundary layer particle formation on cloud droplet number and changes in cloud albedo from 1850 to 2000". In: *Atmospheric Chemistry and Physics* 10.2, pp. 695–705.

Mitchell, EJS et al. (2017). "Heating with Biomass in the United Kingdom: Lessons from New Zealand". In: *Atmospheric Environment* 152, pp. 431–454.

Monahan, Edward C, Donald E Spiel, and Kenneth L Davidson (1986). "A model of marine aerosol generation via whitecaps and wave disruption". In: *Oceanic whitecaps*. Springer, pp. 167–174.

Monks, Sarah A et al. (2017). "The TOMCAT global chemical transport model v1. 6: description of chemical mechanism and model evaluation". In: *Geoscientific Model Development* 10.8, p. 3025.

Moriondo, M et al. (2006). "Potential impact of climate change on fire risk in the Mediterranean area". In: *Climate Research* 31.1, pp. 85–95.

Moss, Richard H et al. (2010). "The next generation of scenarios for climate change research and assessment". In: *Nature* 463.7282, p. 747.

Myhre, Gunnar et al. (2013). "Anthropogenic and natural radiative forcing". In: *Climate change* 423, pp. 658–740.

Nenes, Athanasios and John H Seinfeld (2003). "Parameterization of cloud droplet formation in global climate models". In: *Journal of Geophysical Research: Atmospheres* 108.D14.

Nightingale, Philip D et al. (2000). "In situ evaluation of air-sea gas exchange parameterizations using novel conservative and volatile tracers". In: *Global Biogeochemical Cycles* 14.1, pp. 373–387.

O'Connor, FM et al. (2014). "Evaluation of the new UKCA climate-composition model–Part 2: The Troposphere". In: *Geoscientific Model Development* 7.1, pp. 41–91.

Ostro, Bart and WHO (2004). "Outdoor air pollution: assessing the environmental burden of disease at national and local levels". In:

Ostro, Bart et al. (2018). "Assessing the recent estimates of the global burden of disease for ambient air pollution: Methodological changes and implications for low- and middle-income countries". In: *Environmental research*.

Ots, R. et al. (2017). "Modelling carbonaceous aerosol from residential solid fuel burning with different assumptions for emissions". In: *Atmospheric Chemistry and Physics Discussions* 2017, pp. 1–29. DOI: 10.5194/acp-2017-568. URL: https://www.atmos-chem-phys-discuss.net/acp-2017-568/.

Oudin, Anna et al. (2016). "Association between neighbourhood air pollution concentrations and dispensed medication for psychiatric disorders in a large longitudinal cohort of Swedish children and adolescents". In: *BMJ open* 6.6, e010004.

Pedersen, Marie et al. (2013). "Ambient air pollution and low birthweight: a European cohort study (ESCAPE)". In: *The lancet Respiratory medicine* 1.9, pp. 695–704.

Pham, M et al. (1995). "A three-dimensional study of the tropospheric sulfur cycle". In: *Journal of Geophysical Research: Atmospheres* 100.D12, pp. 26061–26092.

Philip, Sajeev et al. (2014). "Spatially and seasonally resolved estimate of the ratio of organic mass to organic carbon". In: *Atmospheric environment* 87, pp. 34–40.

Pillarisetti, Ajay et al. (2014). "Patterns of stove usage after introduction of an advanced cookstove: the long-term application of household sensors". In: *Environmental science & technology* 48.24, pp. 14525–14533.

Pope, C Arden, Douglas W Dockery, and Joel Schwartz (1995). "Review of epidemiological evidence of health effects of particulate air pollution". In: *Inhalation toxicology* 7.1, pp. 1–18.

Pope, C Arden et al. (1995). "Particulate air pollution as a predictor of mortality in a prospective study of US adults". In: *American journal of respiratory and critical care medicine* 151.3, pp. 669–674.

Pope III, C Arden (2007). "Mortality effects of longer term exposures to fine particulate air pollution: review of recent epidemiological evidence". In: *Inhalation toxicology* 19.sup1, pp. 33–38.

Pope III, C Arden and Douglas W Dockery (2006). "Health effects of fine particulate air pollution: lines that connect". In: *Journal of the air & waste management association* 56.6, pp. 709–742.

Pope III, C Arden et al. (2011). "Lung cancer and cardiovascular disease mortality associated with ambient air pollution and cigarette smoke: shape of the exposure–response relationships". In: *Environmental health perspectives* 119.11, p. 1616.

Prather, Michael J (1986). "Numerical advection by conservation of second-order moments". In: *Journal of Geophysical Research: Atmospheres* 91.D6, pp. 6671–6681.

Pringle, KJ et al. (2009). "The relationship between aerosol and cloud drop number concentrations in a global aerosol microphysics model." In: *Atmospheric Chemistry & Physics* 9.12.

Pringle, KJ et al. (2012). "A multi-model assessment of the impact of sea spray geoengineering on cloud droplet number". In: *Atmospheric Chemistry and Physics* 12.23, pp. 11647–11663.

Raes, Frank et al. (2000). "Formation and cycling of aerosols in the global troposphere". In: *Atmospheric environment* 34.25, pp. 4215–4240.

Rao, Shilpa et al. (2017). "Future air pollution in the Shared Socio-economic Pathways". In: *Global Environmental Change* 42, pp. 346–358.

Rap, Alexandru et al. (2013). "Natural aerosol direct and indirect radiative effects". In: *Geophysical Research Letters* 40.12, pp. 3297–3301.

Reddington, CL et al. (2014). "Contribution of vegetation and peat fires to particulate air pollution in Southeast Asia". In: *Environmental Research Letters* 9.9, p. 094006.

Reddington, CL et al. (2015). "Air quality and human health improvements from reductions in deforestation-related fire in Brazil". In: *Nature Geoscience* 8.10, p. 768.

Regayre, LA et al. (2014). "Uncertainty in the magnitude of aerosol-cloud radiative forcing over recent decades". In: *Geophysical Research Letters* 41.24, pp. 9040–9049.

Regayre, Leighton A et al. (2018). "Aerosol and physical atmosphere model parameters are both important sources of uncertainty in aerosol ERF". In: *Atmospheric Chemistry and Physics* 18.13, pp. 9975–10006.

Rehfuess, Eva A et al. (2014). "Enablers and barriers to large-scale uptake of improved solid fuel stoves: a systematic review". In: *Environmental health perspectives* 122.2, p. 120.

Riccobono, Francesco et al. (2014). "Oxidation products of biogenic emissions contribute to nucleation of atmospheric particles". In: *Science* 344.6185, pp. 717–721.

Ritz, Beate et al. (2016). "Traffic-related air pollution and Parkinson's disease in Denmark: a case–control study". In: *Environmental health perspectives* 124.3, p. 351.

Roden, Christoph A et al. (2009). "Laboratory and field investigations of particulate and carbon monoxide emissions from traditional and improved cookstoves". In: *Atmospheric Environment* 43.6, pp. 1170–1181.

Rossow, William B and Robert A Schiffer (1999). "Advances in understanding clouds from ISCCP". In: *Bulletin of the American Meteorological Society* 80.11, pp. 2261–2287.

Sambandam, Sankar et al. (2015). "Can currently available advanced combustion biomass cook-stoves provide health relevant exposure reductions? Results from initial assessment of select commercial models in India". In: *EcoHealth* 12.1, pp. 25–41.

Schmidt, Anja et al. (2011). "Excess mortality in Europe following a future Laki-style Icelandic eruption". In: *Proceedings of the National Academy of Sciences* 108.38, pp. 15710–15715.

Schmidt, Anja et al. (2012). "Importance of tropospheric volcanic aerosol for indirect radiative forcing of climate". In: *Atmospheric Chemistry and Physics* 12.16, pp. 7321–7339.

Schultz, Martin G et al. (2008). "Global wildland fire emissions from 1960 to 2000". In: *Global Biogeochemical Cycles* 22.2.

Scott, CE et al. (2014). "The direct and indirect radiative effects of biogenic secondary organic aerosol". In: *Atmospheric Chemistry and Physics* 14.1, pp. 447–470.

Seinfeld, JH and SN Pandis (1998). "Chemistry of the atmospheric aqueous phase". In: *Atmospheric Chemistry and Physics: From Air Pollution to Climate Change* 337407.

Seinfeld, John H and Spyros N Pandis (2012). *Atmospheric chemistry and physics: from air pollution to climate change*. John Wiley & Sons.

Sekhon, Rajinder S and RC Srivastava (1971). "Doppler radar observations of drop-size distributions in a thunderstorm". In: *Journal of the Atmospheric Sciences* 28.6, pp. 983–994.

Shaddick, Gavin et al. (2018). "Data integration model for air quality: a hierarchical approach to the global estimation of exposures to ambient air pollution". In: *Journal of the Royal Statistical Society: Series C (Applied Statistics)* 67.1, pp. 231–253.

Shen, Huizhong et al. (2017). "Urbanization-induced population migration has reduced ambient PM2. 5 concentrations in China". In: *Science advances* 3.7, e1700300.

Shi, Liuhua et al. (2016). "Low-concentration PM2. 5 and mortality: Estimating acute and chronic effects in a population-based study". In: *Environmental health perspectives* 124.1, p. 46.

Sihto, S-L et al. (2006). "Atmospheric sulphuric acid and aerosol formation: implications from atmospheric measurements for nucleation and early growth mechanisms". In: *Atmospheric Chemistry and Physics* 6.12, pp. 4079–4091.

Silva, Raquel A et al. (2016). "The effect of future ambient air pollution on human premature mortality to 2100 using output from the ACCMIP model ensemble". In: *Atmospheric chemistry and physics* 16.15, pp. 9847–9862.

Silva, Raquel A et al. (2017). "Future global mortality from changes in air pollution attributable to climate change". In: *Nature Climate Change* 7.9, p. 647.

Silver, B et al. (2018). "Substantial changes in air pollution across China during 2015–2017". In: *Environmental Research Letters* 13.11, p. 114012.

Singh, Gitanjali M et al. (2013). "The age-specific quantitative effects of metabolic risk factors on cardiovascular diseases and diabetes: a pooled analysis". In: *PloS one* 8.7, e65174.

Smith, Kirk R and Majid Ezzati (2005). "How environmental health risks change with development: the epidemiologic and environmental risk transitions revisited". In: *Annu. Rev. Environ. Resour.* 30, pp. 291–333.

Smith, Kirk R and Ambuj Sagar (2014). "Making the clean available: escaping India's Chulha Trap". In: *Energy Policy* 75, pp. 410–414.

Smith, Kirk R et al. (2014a). "Millions dead: how do we know and what does it mean? Methods used in the comparative risk assessment of household air pollution". In: *Annual review of public health* 35, pp. 185–206.

Smith, Lauren T et al. (2014b). "Drought impacts on children's respiratory health in the Brazilian Amazon". In: *Scientific reports* 4, p. 3726.

Spracklen, Dominick V et al. (2009). "Impacts of climate change from 2000 to 2050 on wildfire activity and carbonaceous aerosol concentrations in the western United States". In: *Journal of Geophysical Research: Atmospheres* 114.D20.

Spracklen, Dominick V et al. (2010). "Explaining global surface aerosol number concentrations in terms of primary emissions and particle formation". In: *Atmospheric Chemistry and Physics* 10.10, pp. 4775–4793.

Spracklen, DV et al. (2005a). "A global off-line model of size-resolved aerosol microphysics: I. Model development and prediction of aerosol properties". In: *Atmospheric Chemistry and Physics* 5.8, pp. 2227–2252.

— (2005b). "A global off-line model of size-resolved aerosol microphysics: I. Model development and prediction of aerosol properties". In: *Atmospheric Chemistry and Physics* 5.8, pp. 2227–2252.

— (2005c). "A global off-line model of size-resolved aerosol microphysics: II. Identification of key uncertainties". In: *Atmospheric Chemistry and Physics* 5.12, pp. 3233–3250.

Spracklen, DV et al. (2006). "The contribution of boundary layer nucleation events to total particle concentrations on regional and global scales". In: *Atmospheric Chemistry and Physics Discussions* 6.4, pp. 7323–7368.

Spracklen, DV et al. (2011a). "Aerosol mass spectrometer constraint on the global secondary organic aerosol budget". In: *Atmospheric Chemistry and Physics* 11.23, pp. 12109–12136.

Spracklen, DV et al. (2011b). "Global cloud condensation nuclei influenced by carbonaceous combustion aerosol". In: *Atmospheric Chemistry and Physics* 11.17, pp. 9067–9087.

Steenland, Kyle et al. (2018). "Modeling the potential health benefits of lower household air pollution after a hypothetical liquified petroleum gas (LPG) cookstove intervention". In: *Environment international* 111, pp. 71–79.

Stier, P et al. (2005). "The aerosol-climate model ECHAM5-HAM". In: *Atmospheric Chemistry and Physics* 5.4, pp. 1125–1156.

Stocker, Thomas (2014). *Climate change 2013: the physical science basis: Working Group I contribution to the Fifth assessment report of the Intergovernmental Panel on Climate Change*. Cambridge University Press.

Stohl, Andreas et al. (2015). "Evaluating the climate and air quality impacts of short-lived pollutants". In: *Atmospheric Chemistry and Physics* 15.18, pp. 10529–10566.

Sun, Haolin, Laura Biedermann, and Tami C Bond (2007). "Color of brown carbon: A model for ultraviolet and visible light absorption by organic carbon aerosol". In: *Geophysical Research Letters* 34.17.

Tai, Amos PK, Loretta J Mickley, and Daniel J Jacob (2010). "Correlations between fine particulate matter (PM2. 5) and meteorological variables in the United States: Implications for the sensitivity of PM2. 5 to climate change". In: *Atmospheric Environment* 44.32, pp. 3976–3984.

Thurston, George D et al. (2016). "Ischemic heart disease mortality and long-term exposure to source-related components of US fine particle air pollution". In: *Environmental health perspectives* 124.6, p. 785.

Tiedtke, MICHAEL (1989). "A comprehensive mass flux scheme for cumulus parameterization in large-scale models". In: *Monthly Weather Review* 117.8, pp. 1779–1800.

Todd, MC et al. (2013). "Meteorological and dust aerosol conditions over the western Saharan region observed at Fennec Supersite-2 during the intensive observation period in June 2011". In: *Journal of Geophysical Research: Atmospheres* 118.15, pp. 8426–8447.

Tørseth, Kjetil et al. (2012). "Introduction to the European Monitoring and Evaluation Programme (EMEP) and observed atmospheric composition change during 1972–2009". In: *Atmospheric Chemistry and Physics* 12.12, pp. 5447–5481.

Tsigaridis, K et al. (2014). "The AeroCom evaluation and intercomparison of organic aerosol in global models". In: *Atmospheric Chemistry and Physics* 14.19, pp. 10845–10895.

Tuomisto, Jouni T et al. (2008). "Uncertainty in mortality response to airborne fine particulate matter: Combining European air pollution experts". In: *Reliability Engineering & System Safety* 93.5, pp. 732–744.

Turner, Michelle C et al. (2016). "Long-term ozone exposure and mortality in a large prospective study". In: *American journal of respiratory and critical care medicine* 193.10, pp. 1134–1142.

Turnock, ST et al. (2015). "Modelled and observed changes in aerosols and surface solar radiation over Europe between 1960 and 2009". In: *Atmospheric Chemistry and Physics* 15.16, pp. 9477–9500.

Twomey, S (1959). "The nuclei of natural cloud formation part II: The supersaturation in natural clouds and the variation of cloud droplet concentration". In: *Geofisica pura e applicata* 43.1, pp. 243–249.

Twomey, Sean (1977). "The influence of pollution on the shortwave albedo of clouds". In: *Journal of the atmospheric sciences* 34.7, pp. 1149–1152.

Uppala, Sakari M et al. (2005). "The ERA-40 re-analysis". In: *Quarterly Journal of the royal meteorological society* 131.612, pp. 2961–3012.

Van Der Werf, Guido R et al. (2004). "Continental-scale partitioning of fire emissions during the 1997 to 2001 El Nino/La Nina period". In: *Science* 303.5654, pp. 73–76.

Van Donkelaar, Aaron, Randall V Martin, and Rokjin J Park (2006). "Estimating ground-level PM2. 5 using aerosol optical depth determined from satellite remote sensing". In: *Journal of Geophysical Research: Atmospheres* 111.D21.

Van Donkelaar, Aaron et al. (2010). "Global estimates of ambient fine particulate matter concentrations from satellite-based aerosol optical depth: development and application". In: *Environmental health perspectives* 118.6, p. 847.

Van Donkelaar, Aaron et al. (2016). "Global estimates of fine particulate matter using a combined geophysical-statistical method with information from satellites, models, and monitors". In: *Environmental science & technology* 50.7, pp. 3762–3772.

Van Vuuren, Detlef P et al. (2011). "The representative concentration pathways: an overview". In: *Climatic change* 109.1-2, p. 5.

Vieno, Massimo et al. (2016). "The UK particulate matter air pollution episode of March–April 2014: more than Saharan dust". In: *Environmental Research Letters* 11.4, p. 044004.

Von Schneidemesser, Erika et al. (2015). "Chemistry and the linkages between air quality and climate change". In: *Chemical Reviews* 115.10, pp. 3856–3897.

Wang, Jiandong et al. (2017). "Historical trends in PM2. 5-related premature mortality during 1990–2010 across the northern hemisphere". In: *Environmental health perspectives* 125.3, p. 400.

Wathore, Roshan, Kevin Mortimer, and Andrew P Grieshop (2017). "In-use emissions and estimated impacts of traditional, natural-and forced-draft cookstoves in rural Malawi". In: *Environmental science & technology* 51.3, pp. 1929–1938.

Weagle, Crystal L et al. (2018). "Global Sources of Fine Particulate Matter: Interpretation of PM2. 5 Chemical Composition Observed by SPARTAN using a Global Chemical Transport Model". In: *Environmental science & technology*.

West, J Jason et al. (2013). "Co-benefits of mitigating global greenhouse gas emissions for future air quality and human health". In: *Nature climate change* 3.10, p. 885.

West, J Jason et al. (2016). *What we breathe impacts our health: improving understanding of the link between air pollution and health*.

Westerling, AL and BP Bryant (2008). "Climate change and wildfire in California". In: *Climatic Change* 87.1, pp. 231–249.

Whiteaker, Jeffrey R, David T Suess, and Kimberly A Prather (2002). "Effects of meteorological conditions on aerosol composition and mixing state in Bakersfield, CA". In: *Environmental science & technology* 36.11, pp. 2345–2353.

Wild, Oliver, Xin Zhu, and Michael J Prather (2000). "Fast-J: Accurate simulation of in-and below-cloud photolysis in tropospheric chemical models". In: *Journal of Atmospheric Chemistry* 37.3, pp. 245–282.

Wilkinson, Paul et al. (2009). "Public health benefits of strategies to reduce greenhouse-gas emissions: household energy". In: *The Lancet* 374.9705, pp. 1917–1929.

Winijkul, Ekbordin, Laura Fierce, and Tami C Bond (2016). "Emissions from residential combustion considering end-uses and spatial constraints: Part I, methods and spatial distribution". In: *Atmospheric Environment* 125, pp. 126–139.

Woodward, S (2001). "Modeling the atmospheric life cycle and radiative impact of mineral dust in the Hadley Centre climate model". In: *Journal of Geophysical Research: Atmospheres* 106.D16, pp. 18155–18166.

Xing, Yu-Fei et al. (2016). "The impact of PM2. 5 on the human respiratory system". In: *Journal of thoracic disease* 8.1, E69.

Yin, Peng et al. (2017). "Long-term fine particulate matter exposure and nonaccidental and cause-specific mortality in a large national cohort of Chinese men". In: *Environmental health perspectives* 125.11.

Yoshioka (2017). "Ensembles of global climate model simulations to explore uncertainty in global aerosols and radiative forcing". In: *In prep*.

Zhang, Leiming et al. (2001). "A size-segregated particle dry deposition scheme for an atmospheric aerosol module". In: *Atmospheric Environment* 35.3, pp. 549–560.

Zheng, Yixuan et al. (2017). "Air quality improvements and health benefits from China clean air action since 2013". In: *Environmental Research Letters* 12.11, p. 114020.